Amine-Linked Oligomers of Polycyclic Aromatic Hydrocarbons: Synthesis, Properties and Supramolecular Assembly

Inauguraldissertation

der Philosophisch-naturwissenschaftlichen Fakultät

der Universität Bern

vorgelegt von

Jovana Jevrić

von Montenegro

Leiter der Arbeit:

Prof. Dr. Robert Häner

Departement für Chemie, Biochemie und Pharmazie der Universität Bern

Copyright Notice

You are free to:

Share – copy and redistribute the material in any medium or format

Adapt – remix, transform, and build upon the material

The licensor cannot revoke these freedoms as long as you follow the license terms.

Under the following terms:

Attribution – You must give appropriate credit, provide a link to the license, and indicate if changes were made. You may do so in any reasonable manner, but not in any way that suggests the licensor endorses you or your use.

NonCommercial – You may not use the material for commercial purposes.

No additional restrictions – You may not apply legal terms or technological measures that legally restrict others from doing anything the license permits.

For any reuse or distribution, you must take clear to others the license terms of this work.

Any of these conditions can be waived if you get permission from the copyright holder.

Nothing in this license impairs or restricts the author's moral rights according to Swiss law.

The detailed license agreement can be found at:
https://creativecommons.org/licenses/by-nc/4.0/legalcode

Amine-Linked Oligomers of Polycyclic Aromatic Hydrocarbons: Synthesis, Properties and Supramolecular Assembly

Inauguraldissertation

der Philosophisch-naturwissenschaftlichen Fakultät

der Universität Bern

vorgelegt von

Jovana Jevrić

von Montenegro

Leiter der Arbeit:

Prof. Dr. Robert Häner

Departement für Chemie, Biochemie und Pharmazie der Universität Bern

Von der Philosophisch-naturwissenschaftlichen Fakultät angenommen.

Bern, 18.06.2021

Der Dekan:
Prof. Dr. Zoltan Balogh

Acknowledgements

After four interesting and educational years of my PhD, I would like to thank some important people.

First of all, I would like to thank Robert Häner for giving me the opportunity to do my PhD in his research group. I appreciate that he gave me my scientific freedom and supported me with my ideas.

I would also like to thank my external reviewer, Jean-François Lutz, as well as the chairman of my PhD defense, Philippe Renaud, for agreeing to evaluate my work.

My thanks go to the current as well as past group members for the great time and the good collaboration. Especially, I would like to thank Simon Langenegger, for all the helpful discussions and instructive tips.

Thanks also to all staff members of the in-house services of the department, who were always ready to help when one had a problem.

A big thank you goes to my family, for their support and encouragement to achieve my goals.

The financial support of the Swiss National Science Foundation (SNF) and the University of Bern are gratefully acknowledged.

Last but not least, I would like to thank everyone who accompanied, supported, and helped me during this time.

Shoot for the moon.
Even if you miss, you'll land among the stars.

— Norman Vincent Peale

Contents

Summary

The thesis starts with a general introduction about supramolecular polymers, energy transfer in light-harvesting systems, and electrostatic layering. Thereafter follows the experimental work which is outlined in five chapters.

The first chapter focuses on the electrostatic interaction of positively- and negatively-charged supramolecular polymers. Positively charged phenanthrene vesicles and negatively charged pyrene sheets were alternately deposited on the substrate mica. The challenges and limitations of electrostatic layering with oppositely charged supramolecular polymers will be discussed.

Chapter 2 concentrates on the synthesis and analysis of new cationic supramolecular polymers, oligoamines, respectively. The following oligoamines were synthesized: 3,6-dialkynyl phenanthrene-pyrene-phenanthrene trimer, 2,7-dialkynyl phenanthrene trimer, 1,6-dialkynyl pyrene trimer, 1,6-dialkynyl pyrene trimer with dimethylated amine-bridges, 1,6-dialkynyl pyrene monomer and 4,4'-dialkynyl stilbene trimer. The goal was to find an oligoamine that self-assembles into sheets and could be used for the electrostatic layering, described in the previous chapter. Therefore, atomic force spectroscopy was measured to study the formed assemblies. It was shown that the synthesized molecules tend to self-assemble into various, unreproducible structures. Nevertheless, findings showed that linear structures tend to self-assemble into sheets, but are barely soluble in water-miscible solvents.

In chapter 3, the ideas of the previous two chapters will be combined. A novel linearly-linked stilbene-oligomer is synthesized in which the linkers were changed from dialkynyl to dialkoxy to improve the solubility. The formation of supramolecular polymer sheets was observed. Its synthesis and self-assembly behavior are described.

The last two chapters 4 and 5 are devoted to investigations in supramolecular and DNA based light-harvesting systems using a cationic supramolecular polymer. Different types of chromophore acceptors are tested in both systems, non-covalently- and covalently-linked ones. It will be shown that the oligoamines can be used as donors and acceptors in light-harvesting structures.

1. General Introduction

1.1. Supramolecular Polymers

In contrast to their classical counterparts, the covalent polymers, supramolecular polymers are linked together by highly directional non-covalent interactions of monomeric units.[1,2] Meijer et. al. proposed the following definition: *"Supramolecular polymers are defined as polymeric arrays of monomeric units that are brought together by reversible and highly directional secondary interactions, resulting in polymeric properties in dilute and concentrated solutions, as well as in the bulk. The monomeric units of the supramolecular polymers themselves do not possess a repetition of chemical fragments. The directionality and strength of the supramolecular bonding are important features of systems that can be regarded as polymers and that behave according to well-established theories of polymer physics."*[3]

The non-covalent interactions range from hydrogen bonding, hydrophobic interaction, $\pi - \pi$ interaction, metal-ligand coordination to electrostatic interaction. Since non-covalent interactions lead to reversible and stimuli-responsive systems, materials based on supramolecular polymers are adaptive and dynamic.[4–11] The advantages of these properties are that such materials are self-healing, recyclable, controllably modularized constructed, and so forth.[1,3,12–15]

As water is the environment of all biological processes, the interest in supramolecular polymers in aqueous medium increased in recent years. The self-assembly of supramolecular polymers in aqueous medium is based on hydrophobic effects, hydrophilic interactions, Coulomb interactions, hydrogen bonds, and Van der Waals interactions.[1,16–23]

Meijer et. al. divided the formation of supramolecular polymerizations in three main mechanisms: isodesmic, cooperative, and ring-chain supramolecular polymerization (Figure 1.1).[24,25]
The isodesmic supramolecular polymerization (shown in Figure 1.1(a)) is very similar to the step polymerization for the formation of macromolecules. This mechanism occurs when the strength of non-covalent interactions between monomers is unaffected by the length of the chain. Thus, the length of the forming polymer gets bigger as the concentration of monomers in solution is increased or the temperature decreased.
The second mechanism, ring-chain mediated polymerization (shown in Figure 1.1(b)), happens when an equilibrium between closed rings and linear polymer chains is present. If the monomer concentration is below a critical point, the ends of small polymer chains react with each other to generate closed rings. If the monomer concentration is above the critical point, polymer growth is initiated because the linear chain formation gets more favoured.
The third mechanism, cooperative polymerization (Figure 1.1(c)), is also known as nucleation-elongation mechanism and occurs in the growth of ordered supramolecular polymers. Besides the formation of linear polymers, additional interactions are present during the growth of ordered

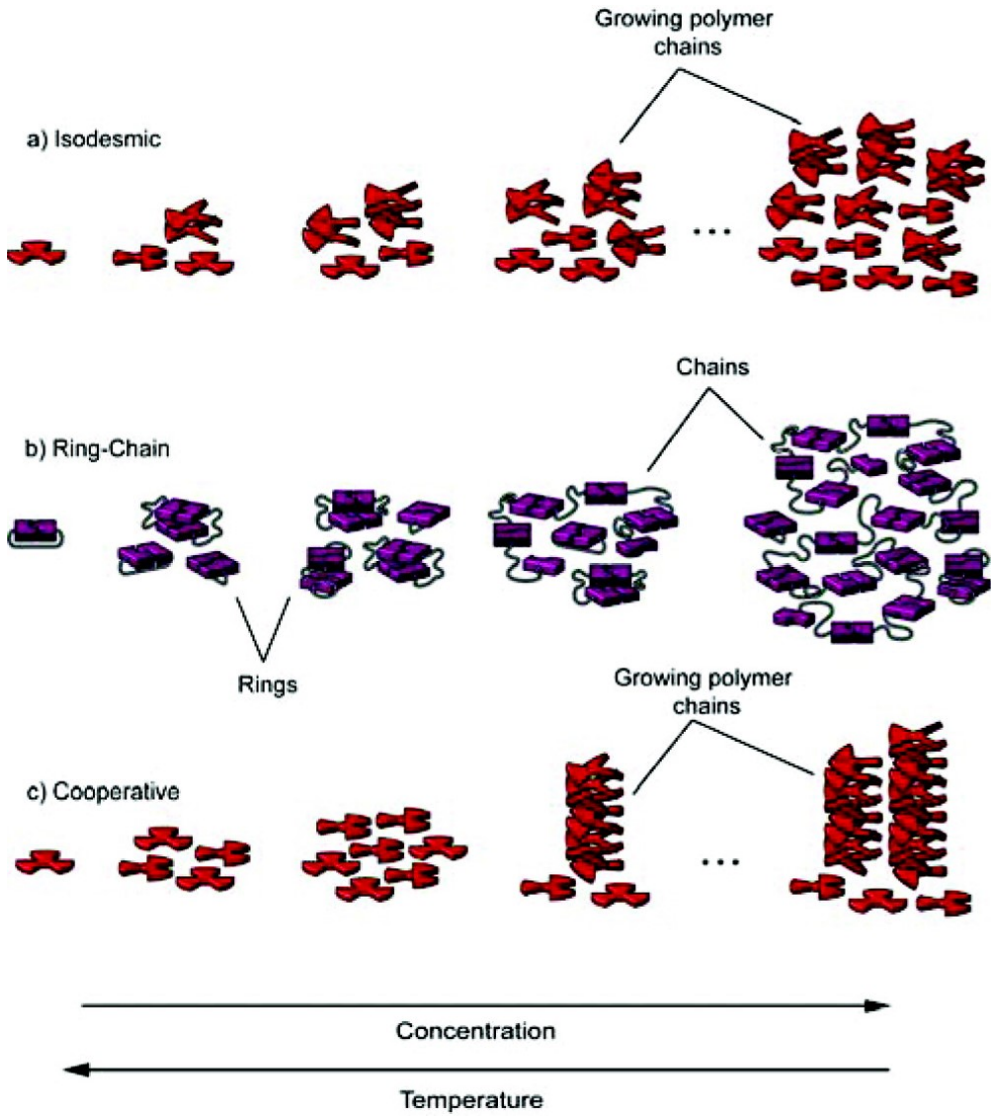

Figure 1.1. Model representation of the three main polymerization mechanisms by which a monomer unit can polymerize into a supramolecular polymer: (a) isodesmic, (b) ring-chain mediated, and (c) cooperative polymerization. Illustration is taken from reference.[24]

supramolecular polymers by cooperative polymerization, such as those that form helices and tubes. During the nucleation step, only a single bond is formed between the monomers (same as in the

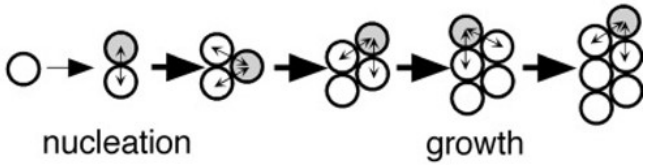

Figure 1.2. Model representation of the cooperative polymerization. Until the nucleus is formed only a single bond is formed between the subunits. After the nucleation, two or more bonds may form during the addition of subunits to the end of a multistranded polymer. Figure adapted from reference.[26]

isodesmic method), meaning that the non-covalent bonds between the subunits are weak (Figure 1.2). After the formation of a nucleus, the addition of further monomer subunits is favoured and the polymer growth initiated.[24–27]
Thus summed up, all three mechanisms are both concentration and temperature dependent.

Supramolecular polymers in an aqueous medium are especially interesting for biomedical applications, as they offer a dynamic nature that allows a high adaptivity when changing e.g. the biological environment.[18] Additionally, the dynamics of supramolecular polymers allow the production of self-healing materials.[28] Also the electronic properties of supramolecular assemblies of π-conjugated system are the reason for their potential application in optoelectronics, like nanoscale photovoltaics and photodetectors.[24,29]

1.2. Light-Harvesting and Energy Transfer

In the previous section, supramolecular polymers were introduced. Their dynamic nature and adaptivity enables the polymerization of different monomeric subunits, and thus various modifications with chromophores are possible. The formation of π-conjugated supramolecular polymers allows energy transfer and/or light-harvesting of such a system.

Photosynthesis is the most commonly known process in nature, in which light energy is captured and stored by an organism and further used for cellular processes. Basically, plants, algae and cyanobacteria produce oxygen and carbohydrates using water, CO_2 and sunlight.[30–32] Figure 1.3 displays graphically the process of photosynthesis in a light-harvesting complex. The light energy is first absorbed by pigments, whereas due to the photon absorption an excited state is created. This leads to a charge separation when the reaction center is reached.

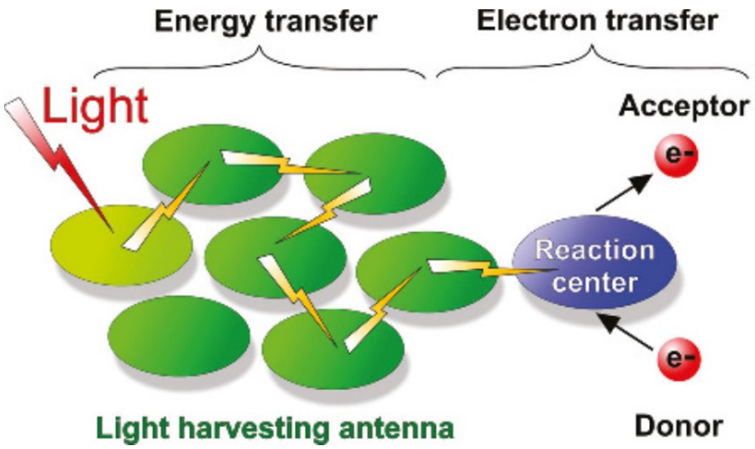

Figure 1.3. Graphical illustration of a light-harvesting complex in organisms. Light is absorbed by a pigment (green), followed by the energy transfer (flashes) throughout the light-harvesting antenna system until it reaches the reaction center (blue). At this point, the electron transfer takes place, and creates an oxidized electron donor and a reduced electron acceptor. Illustration is taken from reference.[30]

In other words said, a light-harvesting complex is an accumulation of pigments that are capable of collecting light and transfer it to the reaction center. In nature, the most important pigments are chlorophylls and carotenoids.
In order to understand the processes occurring in such natural light-harvesting systems, researchers started to study simplified model systems. Thus, artificial light-harvesting complexes were designed which are comprised of electron donors and acceptors that mimic the charge separation function of photosynthetic proteins.[33–43] Thereby, different energy transfers may occur in these systems.

Electronic energy transfer (EET) is a process in which the excitation energy is transferred from one donor-chromophore to an acceptor-chromophore. The EET is especially observed in multichromophoric systems over reasonably large distances (limited by the excited state lifetime) by a series of energy hops.[44–48]
However, if the electrostatic interactions between the chromophores are relatively weak, the energy transfer is described as Förster resonance energy transfer (FRET).[34,49–55] FRETs are based on the electric dipole-dipole interactions between donor and acceptor, and the processes depend on the distance between the interacting chromophores (0.5-10 nm), the relative orientations of the chromophores and the spectral overlap between donor emission and acceptor absorption.[56,57]

Figure 1.4 explains how Förster resonance energy transfer can be spectroscopically determined. Figure 1.4 A1) and A2) show the emission spectra of two hypothetical fluorophores when exciting the donor, fluorophore 1. Their emission maxima are at different wavelengths. The emission of the acceptor (m2, orange), fluorophore 2, is low because it is not absorbing at the same wavelength as the donor and thus not excited. Figure 1.4 B1) and B2) show the fluorescence spectra after mixing the donor and acceptor (red). Figure 1.4 B1) shows the emission spectrum when donor and acceptor (red) are mixed in a low concentration. Comparing the emission of the donor alone (green dashed line) with the one after mixing (red), there is a slight increase in donor-intensity (m1, green arrow), meaning that no energy is transferred to the acceptor. Because we are in a system, where the concentration of both chromophores is low, the distance between the molecules is too large, and thus no FRET occurs. As previously mentioned, the distance of donor to acceptor needs to be in a range of 0.5-10 nm, otherwise, the energy cannot be transferred from the excited donor to the acceptor, and only donor emission is observed (Figure 1.4 C1)). In Figure 1.4 B2) the concentration of chromophores was high, meaning that the distance between the donor and acceptor was small and FRET possible. When exciting the donor, one observes a decrease in donor-intensity (m1, green arrow) and an increase in acceptor-intensity (m2, orange arrow). This shows that an energy transfer occurs. Figure 1.4 C2) shows the distribution of donors (green) and acceptors (orange) at a high concentration. The distances are smaller and that is why the excited donor can transfer the energy to the acceptor, and acceptor emission is observed.

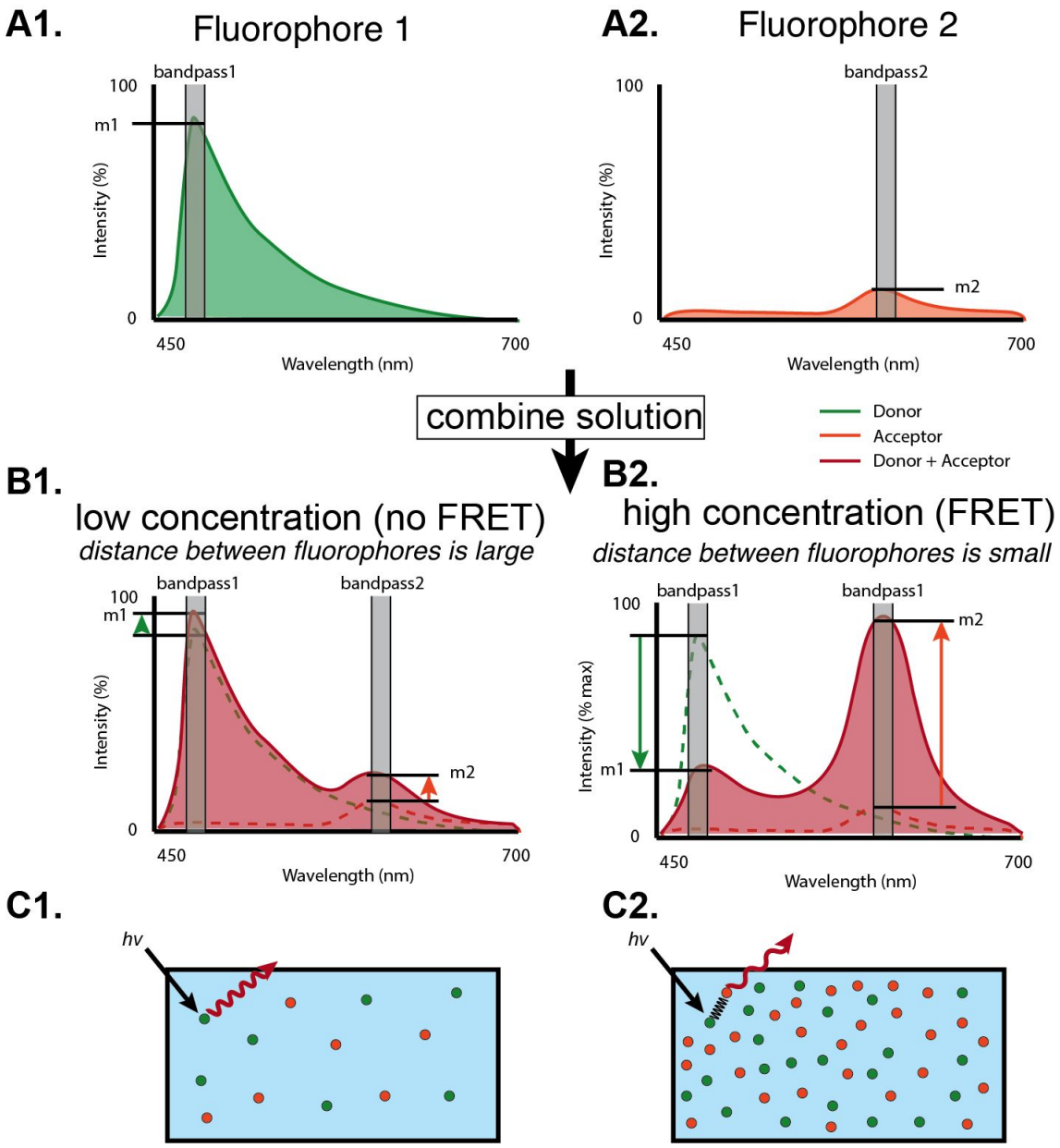

Figure 1.4. The concept of FRET is described. A) The emission spectra of two hypothetical fluorophores are shown, which fluoresce at different wavelengths. B) The emission spectra are shown after the combination of both fluorophores 1 and 2, when mixed in B1) low concentrations and B2) high concentrations. C) Illustration of the sample solution. The distribution of the fluorophores is demonstrated at low (C1) and high (C2) concentrations. Figure adapted from reference.[58]

On the other hand, if the electronic coupling of the interacting chromophores is strong, the electronic excitation is spread coherently.[59] In such a case, the electronic states of the donor and acceptor mix strongly, to produce new, delocalized states within which the energy is shared quantum mechanically among several chromophores. The excitation energy is therefore transferred wavelike (Figure 1.5 (b)).[44] Newer concepts for the description and understanding of light-harvesting phenomena include this theory of quantum coherent energy transfer.[44,59–64]

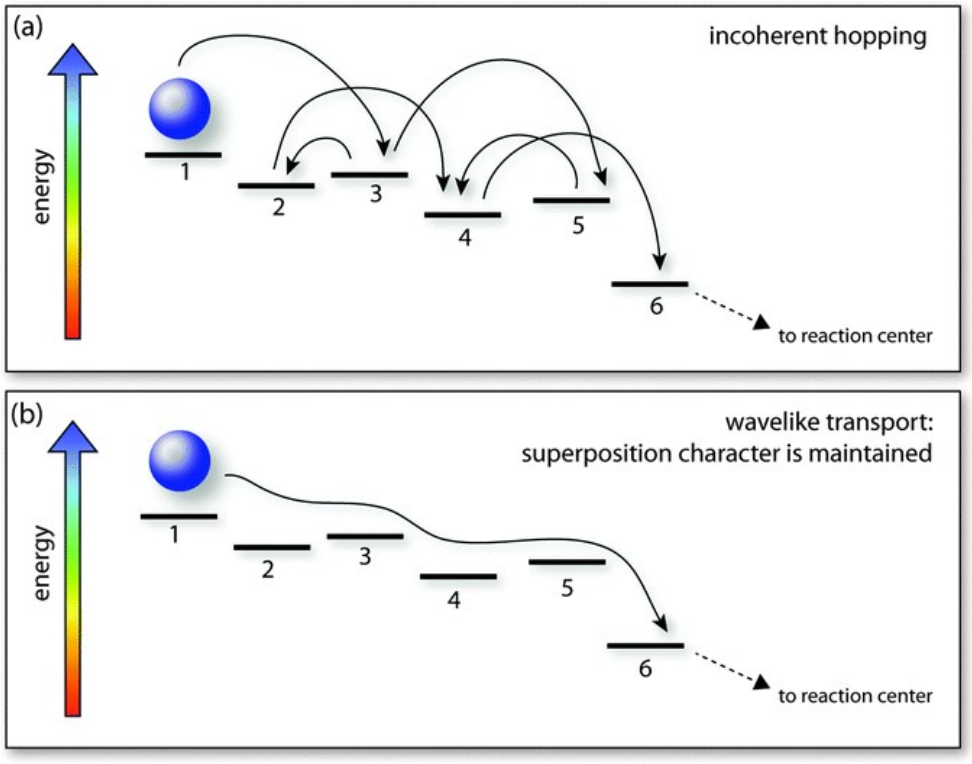

Figure 1.5. The difference between the two mechanisms of excitation energy transfer (EET) is schematically illustrated. (a) Classical EET: the excitation energy hops randomly from one chromophore to another until it reaches the reaction center. (b) Quantum-coherent EET: the excitation energy is quantum-mechanically distributed over several chromophores. Illustration is taken from reference.[44]

1.3. Electrostatic Layering

The interest in producing ultrathin layers for optics and sensors is increasing. These applications need a well-defined and controlled film preparation, with a choice of usable materials depending on its application field.[65–67]

For about 65 years the formation of controlled monolayers was done by the Langmuir-Blodgett technique. In this method, one used amphiphilic molecules which would arrange themselves on the air-water interface and thus form a layer. Afterwards, this layer was transferred onto a solid substrate.[67–70] H. Kuhn et al. experimented in the 70's with synthetic nanoscale multicomposites out of organic molecules using the Langmuir-Blodgett technique. They showed that a FRET transfer between alternating donor- and acceptor layers is possible.[71,72]

The Langmuir-Blodgett technique is an efficient method for the formation of multilayered structures. Nevertheless, a disadvantage of the technique is, that one is limited regarding the choice of suitable molecules for the deposition. Within the years the technique of layer adsorption was improved and even more simplified, called the layer-by-layer (LbL) deposition technique. The LbL deposition technique is based on alternate electrostatic adsorption of oppositely charged materials for the production of multilayered thin films.[66–68,73–75] The advantage is that the repertoire of

possible materials for the formation of multilayered assemblies is extended to polyelectrolytes,[76–79] biomaterials[73,80] or supramolecular assemblies[81,82] to mention some. This method was first described in the 60's by Iler and Kirkland,[83,84] rediscovered in the early 90's from Decher et al.[76,85] and applied since because of its simplicity and low cost. The general procedure of an LbL film formation is explained by the example of Decher and coworkers using poly(styrene sulfonate sodium salt) as the anion and poly(allylamine hydrochloride) as the cation (Figure 1.6).[86]
They immersed a positively charged planar surface into the anionic polyelectrolyte solution (step 1 in Figure 1.6A). This led to the adsorption of a negative monolayer due to electrostatic interactions, meaning that the surface charge was changed from positive to negative (blue layer in Figure 1.6B). Afterwards, the coated substrate was immersed in a rinsing solution (step 2), to remove weakly adsorbed polyanions and prevent contamination of the following solution. In a third step, the coated substrate was immersed into a solution containing the cationic polyelectrolyte (red), leading to an adsorption of another monolayer (red layer in Figure 1.6B) and thus changing the surface charge back to positive. The substrate with the two layers was immersed again into a rinsing solution (step 4) and the cycle could be repeated as long as the desired thickness of the layer was reached.

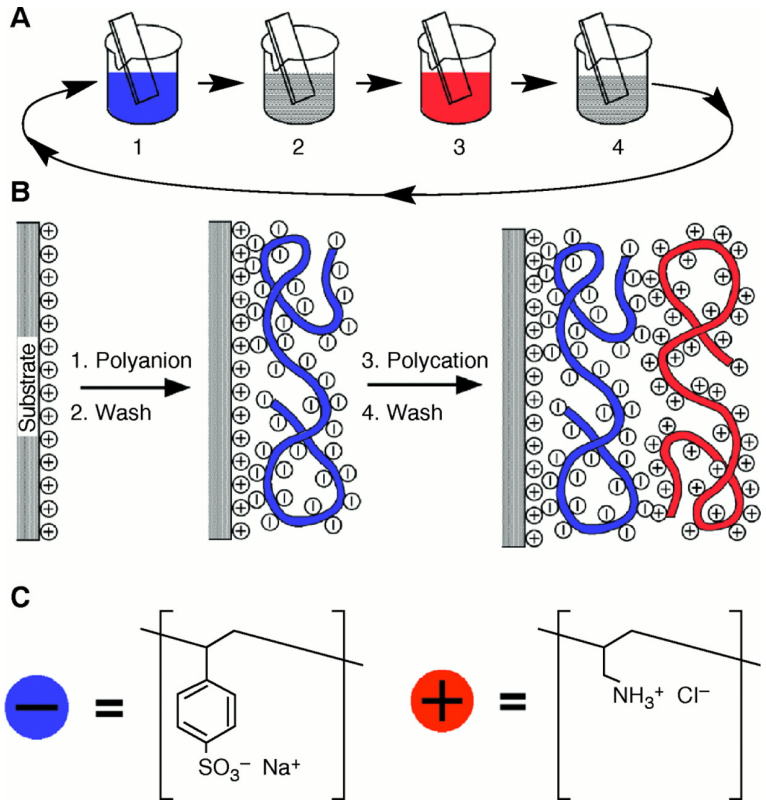

Figure 1.6. Schematical representation of the electrostatic layer-by-layer assembly. A) The deposition of a new layer is shown, whereas steps 1 and 3 show the adsorption of a polyion and steps 2 and 4 the washing steps. B) The first two adsorption steps are shown as a graphic. One starts with the positively charged surface, followed by adsorption of polyanions. The surface charge is reversed with each adsorption step. C) These two molecules were used for the electrostatic interaction: the anion poly(styrene sulfonate sodium salt) and the cation poly(allylamine hydrochloride). Figure adapted from reference.[86]

Several years later, a group from South Korea used as an anion the negatively charged squarylium dye and as a counter-ion poly(diallyldimethylammonium chloride) (PDDA).[77] Squarylium is especially interesting as it can be potentially applied in organic photoreceptors and organic solar cells. As shown in Figure 1.7, they started with a negative charged planar surface and adsorbed first a monolayer of PDDA by immersing it in the solution. After rinsing they could adsorb another monolayer of the squarylium dye. Also, this group could stack as many layers on top of each other as they wanted.

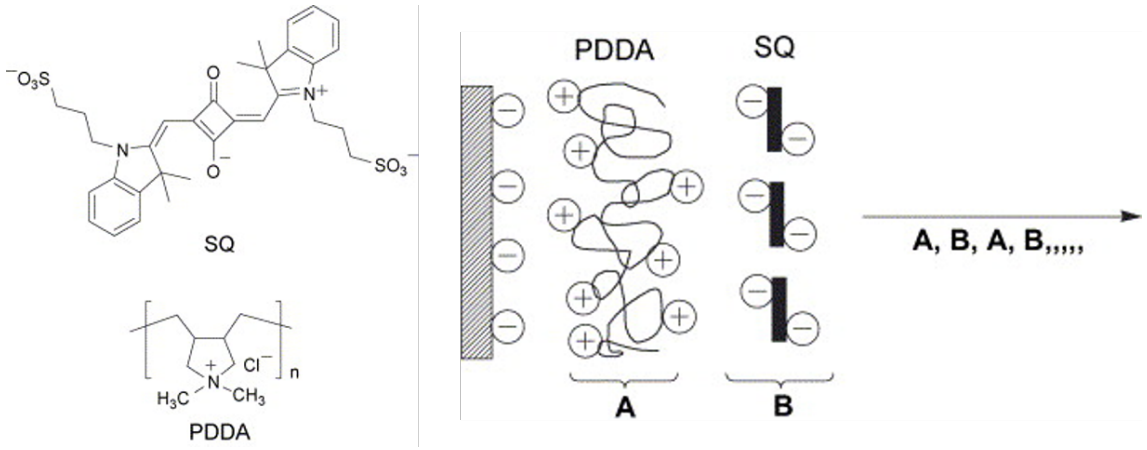

Figure 1.7. Model representation of the electrostatic layer-by-layer self-assembly of squarylium dye (SQ) and poly(diallyldimethylammonium chloride) (PDDA). Illustration is taken from reference.[77]

The LbL technique allows the incorporation of various functionalities into the formation of multilayered films. Sohn et al. investigated FRET in LbL assemblies, by incorporating donor and acceptor pairs of fluorescent dyes into the layers of an LbL assembly and thus control the energy transfer. The dyes were therefore covalently attached to polyelectrolytes and used for the alternate layering. They could control multiple FRET events within the LbL assemblies, by increasing the donor-to-acceptor distances beyond the Förster radius with the addition of polyelectrolyte layers. Such a system could be used for multiple controlled FRET events like producing different colors in light-emitting diodes.[87,88]

So far the focus was on what materials can be used to achieve the desired thin films. Recent studies show, that the assembly method determines the process properties, but also affects the physicochemical properties of the films. This means that the thickness, homogeneity, or even intra- and interlayer film organization is affected by the assembly method. Therefore, the five major technology categories for LbL assembly are presented: immersive, spin, spray, electromagnetic, and fluidic assembly (Figure 1.8).[65,66] Most of the presented methods work on the same principle. One starts with the adsorption of the first material, followed by washing off unbound material. Next, adsorb the second material and repeat the washing step (Figure 1.8 A, C, and D). The other two methods (Figure 1.8 B and E) distinguish themselves from these three by their lack of a washing step.

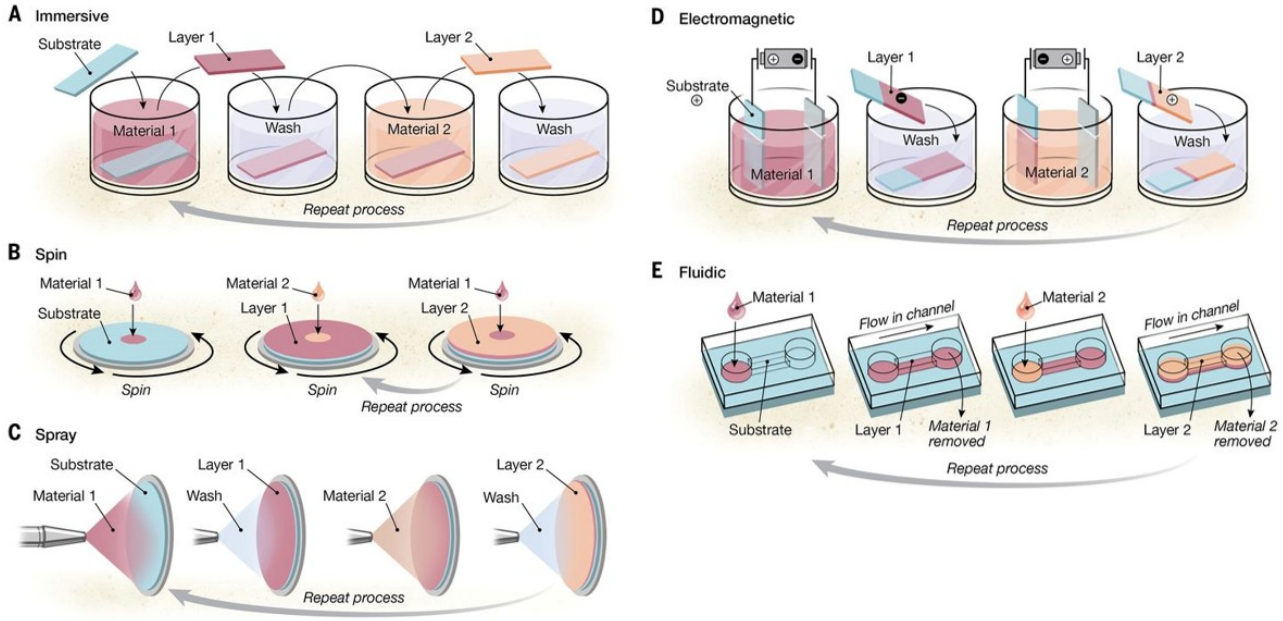

Figure 1.8. Schematical illustration of the five major technology categories and their assembly procedure for LbL film production. A) immersive, B) spin, C) spray, D) electromagnetic and E) fluidic. Illustration is taken from reference.[65]

The immersive assembly (Figure 1.8 A) is the most commonly used method and was previously described in the example of Decher and coworkers.[86] The reason for this is, the ease of use, meaning that one can immerse any shape and size of a substrate in a container with the material solution to be adsorbed. The resulting layers interpenetrate each other, forming indistinct LbL assemblies. One disadvantage is, that one needs quite a lot of material to immerse the substrate. This is why the washing steps are important, so that the material solutions may be reused.

The layers are deposited on a rotating substrate when applying the spin coating method. The excess of material and solvent is therefore removed due to the spinning and no washing step is required. In comparison to the immersive method, thinner and more organized layers are formed by spin-coating. A disadvantage is, that only flat and smooth substrates may be used, otherwise the shear forces during assembly would not allow an even adsorption of a film.

With spray assembly, multilayer films are produced by aerosolizing the coating solutions, and afterwards spraying them onto the substrate. The substrate may be large or nonpolar, but still, the main method to coat complex structures is the immersive assembly. By spraying the material on the substrate, well organized and clear layers are formed in a short time and thus, this method is frequently used for industrial applications.

The electromagnetic assembly is still not such a common technology, as it requires special equipment and expertise. In order to deposit a film, an electric or magnetic field needs to be applied. Usually, electrodes are coated in polymer solutions or one uses a magnetic particulate substrate which can be moved in and out of the coating solutions. The formed layers are thicker and more densely packed than films which are prepared by other assembly techniques.

The fluidic assembly is used for the assembly of multilayers on surfaces that are not easily accessible

to other methods, like inside capillaries. For the deposition of films, fluidic channels are used in which the substrate solution is moved by using pressure or vacuum through the channels. Again specialized equipment and expertise are required for this method.

1.4. Aim of the Thesis

The research of our group is specified on phosphodiester-linked supramolecular polymers in aqueous medium. Not only the self-assembly of different kinds of oligomers was investigated but also their arrangement in DNA,[89–93] their functionalization[94,95] and their properties like acting as a light-harvesting antenna.[96–99]

The aim of this thesis is to change the negatively charged phosphate oligomers to positively charged ones.

To obtain positively charged oligomers we decided to use amine-linked oligomers instead of phosphate and to investigate their self-assembly behavior. Further, the interaction with negatively charged supramolecular polymers was of interest. The goal was to form an electrostatically layered assembly using different supramolecular polymers. In addition, the newly synthesized oligoamines are tested for their light-harvesting properties. On the one hand as positively charged supramolecular polymers and on the other hand in combination with the negatively charged DNA.

2. Electrostatic Assembly of Supramolecular Polymers

Manuscript submitted:

Layered assembly of cationic and anionic supramolecular polymers

J. Jevric, S. M. Langenegger, R. Häner

2.1. Abstract

A 3,6-disubstituted amine-linked phenanthrene trimer (**N-Phe$_3$**) was synthesized which self-assembles into vesicles in an aqueous medium. The cationic oligomer was further used for the electrostatic layer assembly using an anionic supramolecular polymer, the 1,6-disubstituted phosphodiester-linked pyrene trimer (**Py$_3$**). The formed composites were studied in solution and also after the alternate adsorption on mica. Both methods were analyzed by measuring atomic force microscopy (AFM).

2.2. Introduction

The field of supramolecular polymers is rapidly expanding.[2,4,100,101] The properties of supramolecular polymers, such as self-healing, remouldability, and easy recyclability, may lead to future-oriented types of application.[12,102–104] In addition to the commonly used organic solvents, also aqueous conditions can be used for the self-assembly of supramolecular polymers.[1] In particular, the employment of water as a medium opens the possibility of using highly polar and even ionic compounds as building blocks for the assembly of supramolecular systems. Supramolecular polymers assembled in an aqueous medium find applications in biomedical engineering[1,2,18,105–110] sensing,[111] organic electronics,[112] light-harvesting,[90,96,99,113,114] and solar energy conversion.[1,115] For the assembly of supramolecular structures with special spectroscopic and light-harvesting properties, π-conjugated and aromatic molecules are of particular interest.[1,2] We have previously observed light-harvesting properties in various types of supramolecular assemblies of oligophosphates based on phenanthrenes and tetraphenylethylene in aqueous medium.[90,96,98,99] Further, pyrene trimers showed interesting spectroscopic properties due to their self-assembly into nanosheets (Figure 2.1).[116] These polyaromatic oligomers were joined by phosphodiester linkages and, thus, were of anionic nature.[91,96,116–118] Besides these examples of polyphosphoester oligomers,[118,120–122] amine-linked polyaromatic oligomers have not been studied in this context. Under physiological conditions, an amine-based oligomer will be protonated and therefore oppositely charged to the already known oligophosphates. In addition, access to cationic oligomers would bring the further option of forming and studying composites with anionic phosphodiester-linked oligomers. The method of electrostatic layering was first applied in

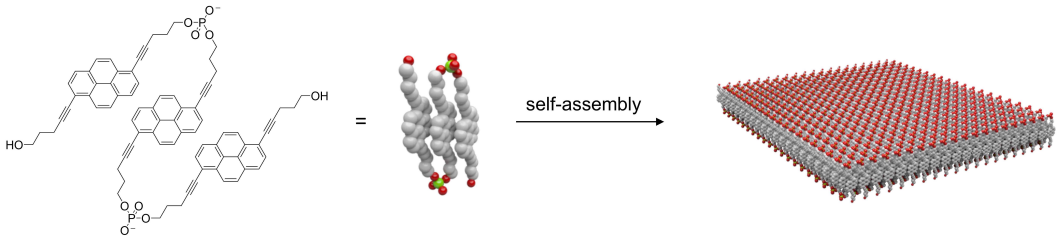

Figure 2.1. Previously investigated 1,6-dialkynyl pyrene with phosphodiester-bridges which self-assembles into nanosheets in aqueous medium. Illustration is taken from reference.[119]

the 60's by Iler[83] and Kirkland,[84] who both made use of microparticles. Around 30 years later, Decher revived the method by the application on a wide range of polyelectrolytes.[76,85] The method has since been used for the preparation of ultrathin-layers and is of high interest for the production of optics and sensors.[65,66,123–127] Herein, the synthesis, the self-assembly, and the spectroscopic properties of a 3,6-dialkynyl-substituted, amine-linked phenanthrene-trimer (**N-Phe$_3$**, Scheme 2.1) are presented. Additionally, the cationic oligomer was used for the formation of nanometer-scaled aggregates in an electrostatic layered assembly[85,123] in combination with an anionic supramolecular polymer.

2.3. Results and Discussion

2.3.1. Synthesis and Analysis of N-Phe$_3$

Synthesis of N-Phe$_3$

First, 4,4'-dibromo-*trans*-stilbene (**1**) was converted into 3,6-dibromophenanthrene (**2**) by an oxidative photochemical cyclization in analogy to literature.[128] A Sonogashira cross-coupling reaction led to a mixture of compounds **3** and **4** which were separated by flash column chromatography. The treatment of compound **3** with hydrazine afforded the amine **5**. Separately, the diol **4** was converted into the bis-aldehyde **6** by a Dess-Martin oxidation. A reductive amination reaction with compounds **5** and **6** finally yielded the oligomer **N-Phe$_3$**, which was purified by preparative TLC (Scheme 2.1).

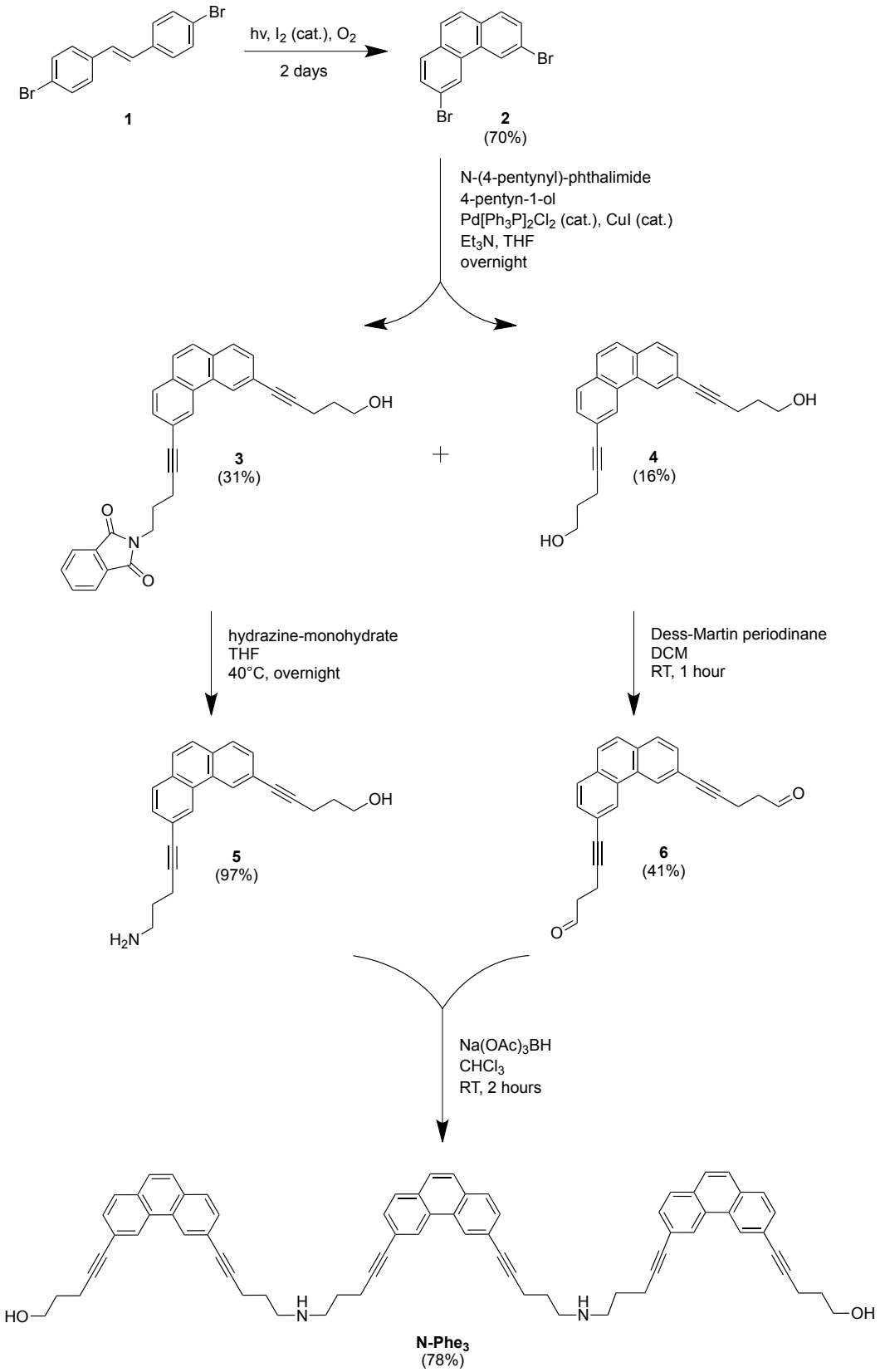

Scheme 2.1 Synthesis of **N-Phe$_3$**.

Self-Assembly Behavior of N-Phe$_3$

The presented amine-linked phenanthrene trimer, **N-Phe$_3$**, was studied in detail.[129] **N-Phe$_3$** self-assembles into vesicles in aqueous medium at pH 4.7. The vesicles are positively charged on the in- and outside, due to hydrophobic effects, which force the protonated amines to be in the aqueous medium and the polycyclic aromatic hydrocarbons to be shielded from water on the inside of a bilayer. Depicted in Figure 2.2 the formation of such a bilayer is graphically illustrated. The thickness of an **N-Phe$_3$** bilayer is approximately 6 nm.

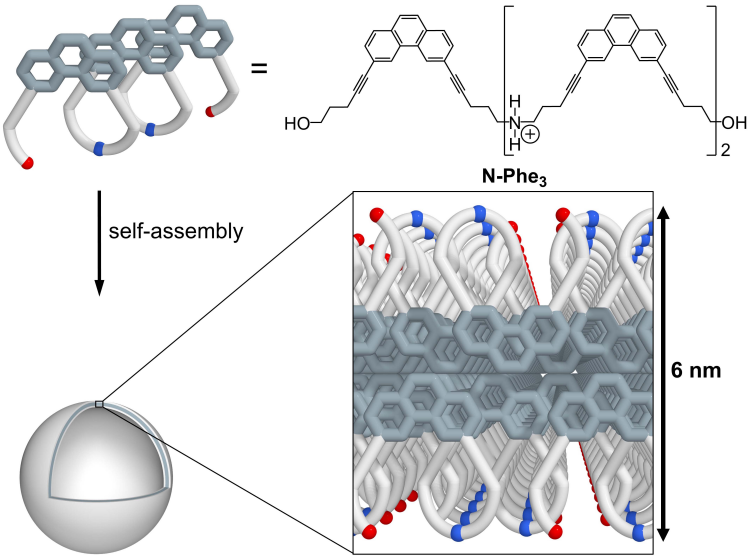

Figure 2.2. Graphical illustration of an **N-Phe$_3$**-vesicle. Blue dots indicate amines, red dots hydroxyl groups. A bilayer of trimers has a calculated height of ~6 nm.

The structures of the objects formed by self-assembly of **N-Phe$_3$** were investigated by AFM on mica. As shown in Figure 2.3, the sample concentration has a strong effect on the course of the self-assembly. At a 1 µM concentration (Figure 2.3A), the formation of a layer with intervening holes was observed. That is why the average height of 5-6 nm suggests that the covered areas correspond to a bilayer of trimers (Figure 2.2). After the increase of the **N-Phe$_3$** concentration to 10 µM, vesicles were observed (Figure 2.3B). This type of concentration dependence in AFM imaging was already noticed in previous work.[91] Apparently, vesicles formed in the solution first, form the mentioned bilayer after the deposition on mica. At higher concentrations (10 µM), vesicles are further adsorbed on this preformed bilayer. The vesicles exhibit a height of 6-30 nm and a width of 50-100 nm (Figure 2.3B).
Further spectroscopic data (UV-vis, fluorescence, TEM) can be found in section 2.5 *Experimental Part*.

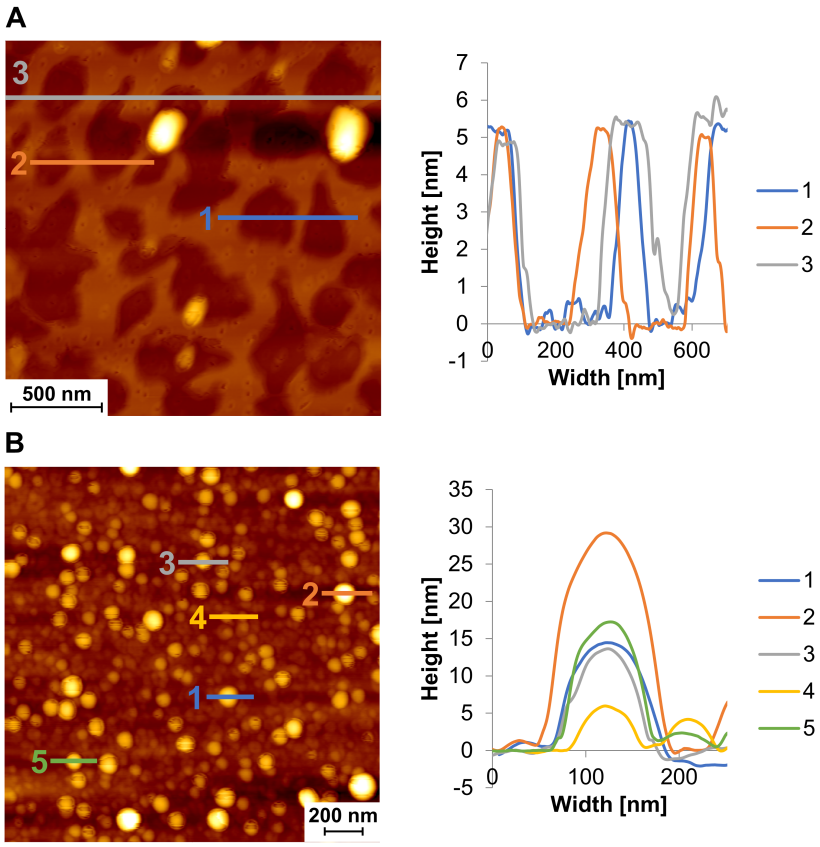

Figure 2.3. Atomic force microscopy (AFM) images of the self-assembled amine-oligomer **N-Phe$_3$** at different concentrations in aqueous medium at 20°C. Conditions: 10 mM sodium acetate buffer (pH 4.71), 10 vol% ethanol, 1 µM (top) and 10 µM (bottom) **N-Phe$_3$**.

2.3.2. Electrostatic Interaction of Oppositely Charged Oligomers in Solution

The question arose whether the **N-Phe$_3$**-vesicles can be covered with another layer by electrostatic interaction. First, the electrostatic interaction with an oppositely charged oligomer in solution was tested. It was checked if it is possible to combine and cover, respectively, **N-Phe$_3$** with a negatively charged supramolecular polymer. Several members in the Häner group showed, that the molecule, 1,6-dipentynyl substituted pyrene with phosphodiester bridges (**Py$_3$**), forms sheets during self-assembly.[116,119,130] This molecule was a possible counteractor, as it assembles to a two-dimensional planar structure in aqueous medium, and therefore could coat the vesicle (Figure 2.4). The difference between the two trimers, **N-Phe$_3$** and **Py$_3$**, is that they both self-assemble in different conditions. Whereas **N-Phe$_3$** aggregates in 10 mM sodium acetate buffer (pH 4.7) with 10% ethanol, **Py$_3$** forms sheets in 10 mM sodium phosphate buffer (pH 7.1), 10 mM sodium chloride and 10% ethanol.

Previous studies regarding finding the optimal conditions for **N-Phe$_3$** showed that the trimer is not meltable in sodium phosphate buffer.[129] The supramolecular assembly was too strongly stabilized in the phosphate buffer at a pH of 7.1 by the doubly negatively charged HPO_4^{2-} ions. The **Py$_3$** was also measured in acetate buffer but no sheets were found during the AFM measurements. From this, we concluded that the combination of the two trimers in solution is not possible in the same

buffer.

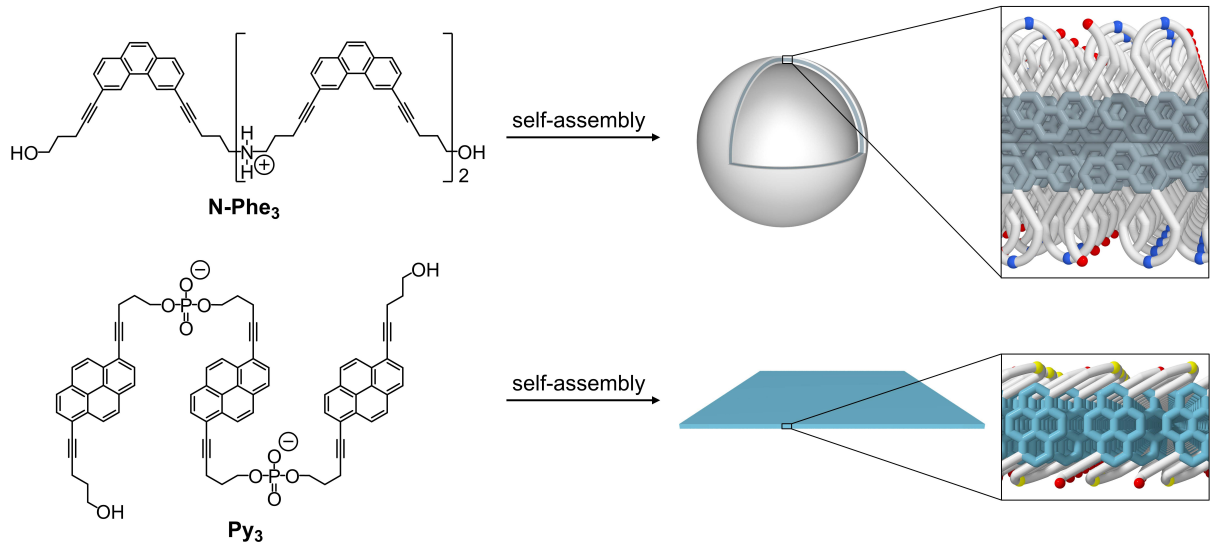

Figure 2.4. The two oligomers and their self-assembled structure are graphically illustrated. The cationic **N-Phe$_3$** self-assembles into vesicles and the anionic **Py$_3$** into sheets.

2.3.3. Electrostatic Layering on a Substrate

Because the layering in solution was not possible, the approach was changed to electrostatic layering on a substrate. The advantage of this change is that both supramolecular polymers are formed in advance in their own conditions and then adsorbed layer by layer where they can interact with each other via electrostatic forces. In our case, we chose mica as the surface, since we already used it for our AFM measurements. The advantage of mica is that unmodified it is perfect for the adsorption of positively charged molecules, and APTES-modified it can be used for the adsorption of negatively charged molecules.

Figure 2.5 depicts the two methods which were used for the electrostatic layering using **N-Phe$_3$**-vesicles and **Py$_3$**-sheets as layers. Basically, there were two options: either start with the negatively charged **Py$_3$**-sheets on APTES-modified mica (Method 1, Figure 2.5B), or start with the positively charged **N-Phe$_3$**-vesicles on unmodified mica (Method 2, Figure 2.5C).

Method 1

Method 1 is graphically illustrated in Figure 2.5B. One starts with an APTES-modified mica on which the **Py$_3$**-sheets (blue) are adsorbed. Next, the **N-Phe$_3$**-vesicles (grey) are adsorbed on top of the sheets as a second layer. Last, the **Py$_3$**-sheets are adsorbed on top of the previous two layers. Figure 2.6 shows the layering process as described in Figure 2.5B. The first layer consists of **Py$_3$**-sheets adsorbed on APTES-modified mica[131] with a height of 2 nm (Figure 2.6A). In a next step, **N-Phe$_3$**-vesicles were added as a second layer, which resulted in a total height of 8 nm for the two layers (Figure 2.6B). Thus, the height of 8 nm consists of the **Py$_3$**-sheets (2 nm) and the **N-Phe$_3$**-vesicles, which are adsorbed as bilayer discs (6 nm). As a third layer, **Py$_3$**-sheets were

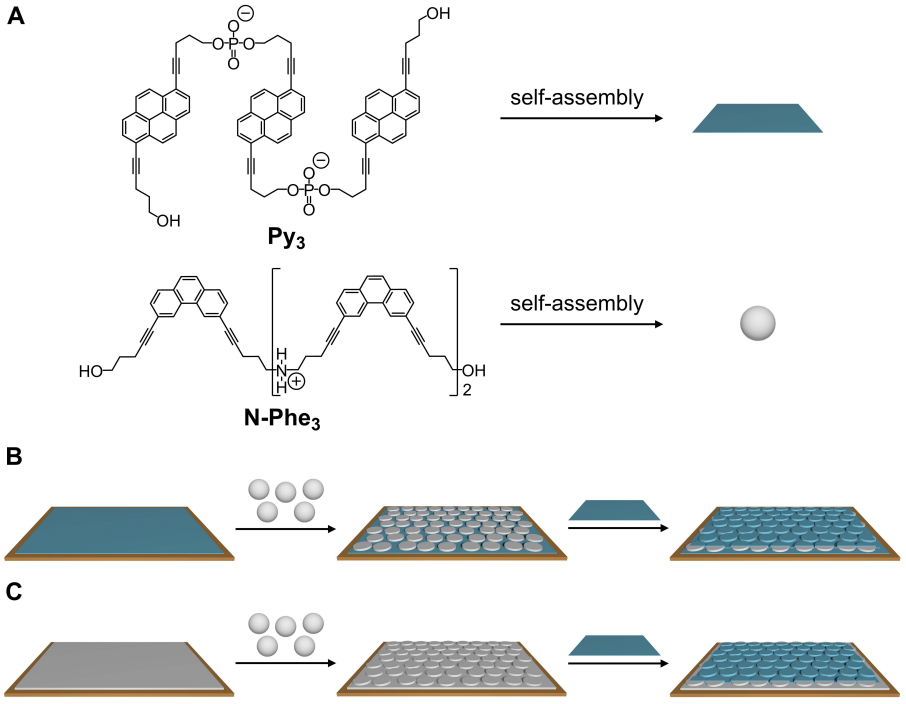

Figure 2.5. Graphical illustration of the electrostatic layered assembly preparation. A) **Py$_3$** self-assembles into negatively charged sheets (blue) and **N-Phe$_3$** into positively charged vesicles (grey). B) First, the **Py$_3$**-sheet (blue) is adsorbed on the substrate (APTES-modified mica, brown), followed by the adsorption of **N-Phe$_3$**-vesicles (grey), ending with the adsorption of **Py$_3$**-sheets on top (Method 1). C) First, the **N-Phe$_3$**-vesicles are adsorbed as a layer on top of nonmodified mica followed by the adsorption of more **N-Phe$_3$**-vesicles on top. Next, **Py$_3$**-sheets are adsorbed on top of the **N-Phe$_3$**-layer (Method 2).

adsorbed again (Figure 2.6C). At this point, two options were possible since the mica was still APTES-modified and therefore, negatively charged **Py$_3$** can easily adsorb on it. Either the third layer of **Py$_3$**-sheets will adsorb on the unoccupied APTES-modified mica or it will ideally adsorb on top of a two-layer construct of **Py$_3$**-sheets with **N-Phe$_3$**-bilayer discs on top (Figure 2.6B). The AFM image in Figure 2.6C shows both possibilities. The height profile indicates that the left aggregate in the AFM image has a height of 8 nm and thus, is a two-layer construct. The right aggregate in the AFM image has a height of 2 nm, which corresponds to a single layer of **Py$_3$**. The height profile also shows the intersection of these two aggregates, which reaches a height of 10 nm, and consists of an overlap of a two-layer assembly (8 nm) and single-layer assembly (2 nm). A complete overlap of the three layers was difficult to observe. This is probably due to the rough surface of the two-layer assembly caused by the adsorption of vesicles as discs (Figure 2.6B). Further measurements are shown in section 2.5.4 *Electrostatic Layering*.

Method 2

Figure 2.5C depicts Method 2 in a graphical illustration. At higher concentrations, **N-Phe$_3$**-vesicles are first adsorbed as a bilayer (grey) on unmodified mica, whereas further vesicles are adsorbed as bilayer discs. In a next step, **Py$_3$**-sheets (blue) are adsorbed.
Figure 2.7 illustrates the electrostatic layering in the order shown in Figure 2.5C. As previously

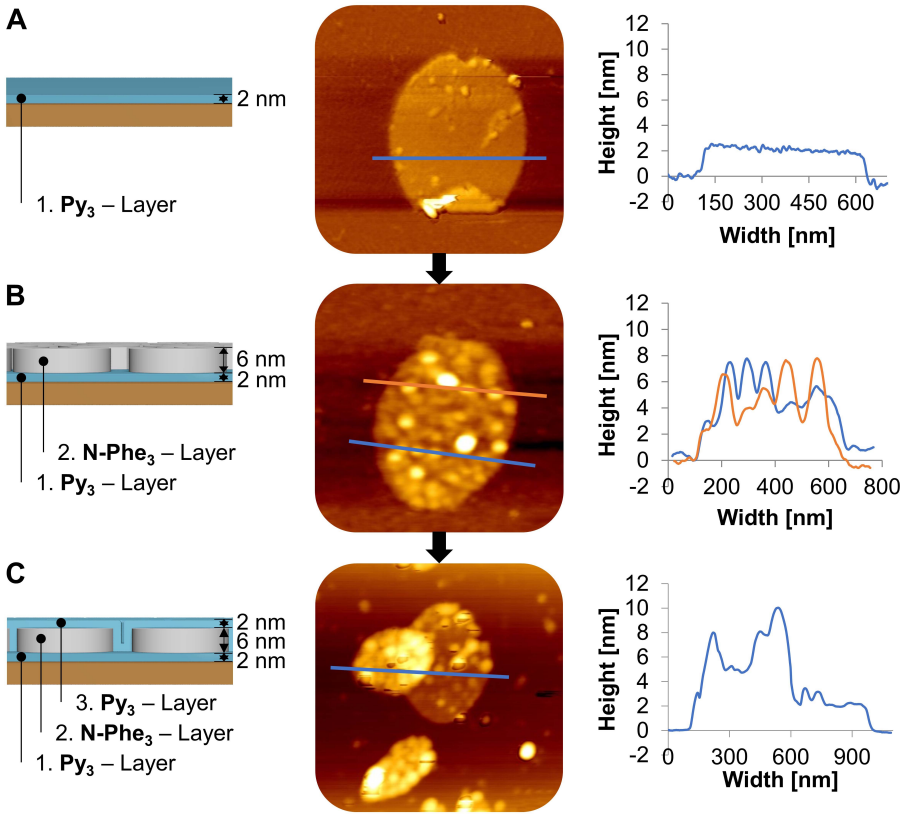

Figure 2.6. Electrostatic assembly starting with **Py_3**-sheets (Method 1). Left: graphical illustration of the layering; middle and right: AFM images and corresponding height profiles. Conditions: 1st and 3rd layer 2 µM **Py_3**, 10 mM sodium phosphate buffer (pH 7.1), 10 mM sodium chloride and 10 vol% ethanol, 2nd layer 10 µM **N-Phe_3**, 10 mM sodium acetate buffer (pH 4.7) and 10 vol% ethanol.

explained in section 2.3.1 *Self-Assembly Behavior of N-Phe_3*, the **N-Phe_3**-vesicles are adsorbed as bilayer discs with a height of 6 nm on top of a surface. At a certain concentration, the surface is fully covered with the discs (Figure 2.3A), and the further adsorption of vesicles as discs happens on top of the already formed **N-Phe_3**-bilayer (Figure 2.7A). Therefore, only the height difference between the upper **N-Phe_3**-discs and the first bilayer layer can be measured. Figure 2.7A shows that the height of the adsorbed discs is as expected around 6 nm. The adsorption of a second layer of **Py_3**-sheets is shown in Figure 2.7B. The rough, positively charged surface of the **N-Phe_3**-discs means that the negatively charged **Py_3**-sheets cannot be adsorbed as a whole, and are torn apart. Nevertheless, the height profiles show, that the height of the area where we have an electrostatic interaction of these two supramolecular assemblies, increases for 2 nm to an approximate total height of 8 nm. This is in agreement with the model (Figure 2.7B, left), where we show that the **N-Phe_3**-discs have a height of 6 nm and the **Py_3**-sheets 2 nm.

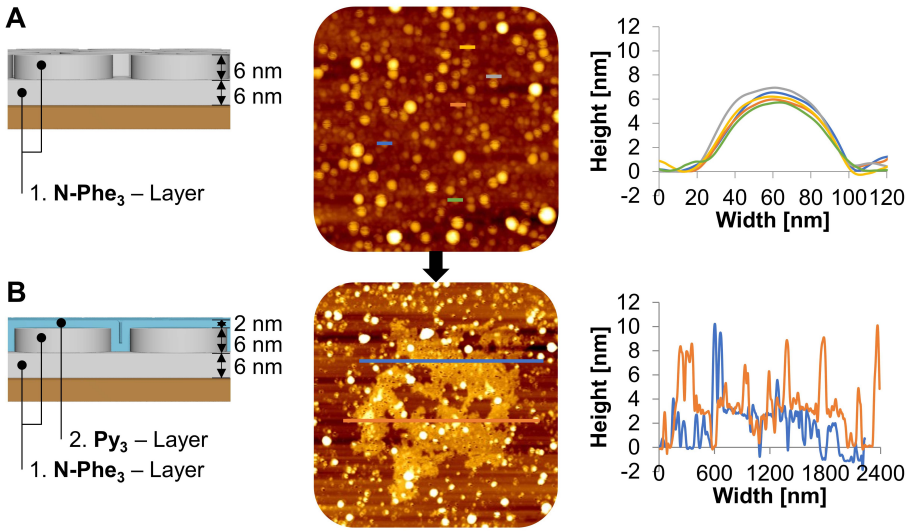

Figure 2.7. Electrostatic assembly starting with $\mathbf{Py_3}$ sheets. Left: graphical illustration of the layering; middle and right: AFM images and corresponding height profiles. Conditions: 1st and 2nd layer 10 µM $\mathbf{N\text{-}Phe_3}$, 10 mM sodium acetate buffer (pH 4.7) and 10 vol% ethanol, 3rd layer 2 µM $\mathbf{Py_3}$, 10 mM sodium phosphate buffer (pH 7.1), 10 mM sodium chloride and 10 vol% ethanol.

Comparison of Method 1 and 2

Both, Method 1 and 2 (Figure 2.5) worked for the electrostatic layering. The limiting factor for the number of layers was the rough surface, which resulted from the adsorption of the vesicles. This meant that the next layer, if not the one after that, had problems with adsorption. Because the surface was rough and corrugated, the electrostatic interaction between the two oligomers $\mathbf{N\text{-}Phe_3}$ and $\mathbf{Py_3}$ could not be guaranteed throughout.

A difference was that the adsorption of $\mathbf{N\text{-}Phe_3}$-vesicles on mica led first to the formation of a bilayer, followed by the further adsorption of vesicles as discs. This was in contrast to the adsorption on $\mathbf{Py_3}$-sheets, where only the adsorption of the $\mathbf{N\text{-}Phe_3}$ discs occurred and no bilayer was formed. This can be explained by the fact that the surfaces of mica and the $\mathbf{Py_3}$-sheet have different charge densities.

2.4. Conclusions and Outlook

In conclusion, it was shown that the cationic $\mathbf{N\text{-}Phe_3}$-vesicles give rise to novel types of electrostatically controlled layered assemblies in combination with anionic supramolecular two-dimensional polymers, which was confirmed by AFM.

Since the two trimers formed the supramolecular polymers ($\mathbf{N\text{-}Phe_3}$-vesicles and $\mathbf{Py_3}$-sheets) under different conditions, the electrostatic interaction in solution could not be studied. It was shown that $\mathbf{N\text{-}Phe_3}$ is not soluble in the $\mathbf{Py_3}$-conditions (phosphate buffer) and $\mathbf{Py_3}$ does not form sheets in acetate buffer.

This is why the approach was changed to the electrostatic layering on the substrate mica. With this proceeding, the problem of finding new, fitting buffer conditions could be circumvented. By

preassembling both trimers in their own conditions to get **N-Phe$_3$**-vesicles and **Py$_3$**-sheets, they could have been alternately layered. The limiting factor was the number of layers due to the rough surface. Starting with **Py$_3$**, three layers were possible to stack on top of each other, whereas only two layers were possible when starting with **N-Phe$_3$**.

These findings increased our interest in the further investigation of amine-linked oligomers and their potential application in electrostatic layering. The next step is to synthesize different oligoamines with the goal that they will self-assemble into sheets and thus, the number of layers of such an electrostatic assembly could be increased. Also, the self-assembly of supramolecular polymers on warm mica is worth a try. By doing so, we hope to coat larger areas with our supramolecular polymers.

2.5. Experimental Part

2.5.1. Synthesis of N-Phe$_3$

3, 6-Dibromophenanthrene (2)

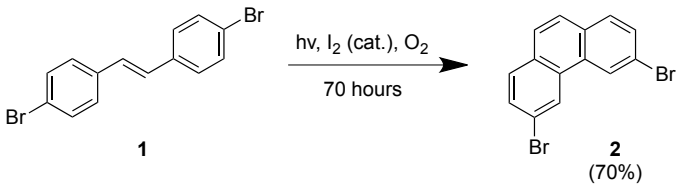

Scheme 2.2 Oxidative photocyclization reaction of compound **1** to obtain compound **2**.

The procedure was done in analogy to reference.[128] The commercially available 4,4'-dibromo-trans-stilbene (**1**) (2.5036 g, 7.41 mmol) and Iodine (0.3638 g, 1.43 mmol) were dissolved in toluene (4 l). The solution was irradiated with a mercury medium pressure UV lamp for 70 hours while air was bubbled through. The reaction was monitored by ^{1}H-NMR. Water (1 l) and an excess of $Na_2S_2O_3$ were added to remove the iodine (color change from pink to beige). The organic phase was evaporated under reduced pressure. The obtained yellow solid was dissolved in boiling DCM (99 ml), methanol (60 ml) was added, and the solution was kept for 2 days in the fridge. The white crystals were filtrated off and washed with cold DCM (7 ml). The filtrate was evaporated and recrystallized again. The combined fractions of compound **2** were obtained in 70% yield (1.7460 g). ^{1}H NMR (300 MHz, $CDCl_3$) δ 8.69 (d, J = 1.6 Hz, 2H), 7.79 – 7.65 (m, 6H).

2-(5-(6-(5-hydroxypent-1-yn-1-yl)phenanthren-3-yl)pent-4-yn-1-yl)isoindoline-1,3-dione (3) and 5,5'-(phenanthrene-3,6-diyl)bis(pent-4-yn-1-ol) (4)

To a degassed solution of 3,6-dibromophenanthrene **2** (1.0016 g, 2.98 mmol) in dry THF (33 ml) and Et_3N (16.5 ml) under an argon atmosphere, $Pd[Ph_3P]_2Cl_2$ (116.7 mg, 0.166 mmol), CuI (51.9 mg, 0.273 mmol), 4-pentynyl-phthalimide (635.9 mg, 2.98 mmol) and 4-pentyn-1-ol (275.5 µl, 2.98 mmol) was added. The black solution was refluxed overnight. The mixture was filtrated, the filtrate was washed with citric acid (10%) and saturated $NaHCO_3$ solution. The solution was dried over Na_2SO_4 and concentrated in vacuo. The crude products **3** and **4** were separated by flash column chromatography on silica gel (hexane/EtOAc 3:1). Compound **3** was isolated as an orange-yellowish solid (437.1 mg, 31%). Compound **4** was isolated as an orange solid (164.7 mg, 16%). **3**: R_f = 0.24 (hexane/EtOAc 1:1). ^{1}H NMR (300 MHz, $CDCl_3$) δ 8.64 (s, 1H), 8.51 (s, 1H), 7.84 – 7.68 (m, 4H), 7.65 (s, 2H), 7.62 –7.41 (m, 4H), 3.98 – 3.86 (m, 4H), 2.71 – 2.54 (m, 4H), 2.10 (p, J = 6.9 Hz, 2H), 1.96 (p, J = 6.6 Hz, 2H). ^{13}C NMR (75 MHz, $CDCl_3$) δ 168.68, 133.96, 132.29, 131.42, 129.71, 128.43, 127.06, 126.42, 123.30, 122.12, 90.34, 81.91, 61.99, 37.69, 31.56, 27.40, 17.68, 16.30. HRMS-NSI (m/z): $[M+H]^+$ calcd for $C_{32}H_{26}NO_3$: 472.1913, found: 472.1907. **4**: R_f = 0.06 (hexane/EtOAc 1:1). ^{1}H NMR (300 MHz, $CDCl_3$) δ 8.69 (s, 2H), 7.77 (d, J = 8.2 Hz, 2H), 7.67 (s, 2H), 7.63 – 7.53 (m, 2H), 3.90 (t, J = 6.2 Hz, 4H), 2.64 (t, J = 6.9 Hz, 4H), 1.94 (p, J =

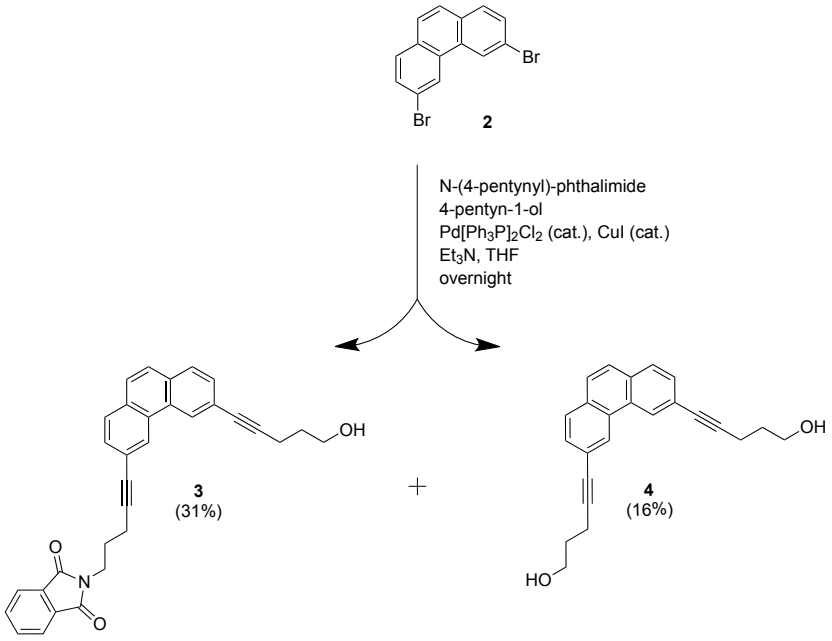

Scheme 2.3 Sonogashira reaction of compound **2** to obtain compounds **3** and **4**.

6.6 Hz, 4H). ^{13}C NMR (75 MHz, $CDCl_3$) δ 131.54, 129.78, 129.61, 128.62, 127.15, 126.28, 122.16, 90.33, 81.83, 62.04, 31.57, 16.30. HRMS-NSI (m/z): $[M+H]^+$ calcd for $C_{24}H_{23}O_2$: 343.1699, found: 343.1693.

5-(6-(5-aminopent-1-yn-1-yl)phenanthren-3-yl)pent-4-yn-1-ol (5)

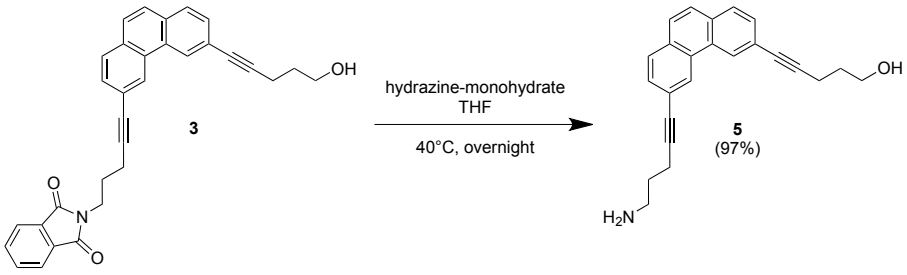

Scheme 2.4 Deprotection of the amine in the phthalimide of compound **3** to obtain compound **5**.

A solution of compound **3** (212.8 mg, 0.451 mmol) and hydrazine-monohydrate (0.18 ml, 3.610 mmol) in THF (9 ml) was stirred at 40 °C, under argon atmosphere overnight. The grey precipitation was filtrated off and the filtrate was diluted with DCM (100 ml). The filtrate was washed two times with 2 M K_2CO_3 (2x 100 ml). The organic phase was dried over K_2CO_3 and concentrated in vacuo. Compound **5** was gained as a yellow sticky solid (149.7 mg, 97%). ^{1}H NMR (300 MHz, $CDCl_3$) δ 8.69 (s, 2H), 7.77 (d, J = 8.2 Hz, 2H), 7.66 (s, 2H), 7.62 – 7.54 (m, 2H), 3.89 (t, J = 6.2 Hz, 2H), 2.94 (t, J = 6.9 Hz, 2H), 2.60 (dt, J = 18.5, 6.9 Hz, 4H), 1.94 (p, J = 6.7 Hz, 2H), 1.82 (p, J = 6.9 Hz, 2H). ^{13}C NMR (75 MHz, $CDCl_3$) δ 131.35, 129.59, 129.46, 128.46, 126.96, 126.18, 122.02, 90.42, 81.68, 61.73, 41.38, 32.48, 31.45, 17.06, 16.16. HRMS-NSI (m/z): $[M+H]^+$ calcd for

$C_{24}H_{24}NO$: 342.1859, found: 342.1852.

5,5'-(phenanthrene-3,6-diyl)bis(pent-4-ynal) (6)

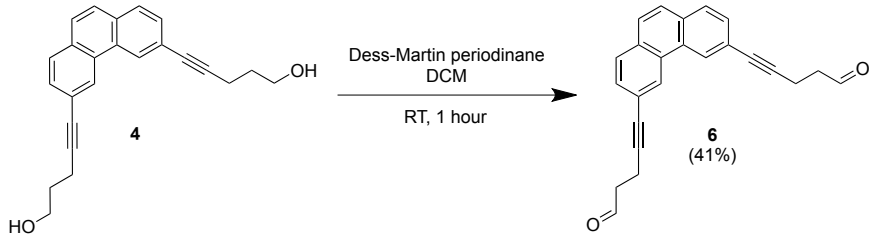

Scheme 2.5 Dess-Martin oxidation of compound **4** to obtain compound **6**.

The procedure was carried out analog to reference.[132] Dess-Martin Periodinane (DMP) (817.2 mg, 1.926 mmol) was dissolved in DCM (9 ml) and placed under argon. Compound **4** (299.8 mg, 0.876 mmol) was dissolved in DCM (9 ml) and was added to the DMP solution. The reaction mixture was stirred at RT for 1 hour. The reaction mixture was diluted with DCM (50 ml) and washed with sat. aq. $NaHCO_3$ solution containing 12.5 g $Na_2S_2O_3$ (50 ml), sat. aq. $NaHCO_3$ solution (50 ml) and water (50 ml). The organic phase was dried over $MgSO_4$ and concentrated in vacuo. The crude product was purified by flash column chromatography on silica gel (hexane/EtOAc 3:1). The product was gained as a white yellowish fluffy solid (120.8 mg, 41%). $R_f = 0.3$ (hexane/EtOAc 2:1). ^{1}H-NMR (300 MHz, $CDCl_3$): δ 9.92 (s, 2H), 8.69 (s, 2H), 7.78 (d, J = 8.2 Hz, 2H), 7.68 (s, 2H), 7.62 – 7.52 (m, 2H), 2.88 – 2.80 (m, 8H). ^{13}C-NMR (75 MHz, $CDCl_3$): δ 200.99, 132.09, 130.20, 130.01, 129.08, 127.68, 126.78, 122.24, 89.16, 82.53, 43.24, 13.41. HRMS-NSI (m/z): $[M+H]^+$ calcd for $C_{24}H_{18}O_2Na$: 361.12, found: 361.1199.

5,5'-((((phenanthrene-3,6-diylbis(pent-4-yne-5,1-diyl))bis(azanediyl))bis(pent-1-yne-5,1-diyl))bis(phenanthrene-6,3-diyl))bis(pent-4-yn-1-ol) (N-Phe$_3$)

The procedure was carried out analog to reference.[133] A solution of **5** (20.2 mg, 0.0591 mmol) and $Na(OAc)_3BH$ (25.5 mg, 0.12 mmol) in $CHCl_3$ (6 ml) was placed under argon and a solution of compound **6** (10.0 mg, 0.0296 mmol) in $CHCl_3$ (3 ml) was added dropwise. The reaction was stirred for two hours. The reaction mixture was diluted with $CHCl_3$ (15 ml), and washed twice with 2 M K_2CO_3 solution. The $CHCl_3$-phase was dried over K_2CO_3 and concentrated under reduced pressure. The crude product was purified by preparative TLC (DCM/MeOH 95:5 + 1% Et_3N) and yielded **N-Phe$_3$** as a white-yellowish solid (22.8 mg, 78%). $R_f = 0.22$ (DCM/MeOH 95:5+1% Et_3N). HRMS-NSI (m/z): $[M+H]^+$ calcd for $C_{72}H_{65}N_2O_2$: 989.50, found: 989.5041.

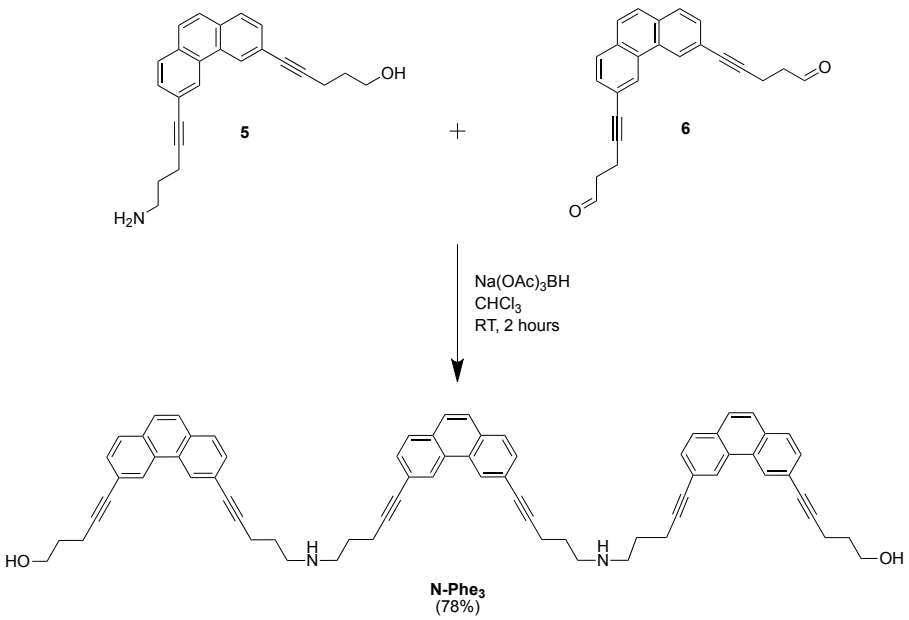

Scheme 2.6 Reductive amination of compounds **5** (2 eq.) and **6** (1 eq.) to obtain compound **N-Phe$_3$**.

2.5.2. Synthesis of Py$_3$

5,5'-(Pyrene-1,6-diyl)bis(pent-4-yn-1-ol) (8)

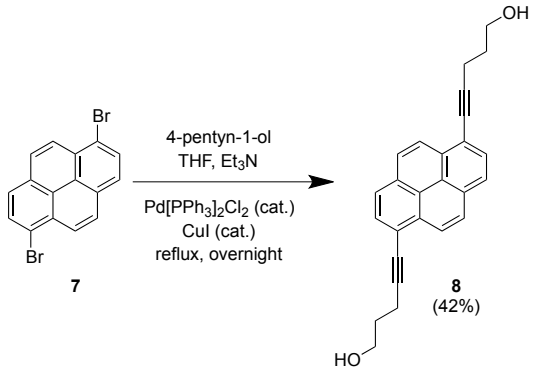

Scheme 2.7 Alkynation of 1,6-dibromopyrene **7** by a Sonogashira reaction to obtain compound **8**.

Compound **8** was synthesized according to literature.[116] 1,6-Dibromopyrene (**7**) (1.0201 g, 2.833 mmol) was dissolved in anhydrous THF (23 ml) and degassed Et_3N (14 ml) under an argon atmosphere and heated to 84°C. 4-Pentyn-1-ol (1 ml, 10.8 mmol) was added, followed by the catalysts $Pd[PPh_3]_2Cl_2$ (52 mg, 0.074 mmol) and CuI (10 mg, 0.053 mmol). The reaction mixture was refluxed at 84°C overnight. TLC (DCM/MeOH 92:8) showed the disappearance of starting material **7**. The reaction mixture was cooled to RT, before it was diluted with DCM (100 ml), and filtrated through Celite 503. The filtrate was washed once with 10% citric acid (100 ml) and once with aq. sat. $NaHCO_3$ (100 ml), dried over Na_2SO_4, filtrated, and concentrated under reduced pressure. The residue was purified by a flash column chromatography on silica gel (DCM/toluene/MeOH 88:10:2). Compound **8** could be isolated as a pure yellow compound (437.4 mg, 42%). $R_f = 0.23$ (DCM/MeOH

97:3). ^{1}H-NMR (300 MHz, $CDCl_3$): δ 8.52 (d, J = 9.1 Hz, 2H), 8.13 – 8.02 (m, 6H), 3.96 (t, J = 6.2 Hz, 4H), 2.79 (t, J = 7.0 Hz, 4H), 2.04 (p, J = 6.6 Hz, 4H).

5-(6-(5-Hydroxypent-1-yn-1-yl)pyren-1-yl)pent-4-yn-1-yl acetate (9)

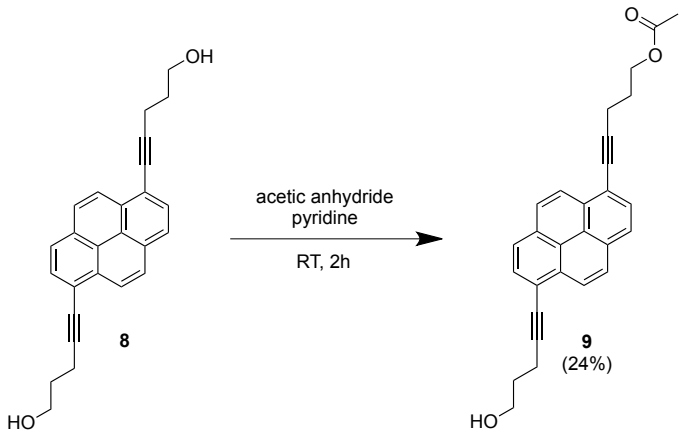

Scheme 2.8 Monoacetylation of compound **8** to obtain compound **9**.

Compound **8** (152.6 mg, 0.416 mmol) was dissolved in pyridine (4.2 ml) under argon. A 2M solution of acetic anhydride (0.2 ml, 0.416 mmol) in pyridine was added dropwise over ten minutes to the dissolved compound **8**. The reaction mixture was stirred at RT for 2 hours. The reaction mixture was diluted with DCM (10ml) and washed with aq. 0.5 M HCl (10 ml), aq. sat. $NaHCO_3$ (10 ml) and with brine (10 ml). The organic phase was dried over $MgSO_4$, filtrated, and the solvent removed under reduced pressure. The residue was purified by a flash column chromatography on silica gel (hexane/EtOAc 3:2). Compound **9** was isolated as a yellow solid (41.1 mg, 24%). R_f = 0.55 (hexane/EtOAc 1:1). ^{1}H-NMR (300 MHz, $CDCl_3$): δ 8.53 (d, J = 11.1 Hz, 2H), 8.15 - 8.03 (m, 6H), 4.36 (t, J = 6.3 Hz, 2H), 3.96 (t, J = 6.2 Hz, 2H), 2.85 - 2.71 (m, 4H), 2.16 - 1.98 (m, 7H). ^{13}C NMR (75 MHz, $CDCl_3$) δ 132.11, 130.86, 130.82, 130.04, 128.05, 128.02, 126.11, 126.07, 124.99, 124.97, 124.31, 119.07, 118.94, 95.65, 94.86, 63.49, 62.05, 31.79, 28.20, 21.15, 16.90, 16.65. HRMS-NSI (m/z): $[M+Na]^+$ calcd for $C_{28}H_{24}O_3Na$: 431.1593, found: 431.1618.

Bis(2-cyanoethyl) (pyrene-1,6-diylbis(pent-4-yne-5,1-diyl)) bis(diisopropylphosphoramidite) (10)

Compound **8** (100.3 mg, 0.274 mmol) was dissolved in anhydrous THF (6 ml) and DIPEA (0.5 ml, 2.93 mmol). 2-Cyanoethyl N,N-diisopropylchlorophosphoramidite (PAM-Cl, 210 mg, 0.887 mmol) was added dropwise at RT and the reaction mixture stirred for 3 hours under argon. TLC (hexane/EtOAc 7:3 + 1% Et_3N) showed the disappearance of starting material. The reaction mixture was concentrated under reduced pressure. The resultant yellow-greenish foam was purified by a short flash column chromatography on silica gel (hexane/EtOAc 8:2 + 1% Et_3N). Product **10** was isolated as a yellow-greenish oil (112.0 mg, 53%). R_f = 0.81 (hexane/EtOAc 6:4 + 1% Et_3N). ^{1}H-NMR (300 MHz, $CDCl_3$): δ 8.55 (d, J = 9.1 Hz, 2H), 8.15 – 7.95 (m, 6H), 4.04 – 3.76 (m, 8H), 3.74 – 3.56 (m, 4H), 2.78 (t, J = 7.0 Hz, 4H), 2.65 (t, J = 6.5 Hz, 4H), 2.14 – 2.01 (m, 4H), 1.26 –

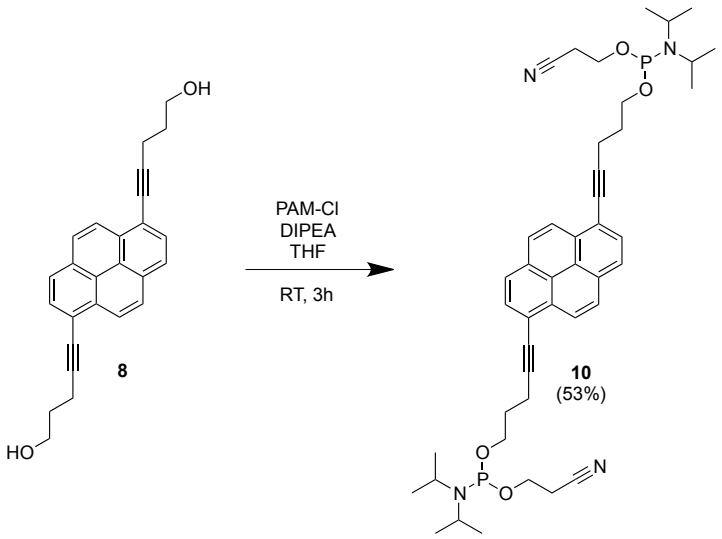

Scheme 2.9 Diphosphitylation of compound **8** to obtain compound **10**.

1.18 (m, 24H). ^{13}C NMR (75 MHz, $CDCl_3$) δ 132.08, 130.76, 130.00, 127.94, 126.14, 124.92, 124.30, 119.17, 117.75, 95.67, 80.05, 62.57, 62.34, 58.62, 58.36, 43.57, 43.27, 43.11, 30.67, 30.57, 24.81, 24.72, 20.55, 20.46, 16.74. ^{31}P-NMR (121 MHz, $CDCl_3$): δ 147.84. HRMS-NSI (m/z): $[M+H]^+$ calcd for $C_{44}H_{57}O_4N_4P_2$: 767.3816, found: 767.3850.

Protected 1,6-dipentynyl substituted pyrene-trimer (11)

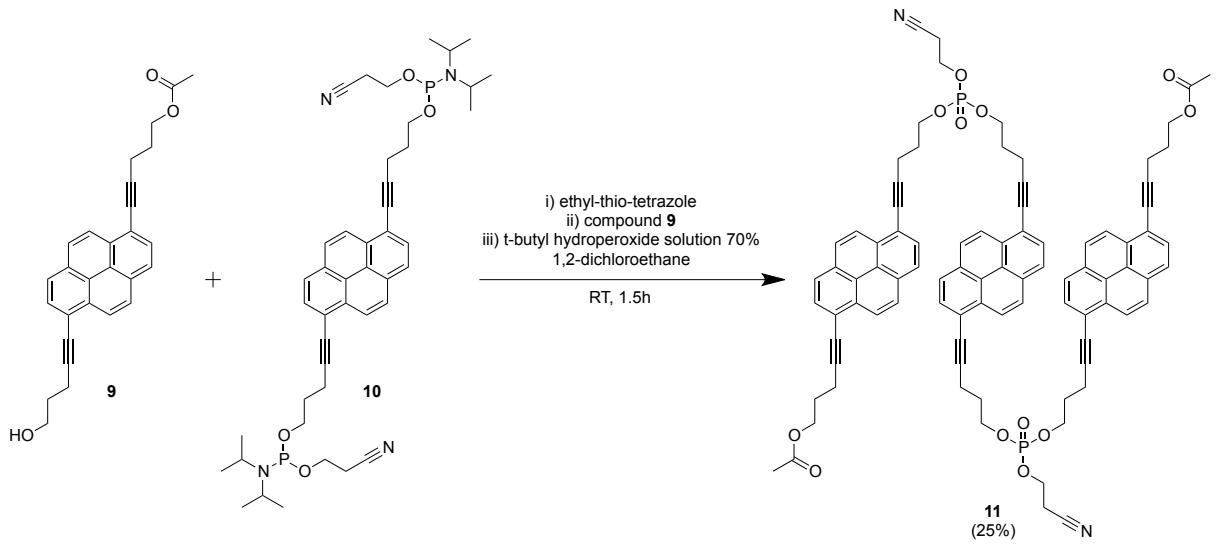

Scheme 2.10 Coupling of compounds **9** and **10** to obtain compound **11**.

A solution of 5-(ethylthio)-1H-tetrazole (9.9 mg, 0.076 mmol) in DCE (0.25 ml) was added under argon atmosphere to a solution of compound **10** (15 mg, 0.02 mmol) in DCE (0.14 ml). Compound **9** (25.1 mg, 0.061 mmol) was dissolved in DCE (0.48 ml) and added to the activated compound **10**. The reaction was stirred at room temperature for one hour. Tert-butyl hydroperoxide solution

(70%, 16.2 µl, 0.117 mmol) was added and the reaction mixture further stirred for 10 minutes. The reaction mixture was diluted with chloroform (15 ml) and washed with aq. sat. $NaHCO_3$ (15 ml) and brine (15 ml). The organic layer was dried over $MgSO_4$, filtrated, and concentrated under reduced pressure. The residue was purified by a preparative TLC (DCM/toluene/MeOH 86:10:4). Compound **11** was isolated as a brown solid (6.9 mg, 25%). R_f = 0.43 (DCM/toluene/MeOH 86:10:4). ^{1}H-NMR (300 MHz, $CDCl_3$): δ 8.54 – 8.30 (m, 6H), 8.14 – 7.86 (m, 18H), 4.51 – 4.25 (m, 16H), 2.91 – 2.66 (m, 16H), 2.22 – 2.04 (m, 18H). ^{31}P-NMR (121 MHz, $CDCl_3$): δ -1.37. HRMS-NSI (m/z): $[M]^+$ calcd for $C_{88}H_{74}O_{12}N_2P_2$: 1412.4712, found: 1412.4648.

1,6-dipentynyl substituted pyrene trimer (Py_3)

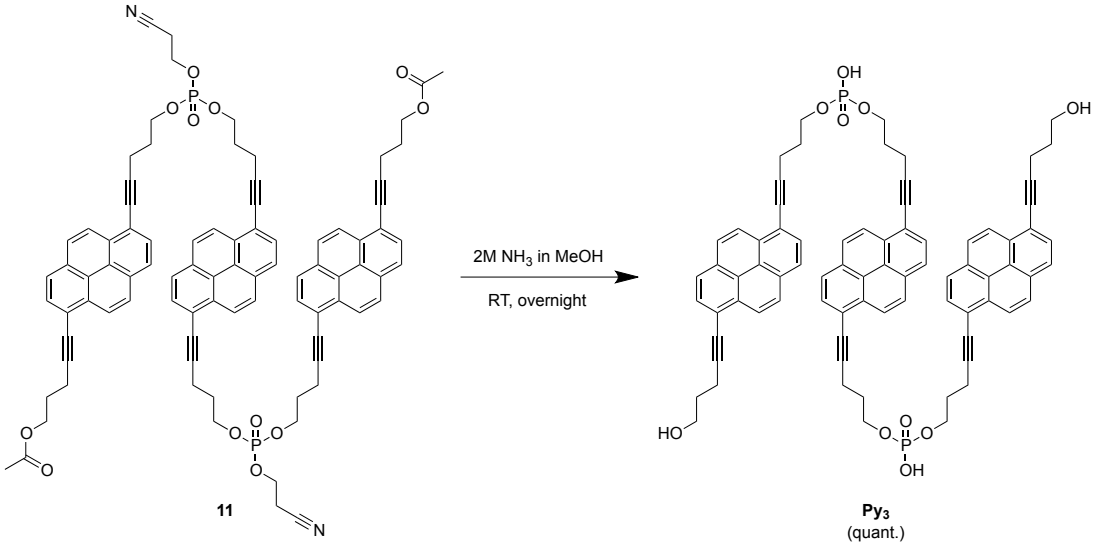

Scheme 2.11 Deprotection of compound **11** to obtain compound **Py_3**.

Compound **11** (6.9 mg, 0.0049 mmol) was dissolved in a solution of 2 mol/l NH_3 in methanol (5 ml) and stirred at RT overnight. The sample was lyophilized, the residue was suspended in MeOH (1 ml) and lyophilized again and yielded the product **Py_3** (6.0 mg, quant.). HRMS-NSI (m/z): $[M\text{-}H]^-$ calcd for $C_{78}H_{64}O_{10}P_2$: 1221.40, found: 1221.39.

2.5.3. Conditions for Supramolecular Polymer Formation

The supramolecular polymer formation of **N-Phe$_3$** was performed via thermal disassembly and reassembly: the samples were prepared in 10 mM sodium acetate buffer (pH 4.7) and 10 vol% ethanol, heated to 70°C and cooled to 20°C with a rate of 0.33°C/min in an Eppendorf Thermomixer Compact.

The formation of **Py_3**-nanosheets was achieved in 10 mM sodium phosphate buffer (pH 7.1), 10 mM sodium chloride and 10 vol% ethanol with a controlled cooling rate of 0.5°C/min from 70°C to 20°C in a Cary 100 spectrophotometer equipped with a Peltier thermostat.

2.5.4. Additional Measurements

UV-vis and Fluorescence Spectra of N-Phe$_3$

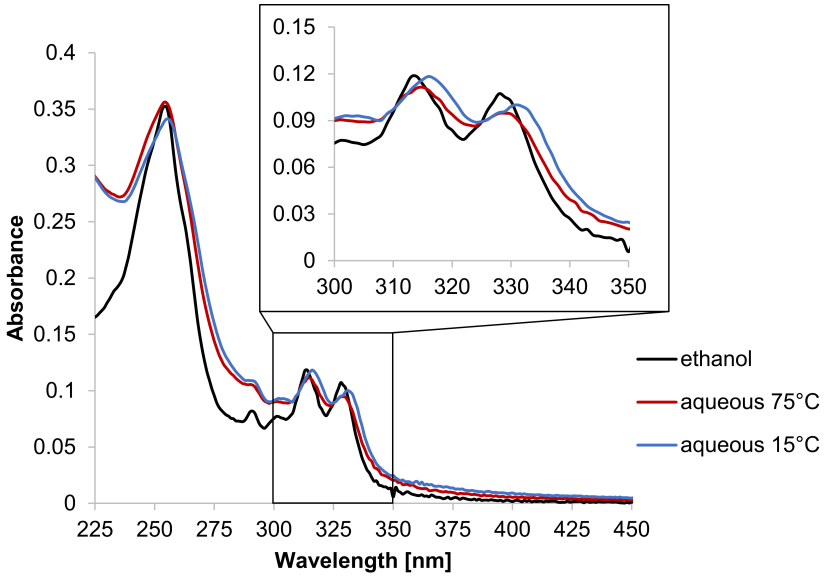

Figure 2.8. UV-vis spectra of **N-Phe$_3$** (1 µM) in ethanol (black) and in an aqueous medium (10 mM sodium acetate buffer pH 4.7, containing 10 vol% ethanol) at 75 °C (red) and 15 °C (blue).

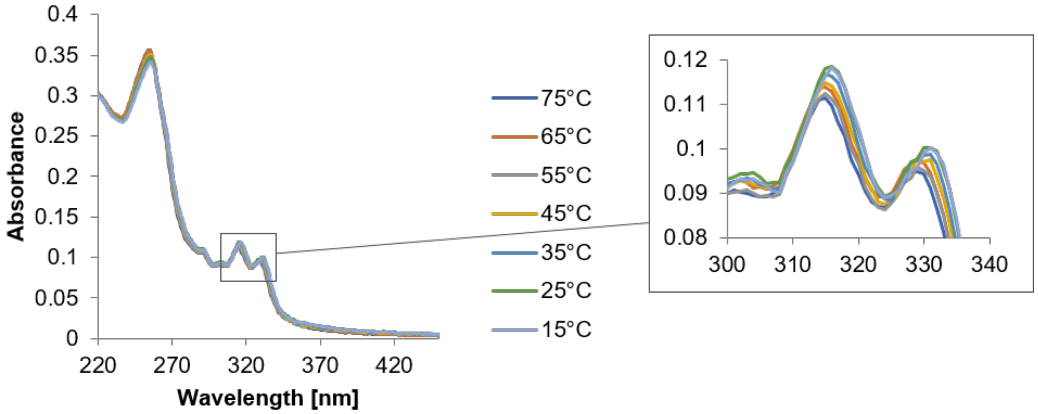

Figure 2.9. Absorption spectra of **N-Phe$_3$** in aqueous medium when cooling down from 75°C to 15°C in 10°C steps. A red-shift of 2 nm is observed between 45°C and 35°C. Conditions: 1 µM **N-Phe$_3$**, 10 mM sodium acetate buffer, 10 vol% ethanol.

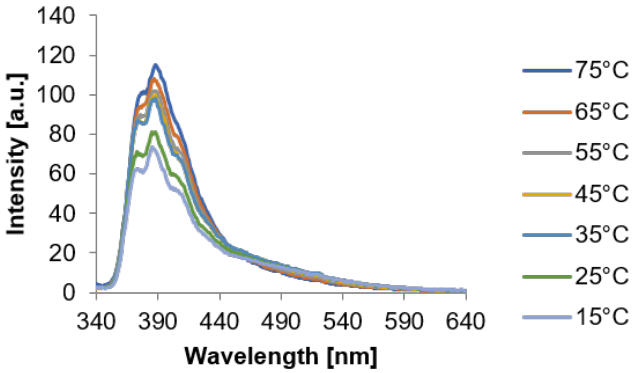

Figure 2.10. Fluorescence spectra of **N-Phe$_3$** in aqueous medium measured every 10°C. Conditions: 1 µM **N-Phe$_3$**, 10 mM sodium acetate buffer, 10 vol% ethanol, λ_{ex} = 330 nm.

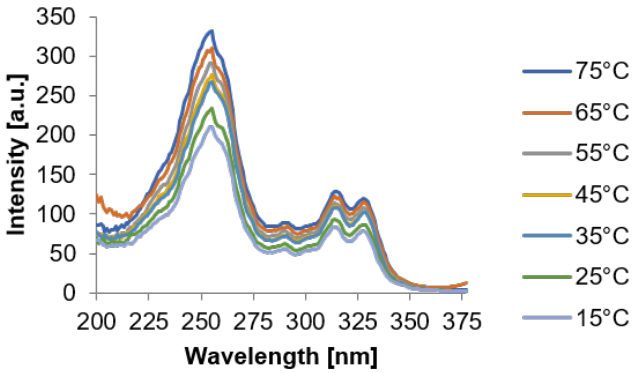

Figure 2.11. Excitation spectra of **N-Phe$_3$** in aqueous medium measured every 10°C. Conditions: 1 µM **N-Phe$_3$**, 10 mM sodium acetate buffer, 10 vol% ethanol, λ_{em} = 387 nm.

TEM Images of N-Phe$_3$

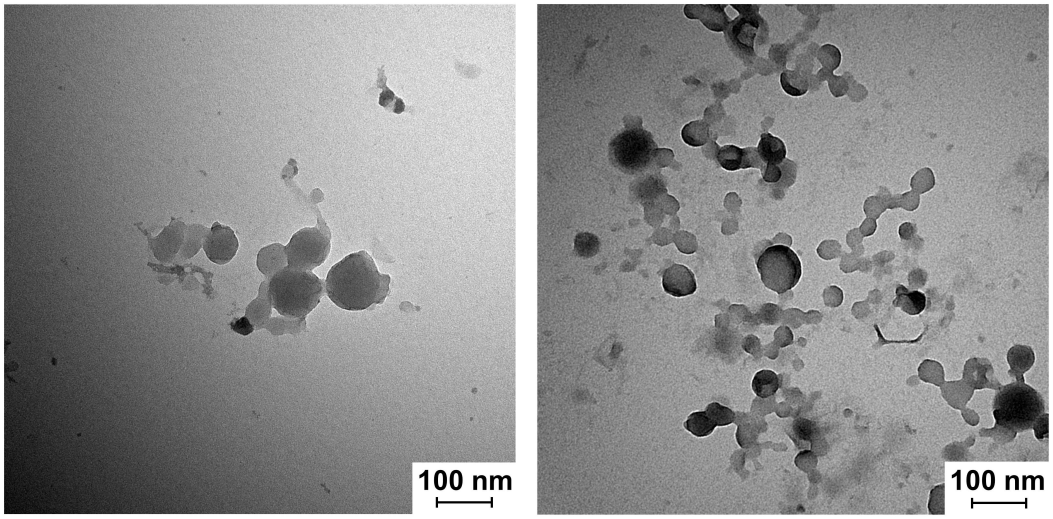

Figure 2.12. Transmission electron microscope (TEM) images of the self-assembled vesicles from the amine-oligomer **N-Phe$_3$**. Conditions: 10 mM sodium acetate buffer (pH 4.71), 10 vol% ethanol, 3 µM (left) and 5 µM (right) **N-Phe$_3$**.

DLS Spectra of N-Phe$_3$

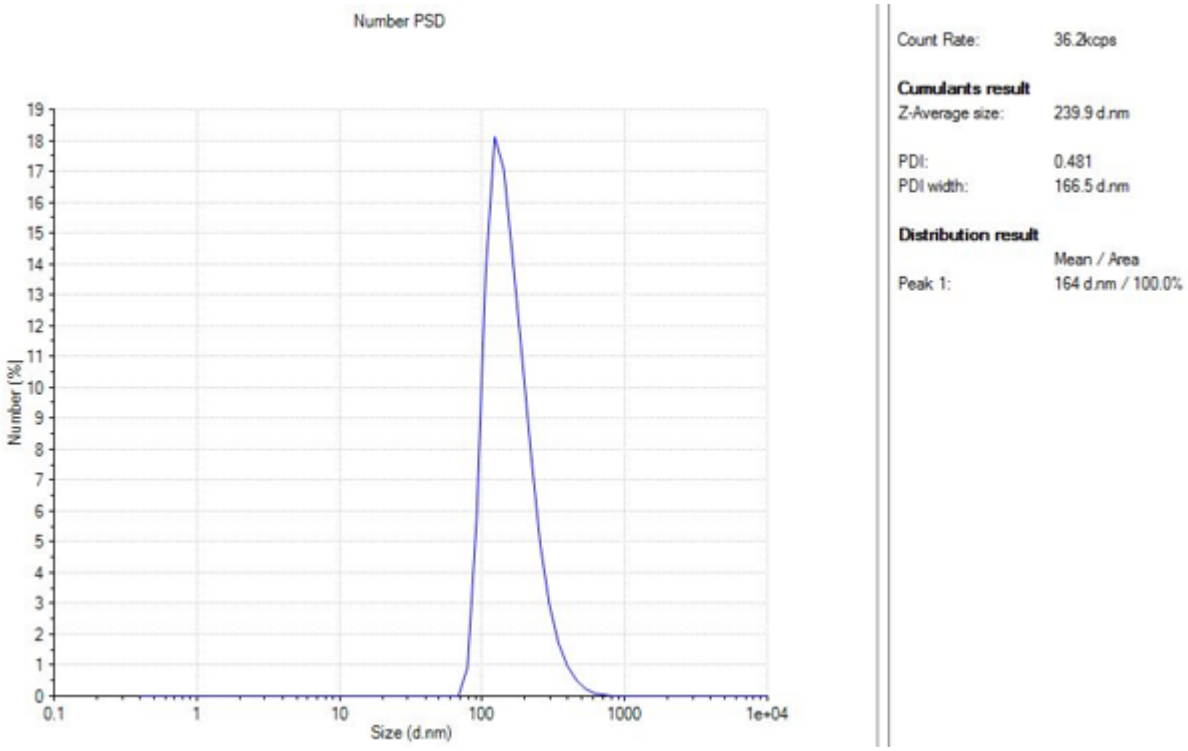

Figure 2.13. Dynamic light scattering (DLS) measurement of the assembled **N-Phe$_3$** in aqueous medium at 20°C. Conditions: 10 mM sodium acetate buffer (pH 4.71), 10 vol% ethanol, 1 µM **N-Phe$_3$**.

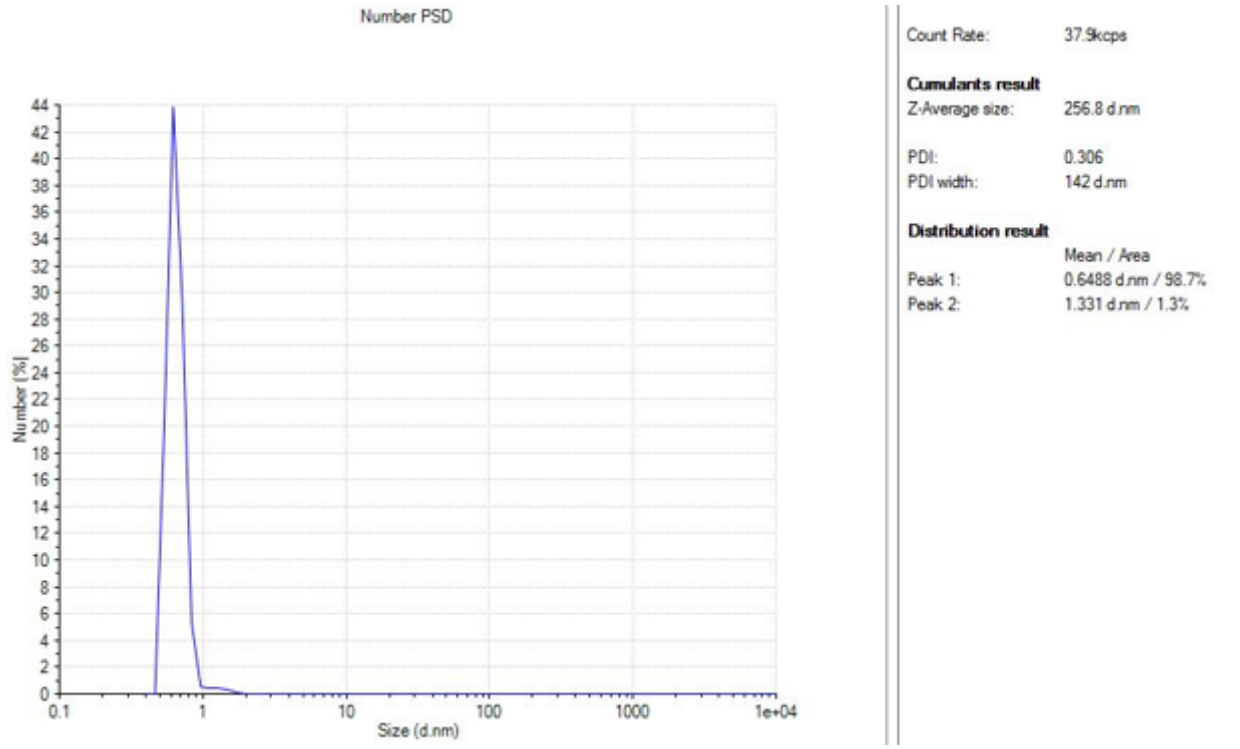

Figure 2.14. Dynamic light scattering (DLS) measurement of the assembled **N-Phe$_3$** in aqueous medium at 70°C. Conditions: 10 mM sodium acetate buffer (pH 4.71), 10 vol% ethanol, 1 µM **N-Phe$_3$**.

Electrostatic Layering

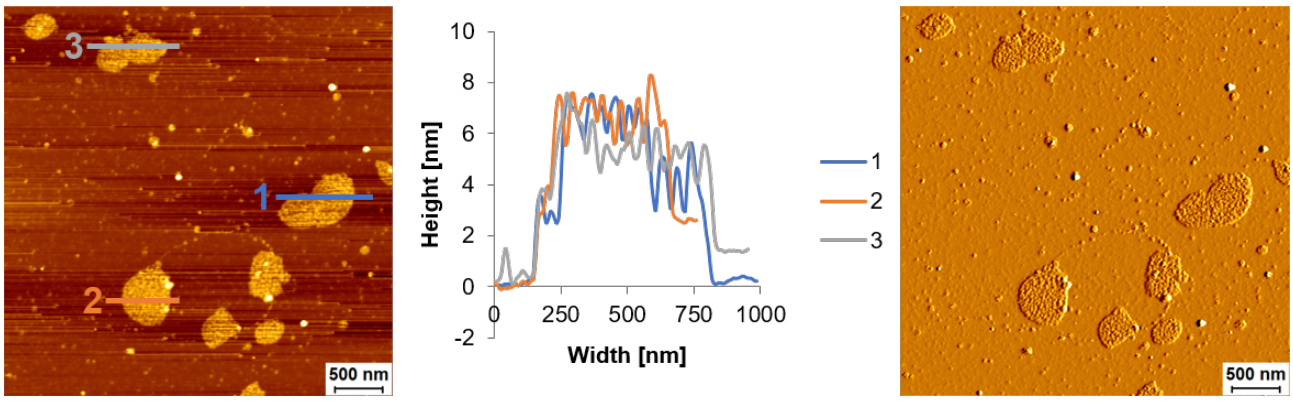

Figure 2.15. AFM measurements of the two layers: 1. **Py$_3$** + 2. **N-Phe$_3$**, their height profiles and the deflection scan (right). Conditions: 1st layer 2 µM **Py$_3$**, 10 mM sodium phosphate buffer (pH 7.1), 10 mM sodium chloride and 10 vol% ethanol, 2nd layer 10 µM **N-Phe$_3$**, 10 mM sodium acetate buffer (pH 4.7) and 10 vol% ethanol.

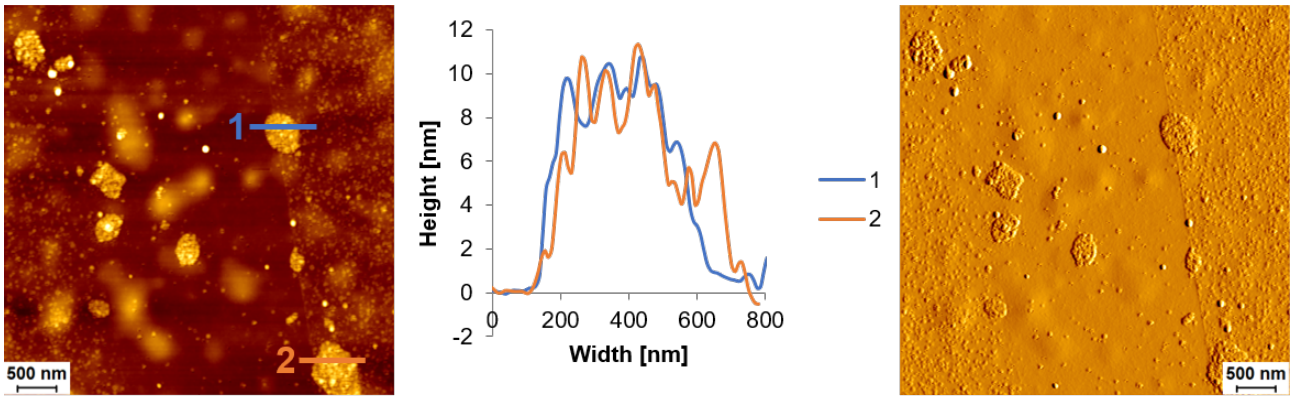

Figure 2.16. AFM measurements of the three layers: 1. **Py_3** + 2. **N-Phe_3** + 3. **Py_3**, their height profiles and the deflection scan (right). Conditions: 1st and 3^3 layer 2 µM **Py_3**, 10 mM sodium phosphate buffer (pH 7.1), 10 mM sodium chloride and 10 vol% ethanol, 2nd layer 10 µM **N-Phe_3**, 10 mM sodium acetate buffer (pH 4.7) and 10 vol% ethanol.

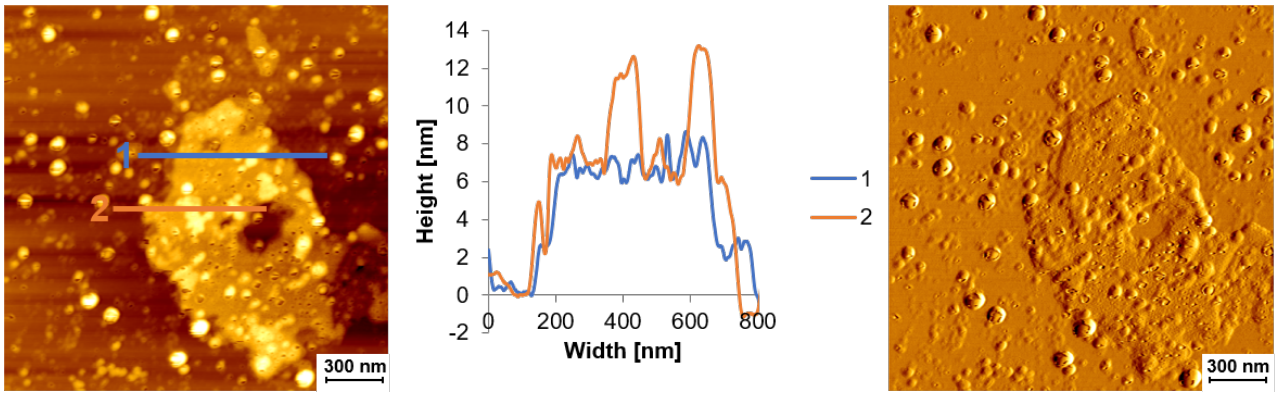

Figure 2.17. AFM measurements of the two layers: 1. **N-Phe_3** + 2. **Py_3**, their height profiles and the deflection scan (right). Conditions: 1st layer 10 µM **N-Phe_3**, 10 mM sodium acetate buffer (pH 4.7) and 10 vol% ethanol, 2nd layer 2 µM **Py_3**, 10 mM sodium phosphate buffer (pH 7.1), 10 mM sodium chloride and 10 vol% ethanol.

3. Synthesis of New Cationic Supramolecular Polymers

3.1. Abstract

The synthesis and analysis of new cationic supramolecular polymers were of particular interest for the previously described chapter 2 *Electrostatic Assembly of Supramolecular Polymers*. The main goal was to find an oligoamine that self-assembles into sheets in order to be able to increase the number of layers. Therefore, the previously used phosphodiester-bridges in the oligomers were changed to amine-bridges. Also, the differences in self-assembly behavior to the corresponding negatively charged oligomers were investigated.
Thus, the following described molecules were spectroscopically analyzed by UV-vis, fluorescence, and AFM. The biggest challenge to overcome during the synthesis of all these molecules was the insolubility of the intermediates and products at a certain point.

3.2. Introduction

Studies of phosphodiester-bridged oligomers in aqueous medium were done in the research group of Prof. R. Häner and showed the formation of different supramolecular polymer assemblies. It was shown that phosphodiester-bridged trimers consisting of the same aromatic unit and linkers, varying in the attachment-position of the linkers, lead to the formation of different supramolecular assemblies due to hydrophobic- and $\pi-\pi$-interactions.[96,97,119,134] (Figure 3.1). Figure 3.1A depicts the self-assembly of 1,6-dialkynyl pyrene trimers into two-dimensional sheets,[119] whereas the 2,7-dialkynyl pyrene trimer forms sheets and tubes[134] (Figure 3.1B). The 2,7-dialkynyl phenanthrene trimer self-assembles into nanotubes[97] compared to the 3,6-dialkynyl phenanthrene trimer which forms fibers[96] (Figure 3.1C and D). It seemed like the formation of two-dimensional structures out of oligomers occurs preferably when the trimers were linearly-linked (Figure 3.1A, B and D).
The question arose, what would happen if we change the backbone from phosphodiesters to amines and thereby change the charge of the trimer backbone from negative to positive when in aqueous medium. Would it still be possible to form two dimensional structures when using linearly-linked oligomers with amine-bridges? Additionally, the change of the phosphodiester-backbone to amines allows us to expand our understanding of supramolecular polymers in aqueous environments. The oligoamines can be investigated in self-assembly behavior by spectroscopic measurements, such as UV-vis, fluorescence, AFM, and TEM. Also, it is possible to investigate in the interactions with phosphate-oligomers, as well as with other molecules. Investigations in light-harvesting properties are possible too and will be discussed in more detail in later chapters. Summed up, a lot of possibilities open up for such oligoamines.
The electrostatic interaction of the **N-Phe$_3$** oligoamine with a phosphate-oligomer has already been explained in more detail in chapter 2. The promising results were the reason to continue the research

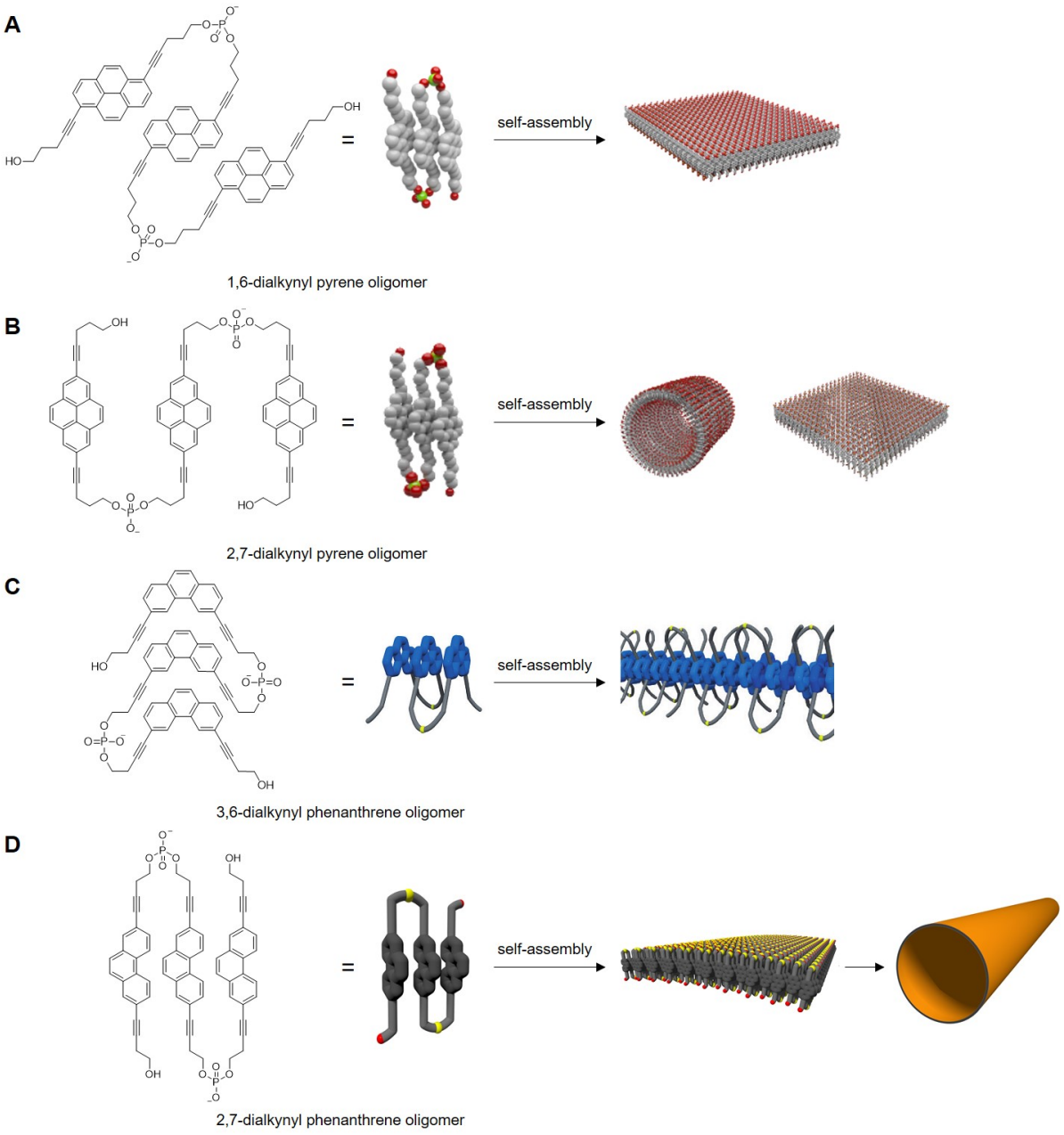

Figure 3.1. Previously investigated different-linked oligomers with phosphodiester-bridges in aqueous medium. A) The 1,6-dialkynyl pyrene oligomer self-assembles into two dimensional sheets.[119] B) The 2,7-dialkynyl pyrene oligomer self-assembles into two-dimensional sheets and tubes.[134] C) The 3,6-dialkynyl phenanthrene trimer forms fibers.[96] D) The 2,7-dialkynyl phenanthrene trimer forms nanotubes.[97] Illustrations are taken from references.

in this field and to prepare even more oligoamines. The goal was to synthesize an oligoamine that forms positively charged supramolecular polymers sheets. These would improve the electrostatic interaction and adsorption of the layers. For that, several different linearly-linked oligoamines were synthesized, varying in linker-length and aromatic unit.

3.3. Results and Discussion

3.3.1. 3,6-Dialkynyl Phenanthrene-Pyrene-Phenanthrene Oligoamine (15)

Oligoamine **15** was primarily synthesized as an acceptor for further studies in light-harvesting properties of **N-Phe$_3$** (see in chapter 5 *Exploration of Light-Harvesting Properties of N-Phe$_3$*), but also to investigate whether the structure of supramolecular polymer will change compared to **N-Phe$_3$**.

Synthesis of 15

The synthesis of **15** is shown in Scheme 3.1. 1,8-Dibromopyrene **12** and 1,6-dibromopyrene **7** were synthesized in close analogy to literature.[135] The separation of these two compounds **12** and **7** was tried to be achieved through crystallization according to different references.[136,137] Only a ratio of **12**/**7** 2:3 could be achieved. Despite the low success in separation, the pentynyl-linkers were synthesized at the mixture of dibromopyrenes by a Sonogashira reaction, whereas the compounds **13** (51%) and **8** (18%) could be well separated by a column chromatography.[135] The hydroxyl-groups of **13** were oxidized to aldehyde-groups by a Dess-Martin oxidation, to obtain compound **14** (64%). Compound **5** was synthesized as described in section 2.3.1. A reductive amination of **14** and **5** was performed to obtain the trimer **15** (5%) as a white solid. The reason for the small yield was the formation of several byproducts and tricky purification steps (extraction, column, recrystallization, prep. TLC).

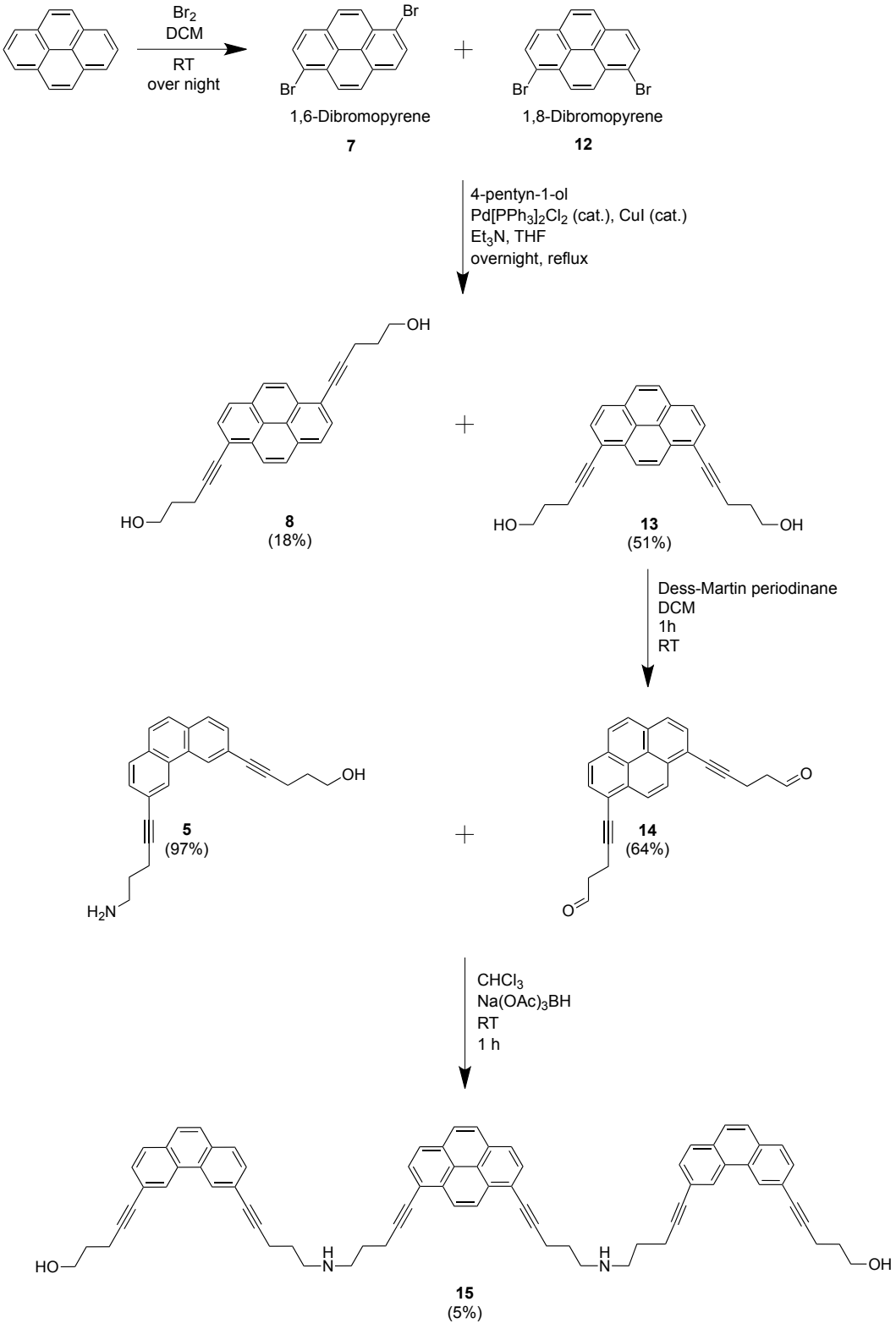

Scheme 3.1 Preparation of amine-linked 3,6-dialkynyl phenanthrene-pyrene-phenanthrene trimer (**15**).

Absorption spectra of 15

Figure 3.2 shows absorption spectra of the trimer **15** in aqueous medium and in pure ethanol. **15** is soluble in ethanol and thus, this curve represents the trimer in a disassembled state. It shows the

phenanthrene maxima at 313 and 327 nm, and the maxima of pyrene at 363 and 383 nm. Further, the absorption spectrum of a sample of **15** (1 µM) in aqueous medium, containing 10 mM sodium acetate buffer and 10% ethanol, heated to 70°C (red), resembles the spectrum of **15** in pure ethanol (green). From this, it can be concluded, that **15** is disassembled at 70°C in aqueous medium. A comparison between the two different conditions, aqueous medium at 20°C and pure ethanol, shows a bathochromic shift (approx. 5-10 nm) and hypochromicity when changing the solvent from ethanol to sodium acetate buffer. This means that at 20°C, the trimer is self-assembled. Also, the peak maxima of **15** (322 nm, 333 nm, 375 nm, 390 nm) are not sharp anymore as in pure ethanol, which indicates aggregation.

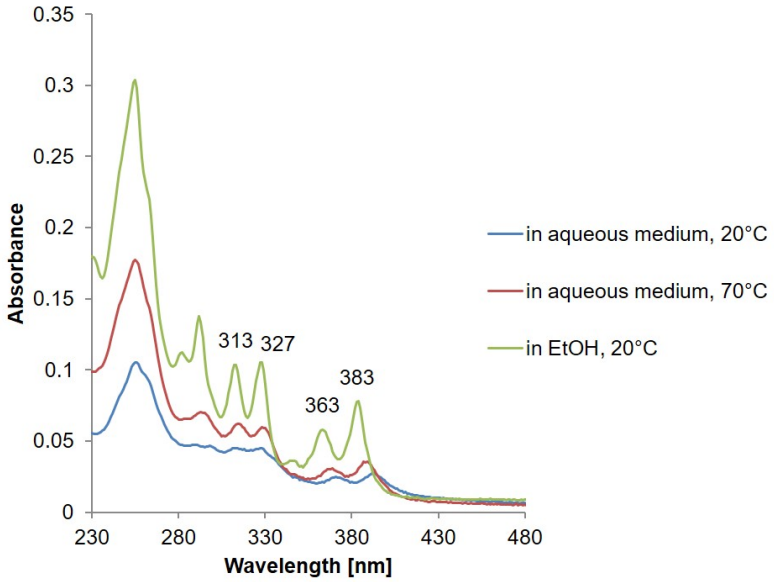

Figure 3.2. Absorption spectra of trimer **15** at 20°C and 70°C in aqueous medium (conditions: trimer **15** (1 µM), 10 mM acetate buffer (pH 4.71), 10 vol% ethanol) and at 20°C in ethanol (trimer **15** 1 µM).

Fluorescence spectra of 15

The fluorescence spectra at different temperatures of **15** in aqueous medium show a peak maximum at 431 nm if the phenanthrene is excited at 322 nm (Figure 3.3). This emission maximum is caused by the pyrene, which was incorporated in the middle of **15**. From literature it is known that a pyrene-phenanthrene-exciplex emission occurs at this wavelength.[138] Phenanthrene emission is observable at the wavelengths 371 nm and 385 nm when **15** is assembled (20°C) and almost vanishes, when the trimer is disassembled (70°C). When disassembled (70°C), the nearest neighbour chromophore of a phenanthrene in trimer **15** is a pyrene, thus mostly the phenanthrene-pyrene exciplex emission at 431 nm is observed.

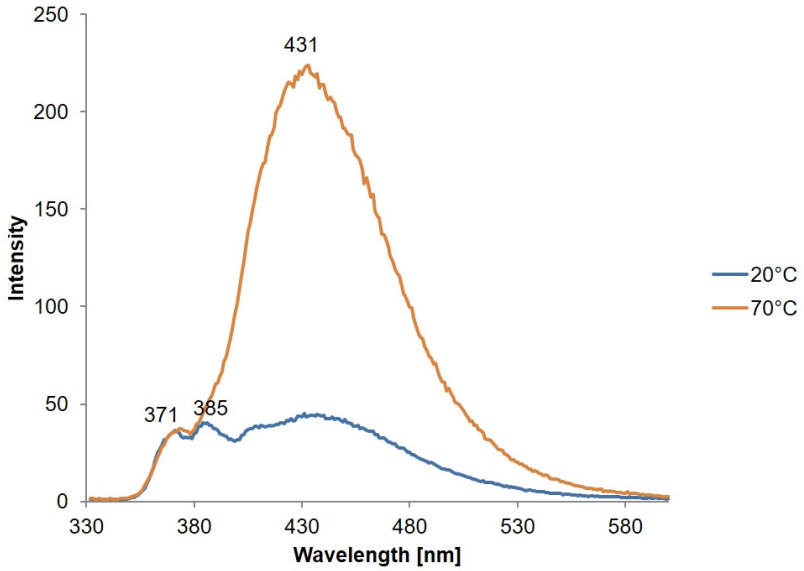

Figure 3.3. Fluorescence spectra at 20°C and 70°C. Conditions: trimer **15** (1 µM), 10 mM acetate buffer (pH 4.71), 10 vol% ethanol, λ_{ex} = 322 nm.

Excitation spectra of 15

By measuring the sample at the emission wavelength of the acceptor, in this case pyrene (433 nm), it can be shown, which wavelengths are responsible for the emission and from where the energy is coming. As shown in Figure 3.4, the excitation spectrum at 433 nm resembles the absorption spectrum of **15** (Figure 3.2).

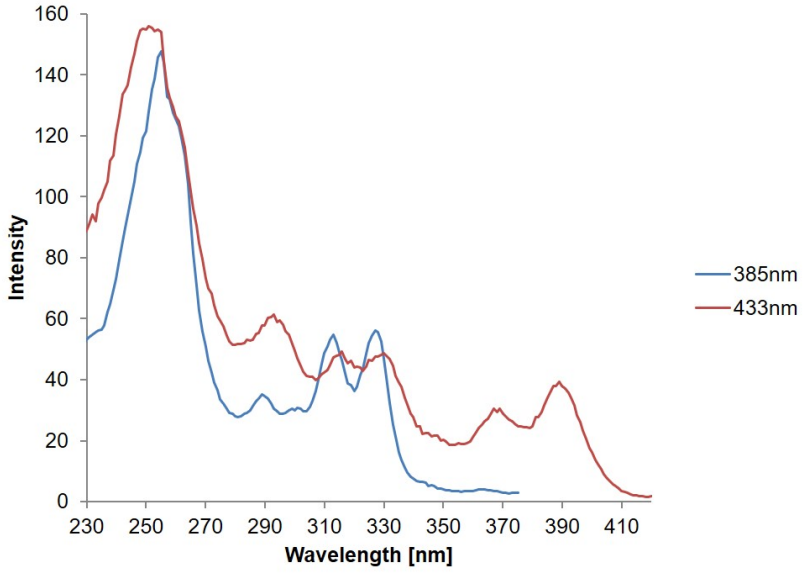

Figure 3.4. Excitation spectra at two different wavelengths of the assembled **15** (20°C). Conditions: trimer **15** (1 µM), 10 mM acetate buffer (pH 4.71), 10 vol% ethanol, $\lambda_{em,blue}$ = 385 nm, $\lambda_{em,red}$ = 433 nm.

If an excitation spectrum is measured at 385 nm, where phenanthrenes are emitting, the spectrum resembles mainly the absorption spectrum of **N-Phe$_3$** (Figure 2.8). Also, a red-shift of 3 nm is observed when measuring the excitation spectrum (at 20°C) at 433 nm, compared to 385 nm.

Visualization of 15 by AFM

Figure 3.5 shows an AFM image in tapping mode of **15** in aqueous medium. As expected from the previous measurements of **N-Phe$_3$**[129] (chapter 2), the newly synthesized compound **15** formed also spherical objects, vesicles, respectively. Their diameter varied between 50-100 nm, and as seen in Figure 3.5 they also had a round shape. The vesicles had a uniform height of around 5-6 nm, which corresponds to a bilayer of the trimer.

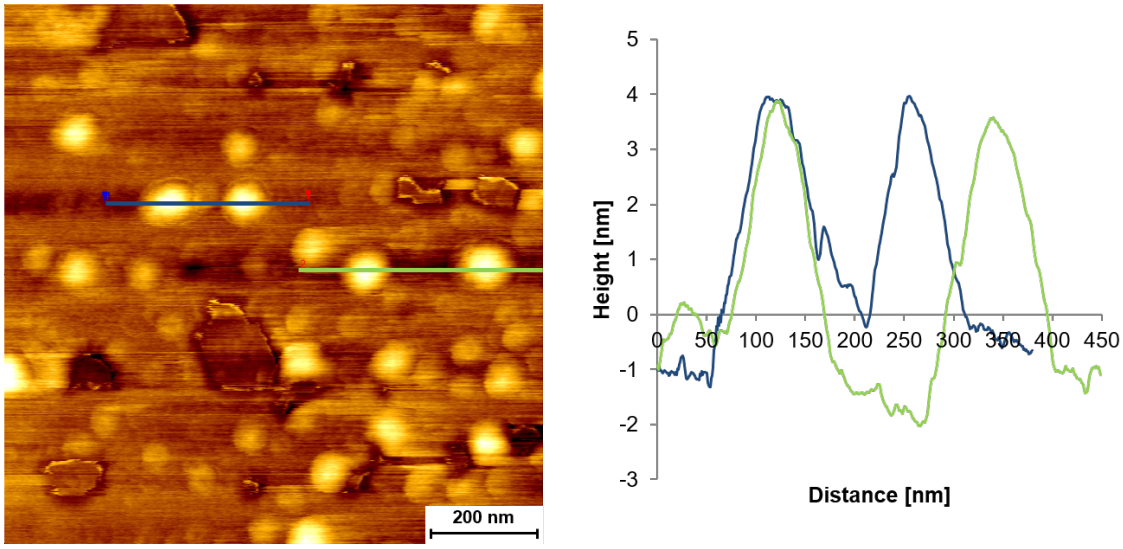

Figure 3.5. Left: Tapping mode AFM image of the assembled **15** on unmodified mica. Right: Height-profile of the formed spheres. Conditions: trimer **15** (3 µM), 10 mM acetate buffer (pH 4.71), 10 vol% ethanol.

3.3.2. 2,7-Dialkynyl Phenanthrene Oligoamine (21)

Synthesis of 21

The synthesis of 2,7-dialkynyl phenanthrene trimer **21** is displayed in Scheme 3.2. In a first step, the commercially available 2,7-dibromophenanthrene **16** was used for a Sonogashira reaction: 4-pentyn-1-ol and 4-pentynyl-phthalimide were attached to the phenanthrene to obtain the compounds **17** (29%) and **18** (14%). The phthalimide-group in compound **17** was afterwards deprotected by the addition of hydrazine (compound **19**, 72%). The hydroxy-groups of **18** were oxidized to aldehydes by a Dess-Martin oxidation, which led to compound **20** (23%). In a last step compounds **19** and **20** were coupled by a reductive amination with $Na(OAc)_3BH$ in chloroform. The target molecule **21** was purified by a preparative TLC (32%).

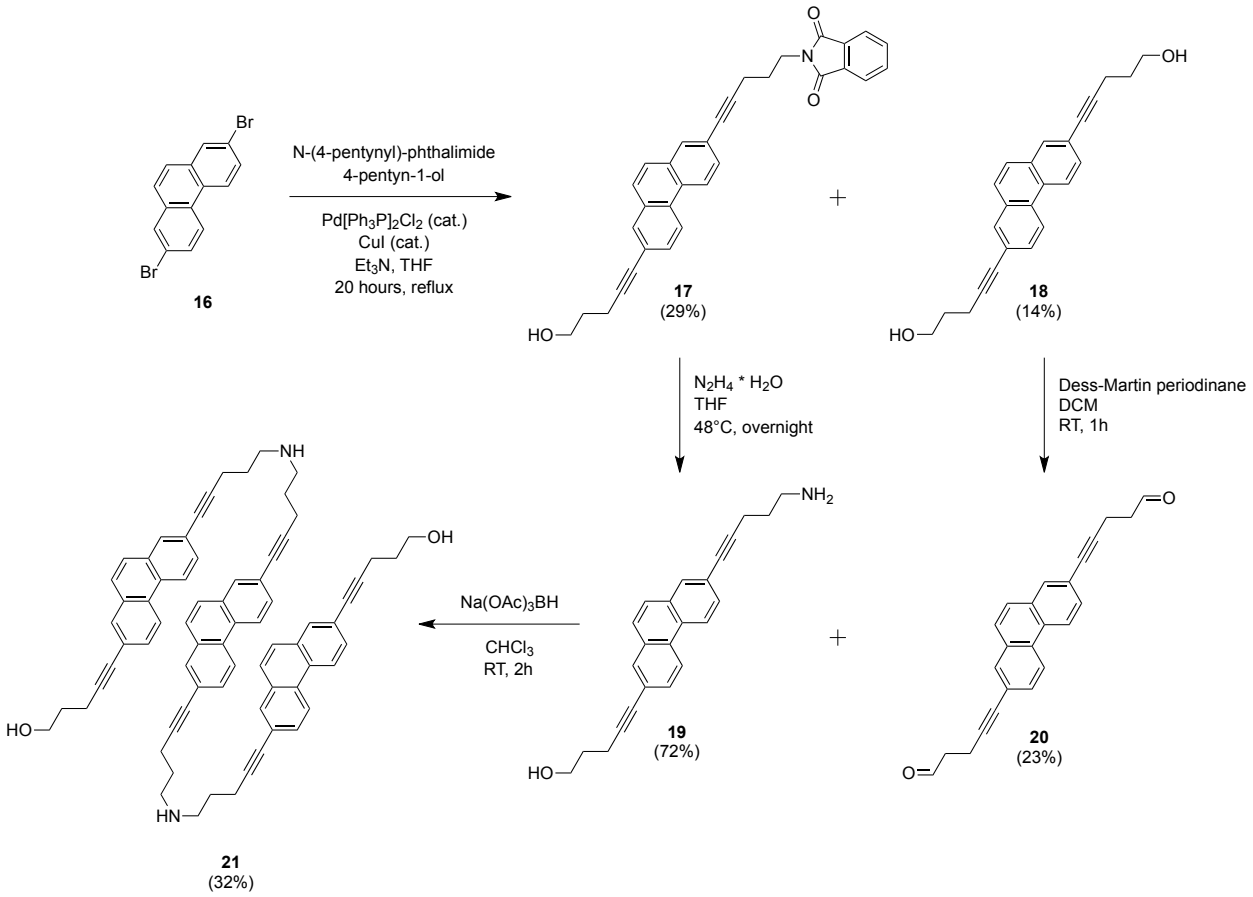

Scheme 3.2 Preparation of amine-linked 2,7-dipentynyl-substituted phenanthrene trimer (**21**).

Absorption Spectra of 21

First experiments were done to find out at which conditions the trimer is assembled at room temperature and disassembled at higher temperature. Figure 3.6 shows the absorption spectra of the trimer in sodium acetate buffer (10 mM, pH 4.69), 70 vol% ethanol and with increasing sodium chloride concentrations (0-20 mM) and in pure ethanol. In ethanol trimer **21** is dissolved, meaning **21** is present in a disassembled state. Comparing the three different samples in aqueous medium at 70°C with the one in pure ethanol, one sees that all the maxima are at the same wavelengths: 267, 274, 293, 303, 317 nm. This means that **21** is disassembled at 70°C in the three samples in aqueous medium. After cooling to 20°C, the sample without any NaCl in 70% ethanol (dark blue), showed a small increase in absorbance compared to the one at 70°C (dark red). In contrast, the samples containing 10 and 20 mM NaCl (at 20°C) showed an increase at higher wavelengths, indicating light scattering. This is observed due to the formation of bigger aggregates in the sample. All three conditions (0-20 mM NaCl) indicated that **21** is disassembled at 70°C and aggregates at 20°C. Further measurements, were done under the conditions 0 and 10 mM sodium chloride, 70% ethanol and 10 mM sodium acetate buffer (pH 4.69).

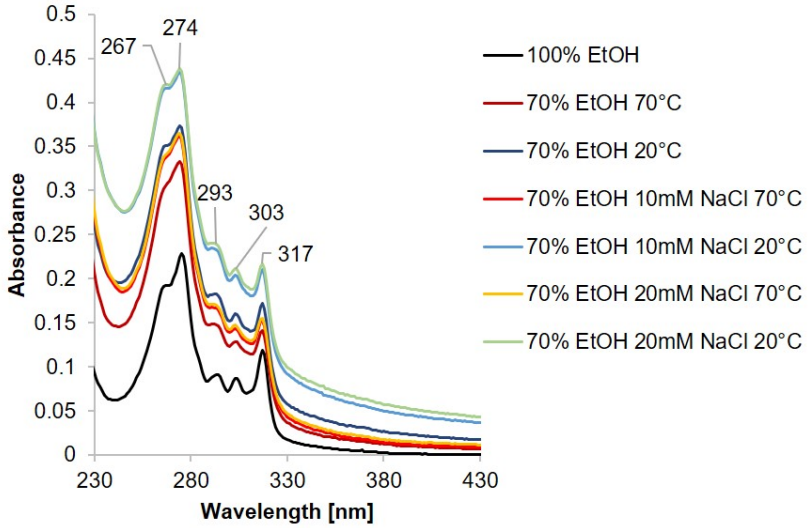

Figure 3.6. Absorption spectra of trimer **21** under different conditions. Conditions: trimer **21** (1 µM), 10 mM sodium acetate buffer (pH 4.69), 70 vol% ethanol, 0-20 mM NaCl and trimer **21** in pure ethanol.

AFM Measurements of 21

0 mM NaCl

The formed structures of **21** without any sodium chloride in 10 mM sodium acetate buffer (pH 4.69) and 70% ethanol were analyzed by measuring AFM. The formation of uniform structures under these conditions was difficult. Various measurements showed different structures, dominated by undefined aggregates and some areas with heights between 1-1.5nm. This means that the formation of identical assemblies was not reproducible. Figure 3.7 shows the rare formation of sheets with a height of approximately 1.5 nm.

The question arose whether an increase in **21**-concentration would lead to bigger, uniform structures. Hence, the concentration was increased to 5 µM and again AFM was measured. Unfortunately, the measurements showed again different structures: sheets, vesicular aggregates, and big undefined aggregates, which were not reproducible. Figure 3.8 and Figure 3.9 indicate AFM images of **21** (5 µM) in 10 mM sodium acetate buffer (pH 4.69) and 70% ethanol. The AFM image in Figure 3.8 (top) depicts the formation of frayed sheets with a height of 2 nm, and the image on the bottom the formation of small aggregates with a height of 3 nm and some large aggregates (70 nm). Also, sheet-like structures with rounded edges were observed, whereas the height of them varies from 2.5-5 nm (Figure 3.9).

The variation in height and lack of reproducibility was the reason to change the conditions.

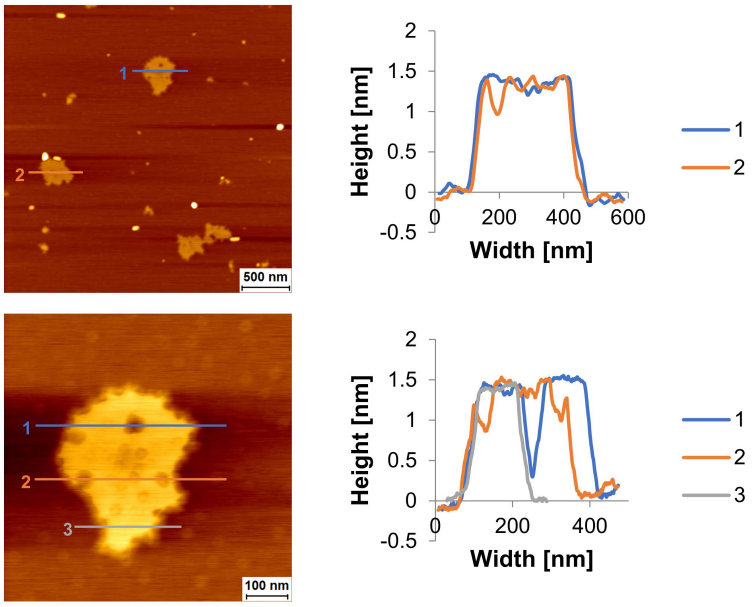

Figure 3.7. AFM image of the adsorbed trimer **21** on unmodified mica. Cross-sections are shown on the right side. Conditions: trimer **21** (1 µM), 10 mM sodium acetate buffer (pH 4.69), 70 vol% ethanol, cooling rate: 13°C/min.

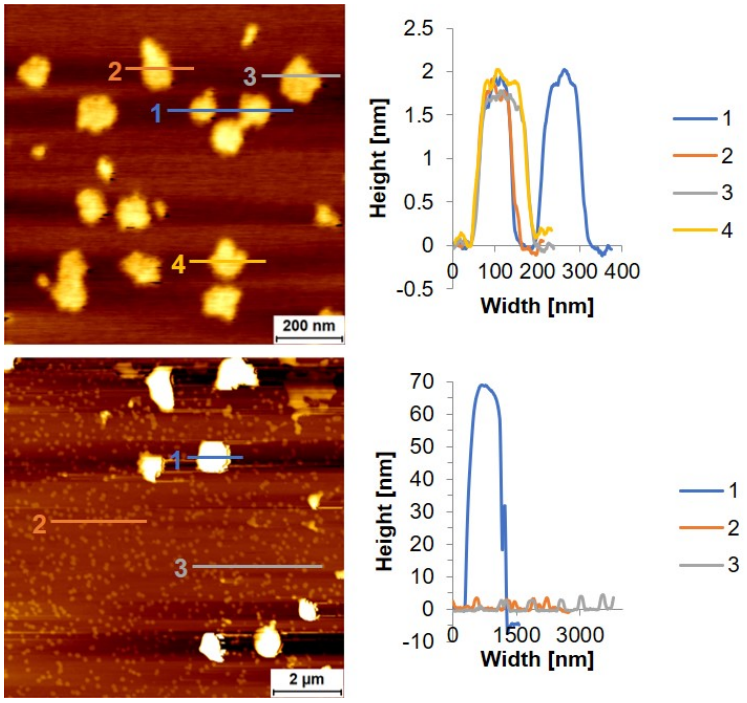

Figure 3.8. AFM image of the trimer **21**. Cross-sections are shown on the right side. Conditions: trimer **21** (5 µM), 10 mM sodium acetate buffer (pH 4.69), 70 vol% ethanol, cooling rate: 13°C/min.

10 mM NaCl

In a next step, atomic force microscopy measurements were done of **21** in 10 mM NaCl, 70% ethanol and 10 mM sodium acetate buffer (pH 4.69). The samples were prepared with different

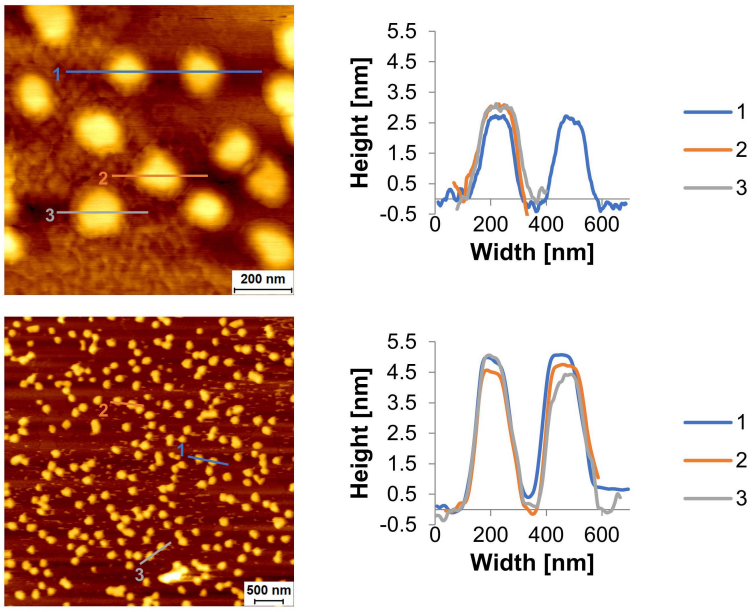

Figure 3.9. AFM image of the trimer **21**. Cross-sections are shown on the right side. Conditions: trimer **21** (5 µM), 10 mM sodium acetate buffer (pH 4.69), 70 vol% ethanol, cooling rate: 13°C/min.

cooling rates (1°C/min and 13°C/min). The data showed the formation of frayed sheets, large vesicular assemblies, and small undefined aggregates, which were not reproducible.
Figure 3.10 indicates the formation of sheets with a height of 1.2 nm. They have frayed edges and sometimes even holes inside the sheet. Figure 3.11 shows large vesicular aggregates with heights of 50-90 nm, and also small undefined aggregates (5-7 nm).
The cooling rate was slowed down from 13°C/min to 1°C/min in order to form the thermodynamically most stable product and as such more uniform structures could form. The AFM measurements indicated the formation of rare roundish sheets and a lot of undefined aggregates, which were not reproducible. Figure 3.12 depicts the formation of sheets with a height of 2-2.2 nm and a lot of undefined small aggregates were distributed around the sheets. The height profiles in Figure 3.13 indicate the formation of undefined roundish aggregates with heights varying between 0.9-5 nm.
Absorption spectra (Figure 3.6) showed light-scattering, indicating the formation of large assemblies when preparing a sample of **21** in an aqueous medium containing 10 mM sodium chloride, 10 mM sodium acetate buffer (pH 4.69) and 70% ethanol. Large assemblies could not be observed by AFM. It could be that they were washed off during AFM sample preparation.
Comparing these results with the ones obtained by the countercharged trimer with phosphodiester-bridges,[97] one could not observe nanotubes. Due to the lack of reproducibility, the investigations were not continued.

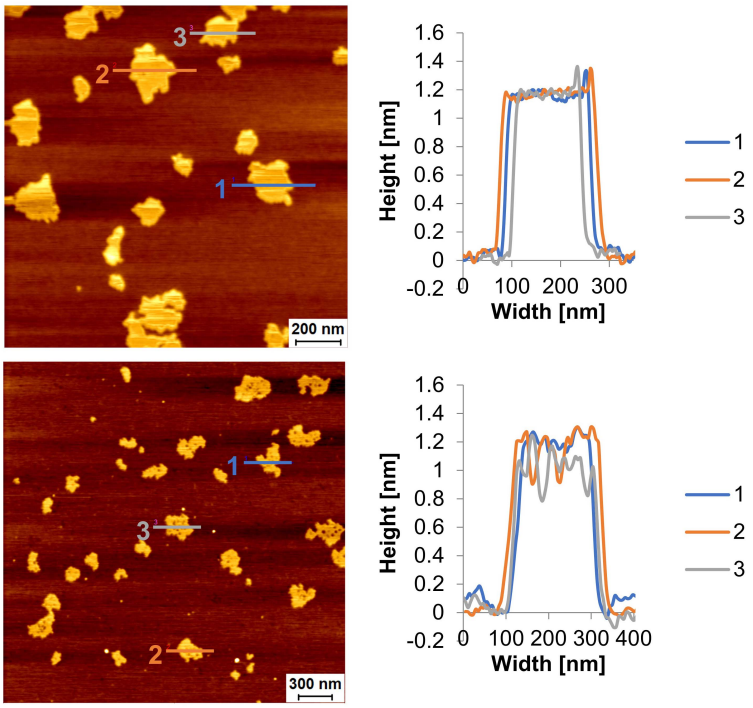

Figure 3.10. AFM image of the trimer **21**. Cross-sections are shown on the right side. Conditions: trimer **21** (1 µM), 10 mM acetate buffer (pH 4.69), 70 vol% ethanol, 10 mM NaCl, cooling rate: 13°C/min.

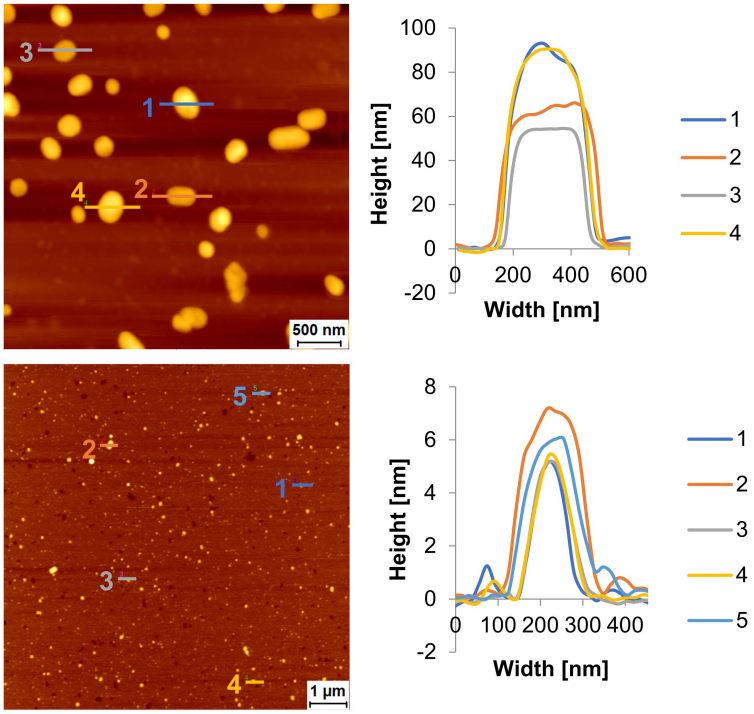

Figure 3.11. AFM image of the trimer **21**. Cross-sections are shown on the right side. Conditions: trimer **21** (1 µM), 10 mM acetate buffer (pH 4.69), 70 vol% ethanol, 10 mM NaCl, cooling rate: 13°C/min.

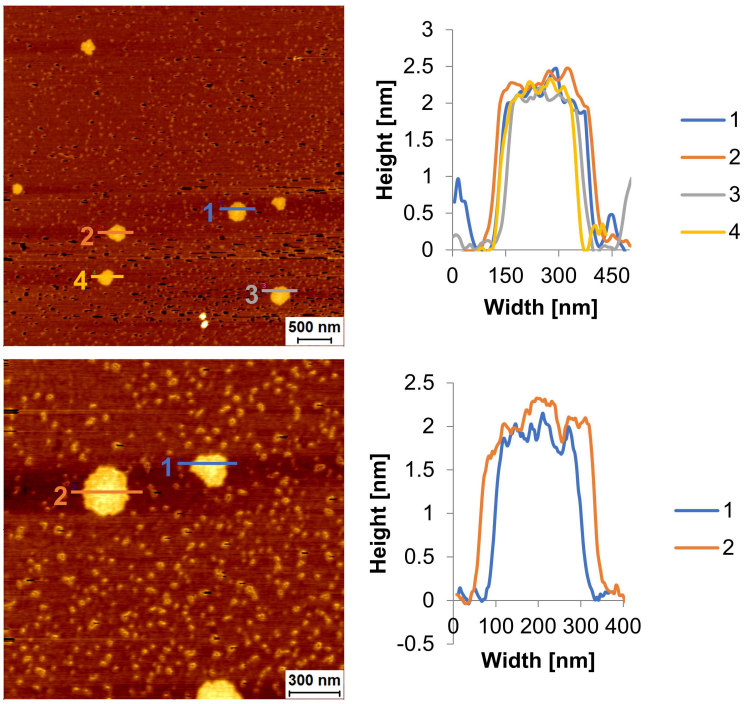

Figure 3.12. AFM image of the adsorbed trimer **21** on unmodified mica. Cross-sections are shown on the right side. Conditions: trimer **21** (1 µM), 10 mM acetate buffer (pH 4.69), 70 vol% ethanol, 10 mM NaCl, cooling rate: 1°C/min.

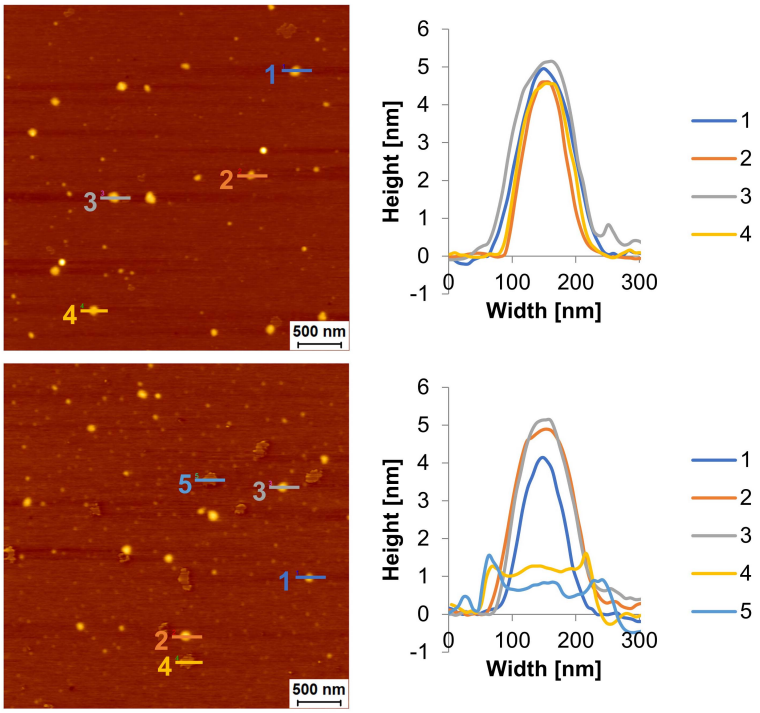

Figure 3.13. AFM image of the adsorbed trimer **21** on unmodified mica. Cross-sections are shown on the right side. Conditions: trimer **21** (1 µM), 10 mM acetate buffer (pH 4.69), 70 vol% ethanol, 10 mM NaCl, cooling rate: 1°C/min.

3.3.3. 1,6-Dialkynyl Pyrene Oligoamine (26)

Previously it was shown, that the change of the 2,7-dialkynyl phenanthrene backbone from phosphate to amine did not lead to the formation of the same assemblies, nanotubes, respectively. Thus another molecule was synthesized and analyzed, the 1,6-dialkynyl pyrene oligoamine.

Synthesis of 26

5-Hexynyl-phthalimide and 5-hexyn-1-ol were added in a ratio 1:1 to the commercially available 1,6-dibromopyrene **7**, in order to be coupled to it by a Sonogashira reaction. The two products, which were used for the further synthesis were isolated by a column chromatography: **22** (29%) and **23** (20%). The phthalimide-group in compound **22** was deprotected with hydrazine in THF to obtain **24** (90%). The two hydroxyl-groups in compound **23** were oxidized to aldehydes with the Dess-Martin periodinane, which resulted in compound **25** (75%). The last reaction was the coupling of compounds **24** and **25** by a reductive amination to afford the trimer **26** (22%) (Scheme 3.3).

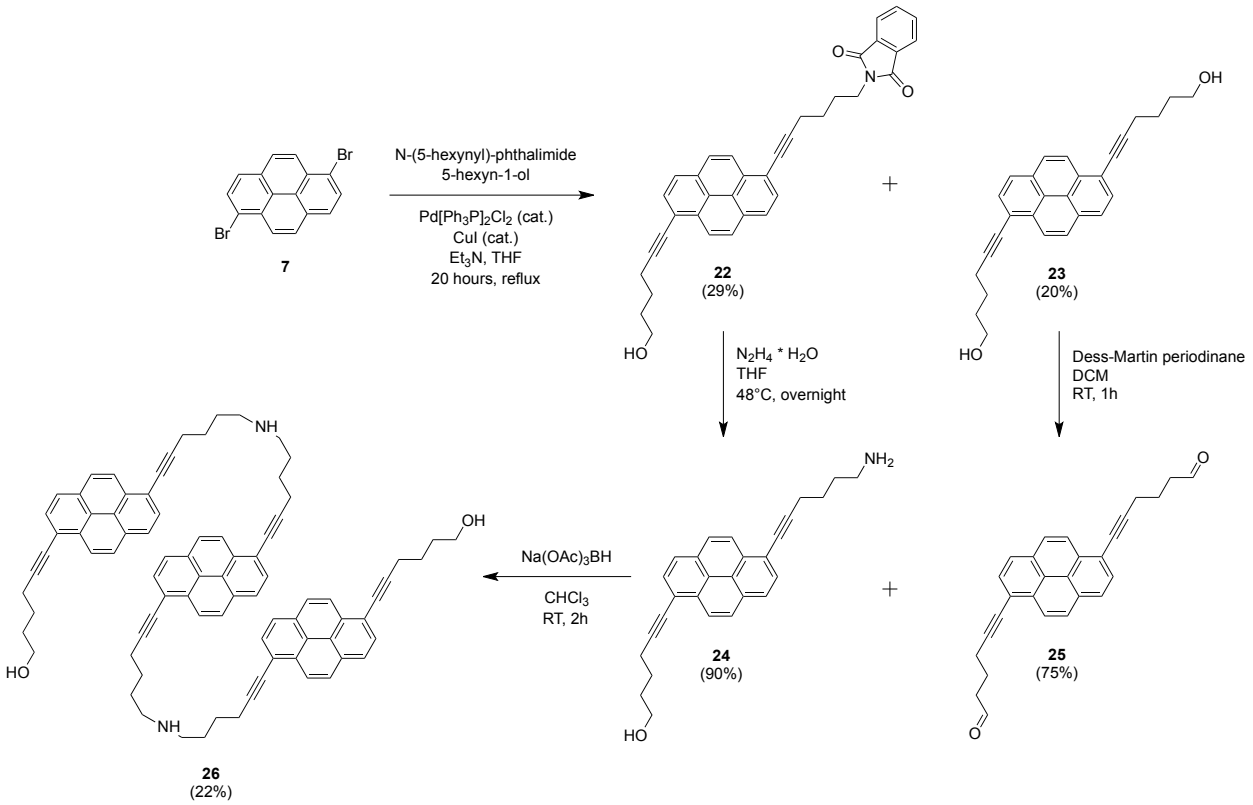

Scheme 3.3 Synthesis of amine-linked 1,6-dihexynyl-substituted pyrene trimer (**26**).

The synthesis of the pyrene trimer **26** showed difficulties at the very end regarding the solubility. The final compound could not be dissolved in any solvents which are miscible with water. That is why the amines were dimethylated in order to have a permanent positive charge on the amine groups and thus, increase the solubility.

3.3.4. 1,6-Dialkynyl Pyrene Oligoamine with Dimethylated Amines (27)

Synthesis of 27

The synthesis of the starting material **26** was performed as described in section 3.5.1. The amines of **26** were dimethylated according to literature.[139] Compound **27** was isolated as an orange-brownish solid.

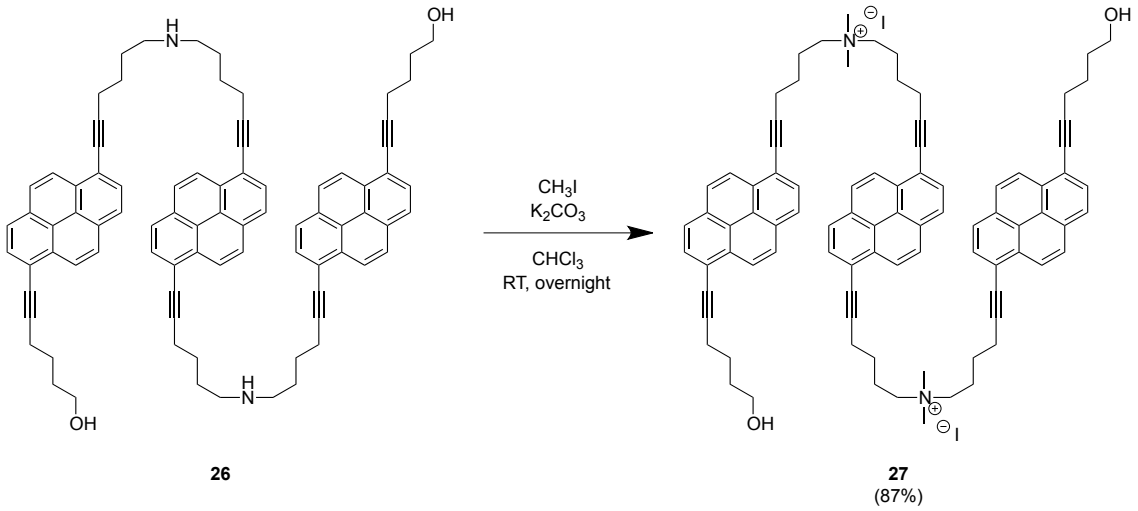

Scheme 3.4 Dimethylation of the amines in **26** to obtain **27**.

Solubility of 27

Trimer **27** was tried to be dissolved in several solvents, which are miscible with water. THF dissolved one part of the solid but still, some particles were in the solution that were insoluble. Acetonitrile, methanol, and isopropanol worked even worse. It looked like only chloroform and dichloromethane could dissolve the solid, which could not be used for the measurements in aqueous medium. It was considered to check pyridine, DMF, and DMSO, but due to their UV-vis cut-off, only DMSO was an option. Unfortunately, DMSO did not work either.

Addition of Salts and Acids to 27

As shown in the previous two subsections, the dimethylation of the amine-groups did not help to increase the solubility of the molecule **27**. It was tried to dissolve molecule **27** in different water-miscible solvents. The last attempt ended with DMSO, which also did not work. Therefore, various salts and acids were added to the trimer in the hope that it will be dissolved. The anions of the added salts and acids should increase the solubility by exchanging them with the iodide.[140,141] The following six salts and acids were tested: **potassium triflate**, **p-toluenesulfonic acid**, **salicylic acid**, **succinic acid**, **L-(+)-lactic acid**, **ammonium hexafluorophosphate**. Unfortunately, neither the addition of salts nor acids dissolved **27**.

3.3.5. 1,6-Dialkynyl Pyrene Monomer (24)

As shown in the previous section (3.3.4 *1,6-Dialkynyl Pyrene Oligoamine with Dimethylated Amines (27)*), oligoamine **27** could not be dissolved in DMSO or another water-miscible solvent. We decided to check if the pyrene monomer (**24**) has better solubility properties (Scheme 3.5).

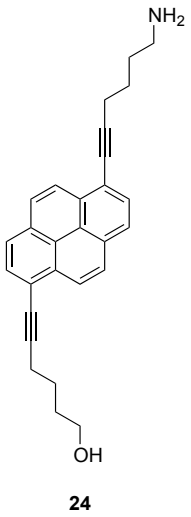

24

Scheme 3.5 Chemical structures of the analyzed pyrene monomer: amine-hydroxy-pyrene (**24**).

Synthesis of Amine-Hydroxy-Pyrene Monomer (24)

Compound **24** was used as a starting material when performing the reductive amination to get the 1,6-dialkynyl pyrene trimer with amine-bridges (**26**). Therefore, the synthesis is described in the previous section 3.3.3 *Synthesis of 26*.

Spectroscopic Analysis of 24

This compound could be well dissolved in ethanol for the following measurements. A stock solution of **24** in ethanol (abs.) was prepared (7099.6 µM) and for the further measurements, four different concentrations (6 µM, 12 µM, 24 µM, and 48 µM) were tested in aqueous medium (10 mM sodium acetate buffer, pH 4.71). Because only the monomer is used for these experiments, the concentration was increased.
Figure 3.14 displays the absorption spectrum of **24** in pure ethanol with maxima at 239, 248, 278, 345, 362 and 384 nm.

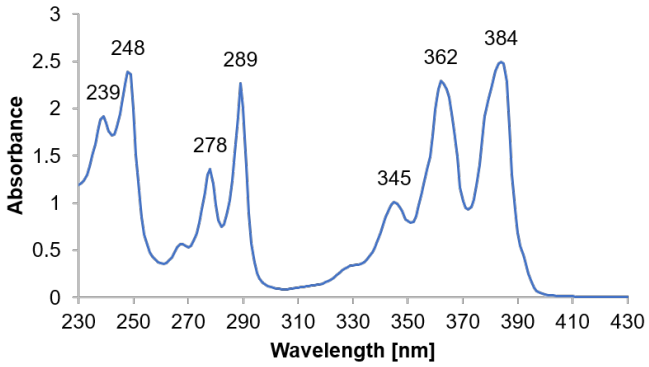

Figure 3.14. Absorption spectrum of monomer **24** in pure ethanol.

Another group member observed at high concentrations of a pyrene monomer a time-dependency in aggregation, respectively slow kinetics, meaning that the aggregation peak at 305 nm increased when waiting at 20°C for a certain time.[142] The question arose whether this is also the case with the monomer **24**. Experiments showed, that the kinetics were not as slow, the full formation of the J-band (305 nm) was reached after 10 minutes (section 3.5.2 *Kinetic Studies of the Amine-Hydroxy Pyrene Monomer (24)*). Thus, for further measurements, this was considered and the samples were measured after waiting for 10 minutes at 20°C, to fully assemble the pyrenes.

Figure 3.15 shows the absorption spectra of compound **24** in sodium acetate buffer with increasing concentrations of sodium chloride. The comparison of both diagrams indicates, that after the addition of 120 mM NaCl a new peak is appearing at 305 nm after cooling to 20°C. This band is typically observed for the 1,6-dialkynyl pyrene trimer with phosphodiester-bridges when it starts to aggregate into sheets (J-band).[116]

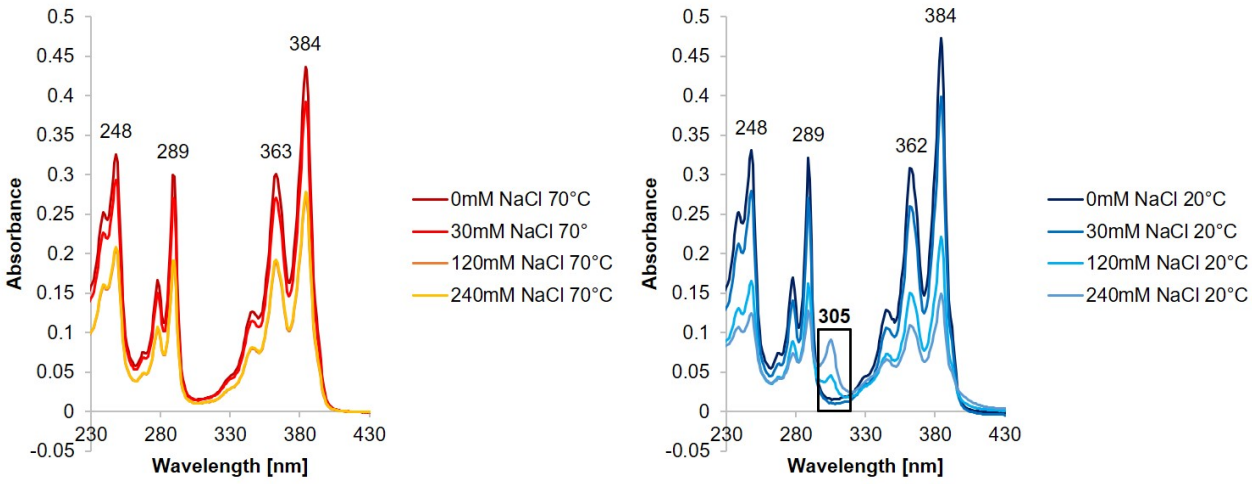

Figure 3.15. Absorption spectra of compound **24** at 70°C (left) and 20°C (right) in aqueous medium after additions of sodium chloride. Conditions: **24** (6 µM) in 10 mM sodium acetate buffer (pH 4.71), increasing concentrations of sodium chloride (0-240 mM).

After the indication that the pyrenes start to aggregate, AFM was measured (Figure 3.16). The

sample with the highest concentration of sodium chloride (240 mM) was chosen, due to the highest J-band. The formation of supramolecular polymers out of **24** was followed by the same procedure as the formation of sheets out of 1,6-dipentynyl substituted pyrene trimers with phosphodiester-bridges (**Py$_3$**, cooling rate 0.5°C/min) except that the adsorption was done on unmodified mica. Several experiments were performed, showing the formation of yarn-like structures (Figure 3.16, left) and round-shaped aggregates (Figure 3.16, right). The yarn-like structures had a quite uniform height of 0.8 nm. The round-shaped aggregates had a varying height of 30-90 nm. It seems like compound **24** did not self-assemble into defined 2D-structures.

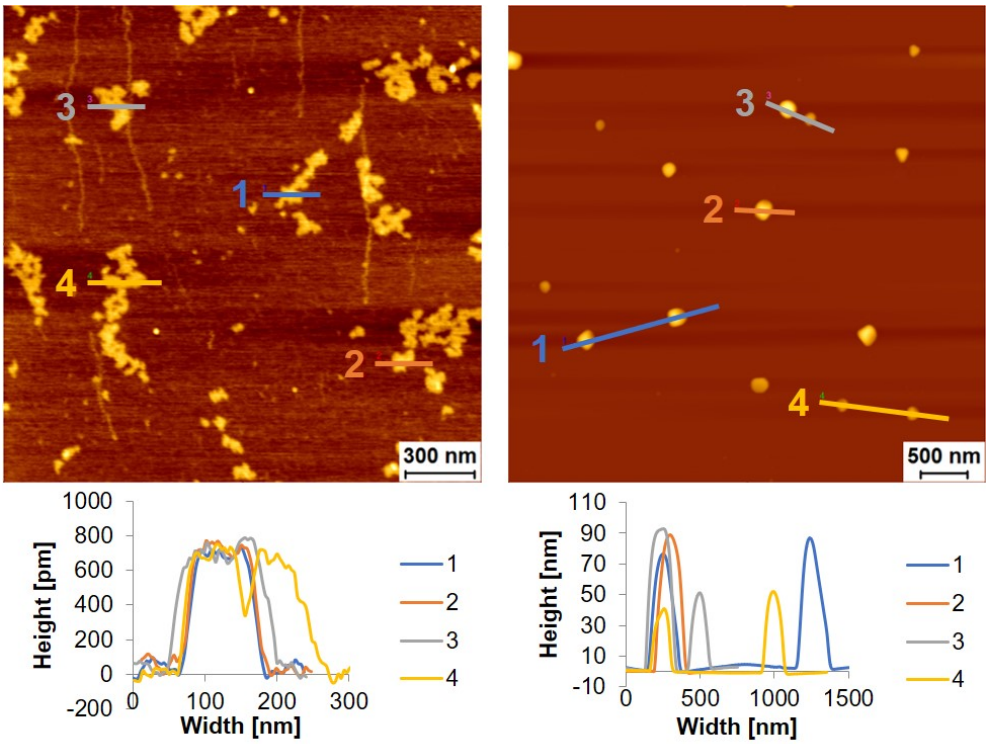

Figure 3.16. AFM measurements of the self-assembled **24** (6 µM) in 10 mM sodium acetate buffer (pH 4.71) and 240 mM NaCl on non-modified mica. Cooling rate: 13°C/min.

To increase the stability of the supramolecular polymers, the concentration of **24** was doubled to 12 µM. The same experiment as before was done: the concentration of sodium chloride was increased. One could observe the formation of the J-band at 305 nm already after the addition of 30 mM NaCl at 20°C. Adding more and more sodium chloride, the J-band reached a maximum after the addition of 60 mM NaCl and afterwards it decreased in intensity (Figure 3.17).
AFM measurements were done with the conditions where the highest intensity of the J-band was observed (60 mM NaCl). Only a few aggregates were deposited on the mica as shown on the left image in Figure 3.18. In a further experiment, the concentration of sodium chloride was doubled to 120 mM. Unfortunately, again only very few undefined aggregates were observed on the mica. There is the possibility that big aggregates were formed in solution and therefore, to find them on the mica is rather difficult. Also, it could be that they were already washed off the mica during the sample preparation due to their large size.

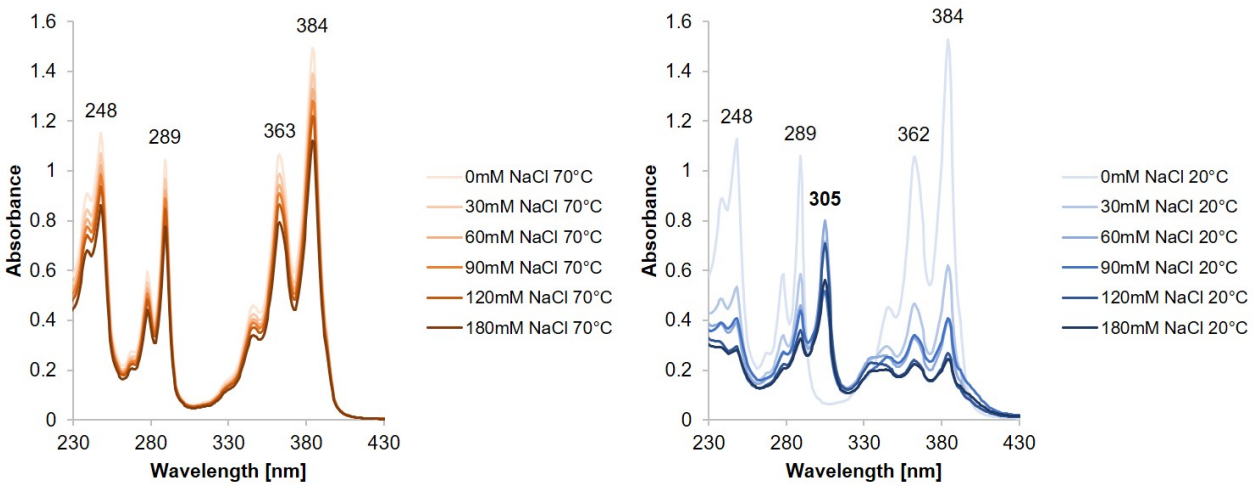

Figure 3.17. Absorption spectra of compound **24** at 70°C (left) and 20°C (right) in aqueous medium after additions of sodium chloride. Conditions: **24** (12 µM) in 10 mM sodium acetate buffer (pH 4.71), increasing concentrations of sodium chloride (0-180mM).

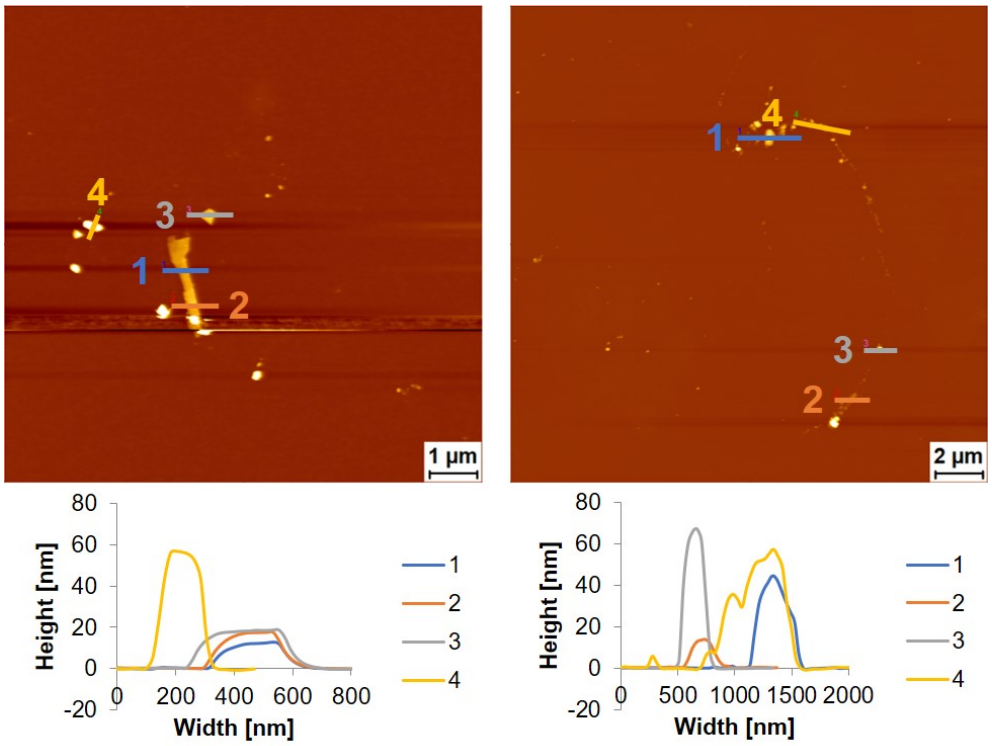

Figure 3.18. AFM measurements of the self-assembled **24** (12 µM) in 10 mM sodium acetate buffer (pH 4.71) and 60 mM NaCl (left) resp. 120 mM NaCl (right) on non-modified mica. Cooling rate: 13°C/min.

In addition to the AFM measurements, also the corresponding thermal UV-vis spectra were recorded of the conditions 6 µM **24** with 240 mM NaCl and 12 µM **24** with 60 mM and 120 mM NaCl (Figure 3.19). All of the spectra indicated a rather low melting point around 40°C. Starting with the sample 6 µM with 240 mM NaCl in sodium acetate buffer (10 mM, pH 4.71), the monomer **24**

starts to assemble at 37°C. After increasing the concentration to 12 µM **24**, Figure 3.19B shows that the aggregation of **24** starts at 42°C when 60 mM NaCl is added, and after doubling the sodium chloride concentration to 120 mM (Figure 3.19C) the self-assembly of **24** starts surprisingly at 37°C. The spectra showed, that the addition of sodium chloride did not help to increase the aggregation temperature of **24**. These low melting points are most likely the problem for the unreproducible AFM data when preparing the mica samples in a room with variable temperature. Unfortunately, neither the increase of the pyrene concentration nor sodium chloride concentration resulted in a higher melting point, and thus further investigations were stopped.

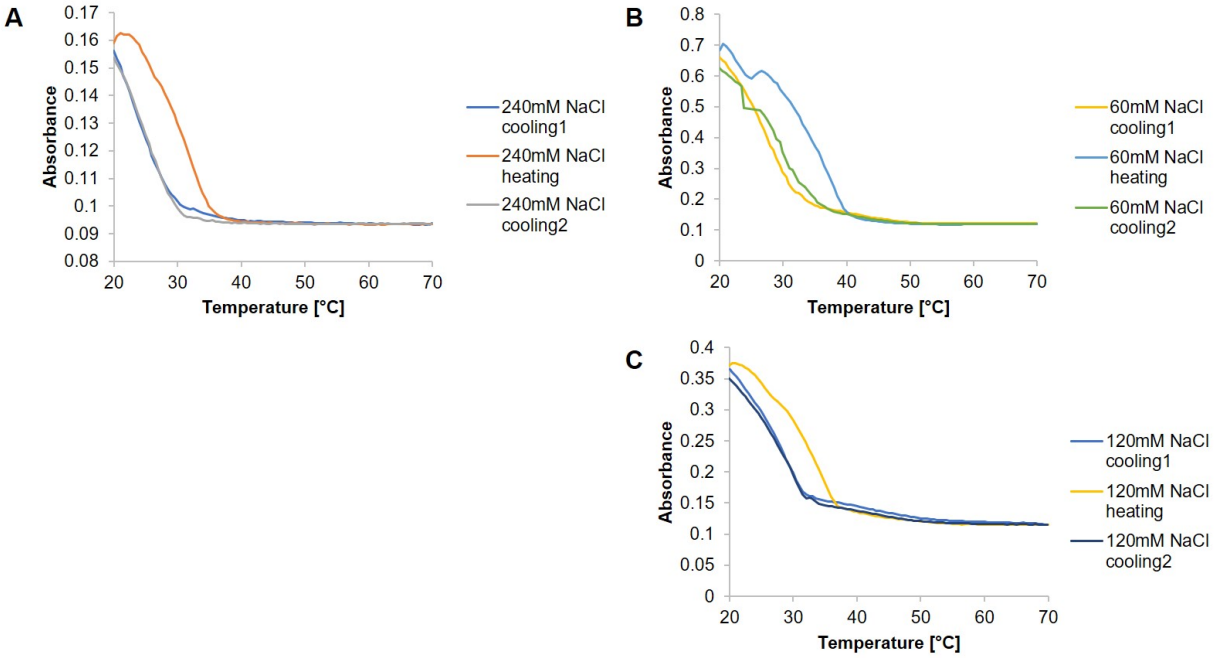

Figure 3.19. Thermal UV-vis spectra of compound **24** under different conditions: A) 6 µM **24** with 240 mM NaCl, B) 12 µM **24** with 60 mM NaCl, and C) 12 µM **24** with 120 mM NaCl, whereas all of them were in a solution of 10 mM sodium acetate buffer (pH 4.71). Cooling rate: 0.5°C/min, λ = 306 nm.

3.3.6. 4,4'-Dialkynyl Stilbene Oligoamine (32)

Synthesis of 32

4-Pentynyl-phthalimide and 4-pentyn-1-ol were added in a ratio of 1:1 to the commercially available 4,4'-dibromo-*trans*-stilbene **1**, in order to be coupled to **1** by a Sonogashira reaction. The purification of the desired products **28** and **29** was rather difficult, due to solubility problems and smearing on the column. Nevertheless, both products were isolated after several flash column chromatographies: **28** (11%) and **29** (12%). The phthalimide-group in compound **29** was deprotected with hydrazine in THF to obtain **30** (57%). The two hydroxyl-groups in compound **28** were oxidized to aldehydes with the Dess-Martin periodinane, which resulted in compound **31** (28%). The last reaction was the coupling of compounds **30** and **31** by a reductive amination to get the trimer **32** (20%) (Scheme 3.3).

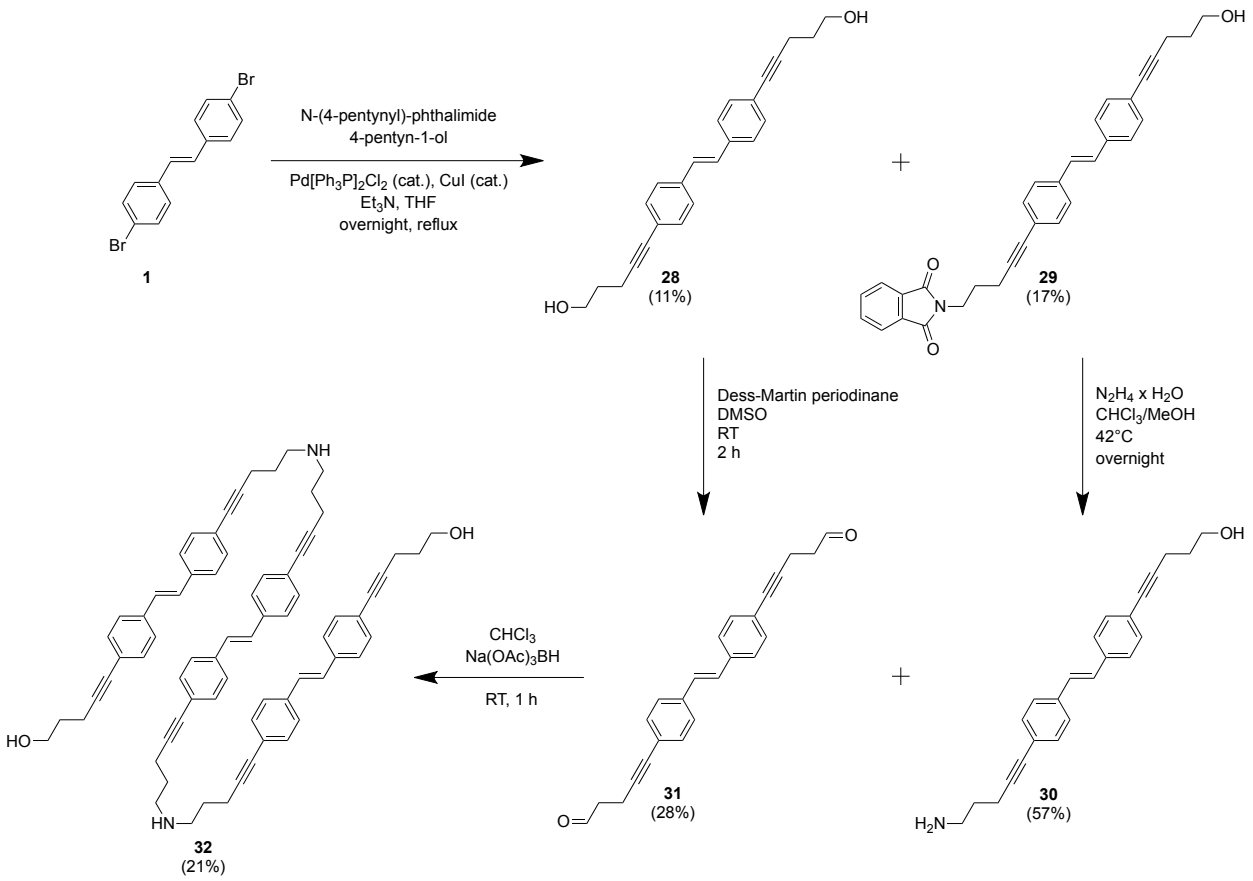

Scheme 3.6 Synthesis of amine-linked 4,4'-dipentynyl-substituted stilbene trimer (**32**).

Generally said, it was a challenge to dissolve the intermediate compounds for their purification but also afterwards, for the further synthesis steps. This had an impact on the yield. The solubility of trimer **32** was bad in water-miscible solvents, it could be dissolved only in a mixture of $CHCl_3$/MeOH (95:5 + 1% Et_3N). Nevertheless, UV-vis and fluorescence spectra were recorded under these conditions.

Spectroscopic Analysis of 32

Figure 3.20 shows the absorption spectra of **32** at two temperatures (58°C and 20°C), when dissolved in a mixture of $CHCl_3$/MeOH (95:5 + 1% Et_3N). The red curve indicates the UV-vis spectrum of **32** at 58°C with the maxima at 330, 342 and 361 nm and a small shoulder at 264 nm. These maxima were also observed in literature for trans-stilbene molecules.[143,144] After cooling to 20°C, the maxima stayed the same, except that the shoulder at 264 nm increased in intensity and evolved as a sharp peak. The induced blue-shift at 264 nm in the absorption spectrum is probably caused by H-aggregates. It is known from literature, that trans-stilbene molecules which are packed in a parallel array ("card pack") are the reason for this spectral shift.[145,146]

Fluorescence spectra at 58°C and 20°C were recorded when exciting the molecule at the wavelength 345 nm (Figure 3.21, left). The fluorescence maxima of **32** at both temperatures (58°C and 20°C)

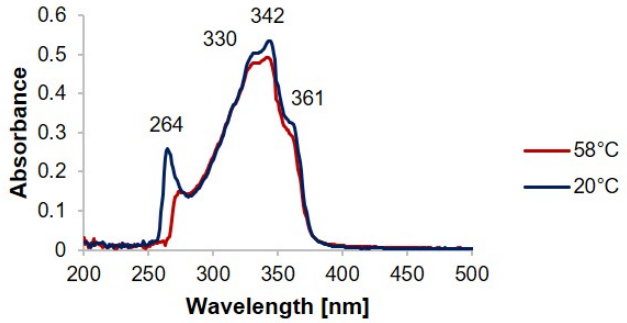

Figure 3.20. Absorption spectra of trimer **32** (20 µM) in a solvent mixture of $CHCl_3$/MeOH (95:5 + 1% Et_3N) at 20°C and 58°C.

are 374 nm, 394 nm, including a shoulder at 416 nm. The maxima in the excitation spectra are 343 and 361 nm (Figure 3.21, right), and thus similar to the absorption spectra which were previously shown (Figure 3.20). The only difference to the absorption spectra is the missing peak at 264 nm (20°C). As previously mentioned, the band at 264 nm is probably an H-band. H-bands reduce the fluorescence efficiency and thus the band cannot be observed in the excitation spectrum.

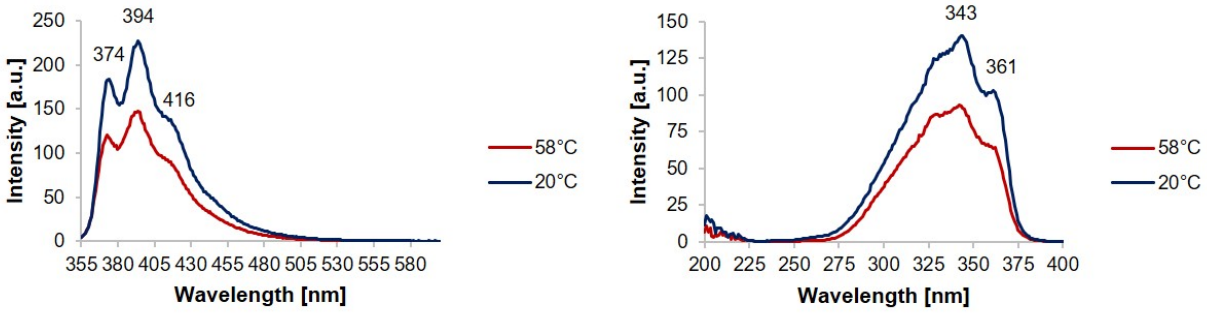

Figure 3.21. Fluorescence (left, λ_{ex} = 345 nm) and excitation (right, λ_{em} = 415 nm) spectra of trimer **32** (20 µM) in a solvent mixture of $CHCl_3$/MeOH (95:5 + 1% Et_3N) at 20°C and 58°C.

3.4. Conclusions and Outlook

Various amine-linked oligomers were successfully synthesized. The subsequent investigations regarding their self-assembly behavior led to different results.

The oligoamines 3,6-dialkynyl phenanthrene-pyrene-phenanthrene trimer (**15**), 2,7-dialkynyl phenanthrene trimer (**21**), and pyrene monomer (**24**) showed the formation of structures when measuring AFM. The self-assembly of oligoamine **15** in aqueous medium showed the formation of vesicles. AFM images indicated a diameter of 50-100 nm with a height of 5-6 nm. The formation of supramolecular polymers out of oligoamine **21** was tested under several conditions, whereas none of those lead to uniform structures. Sheets, undefined aggregates, small and large vesicular shaped assemblies were observed on AFM, which could not be reproduced. Pyrene monomer **24** showed various self-assembled structures on the AFM, which were not reproducible. Yarn-like structures, vesicles but

also undefined aggregates were observed.

The trimer 1,6-dialkynyl pyrene (**26**), the dimethylated species **27** and the 4,4'-dialkynyl stilbene trimer (**32**) were not soluble in water-miscible solvents and no further measurements in aqueous medium could be done. Both amines of the 1,6-dialkynyl pyrene trimer (**26**) were dimethylated to get a permanent positive charge on the trimer and as such increase the water solubility. Unfortunately, this did not help, and neither did the addition of salts and acids to **27** help to increase the solubility in DMSO. Absorption, fluorescence, and excitation spectra of the stilbene oligoamine **32** were measured in a mixture of $CHCl_3$/MeOH (95:5 + 1% Et_3N). The appearance of an H-band at 264 nm was observed.

Poly(ethylene glycols) (PEG) are known for their ability to increase the water solubility of molecules by attaching PEG to them.[147] To improve the solubility of the oligoamines in aqueous solution, it is worth a try to add PEG-linkers on the trimers. Also, another option would be to conduct the experiments with the oligoamines in apolar solvents. This would allow new adsorption methods on mica, such as spin-coating of mica for AFM measurements, which could lead to the formation of large-area and uniform aggregates.[65] Additionally, further investigations in light-harvesting properties of **N-Phe$_3$** will be done by using **15** as an acceptor (chapter 5 *Exploration of Light-Harvesting Properties of N-Phe$_3$*).

3.5. Experimental Part

3.5.1. Synthesis of Oligoamines

3,6-Dialkynyl Phenanthrene-Pyrene-Phenanthrene Oligoamine (15)

1,8-Dibromopyrene (12) and 1,6-Dibromopyrene (7)

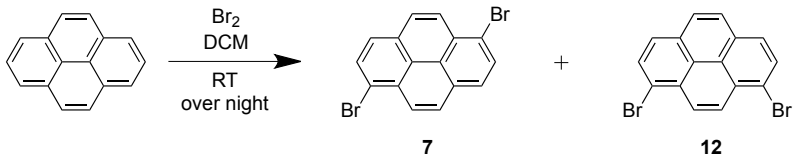

Scheme 3.7 Bromination of pyrene to obtain compounds **7** and **12**.

The procedure was done in analogy to a reference.[135] Pyrene (5.01 g, 0.0248 mol) was dissolved in DCM (88 ml). A solution of bromine (2.5 ml, 0.0485 mol) in DCM (68 ml) was added dropwise to the dissolved pyrene solution. The compounds **12** and **7** slowly precipitated as a grey solid. The mixture was stirred overnight at room temperature. After filtration, the precipitation was recrystallized out of toluene (270 ml). The forming crystals were a mixture of **12** and **7**, whereas compound **7** was present in excess (ratio 4:1). The filtrate was evaporated under reduced pressure and compound **12** was present in excess (ratio 5:3). Both compounds were tried to be separated better by several recrystallizations with toluene and hexane, but mostly a ratio of compounds **7**/**12** 6:4 was obtained. The mixture was used for further synthesis steps. ^{1}H-NMR (300 MHz, $CDCl_3$) of the mixture: δ 8.49 (s, 1H), 8.23 (d, J = 1.9 Hz, 1H), 8.05 – 7.97 (m, 2H).

5,5'-(pyrene-1,8-diyl)bis(pent-4-yn-1-ol) (13) and 5,5'-(pyrene-1,6-diyl)bis(pent-4-yn-1-ol) (8)

The mixture of compounds **12** and **7** (1.0151 g, 2.819 mmol) was dissolved in dry THF (23 ml) and degassed Et_3N (14 ml) under an argon atmosphere and heated to 84°C. 4-Pentyn-1-ol (1 ml, 11.1 mmol) was added, followed by the catalysts $Pd[PPh_3]_2Cl_2$ (46 mg, 0.066 mmol) and CuI (8.6 mg, 0.045 mmol). The reaction mixture was stirred and heated (84°C) under reflux overnight. The reaction mixture was filtrated, diluted with DCM (100 ml), washed with aq. citric acid (10%) (100 ml) and saturated aq. $NaHCO_3$ solution (100 ml). The washed organic phase was dried over Na_2SO_4 and the filtrate concentrated. Both formed compounds **13** and **8** could not be separated by recrystallization. A dry-load column chromatography was done for a separation of the compounds (DCM/toluene/MeOH 87:10:3). Compound **13** could be isolated as an almost pure yellow compound (409.9 mg). The impurities of Glaser coupling were removed by dissolving the compound in DCM (50 ml) and precipitation in cold hexane (150 ml). Compound **13** was isolated as a yellow solid (298 mg, 51%). Compound **8** was purely isolated from the column as a byproduct in respect to the further synthesis (R_f = 0.24 with DCM/MeOH 97:3, 191.1 mg, 18%). **13**: R_f = 0.16 (DCM/MeOH 97:3). ^{1}H-NMR (300 MHz, $CDCl_3$): δ 8.57 (s, 2H), 8.03 (s, 4H), 7.95 (s, 2H), 3.97 (t, J = 6.0 Hz, 4H), 2.79 (t, J = 6.8 Hz, 4H), 2.04 (p, J = 6.4 Hz, 5H). ^{13}C-NMR (75 MHz, $CDCl_3$) of the

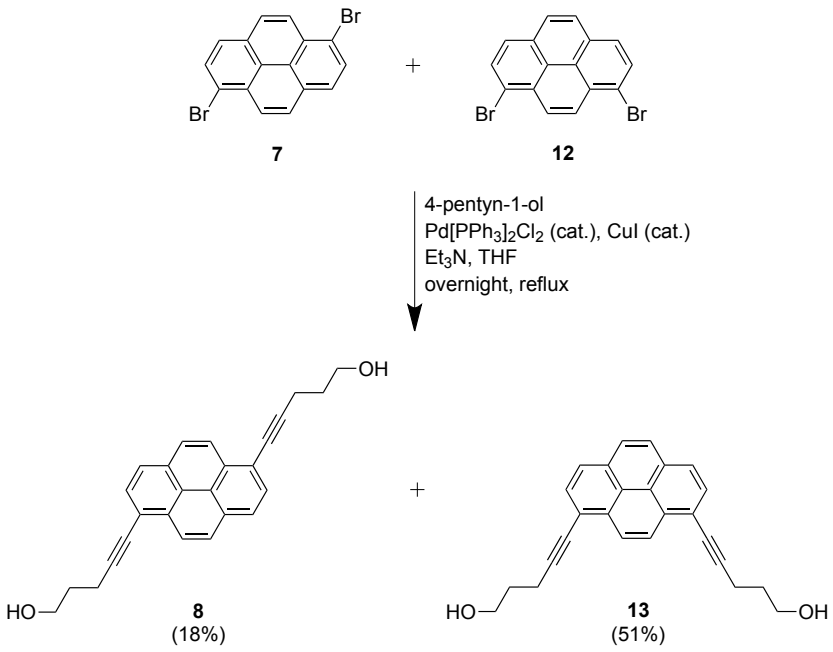

Scheme 3.8 Alkynation of both dibromopyrenes, **12** and **7**, by a Sonogashira reaction to obtain compounds **13** and **8**.

mixture: δ 131.91, 130.97, 129.93, 127.71, 126.32, 124.27, 119.03, 95.69, 80.21, 62.07, 31.79, 16.66. HRMS-NSI (m/z): $[M+Na]^+$ calcd for $C_{26}H_{22}O_2Na$: 389.15, found: 389.15.

5,5'-(pyrene-1,8-diyl)bis(pent-4-ynal) (14)

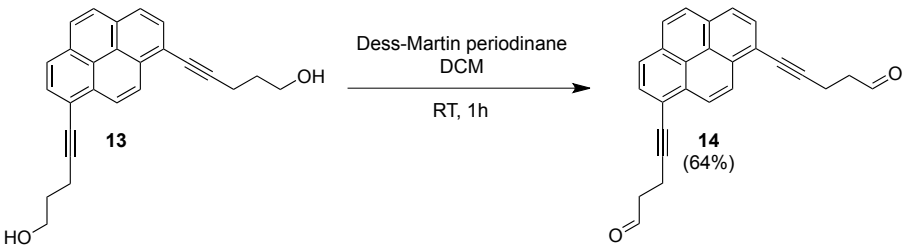

Scheme 3.9 Oxidation of the hydroxy groups from compound **13** to afford **14**.

Dess-Martin periodinane (DMP, 150.1 mg, 0.409 mmol) was dissolved in DCM (4.5 ml). A solution of compound **13** in DCM (4.5 ml) was added dropwise and the reaction mixture was stirred at room temperature for one hour. The reaction mixture was diluted with DCM (50 ml) and washed with sat. aq. $NaHCO_3$ solution containing 12.5 g $Na_2S_2O_3$ (50 ml), sat. aq. $NaHCO_3$ solution (50 ml) and brine (50 ml). The organic phase was dried over $MgSO_4$ and the filtrate concentrated in vacuo. A short dry-load column chromatography (hexane/EtOAc 3:1) was done. Compound **14** was isolated as a yellowish-white compound (94.6 mg, 64%). R_f = 0.56. ^{1}H-NMR (300 MHz, $CDCl_3$): δ 9.98 (s, 2H), 8.58 (s, 2H), 8.04 (d, J = 15.7Hz, 7H), 3.07 – 2.89 (m, 9H). ^{13}C-NMR (75 MHz, $CDCl_3$): δ 200.39, 131.88, 131.03, 129.90, 127.74, 126.26, 124.88, 124.14, 118.57, 93.94, 42.89, 13.23. HRMS-NSI (m/z): $[M]^+$ calcd for $C_{26}H_{18}O_2$: 362.13, found: 362.13.

5,5'-((((pyrene-1,8-diylbis(pent-4-yne-5,1-diyl))bis(azanediyl))bis(pent-1-yne-5,1-diyl))bis(phenanthrene-6,3-diyl))bis(pent-4-yn-1-ol)
(15)

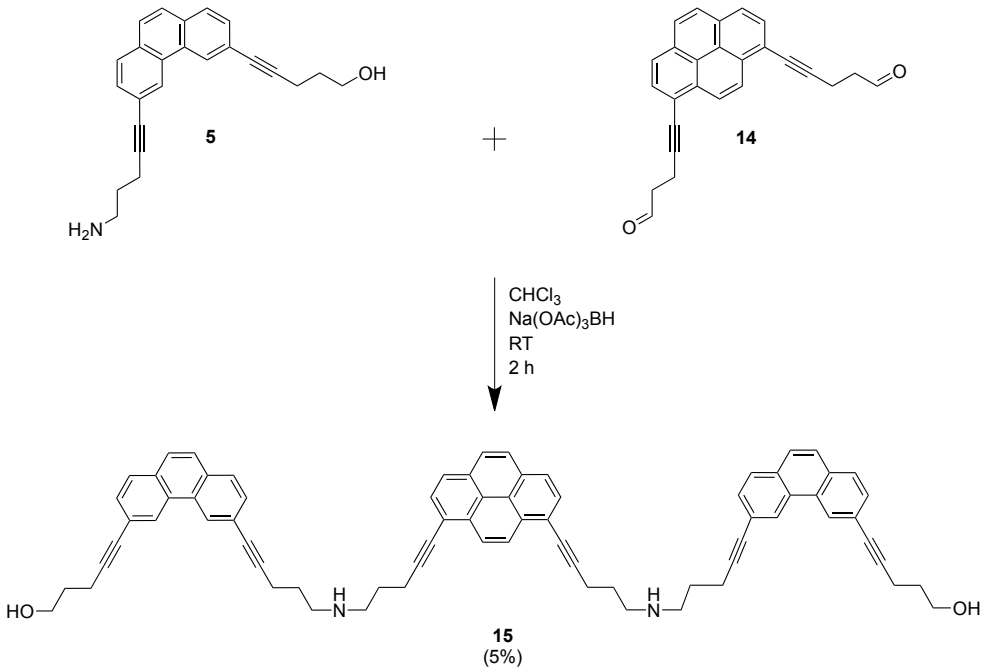

Scheme 3.10 Reductive amination of compounds **5** and **14** to obtain the **15**.

Compound **5** (18.84 mg, 0.0552 mmol) was dissolved in $CHCl_3$ (6 ml) followed by the addition of $Na(OAc)_3BH$ (23.8 mg, 0.1104 mmol). A solution of **14** (10.3 mg, 0.0276 mmol) in $CHCl_3$ (3 ml) was added dropwise over 30 minutes. The reaction mixture was stirred for three hours at room temperature. The reaction mixture was diluted with $CHCl_3$ (12 ml) and filtrated. The filtrate was washed twice with 2 M K_2CO_3 and dried over K_2CO_3. The solvent was concentrated under reduced pressure. A TLC plate was previously soaked in a solution of DCM + 1% Et_3N and let to dry. A basic preparative TLC was done (DCM/MeOH 95:5 + 1% Et_3N). Compound **15** was isolated as a white solid (1.3 mg, 5%). $R_f = 0.24$. HRMS-NSI (m/z): $[M+H]^+$ calcd for $C_{74}H_{65}N_2O_2$: 1013.5036, found: 1013.5041.

2,7-Dialkynyl Phenanthrene Oligoamine (21)

2-(5-(7-(5-hydroxypent-1-yn-1-yl)phenanthren-2-yl)pent-4-yn-1-yl)isoindoline-1,3-dione (17) and 5,5'-(phenanthrene-2,7-diyl)bis(pent-4-yn-1-ol)
(18)

The commercially available compound 2,7-dibromophenanthrene **16** (1.015 g, 3.021 mmol) was dissolved in dry THF (34 ml) and degassed Et_3N (17 ml) under an argon atmosphere. Afterwards, both catalysts, $Pd[Ph_3P]_2Cl_2$ (119.5 mg, 0.17 mmol) and CuI (53 mg, 0.27 mmol), were added. Next, 4-pentynyl-phthalimide (645.6 mg, 3.028 mmol) and 4-pentyn-1-ol (280 µl, 3.029 mmol) were added. The black solution was stirred and heated over night at 84°C under reflux. The reaction

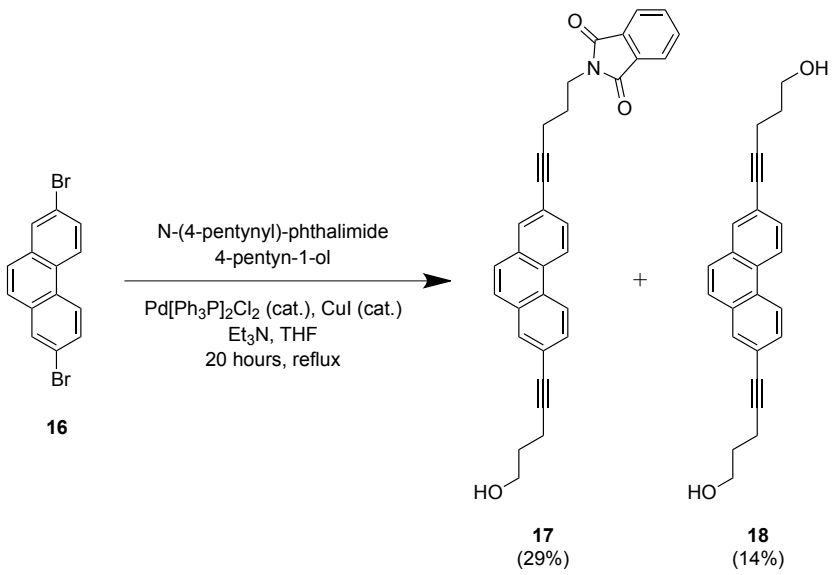

Scheme 3.11 Sonogashira reaction of compound **16** to obtain compounds **17** and **18**.

mixture was filtrated over Celite 503, and washed with aq. citric acid (10%) and sat. aq. $NaHCO_3$ solution. The solution was dried over Na_2SO_4 and concentrated in vacuo. A dry-load silica-gel column chromatography was done (hexane/EtOAc 4:1). Compound **17** was isolated as an orange-yellowish solid (406.4 mg, 29%). Compound **18** was isolated as an orange solid (142.8 mg, 14%). **17**: R_f = 0.41. ^{1}H-NMR (300 MHz, $CDCl_3$): δ 8.54 – 8.40 (m, 2H), 7.91 (d, J = 1.5 Hz, 1H), 7.85 – 7.71 (m, 3H), 7.68 – 7.55 (m, 5H), 7.55 – 7.46 (m, 1H), 3.96 – 3.83 (m, 4H), 2.67 – 2.52 (m, 4H), 2.08 (p, J = 6.9 Hz, 2H), 1.92 (p, J = 6.7 Hz, 2H). ^{13}C-NMR (75 MHz, $CDCl_3$): δ 168.62, 133.98, 132.30, 132.02, 131.68, 129.73, 129.33, 127.01, 123.34, 122.75, 122.15, 90.54, 90.07, 62.01, 37.62, 31.56, 27.43, 17.63, 16.29. HRMS-NSI (m/z): $[M+H]^+$ calcd for $C_{32}H_{26}NO_3$: 472.1897, found: 472.1907. **18**: R_f = 0.32. ^{1}H-NMR (300 MHz, $CDCl_3$): δ 8.53 (d, J = 8.6 Hz, 2H), 7.92 (d, J = 1.6 Hz, 2H), 7.68 – 7.58 (m, 4H), 3.94 – 3.82 (m, 4H), 2.62 (t, J = 6.9 Hz, 4H), 1.92 (p, J = 6.8 Hz, 4H). ^{13}C-NMR (75 MHz, $CDCl_3$): δ 132.07, 131.81, 129.79, 129.36, 127.16, 122.25, 117.61, 90.57, 62.04, 31.57, 16.30. HRMS-NSI (m/z): $[M+H]^+$ calcd for $C_{24}H_{23}O_2$: 343.1691, found: 343.1693.

5-(7-(5-Aminopent-1-yn-1-yl)phenanthren-2-yl)pent-4-yn-1-ol (19)

Compound **17** (50 mg, 0.106 mmol) was dissolved in THF (2.1 ml). The solution was heated to 48°C while stirring. Hydrazine-monohydrate (0.05 ml, 1.031 mmol) was added and the reaction stirred overnight at 48°C. The grey precipitation was filtrated off and the filtrate was diluted with DCM (25 ml). The compound was extracted two times with aq. 2 M K_2CO_3 (2x 20 ml). The organic phase was dried over K_2CO_3 and the solvent evaporated under reduced pressure. A dry-load column chromatography was done (DCM/MeOH 9:1 + 2% Et_3N). Compound **19** was gained as a solid (26.1 mg, 72%). R_f = 0.25 (DCM/MeOH 4:1). ^{1}H-NMR (300 MHz, $CDCl_3$): δ 8.53 (d, J = 8.6 Hz, 2H), 7.95 – 7.88 (m, 2H), 7.68 – 7.58 (m, 4H), 3.88 (t, J = 6.1 Hz, 2H), 2.92 (t, J = 6.9 Hz, 2H), 2.67 – 2.51 (m, 4H), 1.92 (p, J = 6.8 Hz, 2H), 1.80 (p, J = 6.9 Hz, 2H), 1.25 (s, 6H). ^{13}C-NMR (75 MHz, DMSO−d_6): δ 131.62, 131.23, 129.49, 128.58, 127.00, 123.48, 121.84, 117.00,

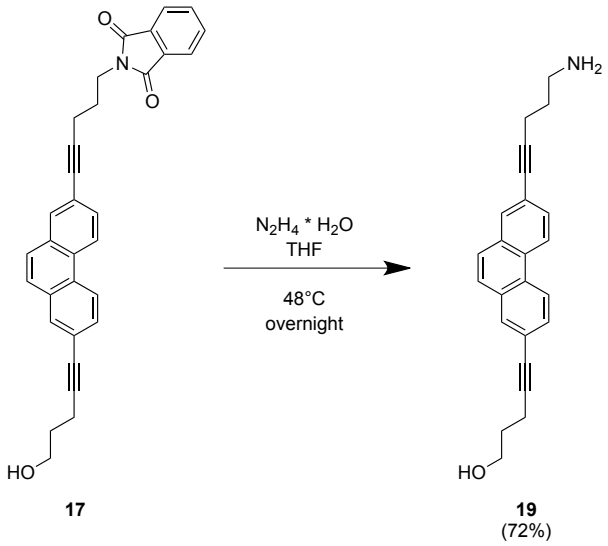

Scheme 3.12 Deprotection of the amine in the phthalimide of compound **17** to obtain compound **19**.

91.93, 59.46, 31.57, 16.26, 15.45. HRMS-NSI (m/z): $[M+H]^+$ calcd for $C_{24}H_{24}NO$: 342.1862, found: 342.1852.

5,5'-(Phenanthrene-2,7-diyl)bis(pent-4-ynal) (20)

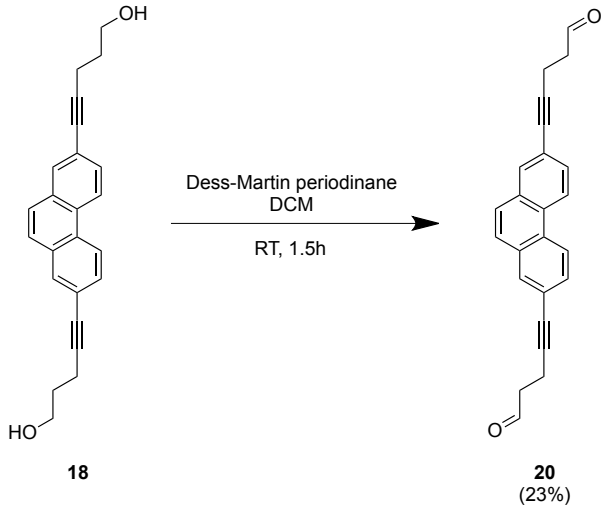

Scheme 3.13 Dess-Martin oxidation of compound **18** to obtain compound **20**.

The procedure was carried out analog to reference.[132] Dess-Martin periodinane (DMP) (178.9 mg, 0.26 mmol) was dissolved in DCM (1 ml) and the solution stirred. A solution of compound **18** (65.1 mg, 0.19 mmol) in DCM (3.5 ml) was added dropwise and stirred for 1.5 hours. The reaction mixture was diluted with DCM (25 ml) and washed with sat. aq. $NaHCO_3$ solution containing 6.5 g $Na_2S_2O_3$ (25 ml), sat. aq. $NaHCO_3$ solution (25 ml) and brine (25 ml). The organic phase was dried over $MgSO_4$ and the solvent evaporated under reduced pressure. A dry-load silica-gel column chromatography (hexane/EtOAc 3:1) was done to remove the remaining DMP ($R_f = 0.05$).

The product was gained as a white yellowish solid (15 mg, 23%). R_f = 0.5. ^{1}H-NMR (300 MHz, $CDCl_3$): δ 9.90 (s, 2H), 8.52 (d, J = 8.6 Hz, 2H), 7.91 (d, J = 1.6 Hz, 2H), 7.68 – 7.57 (m, 4H), 2.82 (s, 8H). ^{13}C-NMR (75 MHz, $CDCl_3$): δ 200.52, 132.06, 131.91, 129.76, 129.46, 127.19, 122.98, 121.93, 88.98, 81.65, 42.79, 12.97. HRMS-NSI (m/z): $[M+Na]^+$ calcd for $C_{24}H_{18}O_2Na$: 361.1207, found: 361.1199.

5,5'-((((Phenanthrene-2,7-diylbis(pent-4-yne-5,1-diyl))bis(azanediyl))bis(pent-1-yne-5,1-diyl))bis(phenanthrene-7,2-diyl))bis(pent-4-yn-1-ol)
(21)

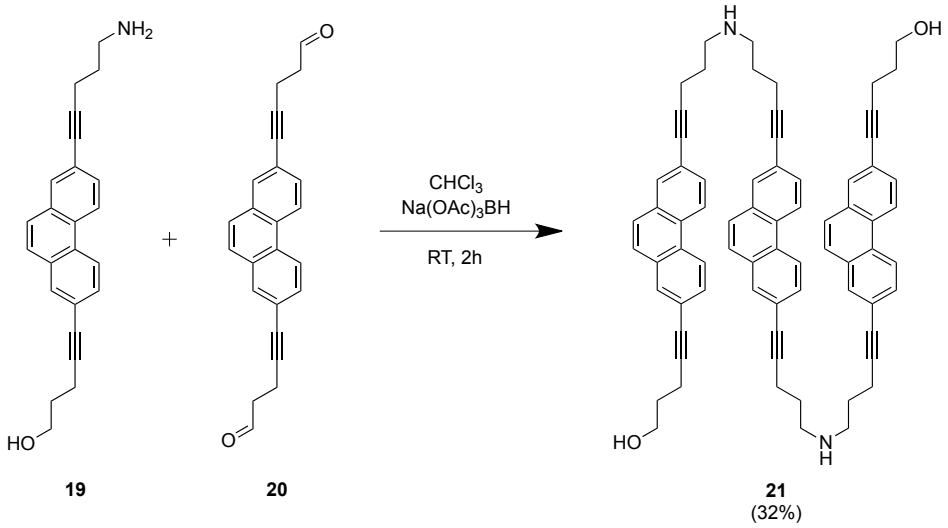

Scheme 3.14 Reductive amination of compounds **19** (2 eq.) and **20** (1 eq.) to obtain trimer **21**.

The procedure was carried out analog to reference.[133] Compound **19** (22.7 mg, 0.0664 mmol) was dissolved in $CHCl_3$ (6 ml), and afterwards $Na(OAc)_3BH$ (28.5 mg, 0.135 mmol) was added. A solution of compound **20** (12.5 mg, 0.0369 mmol) in $CHCl_3$ (3 ml) was added dropwise and the reaction was stirred for two hours. The reaction mixture was diluted with $CHCl_3$ (15 ml), and washed twice with aq. 2 M K_2CO_3 solution. The $CHCl_3$-phase was dried over K_2CO_3 and the filtrate concentrated under reduced pressure. A silica-gel TLC plate (1 mm thick) was soaked in DCM + 1% Et_3N and let it dry. A preparative TLC was done of the crude **21** (DCM/MeOH 95:5 + 1% Et_3N). Compound **21** was dissolved out of the silica-gel with DCM/MeOH (4:1 + 1% Et_3N) (100 ml) and filtrated. The filtrate was evaporated under reduced pressure and a white-yellowish solid was gained. Two additional preparative TLCs had to be done to purify the product **21** (11.6 mg, 32%). R_f = 0.08. HRMS-NSI (m/z): $[M+H]^+$ calcd for $C_{72}H_{65}N_2O_2$: 989.5017, found: 989.5041.

1,6-Dialkynyl Pyrene Oligoamine (26)

2-(6-(6-(6-hydroxyhex-1-yn-1-yl)pyren-1-yl)hex-5-yn-1-yl)isoindoline-1,3-dione (22) and 6,6'-(pyrene-1,6-diyl)bis(hex-5-yn-1-ol) (23)

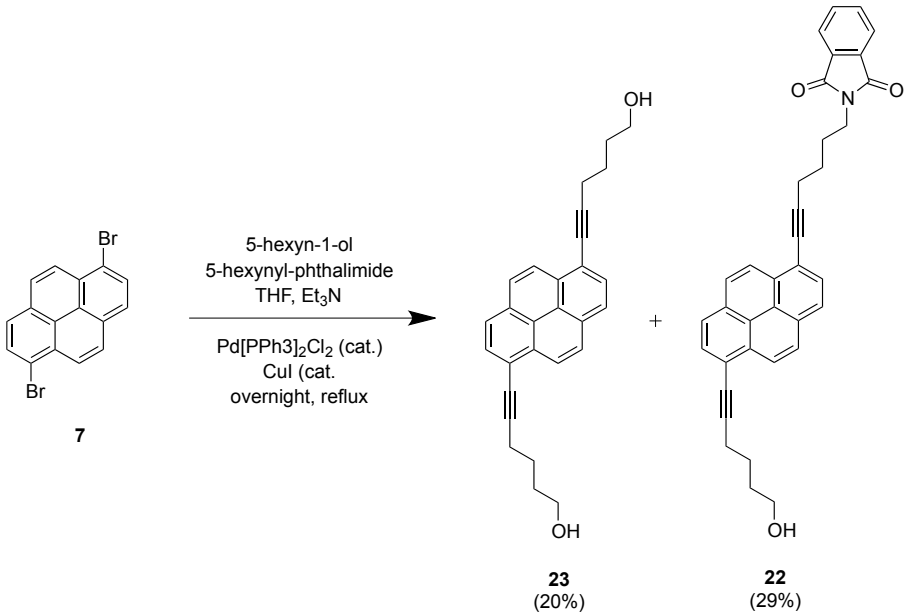

Scheme 3.15 Sonogashira reaction using compound **7** as a starting material to obtain compounds **22** and **23**.

The commercially available compound 1,6-dibromopyrene **7** (253.6 g, 0.704 mmol) was dissolved in dry THF (8.5 ml) and degassed Et_3N (4.2 ml) under an argon atmosphere. Afterwards, both catalysts $Pd[Ph_3P]_2Cl_2$ (28.4 mg, 0.041 mmol) and CuI (13 mg, 0.069 mmol) were added. Next, 5-hexynyl-phthalimide (160.2 mg, 0.705 mmol) and 5-hexyn-1-ol (77.7 µl, 0.705 mmol) were added. The black solution was stirred and heated under reflux (84°C) over night. The reaction was controlled via TLC (hexane/EtOAc 1:1). The mixture was filtrated over Celite 503, washed with aq. citric acid (10%) and sat. aq. $NaHCO_3$ solution. The solution was dried over Na_2SO_4 and the solvent removed under reduced pressure. A dry-load silica-gel column chromatography was done for purification of the molecules **22** and **23** (hexane/EtOAc 4:1). Compound **22** was isolated as an orange-yellowish solid (54.5 mg, 15%). Compound **23** was isolated as an orange solid (28.9 mg, 10%). **22**: R_f = 0.47, ^{1}H-NMR (300 MHz, $CDCl_3$): δ 8.57 – 8.46 (m, 2H), 8.14 – 8.01 (m, 6H), 7.89 – 7.77 (m, 2H), 7.73 – 7.61 (m, 2H), 3.88 – 3.75 (m, 4H), 2.77 – 2.66 (m, 4H), 2.10 – 1.95 (m, 2H), 1.95 – 1.75 (m, 6H). ^{13}C-NMR (75 MHz, $CDCl_3$): δ 134.01, 132.28, 132.13, 130.84, 130.81, 130.08, 130.00, 128.04, 126.18, 126.10, 124.95, 123.34, 119.18, 62.69, 37.74, 32.25, 28.14, 26.33, 25.45, 19.91, 19.69. HRMS-NSI (m/z): $[M]^+$ calcd for $C_{36}H_{29}NO_3$: 523.2126, found: 523.2142. **23**: R_f = 0.41, ^{1}H-NMR (300 MHz, $CDCl_3$): δ 8.54 (d, J = 9.1 Hz, 2H), 8.14 – 8.02 (m, 6H), 3.85 – 3.75 (m, 4H), 2.76 – 2.66 (m, 4H), 1.88 (p, J = 3.2 Hz, 8H). ^{13}C-NMR (75 MHz, $CDCl_3$): δ 132.14, 130.82, 130.04, 128.03, 126.13, 124.97, 124.39, 119.24, 96.21, 62.70, 32.25, 25.45, 19.91. HRMS-NSI (m/z): $[M+H]^+$ calcd for $C_{28}H_{27}O_2$: 395.2001, found: 395.2006.

6-(6-(6-aminohex-1-yn-1-yl)pyren-1-yl)hex-5-yn-1-ol (24)

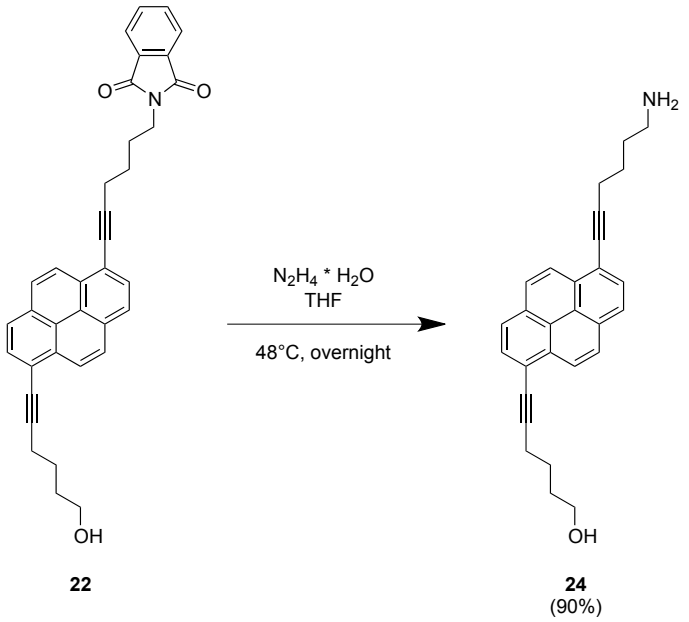

Scheme 3.16 Deprotection of the amine in the phthalimide of compound **22** to obtain compound **24**.

Compound **22** (314 mg, 0.599 mmol) was dissolved in THF (12 ml). The flask was heated to 48°C while stirring. Hydrazine-monohydrate (0.24 ml, 4.79 mmol) was added and the reaction stirred overnight at 48°C. The grey precipitation was filtrated off and the filtrate was diluted with DCM (80 ml). The compound was extracted two times with aq. 2 M K_2CO_3 (2x 80 ml). The organic phase was dried over K_2CO_3 and the solvent evaporated under reduced pressure. A dry-load silica-gel column chromatography was done to purify the product (DCM/MeOH 9:1 + 2% Et_3N). Compound **24** was gained as a solid (212.2 mg, 90%). R_f = 0.18 (DCM/MeOH 4:1), ^{1}H-NMR (300 MHz, DMSO−d_6): δ 8.48 (d, J = 9.1 Hz, 2H), 8.27 (d, J = 8.6 Hz, 4H), 8.12 (d, J = 8.0 Hz, 2H), 3.52 (d, J = 11.9 Hz, 2H), 2.74 – 2.59 (m, 6H), 2.53 – 2.46 (m, 2H), 1.81 – 1.53 (m, 9H). ^{13}C-NMR (75 MHz, DMSO−d_6): δ 131.15, 130.14, 129.89, 128.28, 125.35, 123.38, 118.68, 97.44, 79.15, 60.25, 41.20, 32.71, 31.89, 25.86, 25.09, 19.03. HRMS-NSI (m/z): $[M+H]^+$ calcd for $C_{28}H_{28}NO$: 394.2174, found: 394.2165.

6,6'-(pyrene-1,6-diyl)bis(hex-5-ynal) (25)

The procedure was carried out analog to reference.[132] Dess-Martin periodinane (DMP) (849.4 mg, 2.003 mmol) was dissolved in DCM (9 ml) and the solution stirred. A solution of compound **23** (333.2 mg, 0.845 mmol) in DCM (30.3 ml) was added dropwise and afterwards stirred for two hours at room temperature. The reaction mixture was diluted with DCM (80 ml) and washed with sat. aq. $NaHCO_3$ solution containing 25 g $Na_2S_2O_3$ (100 ml), sat. aq. $NaHCO_3$ solution (100 ml) and brine (100 ml). The organic phase was dried over $MgSO_4$ and the solvent evaporated under reduced pressure. A dry-load silica-gel column chromatography (hexane/EtOAc 2:1) was done to remove the remaining DMP (R_f = 0.05). The product **25** was afforded as a white yellowish solid (245.8 mg,

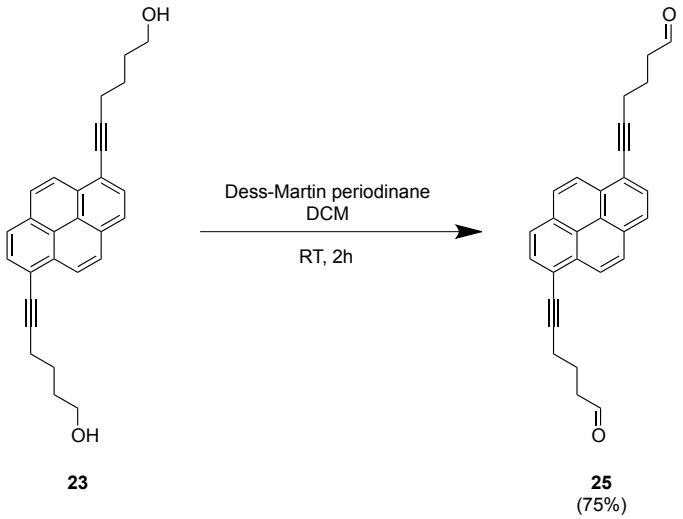

Scheme 3.17 Dess-Martin oxidation of compound **23** to obtain compound **25**.

75%). $R_f = 0.75$, ^{1}H-NMR (300 MHz, $CDCl_3$): δ 9.91 (t, $J = 1.2$ Hz, 2H), 8.52 (d, $J = 9.1$ Hz, 2H), 8.15 – 8.03 (m, 6H), 2.85 – 2.69 (m, 8H), 2.11 (p, $J = 7.0$ Hz, 4H). ^{13}C-NMR (75 MHz, $CDCl_3$): δ 201.96, 132.14, 130.92, 130.11, 128.12, 126.11, 125.05, 124.35, 118.95, 117.62, 95.06, 43.13, 21.57, 19.53. HRMS-NSI (m/z): $[M]^+$ calcd for $C_{28}H_{22}O_2$: 390.1618, found: 390.1614.

6,6'-((((pyrene-1,6-diylbis(hex-5-yne-6,1-diyl))bis(azanediyl))bis(hex-1-yne-6,1-diyl))bis(pyrene-6,1-diyl))bis(hex-5-yn-1-ol) (26)

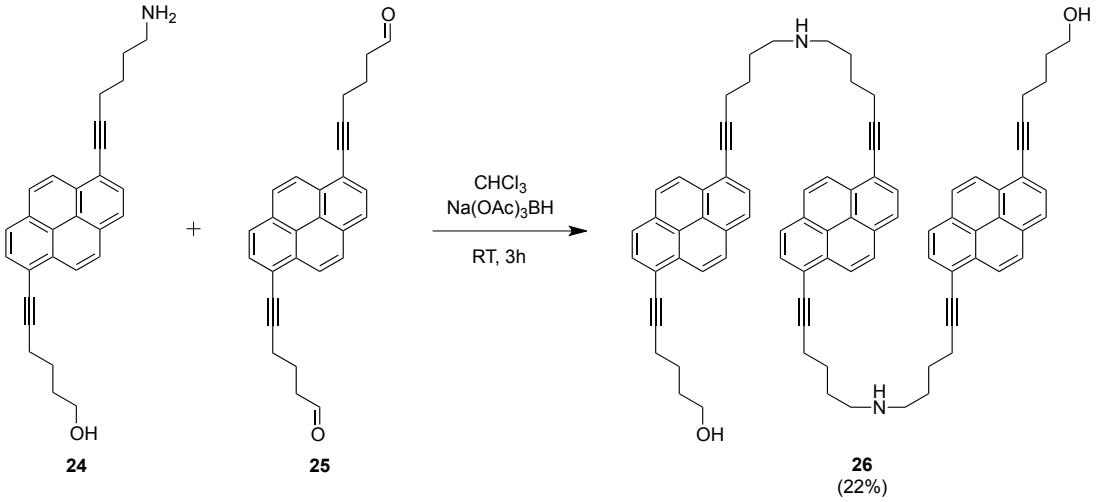

Scheme 3.18 Reductive amination of compounds **24** (2 eq.) and **25** (1 eq.) to obtain trimer **26**.

The procedure was carried out in analogy to reference.[133] To a solution of compound **24** (124.5 mg, 0.316 mmol) in $CHCl_3$ (20 ml), $Na(OAc)_3BH$ (143 mg, 0.664 mmol) was added. A solution of compound **25** (64.9 mg, 0.166 mmol) in $CHCl_3$ (1.65 ml) was added dropwise. The reaction was stirred for three hours at room temperature. The reaction mixture was diluted with $CHCl_3$ (90 ml),

and washed twice with aq. 2 M K_2CO_3 solution (2x 100 ml). The $CHCl_3$-phase was dried over K_2CO_3 and the filtrate concentrated under reduced pressure. A liquid-load silica-gel column chromatography was done (R_f = 0.17, DCM/MeOH 98:2 + 1% Et_3N). Another column had to be done but with a different solvent - DCM/toluene/MeOH 87:10:3 + 1% Et_3N. Compound **26** was gained as a brownish solid (11.8 mg, 22%). R_f = 0.14, HRMS-NSI (*m/z*): $[M+H]^+$ calcd for $C_{84}H_{77}O_2N_2$: 1145.5957, found: 1145.5980.

1,6-Dialkynyl Pyrene with Dimethylated Amines (27)

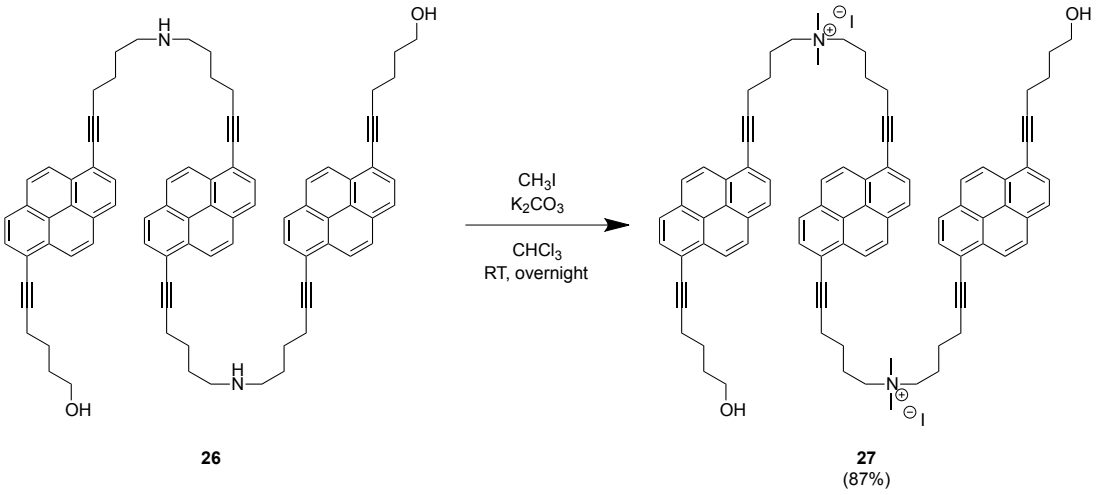

Scheme 3.19 Dimethylation of the amines in compound **26** to obtain compound **27**.

The procedure was carried out in analogy to the reference.[139] The previously described trimer **26** was used as a starting material for the dimethylation of its amines. Compound **26** (11.8 mg, 0.0103 mmol) was dissolved in chloroform (8 ml). Potassium carbonate (115.3 mg, 0.834 mmol) was pestled and added to the dissolved compound **26**. Methyl iodide (0.11 ml, 1.545 mmol) was added dropwise to the mixture, and the reaction stirred overnight at room temperature. The reaction process was controlled by TLC (DCM/MeOH 95:5 + 1% Et_3N, (R_f = 0). The mixture was filtrated to remove the potassium carbonate and the solution washed with water. The organic phase was dried over K_2CO_3 and evaporated under reduced pressure. **27** was isolated as a brown sticky solid (13.1 mg, 87%). HRMS-NSI (*m/z*): $[M+2H]^{2+}$ calcd for $C_{88}H_{86}O_2N_2$: 601.3338, found: 601.3339.

4,4'-Dialkynyl Stilbene Oligoamine (32)

(E)-5,5'-(ethene-1,2-diylbis(4,1-phenylene))bis(pent-4-yn-1-ol) (28) and (E)-2-(5-(4-(4-(5-hydroxypent-1-yn-1-yl)styryl)phenyl)pent-4-yn-1-yl)isoindoline-1,3-dione (29)

The commercially available 4,4'-dibromo-*trans*-stilbene (**1**) (1.0078 g, 2.981 mmol) was dissolved in dry THF (35 ml) and degassed Et_3N (17 ml). Both catalysts $Pd[Ph_3P]_2Cl_2$ (116.6 mg, 0.166 mmol) and CuI (52.6 mg, 0.276 mmol) were added. Next, 4-pentynyl-phthalimide (635.8 mg, 2.981 mmol) and 4-pentyn-1-ol (275.6 µl, 2.981 mmol) were added. The black mixture was stirred and heated

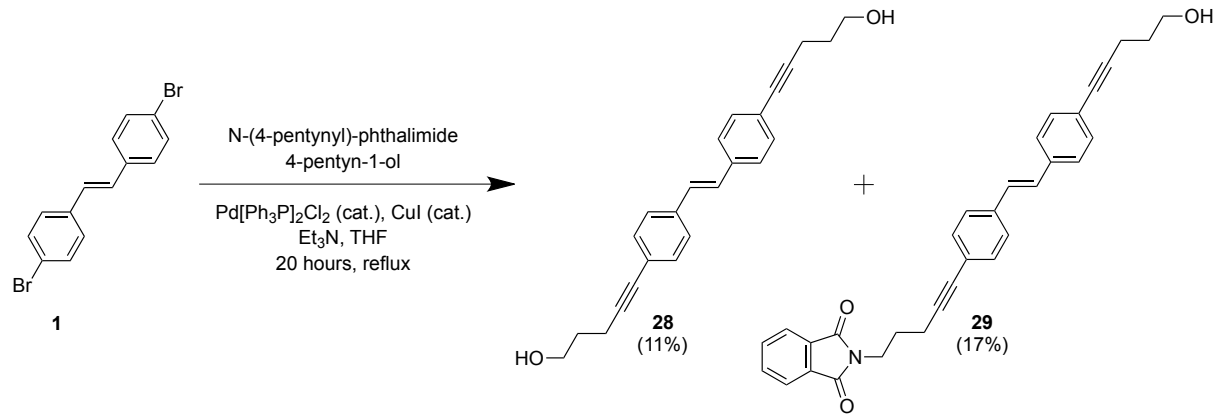

Scheme 3.20 Alkylation of **1** by a Sonogashira reaction to afford **28** and **29**.

under reflux (84°C) overnight. The reaction mixture was diluted with DCM (100 ml), filtrated over Celite 503, washed with aq. citric acid (10%) and sat. aq. $NaHCO_3$ solution. The filtrate was dried over Na_2SO_4 and the solvent removed under reduced pressure. A dry-load silica-gel column chromatography was done to roughly separate the molecules **28** and **29** (DCM/MeOH 99:1). Crude product **28** (120 mg) was repurified by a flash column chromatography on silica-gel (DCM/toluene/MeOH 88:10:2). Further, the crude **28** was dissolved in a mixture of $CHCl_3$/MeOH (4:1) (2 ml) and precipitated with an excess of cold hexane. The precipitation was filtrated and a pure **28** was afforded (53.3 mg). The crude product **29** (620 mg) was also repurified by a flash column chromatography on silica-gel (DCM/MeOH 99:1). The afforded **29** (423.1 mg) from the column was precipitated by dissolving it in a mixture of $CHCl_3$/MeOH (3:1) (2 ml), followed by the addition of an excess cold hexane. The precipitation was filtrated and a pure **29** was obtained (245.1 mg, 17%). This column additionally afforded pure **28** (total: 114.2 mg, 11%). **28**: R_f = 0.33 (DCM/toluene/MeOH 86:10:4). ^{1}H-NMR (300 MHz, DMSO-d_6): δ 7.57 (d, J = 8.1 Hz, 4H), 7.38 (d, J = 8.0 Hz, 4H), 7.27 (s, 2H), 4.54 (t, J = 5.0 Hz, 2H), 3.61 – 3.43 (m, 4H), 2.49 – 2.37 (m, 4H), 1.69 (p, J = 6.6 Hz, 4H). ^{13}C-NMR (75 MHz, DMSO-d_6): δ 136.40, 131.58, 128.44, 126.66, 122.44, 91.64, 80.53, 59.43, 31.57, 15.42. HRMS-NSI (m/z): $[M]^+$ calcd for $C_{24}H_{24}O_2$: 344.1771, found: 344.1771. **29**: R_f = 0.47 (hexane/EtOAc 1:1). ^{1}H-NMR (300 MHz, DMSO-d_6): δ 77.88 – 7.78 (m, 4H), 7.61 – 7.47 (m, 4H), 7.37 (d, J = 8.3 Hz, 2H), 7.28 – 7.16 (m, 4H), 4.54 (t, J = 5.2 Hz, 1H), 3.74 (t, J = 6.7 Hz, 2H), 3.58 – 3.46 (m, 2H), 2.50 – 2.41 (m, 4H), 1.90 (p, J = 6.6 Hz, 2H), 1.69 (p, J = 6.7 Hz, 2H). ^{13}C-NMR (75 MHz, DMSO-d_6): δ 168.02, 134.28, 131.73, 131.58, 131.43, 128.45, 128.42, 126.66, 122.99, 122.14, 117.01, 91.64, 90.87, 80.85, 59.43, 36.95, 31.57, 16.64, 15.42. HRMS-NSI (m/z): $[M+H]^+$ calcd for $C_{32}H_{28}O_3N$: 474.2078, found: 474.2064.

(E)-5-(4-(4-(5-aminopent-1-yn-1-yl)styryl)phenyl)pent-4-yn-1-ol (30)

Compound **29** (76.5 mg, 0.162 mmol) was dissolved in a mixture of $CHCl_3$ (5 ml) and MeOH (3 ml). The solution was heated to 48°C while stirring. Hydrazine-monohydrate (0.07 ml, 1.292 mmol) was added and the reaction stirred overnight at 48°C. The reaction mixture was diluted with DCM (60 ml) and a white precipitation formed. The precipitation was filtered off and the filtrate extracted two times with aq. 2 M K_2CO_3 (2x 60 ml). The organic phase was dried over K_2CO_3 and the solvent

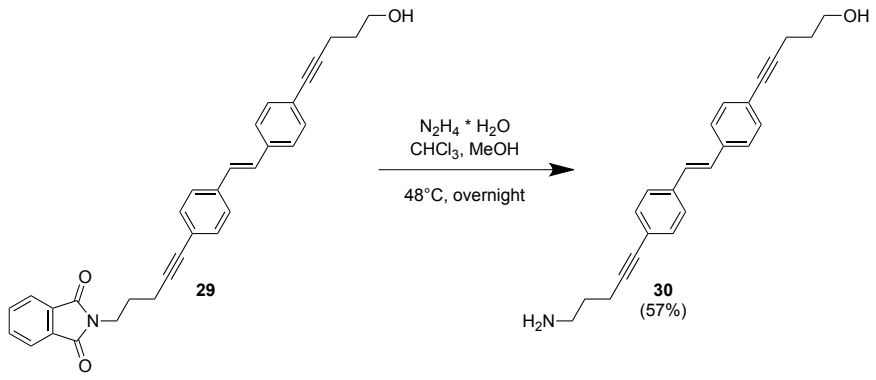

Scheme 3.21 Hydrolysis of the phthalimide in **29** to afford compound **30**.

evaporated under reduced pressure. A liquid-load column chromatography was done (DCM/MeOH 9:1 + 2% Et_3N). Compound **30** was gained as a solid (31.7 mg, 57%). R_f = 0.28 (DCM/MeOH 4:1). ^{1}H-NMR (300 MHz, DMSO-d_6: δ 7.67 – 7.50 (m, 3H), 7.42 – 7.30 (m, 3H), 7.29 – 7.23 (m, 2H), 7.21 – 7.05 (m, 2H), 3.60 – 3.44 (m, 2H), 2.91 – 2.78 (m, 2H), 2.71 – 2.55 (m, 2H), 2.48 – 2.31 (m, 4H), 1.74 – 1.55 (m, 4H). HRMS-NSI (m/z): $[M+H]^+$ calcd for $C_{24}H_{26}ON$: 344.2002, found: 344.2009.

(E)-5,5'-(ethene-1,2-diylbis(4,1-phenylene))bis(pent-4-ynal) (31)

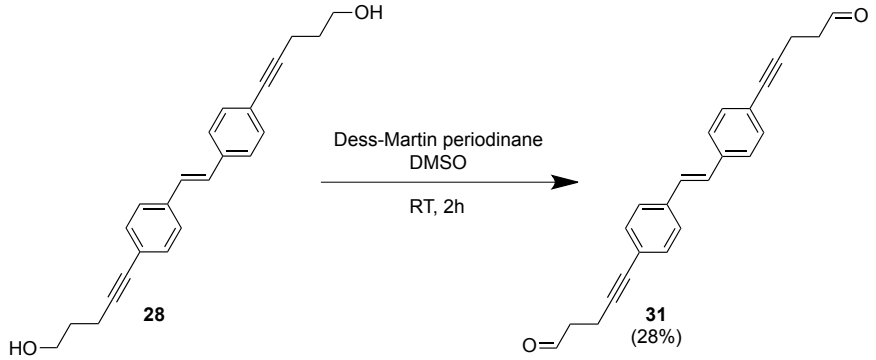

Scheme 3.22 Dess-Martin oxidation of the hydroxy groups in **28** to obtain compound **31**.

The procedure was carried out in analogy to reference.[132] Dess-Martin periodinane (DMP) (169.7 mg, 0.400 mmol) was dissolved in DMSO (2 ml) and the solution stirred. A solution of compound **28** (60.9 mg, 0.177 mmol) in DMSO (3 ml) was added dropwise and afterwards stirred for two hours at room temperature. The reaction mixture was diluted with $CHCl_3$ (50 ml) and washed with sat. aq. $NaHCO_3$ solution containing 12.5 g $Na_2S_2O_3$ (50 ml), sat. aq. $NaHCO_3$ solution (50 ml) and brine (50 ml). The organic phase was dried over $MgSO_4$ and the solvent evaporated under reduced pressure. A liquid-load silica-gel column chromatography (DCM) was done to remove the remaining DMP (R_f = 0.05). The product **31** was afforded as a white yellowish solid (16.9 mg, 28%). R_f = 0.62 (hexane/EtOAc 1:1). ^{1}H-NMR (300 MHz, DMSO-d_6: δ 9.71 (s, 2H), 7.57 (d, J = 8.4 Hz, 4H), 7.37 (d, J = 8.3 Hz, 4H), 7.27 (s, 2H), 2.81 – 2.64 (m, 8H). ^{13}C-NMR (75 MHz, DMSO-d_6: δ 201.76,

136.58, 131.60, 128.52, 126.69, 122.09, 117.02, 90.46, 41.77, 38.69, 12.06. HRMS-NSI (m/z): $[M]^+$ calcd for $C_{24}H_{20}O_2$: 340.1450, found: 340.1458.

5,5'-(((1E,1'E)-(((((((E)-ethene-1,2-diyl)bis(4,1-phenylene))bis(pent-4-yne-5,1-diyl))bis(azanediyl))bis(pent-1-yne-5,1-diyl))bis(4,1-phenylene))bis(ethene-2,1-diyl))bis(4,1-phenylene))bis(pent-4-yn-1-ol)
(32)

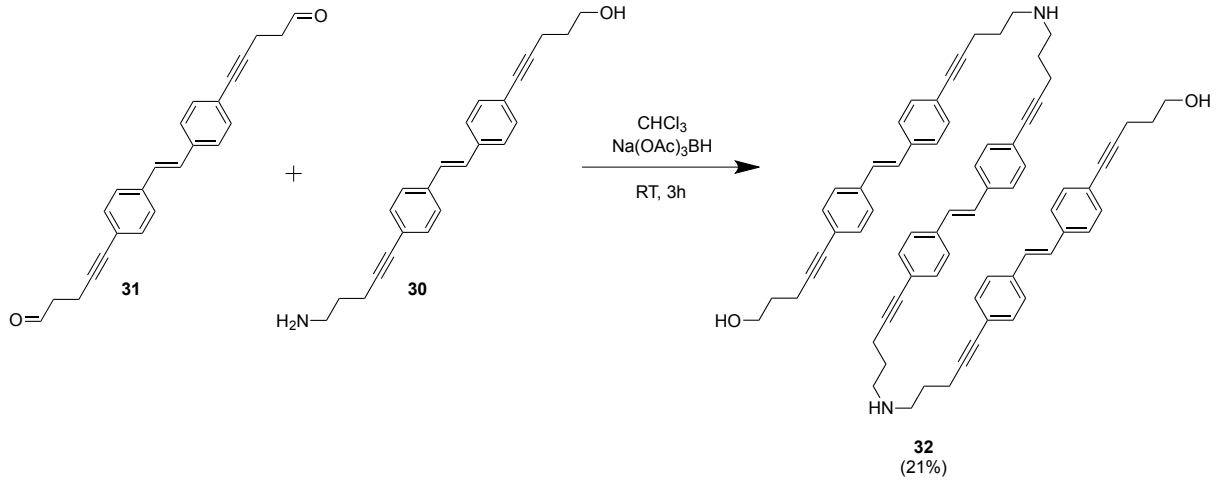

Scheme 3.23 Reductive amination of compounds **30** (2 eq.) and **31** (1 eq.) to obtain trimer **32**.

The procedure was carried out in analogy to reference.[133] To a solution of compound **30** (31.7 mg, 0.092 mmol) in $CHCl_3$ (7 ml), $Na(OAc)_3BH$ (46.9 mg, 0.221 mmol) was added. A solution of compound **31** (16.9 mg, 0.049 mmol) in $CHCl_3$ (3 ml) was added dropwise. The reaction was stirred for three hours at room temperature. The reaction mixture was diluted with $CHCl_3$ (25 ml), and washed twice with aq. 2 M K_2CO_3 solution (2x 30 ml). The $CHCl_3$-phase was dried over K_2CO_3 and the filtrate concentrated under reduced pressure. The crude **32** (110 mg) purified by a preparative basic TLC (DCM/iPrOH 9:1 + 1% Et_3N). The trimer was dissolved out of the silica gel with DCM/MeOH (9:1 + 1% Et_3N, 200 ml). Compound **32** was gained as a white solid (5.3 mg, 21%). R_f = 0.1. HRMS-NSI (m/z): $[M+H]^+$ calcd for $C_{72}H_{71}O_2N_2$: 995.5502, found: 995.5510.

3.5.2. Additional Measurements

Kinetic Studies of the Amine-Hydroxy Pyrene Monomer (24)

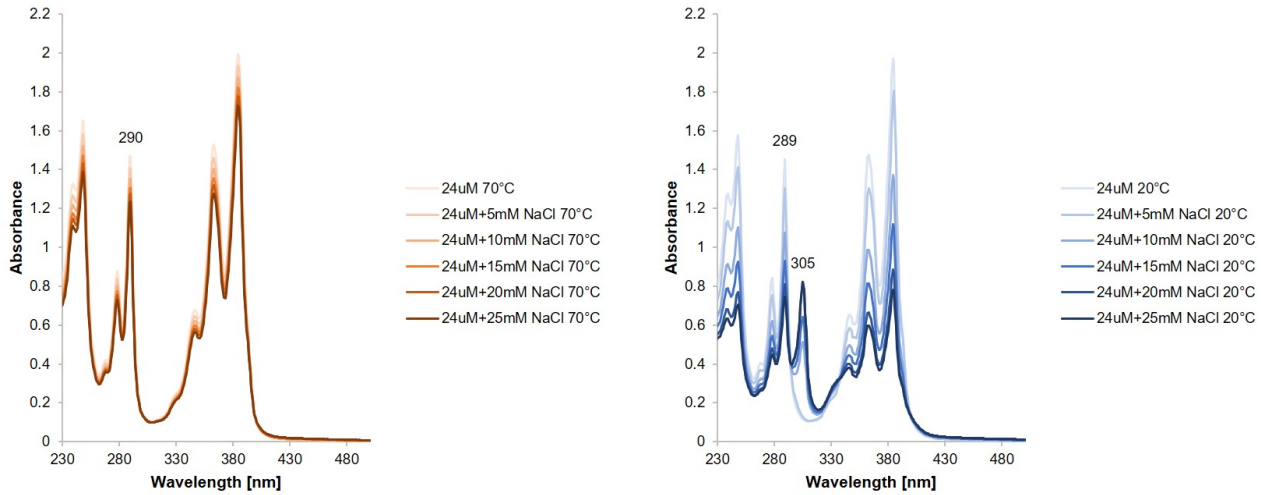

Figure 3.22. Absorption spectra of compound **24** (24 µM) in sodium acetate buffer (10 mM, pH 4.71) at different concentrations of sodium chloride (0-25 mM).

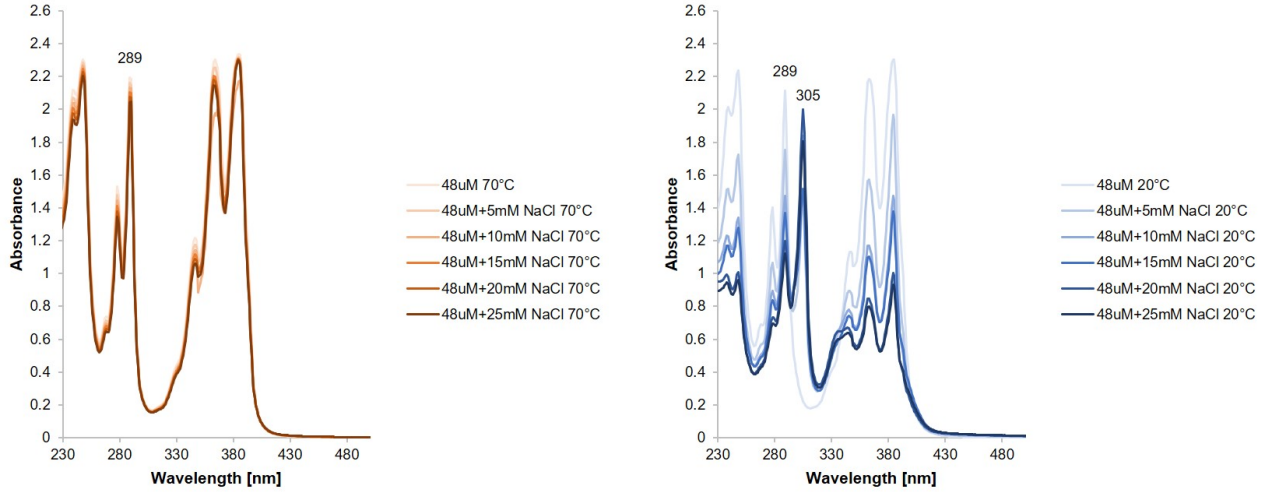

Figure 3.23. Absorption spectra of compound **24** (48 µM) in sodium acetate buffer (10 mM, pH 4.71) at different concentrations of sodium chloride (0-25 mM).

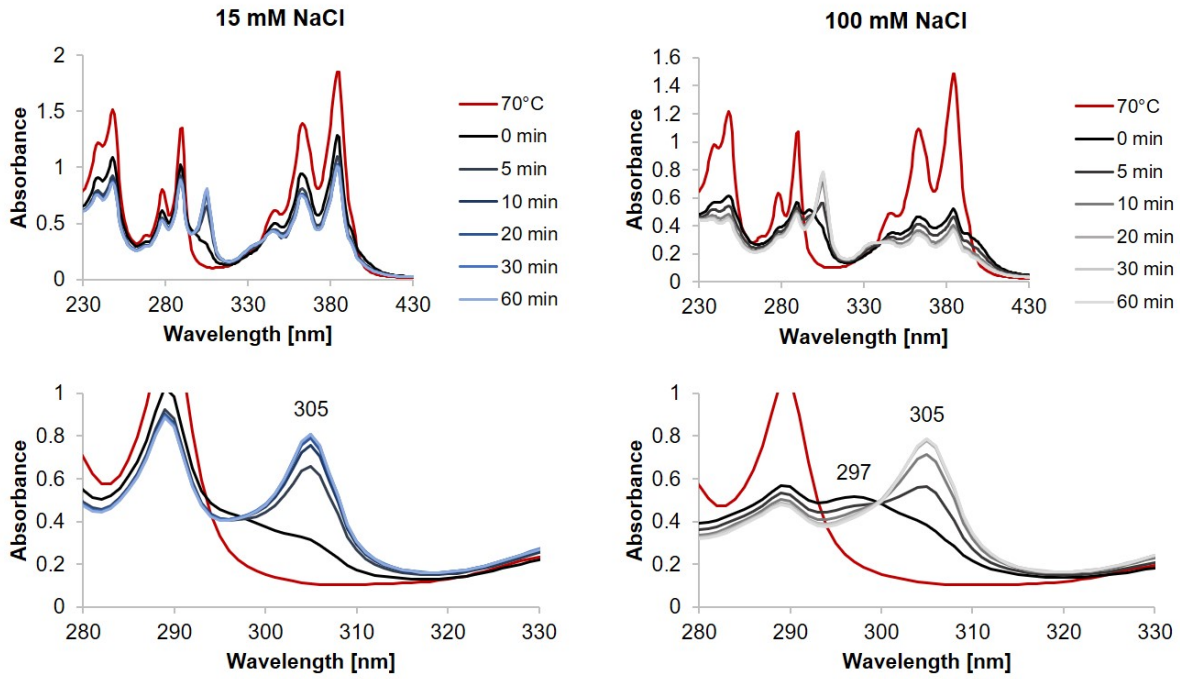

Figure 3.24. Time-dependent absorption spectra of **24** (24 µM) in 10 mM sodium acetate buffer and 15 mM (left) resp. 100 mM NaCl (right). The spectra were recorded after 0, 5, 10, 20, 30 and 60 min at 20°C. The zoom-in of the upper spectra is shown below the corresponding diagram.

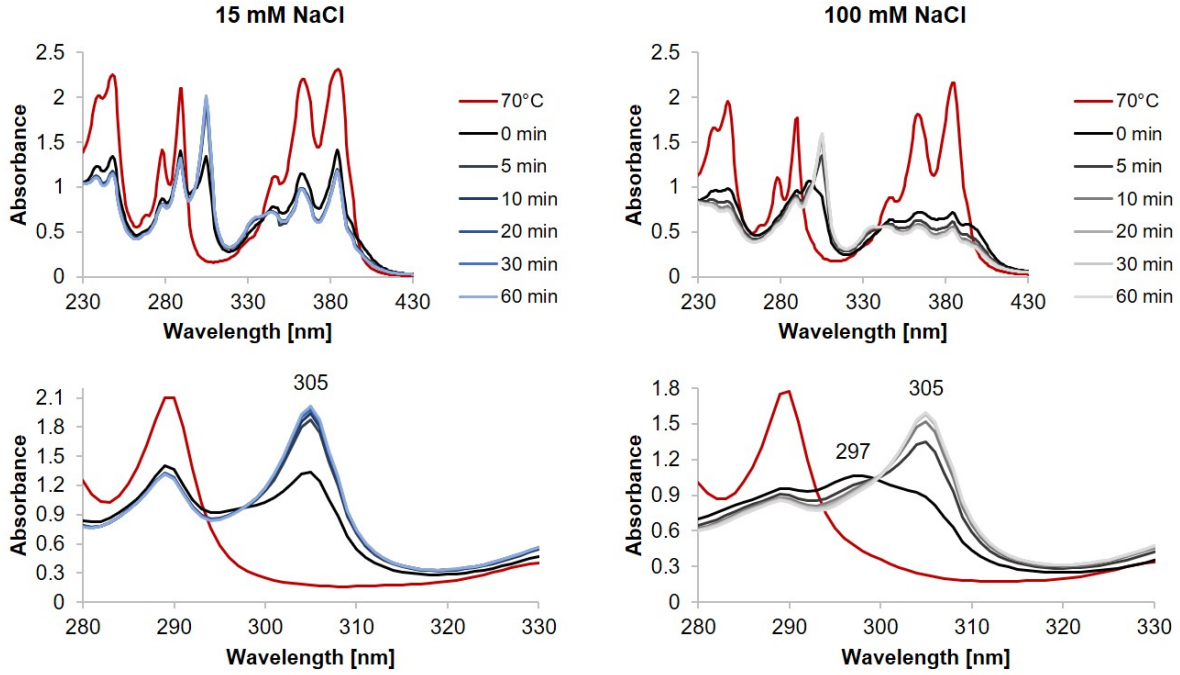

Figure 3.25. Time-dependent absorption spectra of **24** (48 µM) in 10 mM sodium acetate buffer and 15 mM (left) resp. 100 mM NaCl (right). The spectra were recorded after 0, 5, 10, 20, 30 and 60 min at 20°C. The zoom-in of the upper spectra is shown below the corresponding diagram.

4. Stilbene Derivative with Phosphodiester-Bridges

4.1. Abstract

The synthesis and analysis of a 4,4'-dialkoxypropyl-linked stilbene trimer with phosphodiester-bridges are presented. Its self-assembly behavior was investigated with spectroscopic measurements such as UV-vis, fluorescence, and AFM, and the appearance of an H-band was detected. The visualization of the supramolecular polymers was done by AFM and it was shown that sheets with a height of 3 nm were formed.

4.2. Introduction

Our group first started working with dicarboxamide-derived oligomers, later changing to dialkynyl-linked oligomers. Studies showed that the 3,6-dialkynyl phenanthrene has a higher absorption coefficient, and that the stacking is more efficient in comparison to the carboxamide derivatives.[36,92,96,148,149] In addition, the conjugated system is extended with the alkynyl linkers and thus the absorption shifted towards longer wavelengths.

As shown in chapter 3 *Synthesis of New Cationic Supramolecular Polymers*, the synthesis of dialkynyl-linked oligoamines was challenging and brought many solubility problems. The same problem repeated itself when a new oligomer with phosphodiester-bridges was synthesized: 4,4'-dialkynyl-linked stilbene trimer. The idea of synthesizing this trimer was to have an oppositely charged molecule for comparison studies to the previously described oligoamine (subsection 3.3.6 *4,4'-Dialkynyl Stilbene Oligoamine (32)*). Stilbene was previously chosen, because its derivatives are known for their photoresponsive properties such as (*E/Z*)-photoisomerization,[150,151] photochemical cycloaddition, and oxidative photochemical cyclization[152] and were used for the formation of layers.[153,154] Unfortunately, already the first few steps of the 4,4'-dialkynyl stilbene trimer with phosphodiester-bridges synthesis showed troubles with the solubility of the molecules in any solvent (water-miscible and immiscible) and prevented the purification of the products. As a result, the synthesis was not continued.

At about the same time, a group member synthesized a new molecule, the 4,4'-dialkoxy-linked azobenzene trimer with phosphodiester-bridges.[155] He could show that the azobenzene oligomer is forming sheets and thus further confirm our theory that linearly-linked oligomers tend to self-assemble into two-dimensional structures. The change from dialkynyl- to dialkoxyl-linked oligomers had the advantage, that the molecule was less rigid (Figure 4.1). It was shown that stilbenes with dialkoxy-linkers have a good flexibility and π-stacking ability and thus were used in studies with DNA hairpins, meaning that their solubility in aqueous medium was good.[156–160]

Based on this, we assumed that the dialkoxy-linker improves the water-solubility of the stilbene-trimer (Figure 4.1) and due to their linear-linkage should lead to the formation of sheets. Therefore,

the synthesis was adapted and the 4,4'-dialkoxy-linked stilbene trimer with phosphodiester-bridges was prepared.

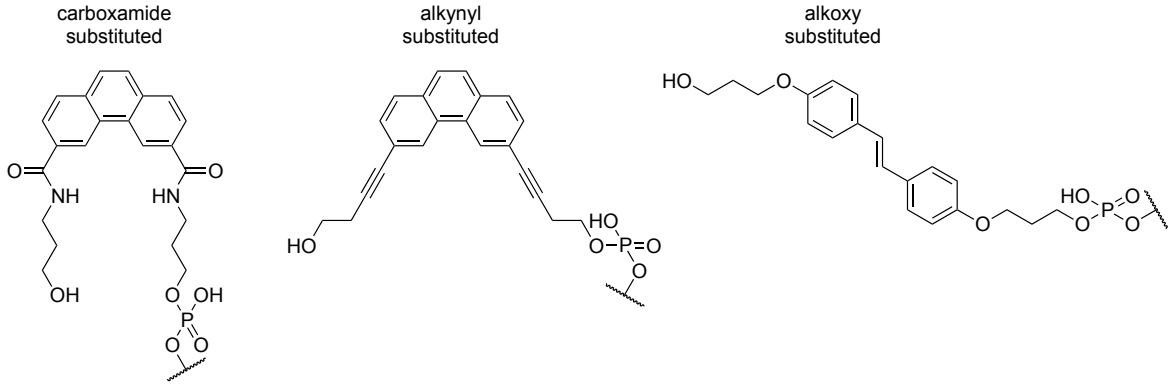

Figure 4.1. The different linkers which were used for the connection of the chromophores: carboxamide, alkynyl, and alkoxy. Examples from the past are shown with phenanthrene as a chromophore.

4.3. Results and Discussion

4.3.1. Synthesis of the Stilbene-Trimer

The chemical synthesis of trimer **38** is shown in Scheme 4.1. The coupling of two 4-hydroxybenzaldehyde by a McMurry reaction afforded (*E*)-4,4'-(ethene-1,2-diyl)diphenol (**33**).[161,162] The crude **33** was further treated with 3-bromo-1-propanol to obtain compound **34**. Recrystallization of **34** in acetone afforded the pure compound (24%). One of the hydroxyl-groups in compound **34** was monoacetylated by the addition of acetic anhydride in pyridine to obtain **35** (32%). Compound **34** was also used for the di-phosphitylation of the hydroxyl-groups to afford **36** (84%). A coupling of compounds **35** and **36** using 5-ethyl-thio-tetrazole as an activator, followed by the oxidation of the intermediate, leading to the formation of **37** (19%). The deprotection of the cyanoethyl ester groups in **37** was performed twice. On a first try, **37** was dissolved in 2M NH_3 and stirred overnight at room temperature. This did not deprotect everything as confirmed by mass spectrometry and RP-HPLC. The second attempt of deprotection was done at 55°C and yielded the final trimer **38** which was purified by RP-HPLC (1%).

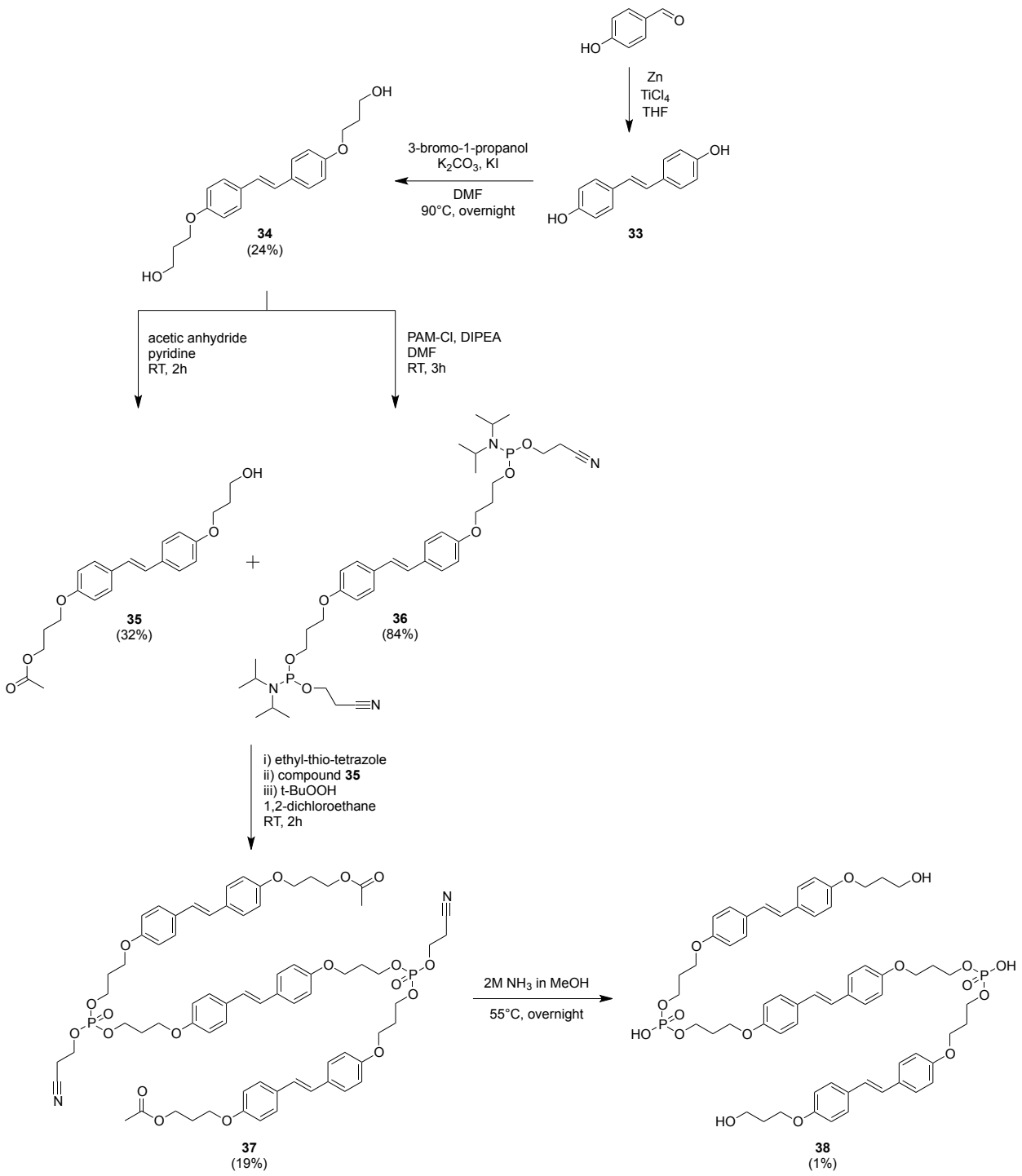

Scheme 4.1 Synthesis pathway to afford the target molecule **38**: 4,4'-dialkoxypropyl-linked stilbene trimer with phosphodiester-bridges.

4.3.2. Spectroscopic Properties

The first step was to find suitable buffer conditions to solubilize the newly synthesized 4,4'-dialkoxy stilbene trimer (**38**). Therefore, **38** was first dissolved in ethanol to have a spectral comparison under which aqueous conditions **38** is dissolved at 70°C.

In ethanol, **38** has two maxima at 296 and 327 nm (Figure 4.2). This means that when the spectra of **38** in aqueous medium at 70°C looked the same as **38** in pure ethanol, **38** was dissolved. Afterwards, **38** was added into a solution of 10 mM sodium phosphate buffer (pH 7.1) and the ethanol content was increased until the spectrum at 70°C looked the same as in ethanol (Figure 4.8 in subsection 4.5.3 *Additional Absorption Spectra of 38*). This experiment showed that with 30% of ethanol the spectrum at 70°C had the same maxima as in pure ethanol (296 and 327 nm) and thus **38** was dissolved (Figure 4.2). After cooling to 20°C the maxima disappeared and a new one appeared at 276 nm. This hypsochromic shift indicated a structural change of **38** in the solution. Thus, for further measurements, the following conditions were used: 1 µM **38** in 10 mM sodium phosphate buffer (pH 7.1) and 30% ethanol.

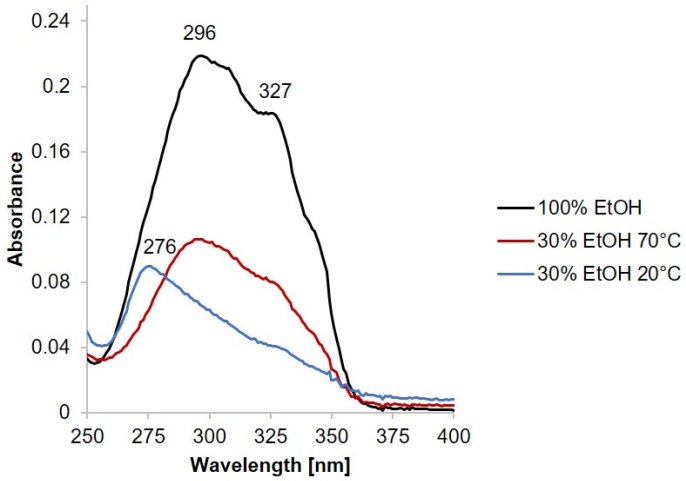

Figure 4.2. Absorption spectra of **38** in pure ethanol (black) and in aqueous medium with 30% ethanol at 70°C (red) and 20°C (blue). Conditions in aqueous medium: trimer **38** (1 µM), 10 mM sodium phosphate buffer (pH 7.1), 30 vol% ethanol.

Next, the aggregation temperature of **38** under the set conditions was determined. Starting from 70°C, every 10°C an absorption spectrum of **38** was recorded until 20°C was reached (Figure 4.3). The idea was to see at which temperature the spectra do not change anymore. At 70°C, two maxima at 296 and 327 nm (same as in Figure 4.2) are present. The change to one maximum at 276 nm occurred after reaching 50°C. This means that the trimer **38** aggregates between 50°C and 60°C. The spectra from 50°C to 20°C look quite similar.

Also, fluorescence and excitation spectra of **38** were measured. Figure 4.4 shows on the left side the fluorescence spectra with a maximum at 384 nm when excited at 275 nm and measured at 70°C and 20°C. The intensity of the assembled **38** (20°C) increased for almost 3.5 times. The diagram on the right side in Figure 4.4 depicts the excitation spectra when measuring the sample at the emission wavelength 386 nm. Also here a big increase in intensity was observed with a maximum at 327 nm (20°C). This maximum correlates with the one observed in the absorption spectrum. In contrast to the UV-vis spectrum, no peak at 276 nm is observable.

The absorption and fluorescence spectra of **38** in the assembled state (30% ethanol, 20°C) were quite different from the spectra of **38** in the disassembled state (pure ethanol) (Figure 4.5). A blue-

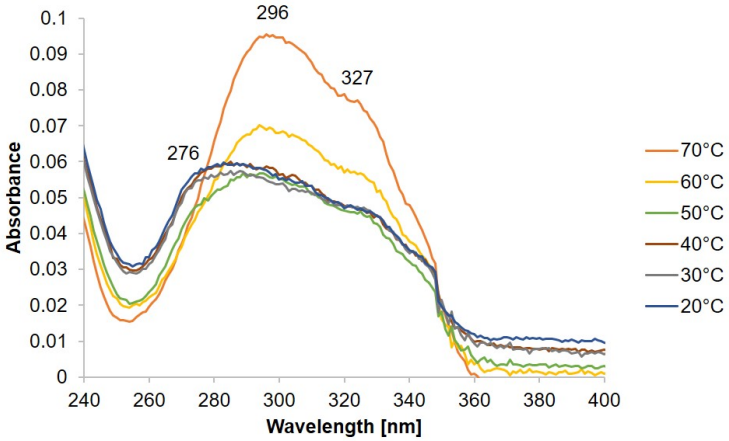

Figure 4.3. Absorption spectra of **38** measured in 10°C steps from 70°C to 20°C. Conditions: trimer **38** (1 µM), 10 mM sodium phosphate buffer (pH 7.1), 30 vol% ethanol.

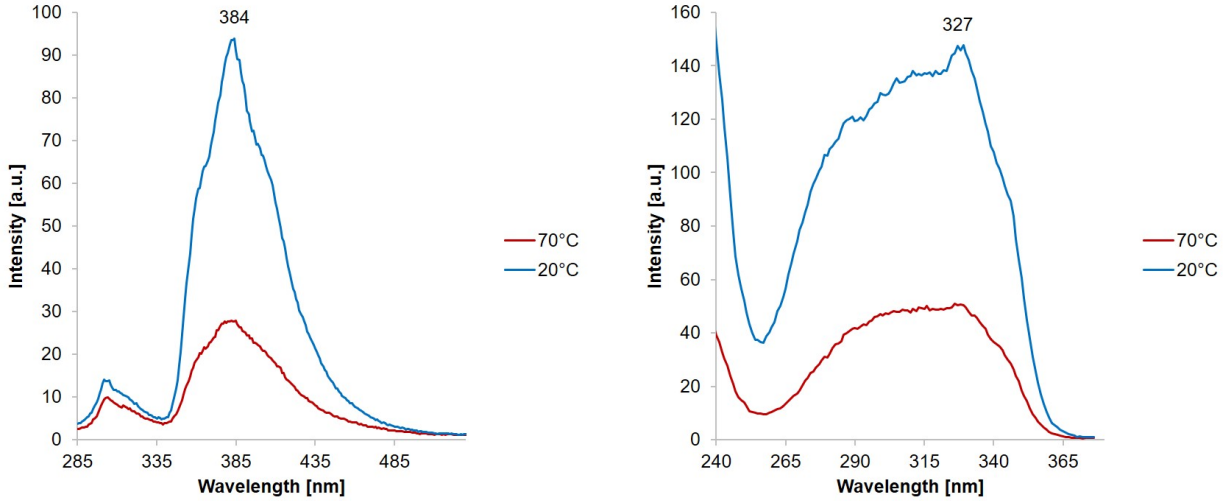

Figure 4.4. Fluorescence (left) and excitation (right) spectra of **38** measured at 70°C (red) and 20°C (blue). Conditions: trimer **38** (1 µM), 10 mM sodium phosphate buffer (pH 7.1), 30 vol% ethanol, λ_{ex} = 275 nm, λ_{em} = 386 nm.

shift was observed in the absorption, the maxima shifted from 296 and 327 nm (disassembled, 100% EtOH) to 276 nm (assembled, 30% EtOH). Additionally, a red-shift in fluorescence is noticeable from 375 nm (disassembled) to 379 nm (assembled). This behavior can be attributed to an H-band. This means that the stilbene molecules orient parallel to each other by self-assembly.[145] This also explains why the excitation spectra (Figure 4.4, right) do not look the same as the absorption spectra. The H-band is not fluorescing and thus not observable in the measurement. This phenomenon was also observed in literature when forming multilayers with stilbene fatty acid derivatives[145,146] and other examples.[153]

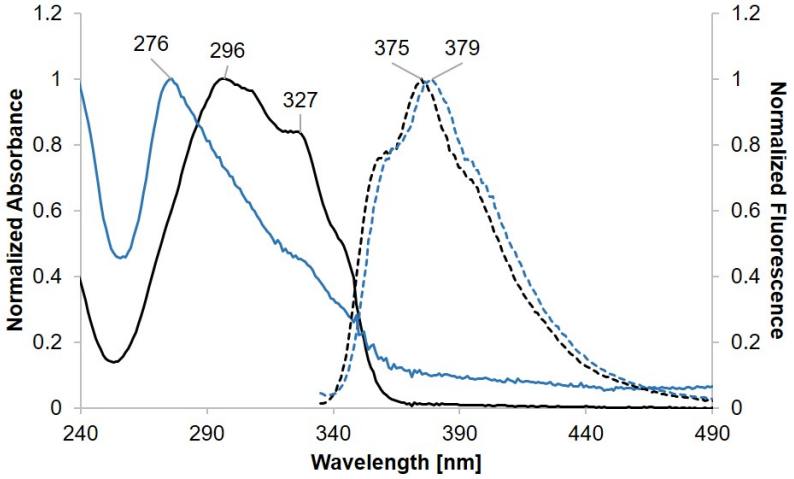

Figure 4.5. Comparison of absorption (solid lines) and fluorescence (dashed lines) spectra of **38** measured at 20°C in pure ethanol (black, disassembled) and with 30% ethanol in aqueous medium (blue, assembled). Conditions in aqueous medium: trimer **38** (1 µM), 10 mM sodium phosphate buffer (pH 7.1), 30 vol% ethanol, λ_{ex} = 325 nm.

4.3.3. Visualization of Stilbene Assemblies

The stilbene trimer **38** self-assembles into sheets in aqueous medium. AFM measurements revealed the adsorption of frayed sheets with a height of 3 nm (Figure 4.6 and Figure 4.7). Some of the sheets look like a hoofprint of a goat (Figure 4.6 and Figure 4.9).
Figure 4.6 depicts that also smaller objects were found with a height of 1 nm, but also sheets with the double-height were observed.

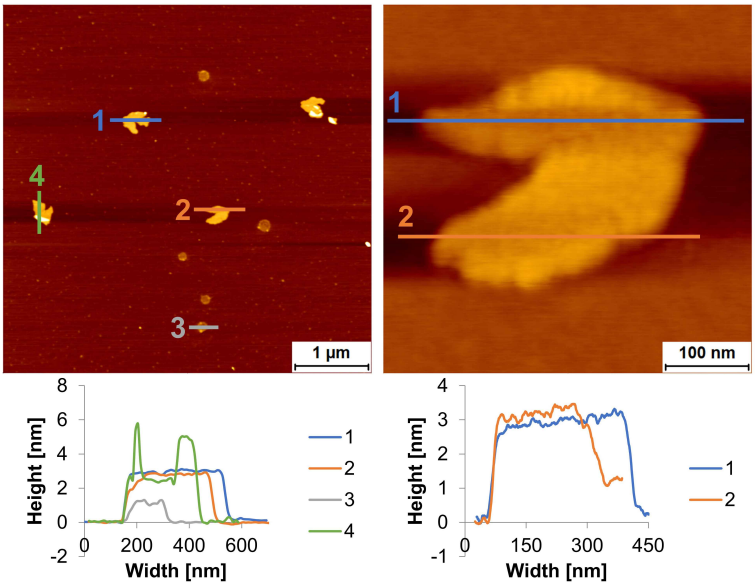

Figure 4.6. AFM measurements of **38** adsorbed on APTES-modified mica and their corresponding height-profiles. Conditions: trimer **38** (1 µM), 10 mM sodium phosphate buffer (pH 7.1), 30 vol% ethanol.

Figure 4.7 indicates the adsorption of several sheets with variable widths, ranging from 300-900 nm. Rarely, big undefined aggregates with a height of 30 nm were observed.

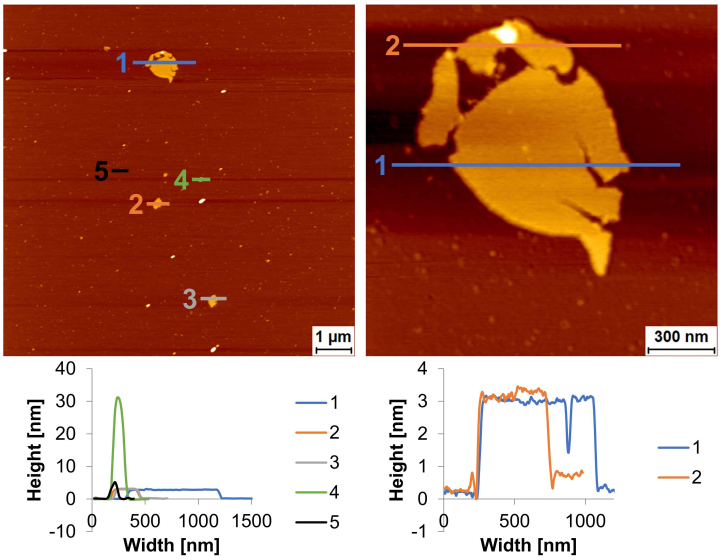

Figure 4.7. AFM measurements of **38** adsorbed on APTES-modified mica and their corresponding height-profiles. Conditions: trimer **38** (1 µM), 10 mM sodium phosphate buffer (pH 7.1), 30 vol% ethanol.

4.4. Conclusions and Outlook

In conclusion, it was demonstrated that the 4,4'-dialkoxy-substituted stilbene trimer with phosphodiester-bridges self-assembles into two-dimensional supramolecular polymers in aqueous medium. The formed nanosheets have a height of 3 nm and vary in width in a range of 300-800 nm. Spectroscopic measurements indicated the appearance of an H-band (276 nm). The change of the linker type from alkynyl to alkoxy improved the solubility of the stilbene. The purification steps were still rather difficult but nevertheless, the desired product was synthesized and could finally be dissolved and studied. The examination of light-harvesting properties with acceptors like 9,10-diphenylanthracene or pyrene, as well as experiments in the field of electrostatic layering, are topics of further investigation. TEM measurements would also be helpful for further understanding of the stilbene trimer and its assembly into sheets. Additionally, it is known that stilbene may undergo a [2+2]-cycloaddition and (*E*/*Z*)-isomerization.[163–166] The [2+2]-cycloaddition would lead to covalently bond polymers as previously shown on the example of photodimerization of anthracene supramolecular assemblies.[167] The (*E*/*Z*)-isomerization would probably lead to a structural change which would be observable on the AFM. Therefore, further investigations in this research topic are of interest.

4.5. Experimental Part

4.5.1. Synthesis of 4,4'-Dialkoxy Stilbene Trimer

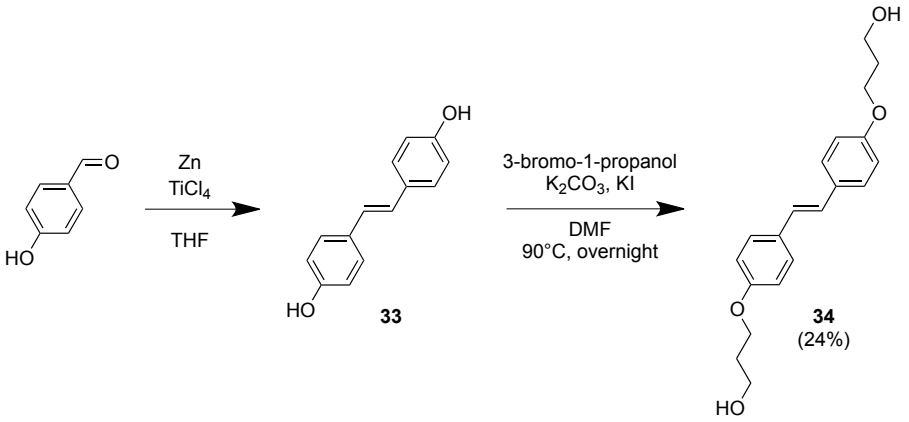

Scheme 4.2 Formation of (*E*)-4,4'-(ethene-1,2-diyl)diphenol (**33**) by a McMurry reaction using 4-hydroxybenzaldehyde as a starting material, followed by an alkylation of **33** to obtain **34**.

(E)-4,4'-(ethene-1,2-diyl)diphenol (33)

The commercially available 4-hydroxybenzaldehyde (10.0486 g, 0.0823 mol) was dissolved in dry THF (670 ml), followed by the addition of Zn dust powder (16.3904 g, 0.2507 mol), which yielded in a grey suspension. The suspension was cooled to 0°C, before $TiCl_4$ (15.20 ml, 0.1385 mol) was added slowly. Afterwards, the reaction mixture was warmed to room temperature, and it was refluxed at 80°C overnight. TLC (DCM/MeOH 95:5) showed the disappearance of starting material. The reaction mixture was cooled to room temperature, before aq. 10% K_2CO_3 (750 ml) was added and the suspension stirred for one hour. The reaction mixture was filtrated through Celite503 and the filter cake was washed thoroughly with THF. The filtrate was acidified with HCl (37%) to about a pH 1. The aqueous phase was extracted with *tert*-butyl methyl ether (3x 200 ml). The combined organic phases were washed once with brine (500 ml), dried over $MgSO_4$, filtrated, and concentrated in vacuo. Due to the low yield after purification, crude **33** was used for further synthesis (9.5831 g, crude). A recrystallization out of 1-butanol[161] yielded the pure product **33** (12%), but this step was not necessary for the further synthesis of **34** and thus, crude **33** was used. pure **33**: ^{1}H-NMR (300 MHz, DMSO-d_6) δ 9.46 (s, 2H), 7.35 (d, J = 8.6 Hz, 4H), 6.90 (s, 2H), 6.74 (d, J = 8.5 Hz, 4H). ^{13}C-NMR (75 MHz, DMSO-d_6) δ 156.76, 128.59, 127.33, 125.20, 115.48.

(E)-3,3'-((ethene-1,2-diylbis(4,1-phenylene))bis(oxy))bis(propan-1-ol) (34)

The synthesis was done in analogy to literature.[168] The crude **33** (4.0549 g, 19.10 mmol) was dissolved in anhydrous DMF (80 ml) whilst heating to 90°C. K_2CO_3 (5.9719 g, 43.21 mmol), potassium iodide (321.4 mg, 1.94 mmol) and 3-bromo-1-propanol (3.39 ml, 38.2 mmol) were added and the dark green suspension was stirred at 90°C overnight. After cooling the reaction mixture to room temperature, water (800 ml) was added. The violet precipitation was filtrated, washed with aq.

K_2CO_3 (10%, 500 ml) and water (2x 500 ml), and dried. The crude product **34** (3.7228 g, 59%) was further recrystallized in acetone, yielding the pure compound **34** (1.4799 g, 24% over two synthesis steps). ^{1}H-NMR (300 MHz, DMSO-d_6) δ 7.48 (d, J = 8.4 Hz, 4H), 7.02 (s, 2H), 6.92 (d, J = 8.3 Hz, 4H), 4.61 (s, 2H), 4.04 (t, J = 6.4 Hz, 4H), 3.56 (t, J = 6.2 Hz, 4H), 1.86 (p, J = 6.3 Hz, 4H). ^{13}C-NMR (75 MHz, DMSO-d_6) δ 158.07, 129.90, 127.39, 125.73, 114.61, 64.57, 57.28, 32.13. HRMS-NSI (m/z): $[M+H]^+$ calcd for $C_{20}H_{25}O_4$: 329.1742, found: 329.1747.

(E)-3-(4-(4-(3-hydroxypropoxy)styryl)phenoxy)propyl acetate (35)

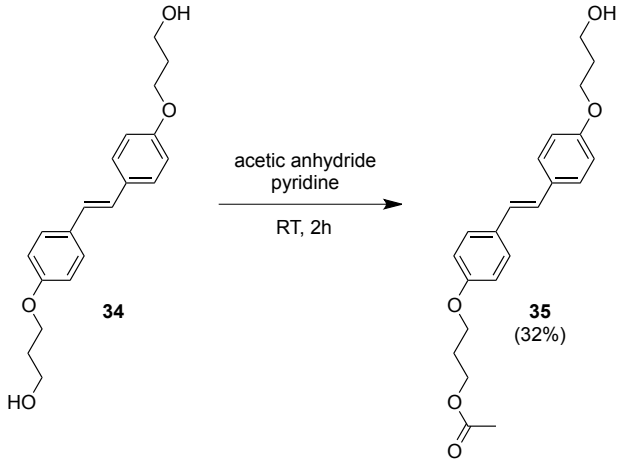

Scheme 4.3 Monoacetylation of **34** to afford **35**.

Compound **34** (201 mg, 0.612 mmol) was dissolved in pyridine (6 ml) under argon. A 2M solution of acetic anhydride (0.3 ml, 0.599 mmol) in pyridine was added dropwise over ten minutes to the dissolved compound **34**. The reaction mixture was stirred at room temperature for 2 hours. The reaction mixture was diluted with DCM (30 ml) and washed with aq. 0.5M HCl (3x 30 ml) solution, aq. sat. $NaHCO_3$ (2x 30 ml) and brine (50 ml). The organic phase was dried over $MgSO_4$, filtrated, and the solvent removed under reduced pressure. The crude **35** was purified by a flash column chromatography on silica-gel (DCM/i-PrOH 98:2). Compound **35** was isolated in a yield of 32% (72.2 mg). R_f = 0.37 (hexane/EtOAc 2:3). ^{1}H-NMR (300 MHz, DMSO-d_6) δ 7.54 – 7.43 (m, 4H), 7.02 (s, 2H), 6.97 – 6.87 (m, 4H), 4.55 (t, J = 5.2 Hz, 1H), 4.16 (t, J = 6.4 Hz, 2H), 4.10 – 3.99 (m, 4H), 3.62 – 3.50 (m, 2H), 2.10 – 1.96 (m, 5H), 1.93 – 1.79 (m, 2H). ^{13}C-NMR (75 MHz, DMSO-d_6) δ 170.41, 158.09, 157.79, 130.14, 129.87, 127.41, 125.87, 125.67, 114.65, 114.61, 64.57, 64.25, 60.83, 57.28, 32.13, 28.07, 20.70. HRMS-NSI (m/z): $[M]^+$ calcd for $C_{22}H_{26}O_5$: 370.1769, found: 370.1775.

(E)-bis(2-cyanoethyl) (((ethene-1,2-diylbis(4,1-phenylene))bis(oxy))bis(propane-3,1-diyl)) bis(diisopropylphosphoramidite) (36)

Compound **34** (118.5 mg, 0.361 mmol) was dissolved in DMF (4 ml) and DIPEA (0.66 ml, 3.811 mol). PAM-Cl (0.16 ml, 0.717 mmol) was added dropwise at room temperature and the reaction mixture stirred for three hours. The reaction mixture was diluted with DCM (40 ml) and washed with

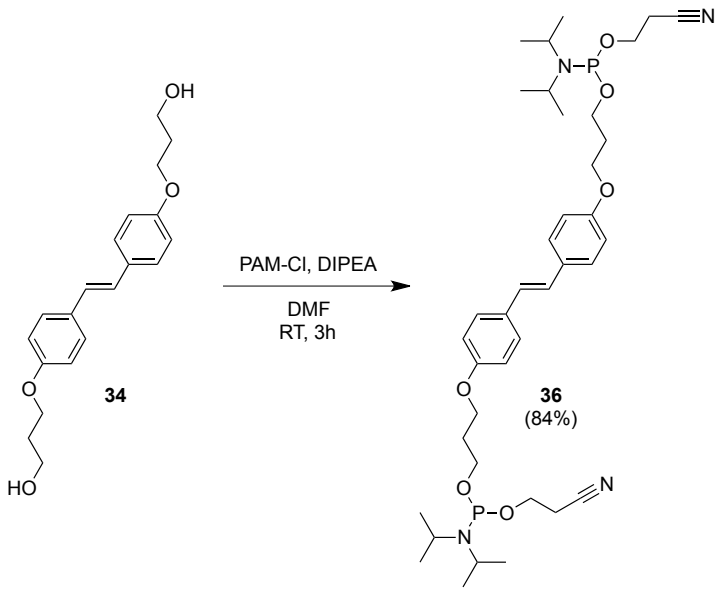

Scheme 4.4 Diphosphitylation of **34** to afford **36**.

water (3x 80 ml) and brine (3x 60 ml). The organic phase was dried over K_2CO_3, filtrated and the solvent evaporated under reduced pressure. A short column chromatography was done on silica gel (DCM/MeOH 99:1 + 1% Et_3N). Compound **36** was isolated in a yield of 84% (219.6 mg). $R_f = 0.83$ (hexane/EtOAc 2:3 + 1% Et_3N). ^{1}H-NMR (300 MHz, DMSO-d_6) δ 7.52 – 7.43 (m, 4H), 7.02 (s, 2H), 6.96 – 6.86 (m, 4H), 4.07 (t, J = 6.2 Hz, 4H), 3.85 – 3.64 (m, 8H), 3.64 – 3.47 (m, 4H), 2.80 – 2.70 (m, 4H), 1.99 (p, J = 6.2 Hz, 4H), 1.26 – 1.03 (m, 25H). ^{13}C-NMR (75 MHz, DMSO-d_6) δ 157.93, 130.00, 127.40, 125.77, 118.98, 114.60, 64.15, 59.76, 59.54, 58.28, 58.04, 42.51, 42.34, 30.47, 24.39, 24.30, 22.23, 19.89, 19.79. ^{31}P-NMR (121 MHz, DMSO-d_6) δ 146.55. HRMS-NSI (m/z): $[M+H]^+$ calcd for $C_{38}H_{59}O_6N_4P_2$: 729.3914, found: 729.3904.

Protected dialkoxypropyl-substituted stilbene trimer (37)

A solution of 5-(ethylthio)-1H-tetrazole (26.9 mg, 0.207 mmol) in DCE (0.5 ml) was added under argon atmosphere to a solution of compound **36** (53.8 mg, 0.074 mmol) in DCE (0.72 ml). Compound **35** was dissolved in DCE (2 ml) and added to the activated compound **36**. The reaction mixture was stirred at room temperature for one hour. *Tert*-butyl hydroperoxide solution (70%, 0.06 ml, 0.433 mmol) was added and the reaction mixture further stirred for 30 minutes. The reaction mixture was diluted with DCM (100 ml) and washed with aq. sat. $NaHCO_3$ (100 ml) and brine (100 ml). The organic phase was dried over $MgSO_4$, filtrated and the solvent evaporated under reduced pressure. The residue was purified by two preparative TLCs (DCM/toluene/MeOH 86:10:4). Compound **37** was isolated as a white solid (18.4 mg, 19%). $R_f = 0.47$. HRMS-NSI (m/z): $[M-H]^-$ calcd for $C_{70}H_{79}N_2O_{18}P_2Na$: 1321.4779, found: 1321.4753.

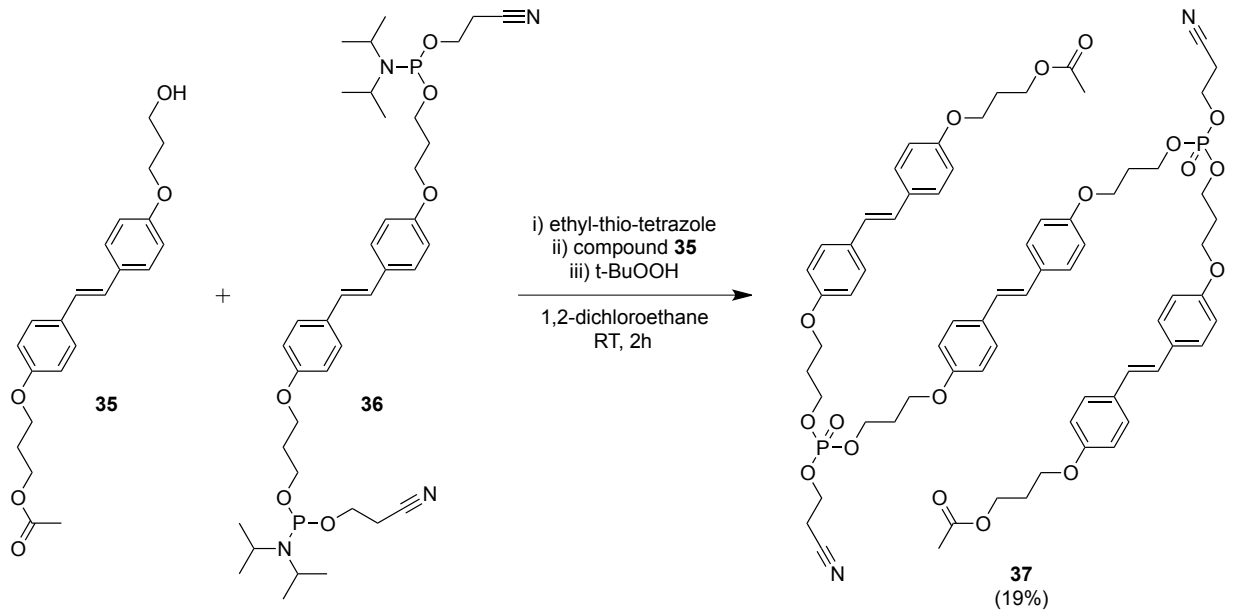

Scheme 4.5 Coupling of **35** and **36** to obtain the protected trimer **37**.

4,4'-Dialkoxypropyl-substituted stilbene trimer with phosphodiester-bridges (38)

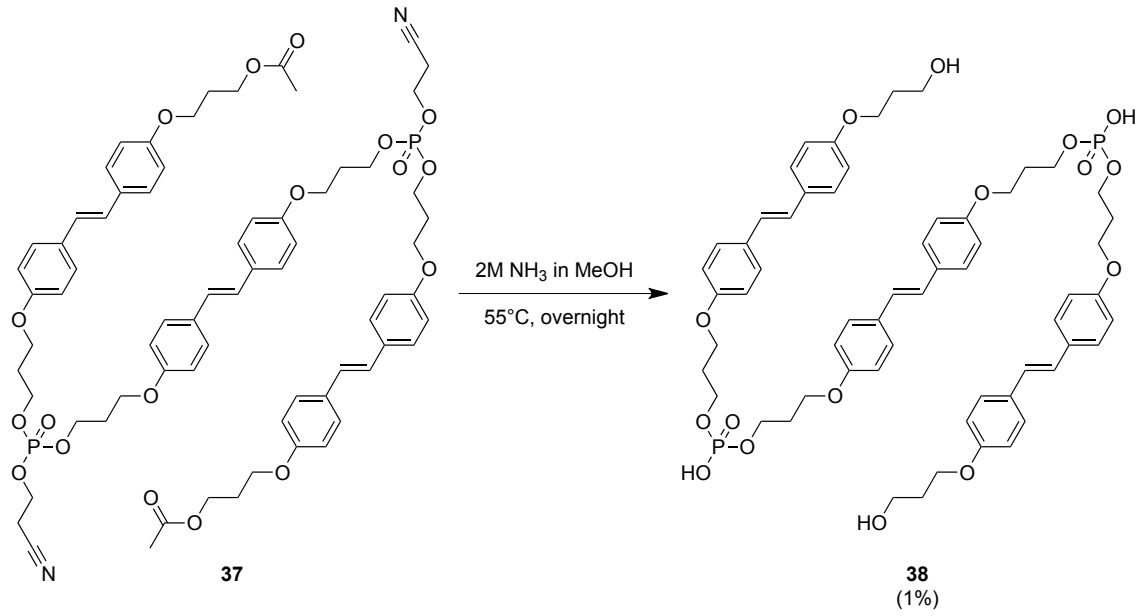

Scheme 4.6 Deprotection of **37** to obtain trimer **38**.

Compound **37** (18.4 mg, 0.014 mmol) was dissolved in a solution of 2 mol/l NH_3 in methanol (20 ml) and stirred at room temperature overnight. The sample was lyophilized, the residue was suspended in a mixture of water/EtOH (1:1, 1 ml), lyophilized again, suspended in water (1 ml) and lyophilized. Analysis with RP-HPLC and mass spectrometry showed, that **37** was not fully deprotected. Therefore **37** was again dissolved in a solution of 2 mol/l NH_3 in methanol (30 ml) and stirred at 55°C overnight. The sample was lyophilized, the residue was suspended in a mixture

of water/EtOH (1:1, 1 ml), lyophilized again, suspended in water (1 ml) and lyophilized. The crude **38** was purified by RP-HPLC (Dr. Maisch, ReproSil 100 C8, 5 µm, 250x4 mm) with the solvents A: 25 mM 1,1,1,3,3,3-hexafluoro-2-propanol, 2.1 mM TEA (pH 7.4), solvent B – acetonitrile, with a flow of 1 ml/min and at a temperature of 40°C. The gradient was set as follows: B[%] (t_R [min]) = 10 (0); 10 (2); 80 (22); 100 (25); 100 (27). Compound **38** was isolated (0.21 mg, 1%). The yield was determined by UV-vis spectroscopy measurements using the ε of the monomer **34** in ethanol (28'259 $l*mol^{-1}*cm^{-1}$). HRMS-NSI (m/z): $[M\text{-}2H]^{2-}$ calcd for $C_{60}H_{68}O_{16}P_2$: 553.1971, found: 553.1957.

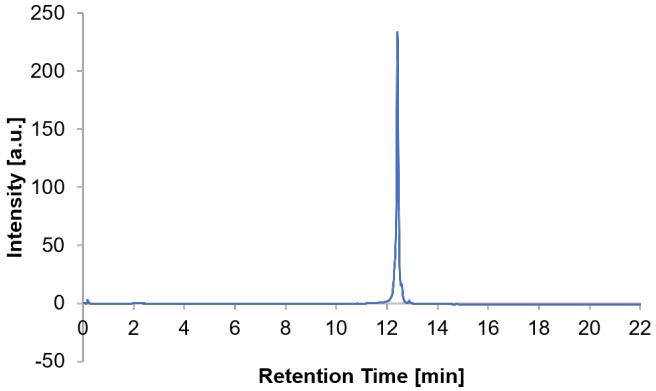

Scheme 4.7 The HPLC trace of **38** monitored at λ = 330 nm

4.5.2. Conditions for Supramolecular Polymer Formation

The supramolecular polymer formation of **38** was performed via thermal disassembly and reassembly: the samples were prepared in 10 mM sodium phosphate buffer (pH 7.1) and 30 vol% ethanol, heated to 70°C and cooled to 20°C with a controlled rate of 13°C/min in a Cary 100 spectrophotometer equipped with a Peltier thermostat.

4.5.3. Additional Absorption Spectra of 38

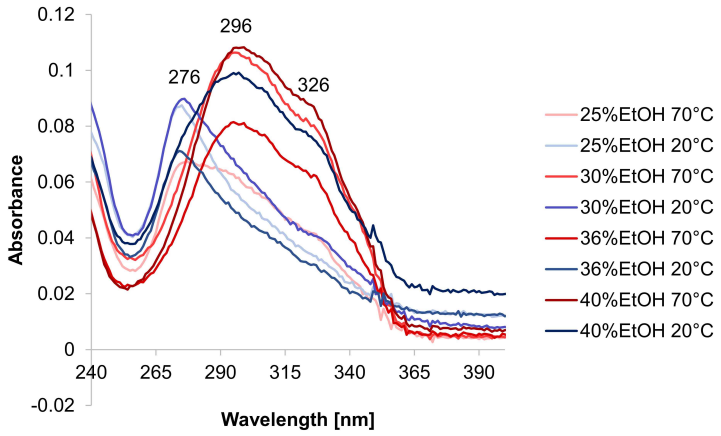

Figure 4.8. Absorption spectra of **38** with increasing additions of ethanol at 70°C (red) and 20°C (blue). Conditions: trimer **38** (1 µM), 10 mM sodium phosphate buffer (pH 7.1), 25-40 vol% ethanol.

4.5.4. Additional AFM Measurements

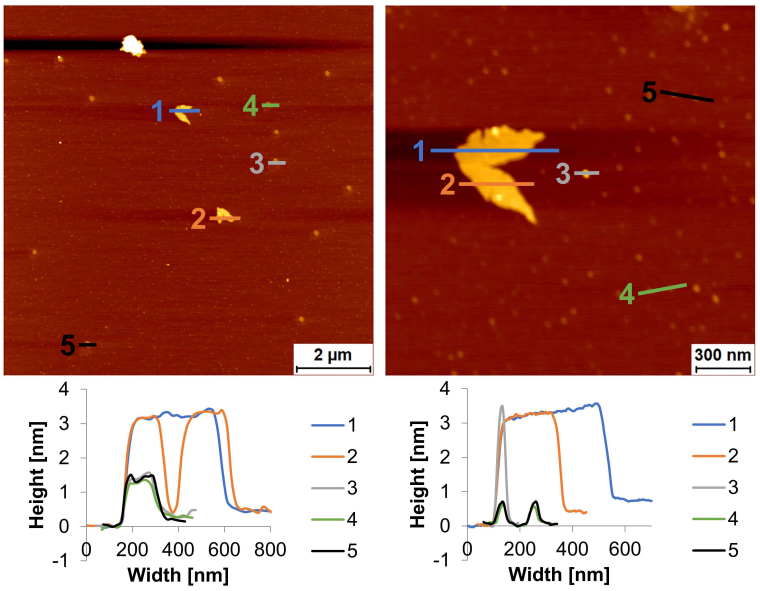

Figure 4.9. AFM measurements of **38** adsorbed on APTES-modified mica and their corresponding height-profiles. Conditions: trimer **38** (1 µM), 10 mM sodium phosphate buffer (pH 7.1), 30 vol% ethanol.

5. Exploration of Light-Harvesting Properties of N-Phe$_3$

5.1. Abstract

Light-harvesting properties in **N-Phe$_3$**-vesicles were investigated by carrying out dotting experiments with two different acceptor molecules: 9,10-diphenylanthracene (**DPA**) and 3,6-dialkynyl phenanthrene-pyrene-phenanthrene oligoamine (**15**). Two different approaches were tested, the use of the acceptor pyrene (in **15**) that was added as a trimer and the addition of a monomer acceptor, **DPA**. Spectroscopic analysis proved the occurrence of an energy transfer to the acceptor molecules when exciting the phenanthrene-donor in **N-Phe$_3$**.

5.2. Introduction

In recent years, the interest in artificial light-harvesting complexes (LHCs) has significantly increased.[39–43,169–176] An important aspect for an efficient energy transfer is a good structural organization of molecules.[177] Supramolecular polymers are particularly suitable for this purpose and allow the ordered arrangement of donor and acceptor building blocks in artificial LHCs. The dynamic nature of supramolecular polymers is an advantage when it comes to modification, like adding different chromophores as acceptors in artificial LHCs.[42,96,97,178–180] The formation of efficient, supramolecular 1D and 2D light-harvesting systems has been previously reported in our group.[36,90,96–99]
It was shown that supramolecular light-harvesting fibers were formed by self-assembly of 3,6-dialkynyl phenanthrene trimers with phosphodiester-bridges (oligomer A, Figure 5.1).[96] In oligomer B the acceptor pyrene was covalently attached to the trimer of phenanthrene-donors. Figure 5.1 illustrates schematically the formation of light-harvesting fibers, in which the pyrene units were embedded at rare positions. The excitation of phenanthrenes led to an energy transfer to the pyrene unit and already minute amounts of pyrene could be detected. The fluorescence quantum yield reached 50% after the addition of only 1.5% pyrene.
In a follow-up study it was shown that even the addition of monomer acceptor molecules to oligomer A, lead to the formation of supramolecular polymer fibers and energy transfer (Figure 5.2).[99]
Herein we describe the investigation in light-harvesting properties of the 3,6-dialkynyl phenanthrene oligoamine vesicles (**N-Phe$_3$**) doped with different kinds of acceptors. Therefore, the pyrene in the previously presented 3,6-dialkynyl phenanthrene-pyrene-phenanthrene oligoamine **15** (subsection 3.3.1 *3,6-Dialkynyl Phenanthrene-Pyrene-Phenanthrene Oligoamine (15)*) is incorporated into a trimer, and 9,10-diphenylanthracene (**DPA**) was chosen as the monomer acceptor. The chemical structures of the investigated molecules are shown in Scheme 5.1.

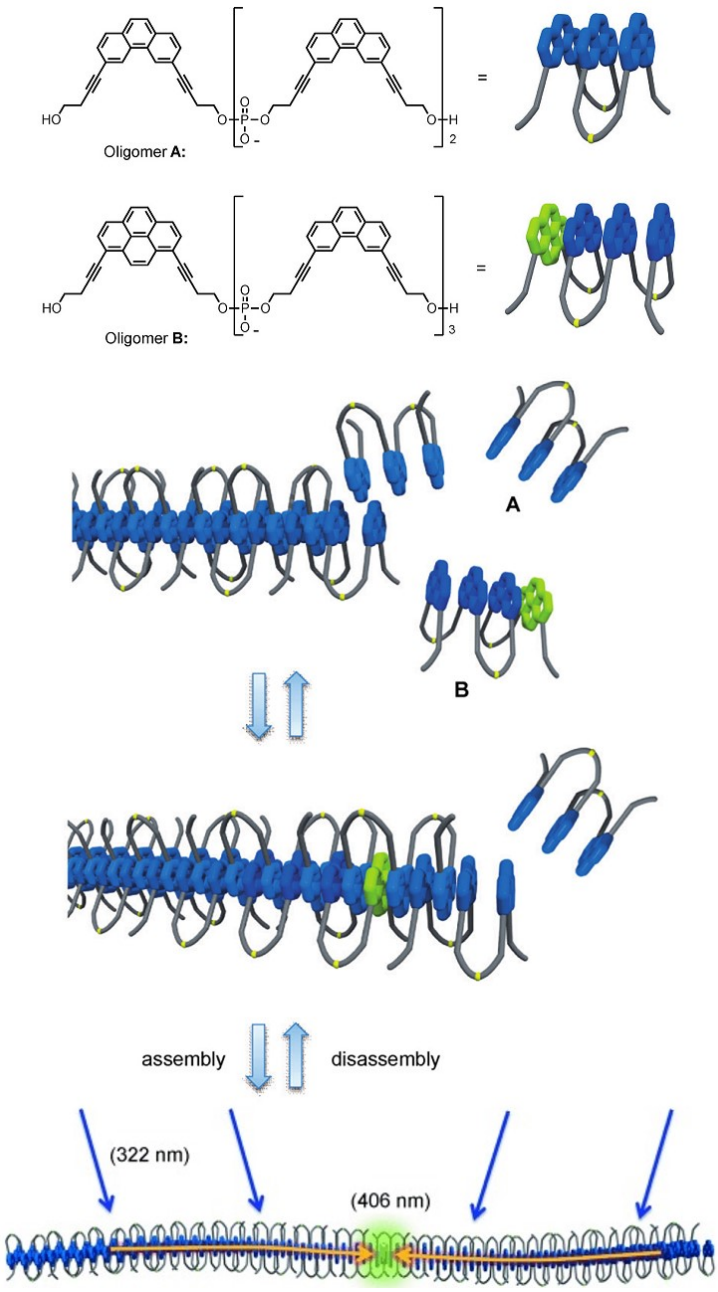

Figure 5.1. Graphical illustration of the supramolecular polymerization of oligomer A and B into pyrene-doped phenanthrene fibers. The chemical structure of oligomer B shows that the acceptor pyrene was covalently attached to the phenanthrene trimer. The excitation of phenanthrenes (blue arrows) leads to an energy transfer (yellow) to the acceptor pyrene (green). Illustration is taken from reference.[96]

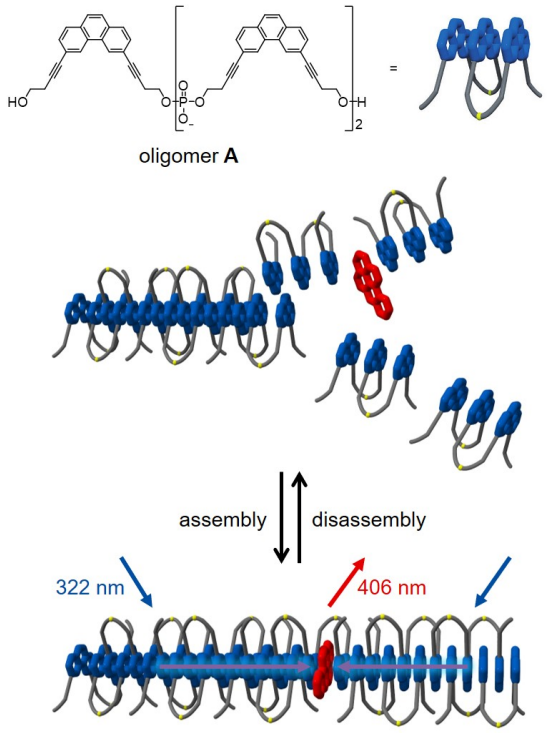

Figure 5.2. Graphical illustration of an idealized assembly process of 3,6-dialkynyl phenanthrene trimers (oligomer A) into supramolecular polymer fibers with non-covalently linked acceptor molecules. The acceptor molecule is randomly integrated into the forming fiber. Energy is transferred from the excited phenanthrenes (blue) to the chromophore (benzo[a]pyrene, red). Figure adapted from reference.[99]

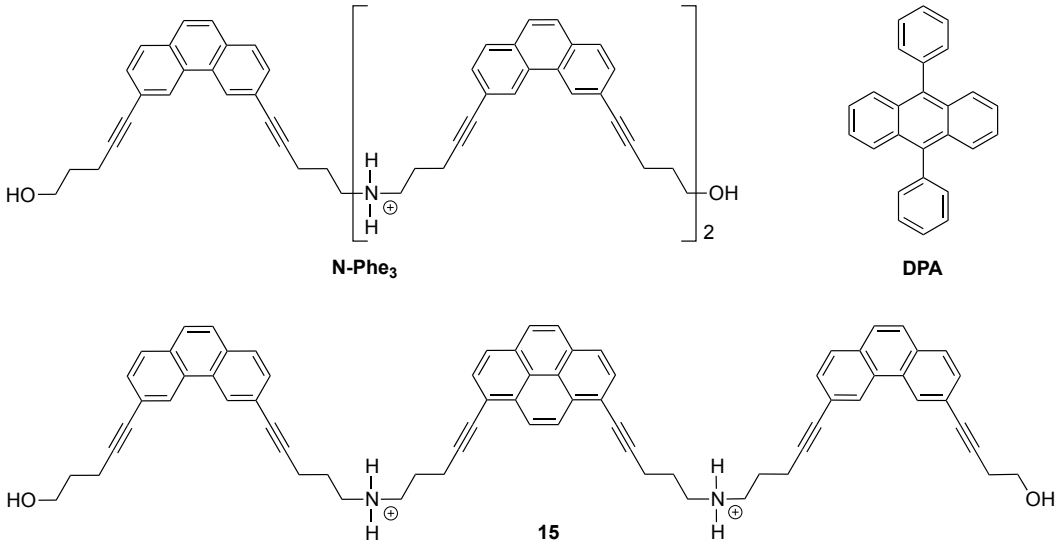

Scheme 5.1 Chemical structures of the donor **N-Phe$_3$** and both acceptors 3,6-dialkynyl phenanthrene-pyrene-phenanthrene oligoamine **15** and 9,10-diphenylanthracene (**DPA**). The pyrene acceptor in **15** was incorporated into the trimer, and **DPA** was investigated as a monomer acceptor.

5.3. Results and Discussion

5.3.1. 9,10-Diphenylanthracene (DPA)

Previous studies showed that **DPA** (Scheme 5.1) was a good acceptor when adding it as a monomer to a sample of 3,6-dialkynyl phenanthrene trimer with phosphodiester-bridges.[99] In order to be sure that only the donor is transferring the energy to the acceptor, one needs to assure to excite the donor at a wavelength where the acceptor is not or very low absorbing. Comparing the absorption spectra of **N-Phe$_3$** (subsection 2.5.4 *Additional Measurements*, Figure 2.8) and **DPA** (Figure 5.5), they do not overlap, and thus **DPA** was chosen as an acceptor for the investigations in light-harvesting properties of **N-Phe$_3$**. **DPA** is most probably incorporated into the membrane of the forming **N-Phe$_3$**-vesicles during the self-assembly process.

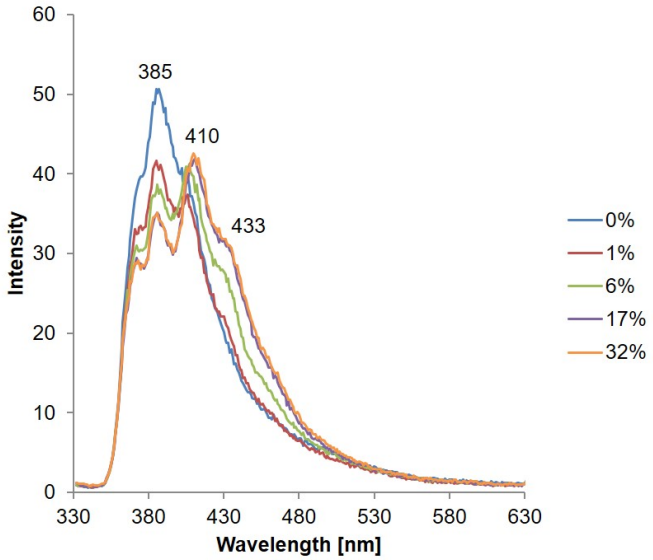

Figure 5.3. Fluorescence spectra of trimer **N-Phe$_3$** in aqueous solution with increasing concentrations of **DPA**. Conditions: trimer **N-Phe$_3$** (1 µM), 10 mM acetate buffer (pH 4.71), 10 vol% ethanol, λ_{ex} = 322 nm.

Figure 5.3 displays emission spectra of the assembled supramolecular polymer (at 20°C), consisting of **N-Phe$_3$** with increasing amounts of **DPA**. To check, whether **N-Phe$_3$** can transfer the energy to the acceptor **DPA**, the sample was excited at the wavelength 322 nm, where only phenanthrene is absorbing, respectively. After the first addition of **DPA** (1%, red), the intensity of the phenanthrene maximum at 385 nm decreased, and a new peak started to appear at 433 nm. This new band was induced by **DPA**. The same effect was observed for further additions of **DPA**. This shows that the energy which was absorbed by phenanthrenes is transferred to **DPA** acceptor molecules.
The quantum yield was determined for every addition of **DPA** (with quinine sulfate in 0.05 M H_2SO_4 as a reference[181]). After each addition of **DPA**, the fluorescence quantum yield of the system stayed constant ($\phi_F \approx 3.4\%$). This indicates, that during the energy transfer from **N-Phe$_3$** to **DPA** (Table 5.1) almost no energy was lost via radiation-less relaxation.

Table 5.1. Quantum yield calculations for **N-Phe$_3$** with increasing additions of **DPA**. Quinine sulfate ($\phi_R{}^{QS}$ = 0.546) in 0.05 M H_2SO_4 was used as a reference.[181] Conditions: **N-Phe$_3$** (1 µM), 10 mM acetate buffer (pH 4.71) and 10 vol% ethanol.

Concentration of DPA [µM]	**mol% of DPA**	ϕ_F [%]
0	0	3.4
0.030	1.00	3.3
0.148	5.94	3.6
0.324	16.78	3.8
0.441	31.56	3.5

5.3.2. 3,6-Dialkynyl Phenanthrene-Pyrene-Phenanthrene (15)

Because the addition of monomers as acceptors to **N-Phe$_3$** worked well as a light-harvesting system, the next step was to add the acceptor molecule as a trimer. The acceptor pyrene was previously described in chapter 3 *Synthesis of New Cationic Supramolecular Polymers*.
Figure 5.4 shows the fluorescence spectra of the doped **N-Phe$_3$**. **15** was admixed such that the total pyrene content increased from 1-20%. After the addition of 20% of pyrene per total phenanthrene content, a new band appeared at 428 nm, which was due to the pyrene, respectively pyrene-phenanthrene-exciplex formation.[138]

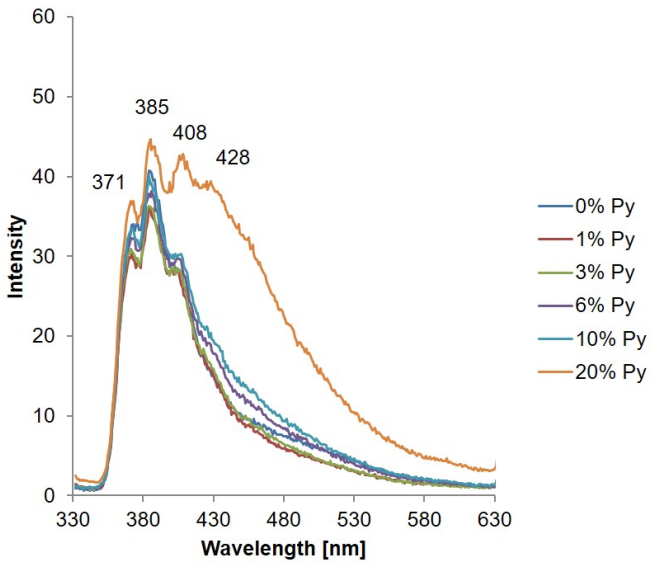

Figure 5.4. Fluorescence spectra of trimer **N-Phe$_3$** in aqueous solution with increasing concentrations of pyrene (Py) by adding **15**. Conditions: trimer **N-Phe$_3$** (1 µM), 10 mM acetate buffer (pH 4.71), 10 vol% ethanol, λ_{ex} = 322 nm.

The quantum yield was calculated after each addition of pyrene (Table 5.2). Quinine sulfate in 0.05 M H_2SO_4 was used as a reference for the quantum yield determination.[181] As depicted in

Table 5.2, the quantum yield increased from 3.4% (0% pyrene) to 9.2% (20% pyrene). This increase in fluorescence quantum yield and the exciplex formation (at 428 nm) show that there is an energy transfer from phenanthrene to pyrene.

Table 5.2. Quantum yield calculations for **N-Phe$_3$** with increasing additions of **15**. Quinine sulfate ($\phi_R{}^{QS}$ = 0.546) in 0.05 M H_2SO_4 was used as a reference.[181] Conditions: **N-Phe$_3$** (1 µM), 10 mM acetate buffer (pH 4.71) and 10 vol% ethanol.

Concentration of 15 [µM]	**mol% of pyrene**	ϕ_F **[%]**
0	0	3.4
0.030	0.98	3.4
0.095	3.01	3.7
0.205	6.08	4.4
0.370	10.00	5.9
0.994	20.16	9.2

5.4. Conclusions and Outlook

In conclusion, it was shown that the supramolecular **N-Phe$_3$**-vesicles exhibit an energy transfer from phenanthrene (donor) to the acceptors **DPA** and pyrene.

The highest fluorescence quantum yields were observed when adding the acceptor pyrene as a phenanthrene-pyrene-phenanthrene trimer (**15**) to the donor phenanthrene. With this approach, a fluorescence quantum yield of 9.2% was reached by doping the vesicles with a total amount of 20% pyrene. Additionally, exciplex formation between phenanthrene and pyrene (428 nm) could be observed after the excitation of phenanthrenes. By incorporation of pyrene into a trimer (**15**), one could ensure better integration of the acceptor into the supramolecular polymer. Also, the acceptor **DPA** showed an energy transfer. The fluorescence quantum yields stayed the same as for **N-Phe$_3$** after each increase in **DPA**-concentration.

Previously done work with the 3,6-dialkynyl phosphodiester-bridged phenanthrene trimer showed, that the energy transfer was more efficient when adding a trimer incorporating the acceptor[96] than when adding monomer acceptors.[99] This phenomenon could be observed in the case of 3,6-dialkynyl phenanthrene trimer with amine-bridges too. A contrast to the oppositely charged trimer is, that the energy transfer was much weaker when adding pyrene as **15**. This can be explained by the difference in supramolecular polymer structures. **N-Phe$_3$** self-assembles into vesicles and the oppositely charged oligomer with phosphodiester-bridges forms fibers. Therefore, the arrangement of phenanthrenes in the supramolecular polymers is different and has an impact on the efficiency of energy transfer.

The DNA-scaffold can be used for the precise positioning of chromophores. Thus, the incorporation of **N-Phe$_3$** into DNA would lead to a potential light-harvesting complex. Next to the aromatic interactions between DNA and **N-Phe$_3$**, also the positively charged amine-backbone of the **N-Phe$_3$**

can electrostatically interact with the negatively charged DNA phosphate backbone.

5.5. Experimental Part

5.5.1. Conditions for the Formation of the Light-Harvesting Complex

The supramolecular polymer, **N-Phe$_3$**-vesicles, was formed by heating the sample to 70°C and cooling it to 20°C with a controlled rate of 13°C/min in a Cary 100 spectrophotometer equipped with a Peltier thermostat. After each addition of an acceptor, the sample was heated again to 70°C and cooled to 20°C, as previously described.

5.5.2. Additional Measurements

Absorption and Fluorescence Spectra of DPA

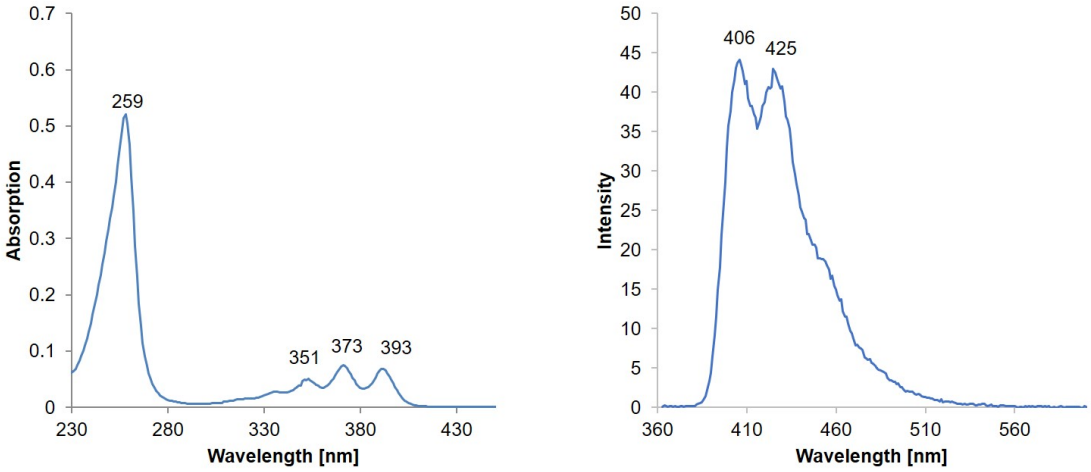

Figure 5.5. Absorption (left) and fluorescence (right) spectra of 9,10-diphenylanthracene (**DPA**) in ethanol. Conditions: 5 µM **DPA**, λ_{ex} = 353 nm, slit$_{ex}$ = 2.5 nm.

Fluorescence Quantum Yield Determination of N-Phe$_3$ + DPA

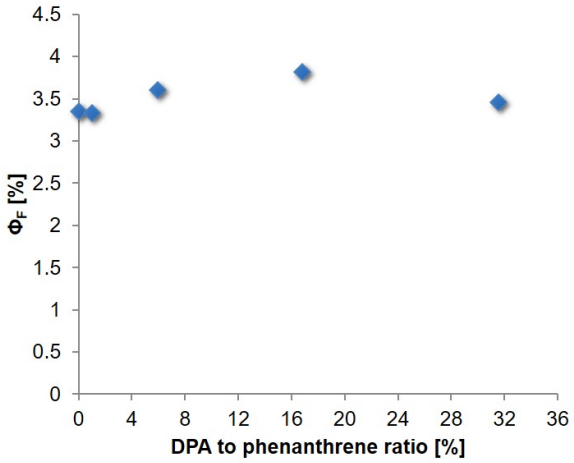

Figure 5.6. Fluorescence quantum yields with increasing concentrations of **DPA**. Conditions: **N-Phe$_3$** (1 µM), 10 mM acetate buffer (pH 4.71) and 10 vol% ethanol.

Fluorescence Quantum Yield Determination of N-Phe$_3$ + 15

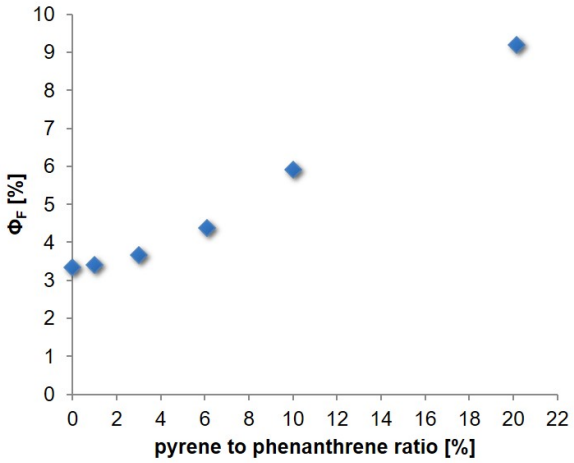

Figure 5.7. Fluorescence quantum yields with increasing concentrations of pyrene, by adding **15**. Conditions: **N-Phe$_3$** (1 µM), 10 mM acetate buffer (pH 4.71) and 10 vol% ethanol.

6. DNA as a Scaffold for Light-Harvesting Dyes

6.1. Abstract

The incorporation of the oligoamine **N-Phe$_3$** into a DNA light-harvesting system and its energy transfer efficiency to three different acceptor molecules (cyanine dye and pyrene derivatives) was investigated. Two different variations of the implementation of acceptors into the DNA duplex were tested: covalently-linked acceptor at the 5'-end of a single-strand DNA or the addition of a positively charged trimer to the formed DNA duplex. Spectroscopic measurements confirmed the energy transfer from **N-Phe$_3$** to the acceptor molecules after excitation of the phenanthrene donors.

6.2. Introduction

DNA light-harvesting systems have always been of interest due to their great advantages.[108,182,183] By using DNA as a scaffold it is possible to precisely position (nm-scale) a chromophore into the self-assembling duplex. Such DNA-chromophore systems can be further used for energy harvesting, biosensing, nanoimaging, and a lot more.[36,89,92,101,184–198] Often, people used Förster resonance energy transfer (FRET) as an energy-transfer in such systems.[185–187,199,200] Previously, we could show that by mixing DNA photonic wires with light-harvesting supramolecular polymers, the energy can be transferred with an efficiency of 59% (Figure 6.1).[98] The excitation energy collected from the phenanthrenes is transferred stepwise via the intermediate Cy3 (green) and Cy5 chromophores (yellow) to the final acceptor Cy5.5 (red) via FRET.

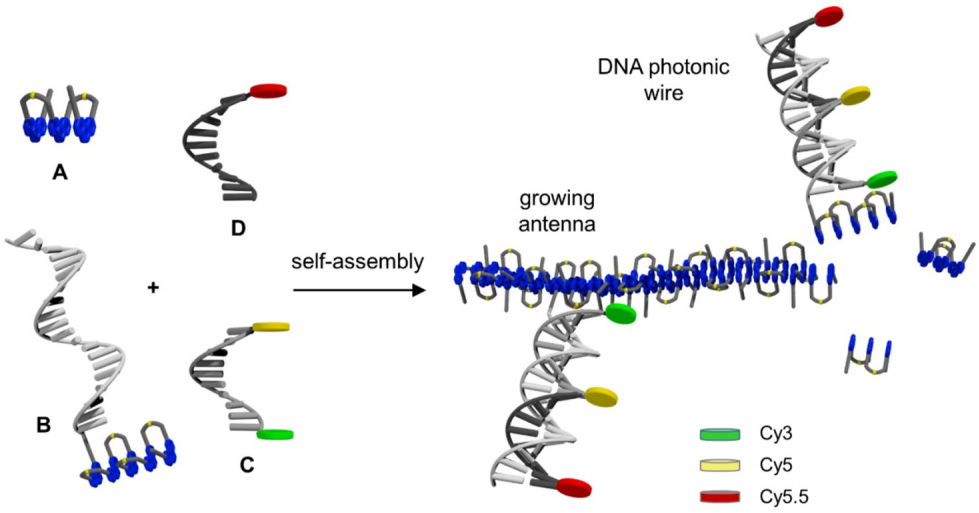

Figure 6.1. Graphical illustration of the self-assembly of a light-harvesting complex composed of phenanthrene trimers (A), a phenanthrene-modified oligonucleotide (B), and cyanine-modified oligonucleotides (C and D). Figure adapted from reference.[98]

Wang et al.[201] used a cationic water-soluble conjugated polymer, poly(1,4-phenylene)-2,7-[9,9-bis(6'-N,N,N-trimethylammonium)-hexyl]fluorene diiodide, with light-harvesting properties as a sensor and a double-stranded DNA in which ethidium bromide intercalates. Additionally, they attached fluorescein at one end of the dsDNA, which showed a more efficient energy transfer. By exciting the cationic polymer the energy is transferred via FRET first to the fluorescein (ET-1) then further to the ethidium bromide (EB, ET-2), where EB emits the light (Figure 6.2). They could show that fluorescein provided a FRET gate to dyes which are intercalated within DNA and that they are optically amplified by the properties of the conjugated polymer.
The question arose, whether it is possible to create a good light-harvesting system when the cationic **N-Phe$_3$** is added to a modified DNA. The **N-Phe$_3$** would act as a donor, the modification on the DNA as an acceptor, and the DNA as a framework.

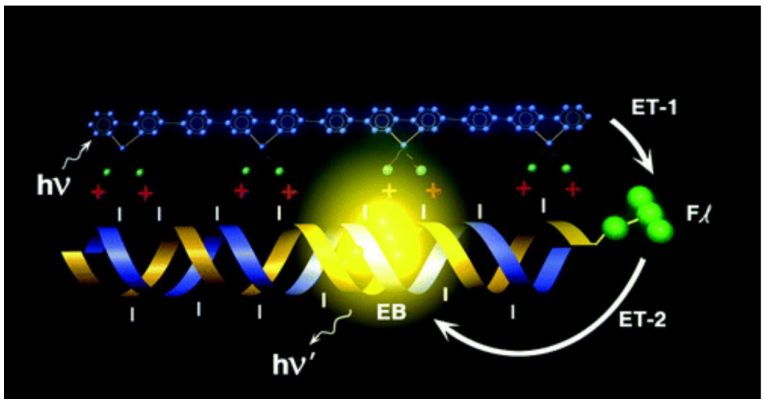

Figure 6.2. Model representation of the double-stranded DNA sequence sensor system and how the energy transfer takes place. The cationic polymer attaches via electrostatic forces to a duplex DNA, containing ethidium bromide (EB) in the middle of the duplex and fluorescein (Fl) at the beginning. After excitation of the cationic polymer, two energy transfers (ET-1 and ET-2) are occurring. Figure adapted from reference.[201]

6.3. Results and Discussion

6.3.1. Acceptor Cy3

Figure 6.3 shows schematically, how the experiment was performed. Two complementary DNA oligomers were purchased from Microsynth - one of them had a **Cy3** (pink) attached at the 5'-end of the DNA-strand (**ssDNA-Cy3**), which acted as an acceptor in this light-harvesting system (Table 6.1). After the hybridization of these DNA single strands, **N-Phe$_3$** (blue) was added in increasing concentrations and after each addition, spectroscopic measurements were done. Thereby, the added **N-Phe$_3$** can interact with the DNA at the minor and/or major groove (left in Figure 6.3) and/or via intercalation (right in Figure 6.3). When phenanthrene is excited at 320 nm, the energy is transferred from one to another phenanthrene across the DNA to the **Cy3** molecule, which emits the light at 550 nm.

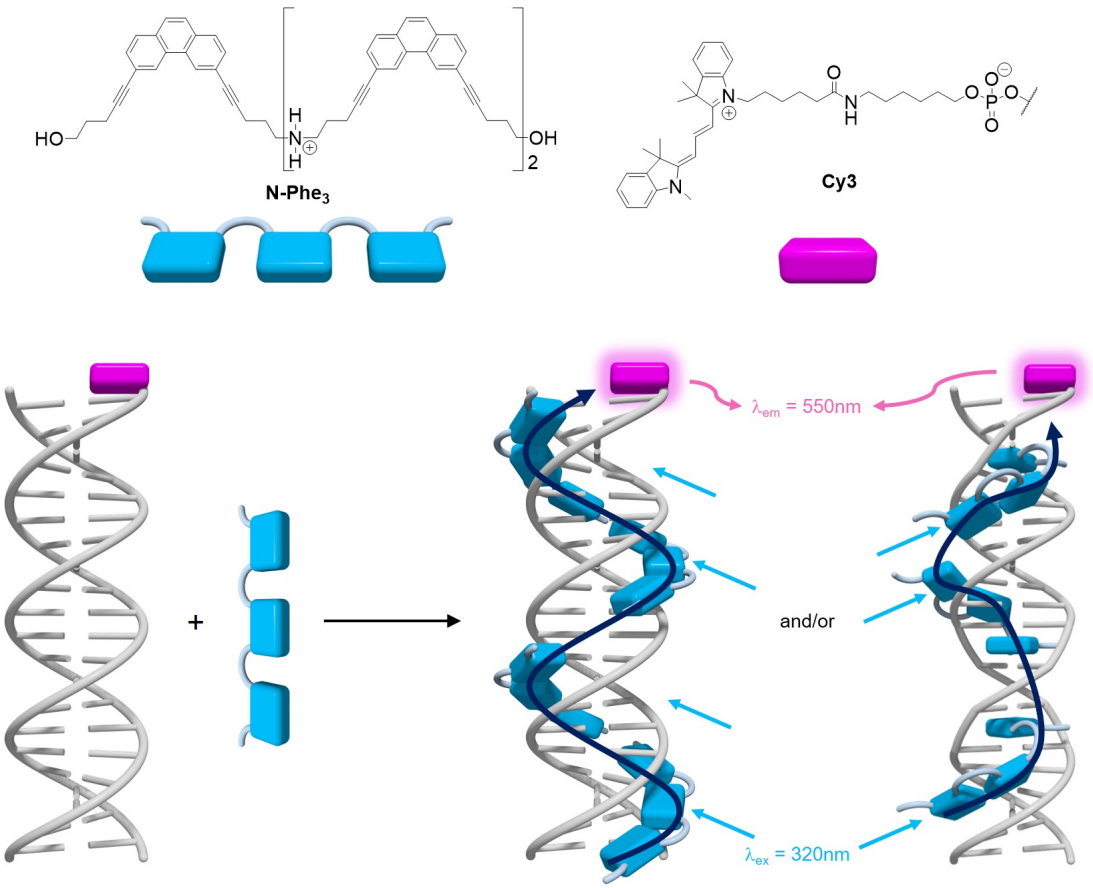

Figure 6.3. Schematic illustration of the performed experiment. A double-strand DNA was formed, whereas one strand has the acceptor **Cy3** (pink) at the 5'-end. After the addition of **N-Phe$_3$** (blue) to the solution, an interaction with the DNA at the minor and/or major groove (left) and/or by intercalation (right) is possible. After excitation of the phenanthrenes, the energy is transferred across the DNA to the acceptor **Cy3**.

Table 6.1. Sequences of the used DNA-strands, purchased from Microsynth.

	Sequence
ssDNA	5' – CAA GGT CCG ATG CAA GGA AG – 3'
ssDNA-Cy3	3' – GTT CCA GGC TAC GTT CCT TC(**Cy3**) – 5'

Fluorescence Spectra

Figure 6.4 shows the fluorescence spectra of the previously described experiment. When only the **N-Phe$_3$** is added in the aqueous solution and the phenanthrenes excited at 320 nm, the intensity increased where the phenanthrene emits the light (390 nm, left diagram). In presence of the DNA duplex containing **Cy3** (**dsDNA-Cy3**) and additions of **N-Phe$_3$**, the emission of **Cy3** (572 nm) strongly increases and the one of phenanthrene (390 nm) shows only a weak increase (right diagram in Figure 6.4). Comparing the left control diagram and the right sample diagram, one sees that the phenanthrene emission (390 nm) is much weaker in presence of **Cy3**, meaning that the energy of

the phenanthrenes was transferred to **Cy3**.

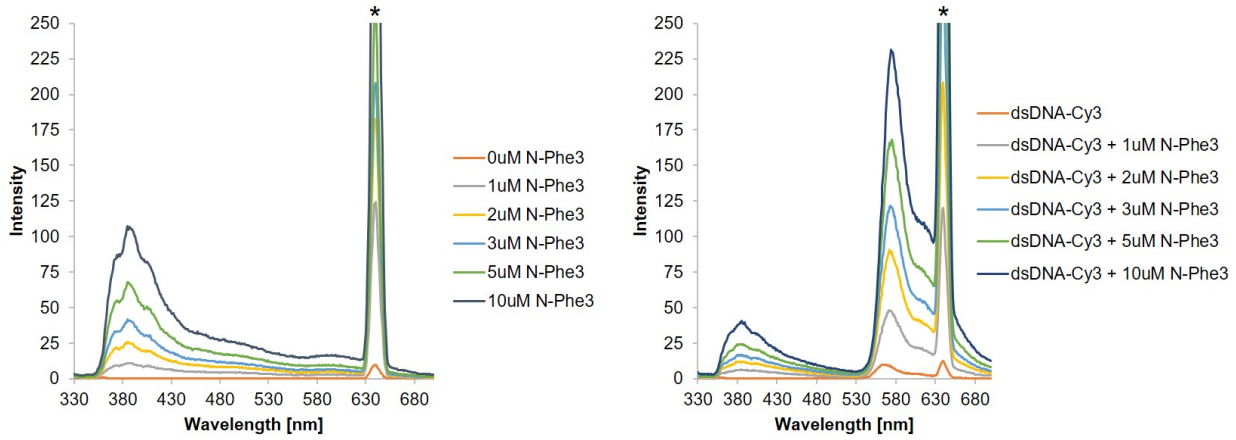

Figure 6.4. Fluorescence spectra of the DNA light-harvesting system experiments with **Cy3** as an acceptor. The one on the left is a control experiment, without any DNA, only with the acceptor **N-Phe$_3$**. On the right side, the DNA with **Cy3** was added and spectra measured with increasing concentrations of **N-Phe$_3$**. Conditions: **ssDNA** (1 µM), **ssDNA-Cy3** (1 µM), 10 mM sodium acetate buffer (pH 4.69), λ_{ex} = 320 nm. * = second-order transmission artefact at 640 nm.

Additionally, the increase of the emission-area was compared between the additive calculation of **N-Phe$_3$** and **dsDNA-Cy3** spectra and the measured spectrum of **dsDNA-Cy3** in presence of **N-Phe$_3$** (Figure 6.5). If there is no energy transfer, then the measured spectra should look like the added up ones. If there is an energy transfer, the donor phenanthrene will transfer the energy to the acceptor, which will fluoresce in a higher intensity and thus, the integrated fluorescence area is getting larger. The measurements showed that the emission-area becomes 1.58 times bigger than the calculated ones (**dsDNA-Cy3** + 1 µM **N-Phe$_3$**), meaning that an energy transfer is taking place.

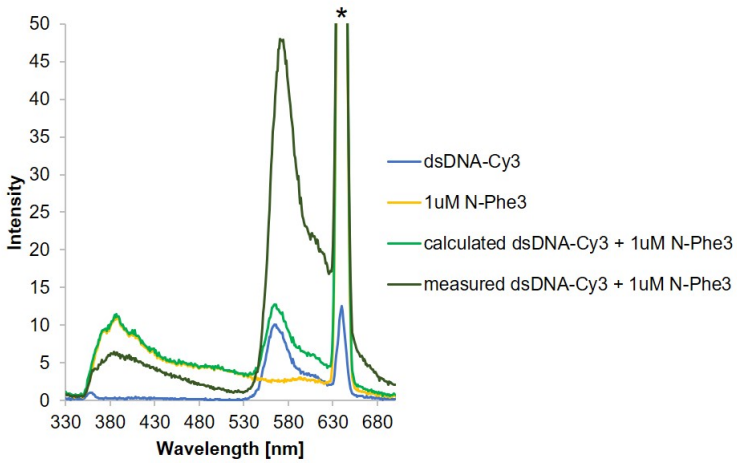

Figure 6.5. Measured and additive calculated spectra of the duplex **dsDNA-Cy3** in presence of **N-Phe$_3$**. Conditions: **ssDNA** (1 µM), **ssDNA-Cy$_3$** (1 µM), **N-Phe$_3$** (1 µM), 10 mM sodium acetate buffer (pH 4.69). λ_{ex} = 320 nm. * = second-order transmission artefact at 640 nm.

Additionally, the same experiments were also done with the DNA single-strand **ssDNA-Cy3**. If one compares the intensity increase at 572 nm (**Cy3**) with the **N-Phe$_3$**/DNA-ratio, there is a difference observable between single- and double-stranded DNA (Figure 6.6). When only **ssDNA-Cy3** is used for the measurements, the maximum intensity is reached at 5 µM **N-Phe$_3$**; when measuring with **dsDNA-Cy3** the maximum is at 10 µM **N-Phe$_3$**. The single-strand has only half the amount of negative charges at the backbone in comparison to the duplex and therefore, only half as many cations, **N-Phe$_3$** respectively, can bind to it. This means that the interaction is primarily electrostatic. At a certain concentration of **N-Phe$_3$** (5 µM for **ssDNA-Cy3**, 10 µM for **dsDNA-Cy3**), the DNA starts to precipitate. This can be observed by the intensity decrease and also the solution turned milky.

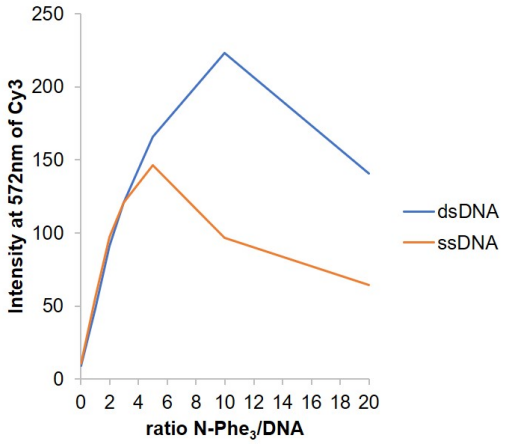

Figure 6.6. Comparison of the **Cy3**-emission in single-strand DNA (orange) with the duplex (blue).

Absorption Spectra

Figure 6.7 shows the absorption spectra of **N-Phe$_3$** alone, and after the addition to **dsDNA-Cy3** or **ssDNA-Cy3**. The grey spectrum shows the absorption of only **N-Phe$_3$** (10 µM). In comparison to the spectra after the addition of **N-Phe$_3$** to **dsDNA-Cy3** or **ssDNA-Cy3** a slight shift (1 nm) is observed (zoom-in, Figure 6.7). This shift indicates that there is a structural change upon binding to the DNA. When 10 µM **N-Phe$_3$** was added to the **dsDNA-Cy3** (blue), no scattering occurred, but if it was added to 10 µM of **ssDNA-Cy3** (yellow), the solution turned murky and scattering was observed at longer wavelengths. At half of the concentration, 5 µM **N-Phe$_3$**, the orange curve exhibited almost half of the intensity of the duplex (blue), but otherwise looked the same in shape and peak maxima. This was in correlation with the previously shown data in Figure 6.6.

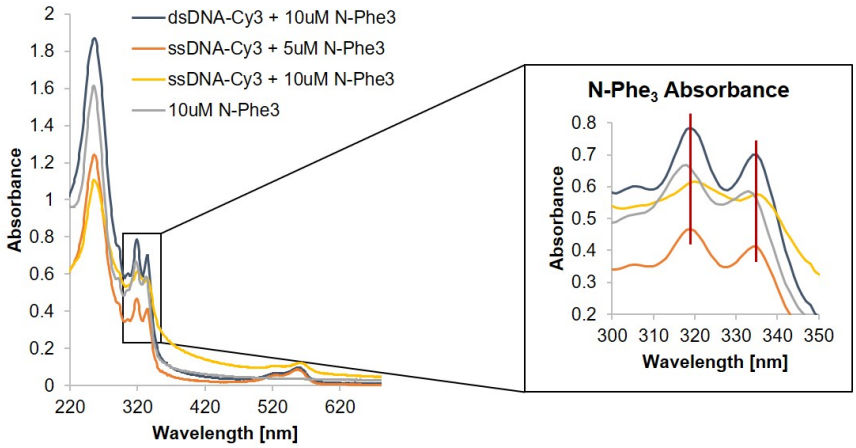

Figure 6.7. Absorption spectra of the DNA light-harvesting system experiments with **Cy3** as an acceptor. Spectra are shown of **N-Phe$_3$** (grey) and after its addition to **dsDNA-Cy3** (blue) and **ssDNA-Cy3** (orange and yellow). Conditions: **ssDNA** (1 µM), **ssDNA-Cy3** (1 µM), 10 mM sodium acetate buffer (pH 4.69).

6.3.2. Acceptor Py$_4$

It was shown that the energy transfer from phenanthrenes to **Cy3** in DNA works, that is why a pyrene acceptor was tried out: **Py$_4$** (Figure 6.8). Therefore, again **N-Phe$_3$** was titrated to the solution after the formation of the DNA duplex **ssDNA*****ssDNA-Py$_4$** (**dsDNA-Py$_4$**) (Table 6.2). The rest of the experiment was performed as described before. There are several options on how **N-Phe$_3$** may interact with DNA: interaction with the major and/or minor groove and/or intercalation (Figure 6.8). The phenanthrenes were excited at a wavelength of 320 nm, the energy transferred from phenanthrene across the DNA to the acceptor **Py$_4$**, which emitted the light at two wavelengths: 406 nm (pyrene monomer) and 500 nm (pyrene excimer).

Table 6.2. Sequences of the used DNA-strands. **ssDNA** was purchased from Microsynth and **ssDNA-Py$_4$** was synthesized by Nutcha Bürki.[130]

	Sequence
ssDNA	5' – CAA GGT CCG ATG CAA GGA AG – 3'
ssDNA-Py$_4$	3' – GTT CCA GGC TAC GTT CCT TC(Py)$_4$ – 5'

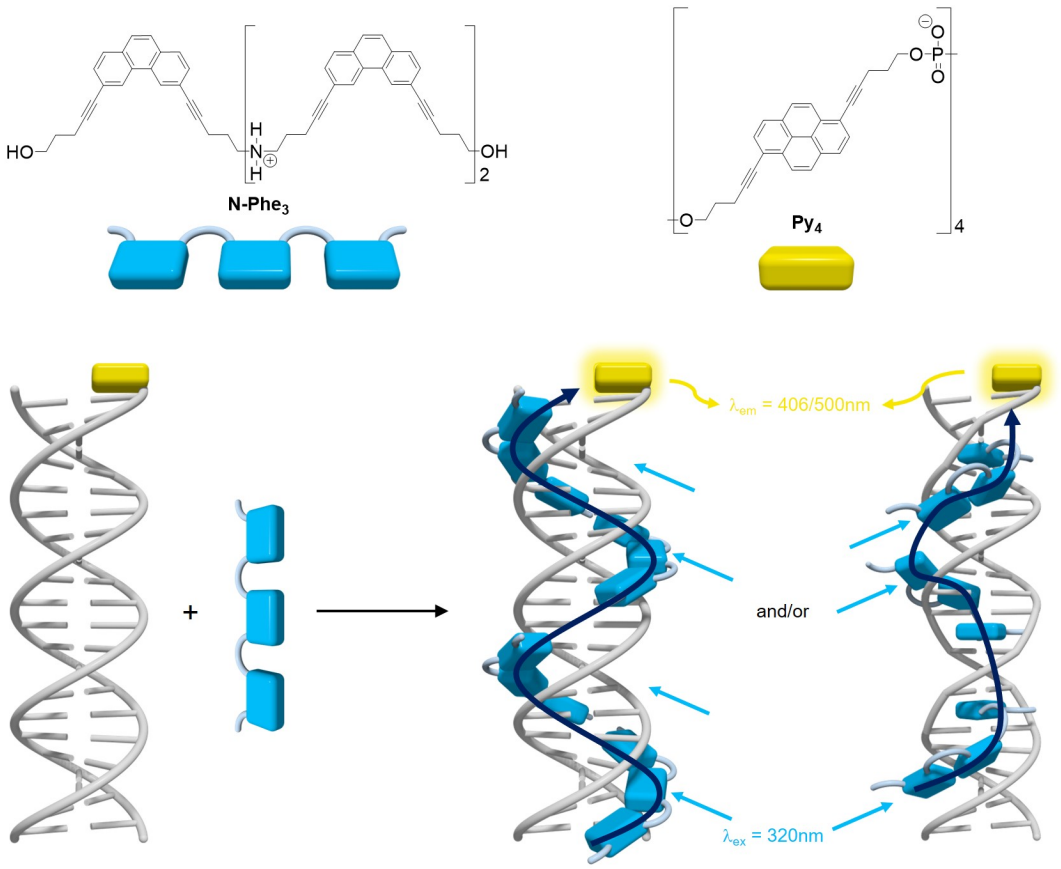

Figure 6.8. Schematic illustration of the performed experiment. Two single-strands were hybridized, whereas one of them has four pyrenes (**Py$_4$**) (yellow) attached at the 5'-end. **N-Phe$_3$** (blue) was titrated to the solution, where it can interact with the DNA at the minor and/or major groove (left) and/or by intercalation (right). After excitation of phenanthrenes, the energy is transferred across the DNA to the acceptor **Py$_4$**.

Fluorescence Spectra

Figure 6.9 shows two diagrams, on the left side are the emission spectra of only **N-Phe$_3$** as a control and on the right side **N-Phe$_3$** is added to the **dsDNA-Py$_4$**. The first blue curve in the right diagram shows the emission of only the **dsDNA-Py$_4$**, showing slight pyrene monomer emission at 406 nm and pyrene excimer fluorescence at 525 nm. After the addition of 1 µM **N-Phe$_3$** to the **dsDNA-Py$_4$** (orange curve), the pyrene excimer emission is still observable but blue-shifted to 500 nm. Additionally, a slight increase in intensity is observed around 430 nm, caused by phenanthrene-pyrene exciplex formation. This further goes on until the addition of 5 µM **N-Phe$_3$**. A comparison between the control spectra on the left side and the sample on the right side, shows that the phenanthrene emission at 386 nm is lower in the sample, indicating an energy transfer from phenanthrene to pyrene. After the addition of 10 µM **N-Phe$_3$** to **dsDNA-Py$_4$**, the phenanthrene emission at 386 nm showed an increase, which could probably mean, that not all the phenanthrenes are interacting with the DNA anymore. At a concentration of 20 µM **N-Phe$_3$** a prominent phenanthrene emission is observed, similar in intensity as the control. This shows that also the further addition of phenanthrenes did not interact with the DNA. On top also a precipitation is observed

in the sample, indicating the precipitation of the DNA.

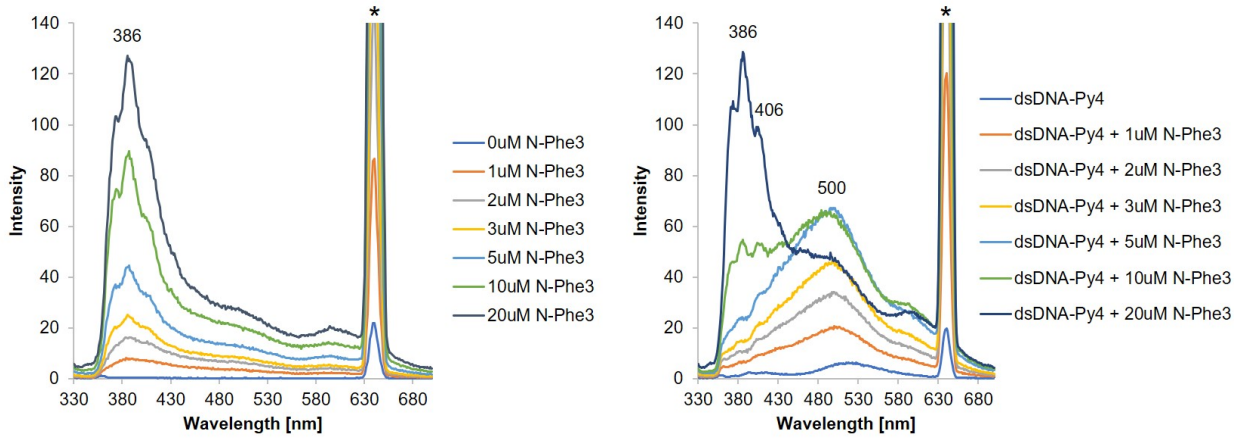

Figure 6.9. Fluorescence spectra of the DNA light-harvesting system with **Py_4** as an acceptor. Left: control experiment, where only **N-Phe_3** is added in buffer. Right: duplex **dsDNA-Py_4** is preformed out of **ssDNA*ssDNA-Py_4**, followed by the addition of **N-Phe_3**. Conditions: **ssDNA** (1 µM), **ssDNA-Py_4** (1 µM), 10 mM sodium acetate buffer (pH 4.69), λ_{ex} = 320 nm. * = second-order transmission artefact at 640 nm.

Like before, also here the spectra were summed up to check how big the emission-shift and emission-area change is. Figure 6.10 shows in dark green the measured interaction of **dsDNA-Py_4** with the addition of 1 µM **N-Phe_3**. The distinct maximum at 500 nm is caused by pyrene excimer emission, additionally, a slight shoulder is observed around 430 nm, indicating phenanthrene-pyrene exciplex emission, and last but not least pyrene monomer emission at 406 nm is observed too. The light-green spectrum in Figure 6.10 shows the theoretical added up spectra of **dsDNA-Py_4** and 1 µM **N-Phe_3**. This spectrum depicts the theoretical case in which both the duplex DNA with acceptor and **N-Phe_3** are in solution but not interacting. After excitation of phenanthrene, one would mostly observe phenanthrene emission at 386 nm, and a weak emission of pyrene (500 nm). Pyrene still absorbs very little at 320 nm, that is why one sees the weak emission. A comparison of the measured to the calculated spectrum shows a big increase in pyrene excimer emission (500 nm) and a slight decrease in phenanthrene emission (386 nm). This means that after exciting the phenanthrenes at 320 nm, the energy is transferred along the DNA to the pyrene acceptor due to the interaction of phenanthrene with DNA.

Figure 6.11 shows two additional diagrams with comparisons between calculated and measured spectra after the additions of 5 µM and 10 µM **N-Phe_3**. They indicate the decrease in **N-Phe_3**-emission at 386 nm (yellow) after measuring a spectrum of **N-Phe_3** added to **dsDNA-Py_4** (dark green spectra) even better than Figure 6.10. The integrated fluorescence area from the measured spectrum after the addition of 5 µM **N-Phe_3** even doubled in comparison to the calculated one.

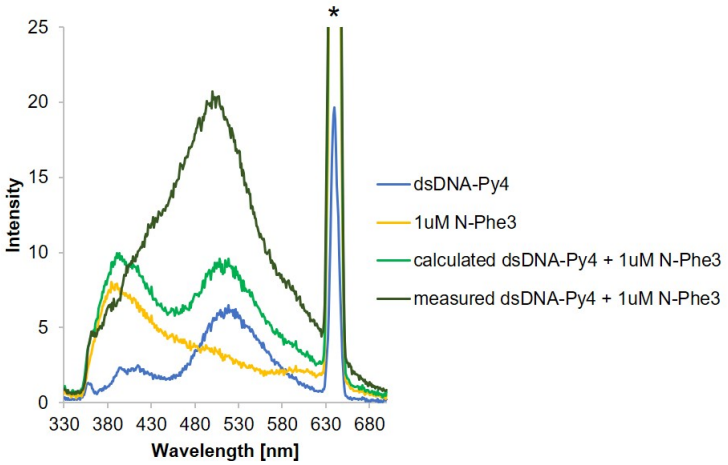

Figure 6.10. Measured and additive calculated spectra of the duplex **dsDNA-Py$_4$** in presence of **N-Phe$_3$**. Conditions: **ssDNA** (1 µM), **ssDNA-Py$_4$** (1 µM), **N-Phe$_3$** (1 µM), 10 mM sodium acetate buffer (pH 4.69), λ_{ex} = 320 nm. * = second-order transmission artefact at 640 nm.

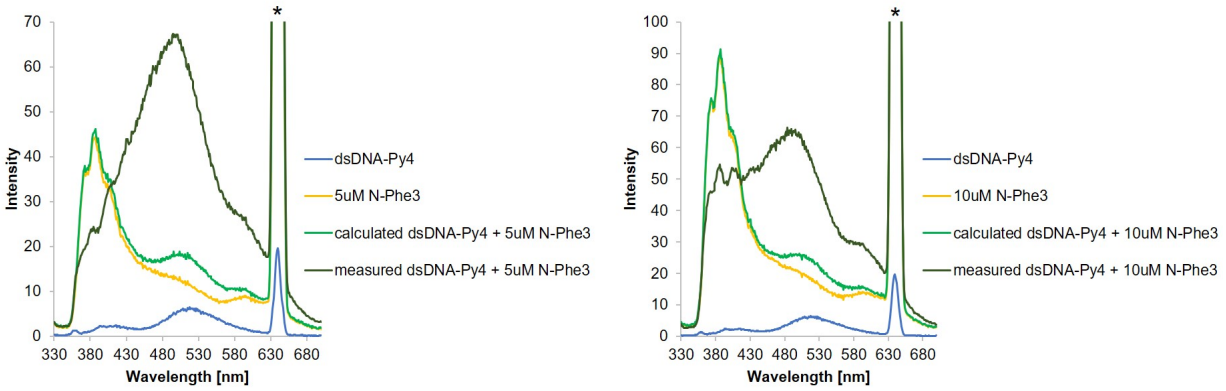

Figure 6.11. Measured and calculated spectra of the duplex in presence of **N-Phe$_3$**. Conditions: **ssDNA** (1 µM), **ssDNA-Py$_4$** (1 µM), **N-Phe$_3$** (5 resp. 10 µM), 10 mM sodium acetate buffer (pH 4.69), λ_{ex} = 320 nm. * = second-order transmission artefact at 640 nm.

6.3.3. Acceptor Pyrene in 15

Since the experiments with **Cy3** and **Py$_4$** as an acceptor worked, another acceptor was tried out: pyrene in **15**. As shown in Figure 6.12 this trimer has also a positively charged backbone due to its protonated amines in aqueous medium. Therefore, the acceptor (**15**) was added to the solution of an unmodified DNA duplex **ssDNA*ssDNA2** (Table 6.3) in the same concentration as the DNA. The rest of the experiment was performed as previously described and schematically shown in Figure 6.12 and Figure 6.13. These two figures show the possibilities of interactions between **N-Phe$_3$** and **15** with DNA: binding to the minor and/or major groove and/or intercalation. The phenanthrenes were excited at a wavelength of 320 nm, the energy was transferred from phenanthrenes across the DNA to the pyrene in **15**, which emitted the light at 430 nm. The emission at 430 nm is caused by an exciplex formation between phenanthrene and pyrene.

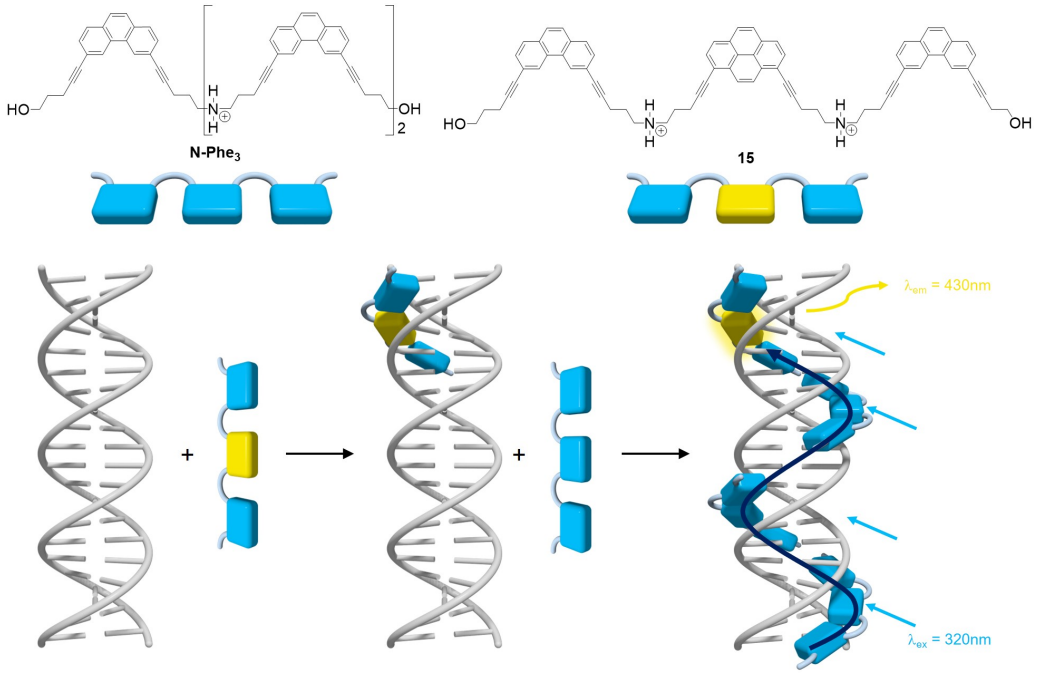

Figure 6.12. Schematic illustration of the binding to the major and/or minor groove. A duplex was preformed, followed by the addition of the acceptor **15**. **N-Phe$_3$** was titrated to the solution, where both, acceptor and donor, can interact with the DNA in the major and/or minor groove. After excitation of phenanthrenes, the energy is transferred across the DNA to the acceptor **15**.

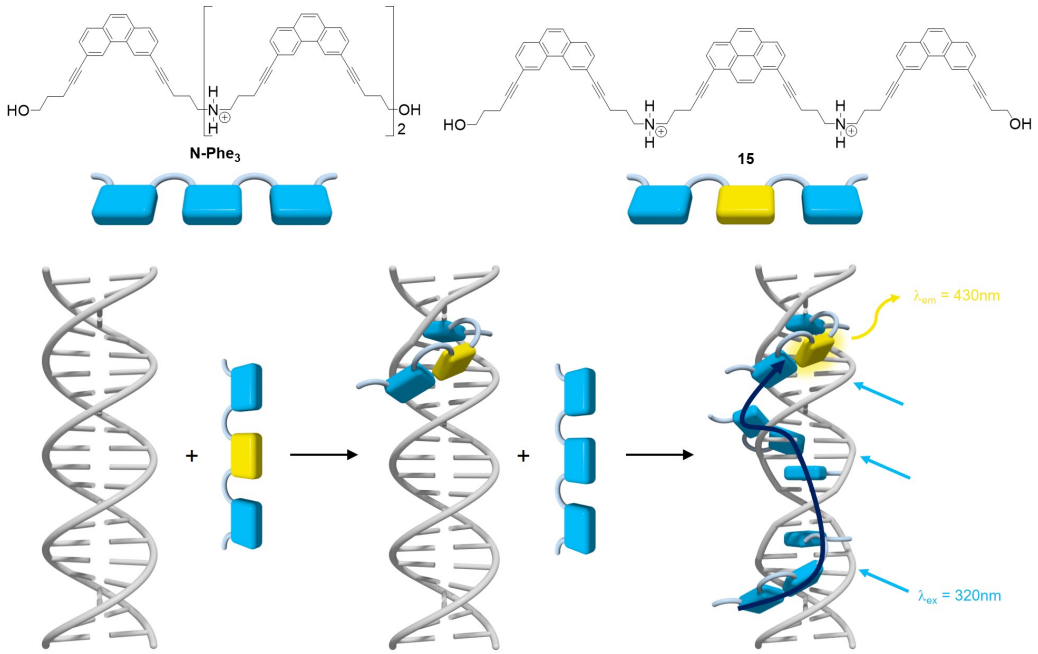

Figure 6.13. Schematic illustration of the binding by intercalation. A duplex was preformed, followed by the addition of the acceptor **15**. **N-Phe$_3$** was titrated to the solution, where both, acceptor and donor, can interact with the DNA by intercalation. After excitation of phenanthrenes, the energy is transferred across the DNA to the acceptor **15**.

Table 6.3. Sequences of the used DNA-strands, purchased from Microsynth.

	Sequence
ssDNA	5' – CAA GGT CCG ATG CAA GGA AG – 3'
ssDNA2	3' – GTT CCA GGC TAC GTT CCT TC – 5'

Fluorescence Spectra

Figure 6.14 displays two diagrams, a control of only **N-Phe$_3$** (left) and the sample in which **dsDNA+15** was doped with increasing **N-Phe$_3$**-concentrations. The first measured spectrum in the sample (right diagram) was only the DNA duplex with the acceptor **15** (**dsDNA+15**). The emission spectrum shows a slight pyrene monomer emission at 405 nm and a maximum at 500 nm, which is probably caused by a phenanthrene-pyrene exciplex or pyrene excimer. The addition of the donor **N-Phe$_3$** (1 µM, orange) shows pyrene monomer emission (405 nm), phenanthrene-pyrene exciplex emission at 426 nm, a shoulder at 500 nm, and very low phenanthrene emission (373, 385 and 405 nm). This is in contrast to the control (left diagram), where only 1 µM **N-Phe$_3$** is emitting at 373, 385 and 405 nm. Further additions of **N-Phe$_3$** showed the same. Therefore, an energy transfer occurs from phenanthrene across the DNA to pyrene in **15**.

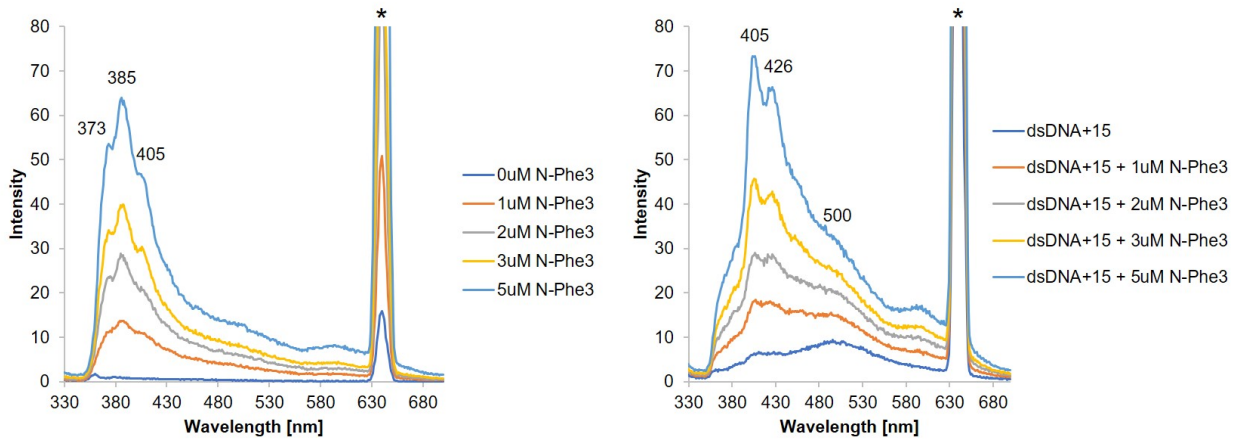

Figure 6.14. Fluorescence spectra of the DNA light-harvesting system with **15** as an acceptor. Left: control experiment, where only **N-Phe$_3$** is added in buffer. Right: duplex **ssDNA*ssDNA2** is preformed, the acceptor **15** added and then the concentration of **N-Phe$_3$** increased after every measurement. Conditions: **ssDNA** (1 µM), **ssDNA2** (1 µM), **15** (1 µM), 10 mM sodium acetate buffer (pH 4.69), λ_{ex} = 320 nm. * = second-order transmission artefact at 640 nm.

Figure 6.15 shows the emission spectra of only **dsDNA+15** (blue), only **N-Phe$_3$** (yellow), when mathematically adding these two spectra (light-green, calculated) and when the real sample is measured, where **N-Phe$_3$** is interacting with **dsDNA+15**. The figure nicely illustrates an emission red-shift after mixing **N-Phe$_3$** to **dsDNA+15**, causing distinct pyrene monomer emission (406 nm) and phenanthrene-pyrene exciplex emission (428 nm). The phenanthrene emission at 385 nm is almost half as low in the measured sample, compared to only **N-Phe$_3$** (yellow) or the calculated

spectrum (light-green). This indicates that the energy is transferred from phenanthrene across the DNA to the acceptor pyrene.

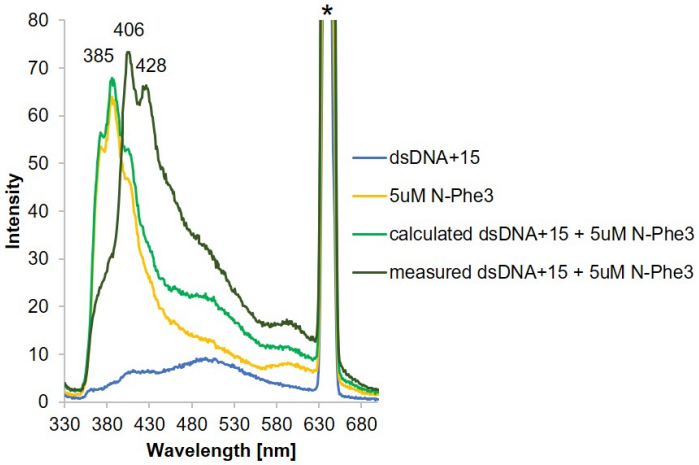

Figure 6.15. Measured and additive calculated spectra of the duplex **dsDNA+15** in presence of **N-Phe$_3$**. Conditions: **ssDNA** (1 µM), **ssDNA2** (1 µM), **N-Phe$_3$** (5 µM), 10 mM sodium acetate buffer (pH 4.69). λ_{ex} = 320 nm. * = second-order transmission artefact at 640 nm.

Absorption Spectra

Figure 6.16 shows the absorption spectra of only **N-Phe$_3$**, and after the addition to **dsDNA+15**. The spectrum of only 10 µM **N-Phe$_3$** (yellow) showed a slight blue-shift (1 nm) in comparison to after the addition to **dsDNA+15** (blue). This shift indicated a structural change of phenanthrene and an interaction between **N-Phe$_3$** and the DNA after mixing them together.

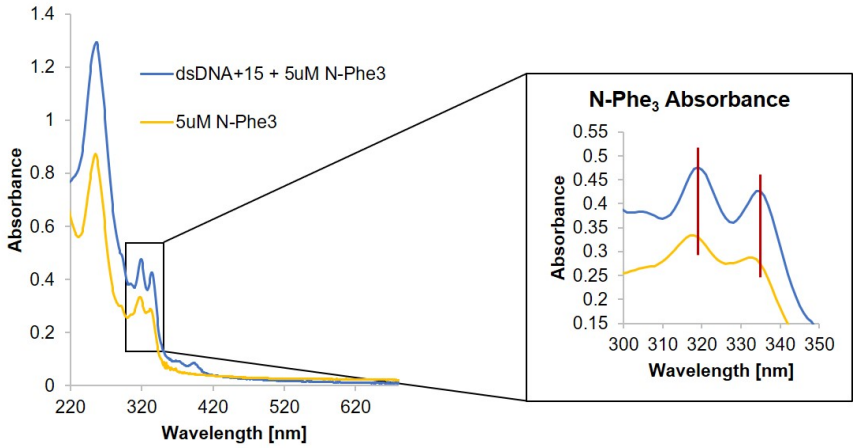

Figure 6.16. Absorption spectra of DNA light-harvesting system experiments with **15** as the acceptor and **N-Phe$_3$** as the donor. Spectra are shown of **N-Phe$_3$** (yellow) and after its addition to **dsDNA+15** (blue). Conditions: **ssDNA** (1 µM), **ssDNA2** (1 µM), **15** (1 µM), 10 mM sodium acetate buffer (pH 4.69).

6.4. Conclusions and Outlook

The energy transfer across DNA using the light-harvesting supramolecular polymer **N-Phe$_3$** was shown. Three different acceptors were tested in energy collecting efficiency: **Cy3**, **15**, and **Py$_4$**, and all of them showed light-harvesting properties. In the future, it would be interesting to change the length of the DNA strands and thus extend the light-harvesting antenna. Of course one could also place the acceptor in the middle of the DNA and thus the energy transfer from the donor to the acceptor could occur from both ends of the DNA strand. The use of a diamine-phenanthrene monomer could probably lead to a better interaction with the DNA, due to less steric hindrance of the smaller molecule. To get a more defined interaction of non-covalently attached acceptors (such as **15**) with the DNA, well-known intercalators (ethidium bromide or acridine orange) may be tested.

6.5. Experimental Part

6.5.1. Conditions for the Formation of the DNA Light-Harvesting Complex

First, the DNA duplexes were formed by heating the DNA single-strands (including the acceptor) to 70°C and cooling to 20°C with a controlled rate of 13°C/min in a Cary 100 spectrophotometer equipped with a Peltier thermostat. Afterwards, **N-Phe$_3$** was added in increasing amounts, without any heating/cooling steps in between.

6.5.2. Additional Measurements

Fluorescence Quantum Yield for Cy3-Acceptor

Table 6.4. Quantum yield calculations for the DNA light-harvesting system using **Cy3** as an acceptor with increasing additions of **N-Phe$_3$**. Quinine sulfate (${\phi_R}^{QS} = 0.546$) in 0.5 M H_2SO_4 was used as a reference.[181] Conditions: 1 µM **ssDNA**, 1 µM **ssDNA-Cy3**, 10 mM acetate buffer (pH 4.71) and 10 vol% ethanol.

Concentration of N-Phe$_3$ [µM]	ϕ_F [%]
1	5.4
2	5.1
3	4.7
5	3.7
10	2.4

Bibliography

[1] E. Krieg, M. M. C. Bastings, P. Besenius, B. Rybtchinski, *Chemical Reviews* **2016**, *116*, 2414–2477.

[2] L. Yang, X. Tan, Z. Wang, X. Zhang, *Chemical Reviews* **2015**, *115*, 7196–7239.

[3] L. Brunsveld, B. J. B. Folmer, E. W. Meijer, R. P. Sijbesma, *Chemical Reviews* **2001**, *101*, 4071–4097.

[4] J. F. Lutz, J. M. Lehn, E. W. Meijer, K. Matyjaszewski, *Nature Reviews Materials* **2016**, *1*, 1–14.

[5] J.-M. Lehn, *Angewandte Chemie International Edition* **2015**, *54*, 3276–3289.

[6] F. J. Hoeben, P. Jonkheijm, E. W. Meijer, A. P. Schenning, *Chemical Reviews* **2005**, *105*, 1491–1546.

[7] S. L. Li, T. Xiao, C. Lin, L. Wang, *Chemical Society Reviews* **2012**, *41*, 5950–5968.

[8] C. Li, J. Zuo, *Advanced Materials* **2020**, *32*, 1903762.

[9] J. Park, S. Murayama, M. Osaki, H. Yamaguchi, A. Harada, G. Matsuba, Y. Takashima, *Advanced Materials* **2020**, *32*, 2002008.

[10] S. Burattini, H. M. Colquhoun, J. D. Fox, D. Friedmann, B. W. Greenland, P. J. Harris, W. Hayes, M. E. MacKay, S. J. Rowan, *Chemical Communications* **2009**, 6717–6719.

[11] X. Ma, H. Tian, *Accounts of Chemical Research* **2014**, *47*, 1971–1981.

[12] T. Aida, E. W. Meijer, *Israel Journal of Chemistry* **2020**, *60*, 33–47.

[13] W. H. Binder, *Self-Healing Polymers: From Principles to Applications*, Wiley-VCH Verlag GmbH & Co. KGaA, Weinheim, Germany, **2013**, pp. 1–425.

[14] L. R. Hart, J. L. Harries, B. W. Greenland, H. M. Colquhoun, W. Hayes, *Polymer Chemistry* **2013**, *4*, 4860–4870.

[15] M. Ahmadi, S. Seiffert, *Macromolecules* **2021**, *54*, 1388–1400.

[16] J. H. Hirschberg, L. Brunsveid, A. Ramzi, J. A. Vekemans, R. P. Sijbesma, E. W. Meijer, *Nature* **2000**, *407*, 167–170.

[17] A. Arnaud, J. Belleney, F. Boué, L. Bouteiller, G. Carrot, V. Wintgens, *Angewandte Chemie International Edition* **2004**, *43*, 1718–1721.

[18] R. Dong, Y. Zhou, X. Huang, X. Zhu, Y. Lu, J. Shen, *Advanced Materials* **2015**, *27*, 498–526.

[19] L. Brunsveld, J. A. Vekemans, J. H. Hirschberg, R. P. Sijbesma, E. W. Meijer, *Proceedings of the National Academy of Sciences of the United States of America* **2002**, *99*, 4977–4982.

[20] T. E. Kaiser, H. Wang, V. Stepanenko, F. Würthner, *Angewandte Chemie International Edition* **2007**, *46*, 5541–5544.

[21] C. Wang, Z. Wang, X. Zhang, *Accounts of Chemical Research* **2012**, *45*, 608–618.

[22] W. Li, Y. Kim, M. Lee, *Nanoscale* **2013**, *5*, 7711–7723.

[23] D. Görl, X. Zhang, F. Würthner, *Angewandte Chemie International Edition* **2012**, *51*, 6328–6348.

[24] T. F. A. De Greef, M. M. J. Smulders, M. Wolffs, A. P. H. J. Schenning, R. P. Sijbesma, E. W. Meijer, *Chemical Reviews* **2009**, *109*, 5687–5754.

[25] A. Harada, *Supramolecular Polymer Chemistry*, Wiley-VCH Verlag GmbH & Co. KGaA, Weinheim, Germany, **2011**.

[26] L. Romberg, M. Simon, H. p. Erickson, *Journal of Biological Chemistry* **2001**, *276*, 11743–11753.

[27] D. Zhao, J. S. Moore, *Organic and Biomolecular Chemistry* **2003**, *1*, 3471–3491.

[28] P. Cordier, F. Tournilhac, C. Soulié-Ziakovic, L. Leibler, *Nature* **2008**, *451*, 977–980.

[29] Y. Yamamoto, T. Fukushima, Y. Suna, N. Ishii, A. Saeki, S. Seki, S. Tagawa, M. Taniguchi, T. Kawai, T. Aida, *Science* **2006**, *314*, 1761–1764.

[30] R. E. Blankenship, *Molecular Mechanisms of Photosynthesis*, (Ed.: R. E. Blankenship), Blackwell Science Ltd, Oxford, UK, **2002**, pp. 1–321.

[31] M. P. Johnson, *Essays in Biochemistry* **2016**, *60*, 255–273.

[32] E. Rabinowitch, *Journal of Physical Chemistry* **1957**, *61*, 870–878.

[33] M. R. Wasielewski, *Chemical Reviews* **1992**, *92*, 435–461.

[34] R. Croce, H. Van Amerongen, *Nature Chemical Biology* **2014**, *10*, 492–501.

[35] N. Aratani, D. Kim, A. Osuka, *Accounts of Chemical Research* **2009**, *42*, 1922–1934.

[36] F. Garo, R. Häner, *Angewandte Chemie International Edition* **2012**, *51*, 916–919.

[37] N. Sakai, S. Matile, *Beilstein J. Org. Chem* **2012**, *8*, 897–904.

[38] I. McConnell, G. Li, G. W. Brudvig, *Chemistry and Biology* **2010**, *17*, 434–447.

[39] A. Maity, A. Dey, M. Gangopadhyay, A. Das, *Nanoscale* **2018**, *10*, 1464–1473.

[40] C. L. Sun, H. Q. Peng, L. Y. Niu, Y. Z. Chen, L. Z. Wu, C. H. Tung, Q. Z. Yang, *Chemical Communications* **2018**, *54*, 1117–1120.

[41] T. Brixner, R. Hildner, J. Köhler, C. Lambert, F. Würthner, *Advanced Energy Materials* **2017**, *7*, 1–33.

[42] K. V. Rao, K. K. Datta, M. Eswaramoorthy, S. J. George, *Chemistry - A European Journal* **2012**, *18*, 2184–2194.

[43] T. Xiao, W. Zhong, L. Zhou, L. Xu, X. Q. Sun, R. B. Elmes, X. Y. Hu, L. Wang, *Chinese Chemical Letters* **2019**, *30*, 31–36.

[44] E. Collini, *Chem. Soc. Rev* **2013**, *42*, 4947.

[45] A. Y. Borisov, V. I. Godik, *BBA Reviews On Bioenergetics* **1973**, *301*, 227–248.

[46] W. S. Struve in *Anoxygenic Photosynthetic Bacteria*, (Eds.: R. E. Blankenship, M. T. Madigan, C. E. Bauer), Springer, Dordrecht, **1995**, Chapter 15, pp. 297–313.

[47] T. Förster, *Discussions of the Faraday Society* **1959**, *27*, 7–17.

[48] R. van Grondelle, *Biochimica et Biophysica Acta - Reviews On Bioenergetics* **1985**, *811*, 147–195.

[49] P. Rajdev, S. Ghosh, *The Journal of Physical Chemistry* **2019**, *123*, 327–342.

[50] S. Jang, M. D. Newton, R. J. Silbey, *The American Physical Society* **2004**, *92*, 218301–218302.

[51] T. Förster, *Annalen der Physik* **1948**, *437*, 55–75.

[52] D. L. Andrews, D. S. Bradshaw, R. Dinshaw, G. D. Scholes in *Photonics*, *Vol. 4*, (Ed.: D. L. Andrews), John Wiley & Sons, **2015**, Chapter 3, pp. 101–127.

[53] H. Sahoo, *Journal of Photochemistry and Photobiology C: Photochemistry Reviews* **2011**, *12*, 20–30.

[54] K. E. Sapsford, L. Berti, I. L. Medintz, *Angewandte Chemie International Edition* **2006**, *45*, 4562–4589.

[55] J. R. Lakowicz in *Principles of Fluorescence Spectroscopy*, **2006**, Chapter 13, pp. 443–475.

[56] A. R. Clapp, I. L. Medintz, H. Mattoussi, *ChemPhysChem* **2006**, *7*, 47–57.

[57] H. Wang, B. Yue, Z. Xie, B. Gao, Y. Xu, L. Liu, H. Sun, Y. Ma, *Physical Chemistry Chemical Physics* **2013**, *15*, 3527–3534.

[58] C. Neveu, Concept of FRET, `https://commons.wikimedia.org/w/index.php?curid=47158737`, Accessed: 2021-04-28.

[59] J. Strümpfer, M. Şener, K. Schulten, *J. Phys. Chem.Lett* **2012**, *3*, 536–542.

[60] T. C. Yen, Y. C. Cheng, *Procedia Chemistry* **2011**, *3*, 211–221.

[61] G. S. Engel, T. R. Calhoun, E. L. Read, T.-K. Ahn, T. Mančal, Y.-C. Cheng, R. E. Blankenship, G. R. Fleming, *Nature* **2007**, *446*, 782–786.

[62] E. Collini, G. D. Scholes, *Science* **2009**, *323*, 369–373.

[63] I. Hwang, G. D. Scholes, *Chemistry of Materials* **2011**, *23*, 610–620.

[64] D. Beljonne, C. Curutchet, G. D. Scholes, R. J. Silbey, *Journal of Physical Chemistry B* **2009**, *113*, 6583–6599.

[65] J. J. Richardson, M. Björnmalm, F. Caruso, *Science* **2015**, *348*, aaa2491.

[66] J. J. Richardson, J. Cui, M. Björnmalm, J. A. Braunger, H. Ejima, F. Caruso, *Chemical Reviews* **2016**, *116*, 14828–14867.

[67] R. F. De Oliveira, A. De Barros, M. Ferreira in *Nanostructures*, Elsevier Inc., **2017**, pp. 105–123.

[68] G. Decher, J. B. Schlenoff, *Multilayer Thin Films: Sequential Assembly of Nanocomposite Materials*, Wiley-VCH Verlag, **2006**, p. 543.

[69] J. A. Zasadzinski, R. Viswanathan, L. Madsen, J. Garnaes, D. K. Schwartz, *Science* **1994**, *263*, 1726–1733.

[70] I. R. Peterson, *Journal of Physics D: Applied Physics* **1990**, *23*, 379–395.

[71] O. Inacker, H. Kuhn, D. Möbius, D. Debuch, *Zeitschrift fur Physikalische Chemie* **1976**, *101*, 337–360.

[72] H. Kuhn, D. Möbius, *Angewandte Chemie International Edition* **1971**, *10*, 620–637.

[73] K. Ariga, T. Nakanishi, T. Michinobu, *Journal of Nanoscience and Nanotechnology* **2006**, *6*, 2278–2301.

[74] M. J. McShane, Y. M. Lvov in *Dekker Encyclopedia of Nanoscience and Nanotechnology, Third Edition*, Taylor & Francis, **2014**, pp. 1342–1358.

[75] K. Ariga, Y. Yamauchi, G. Rydzek, Q. Ji, Y. Yonamine, K. C.-W. Wu, J. P. Hill, *Chemistry Letters* **2014**, *43*, 36–68.

[76] G. Decher, J.-d. Hong, *Makromol. Chem. Macromol. Symp.* **1991**, *46*, 321–327.

[77] S. H. Kim, C. H. Ahn, S. Y. Park, C. J. Shin, H. J. Suh, *Dyes and Pigments* **2006**, *69*, 108–110.

[78] N. A. Kotov, I. Dekany, J. H. Fendler, *Journal of Physical Chemistry* **1995**, *99*, 13065–13069.

[79] G. B. Sukhorukov, E. Donath, H. Lichtenfeld, E. Knippel, M. Knippel, A. Budde, H. Möhwald, *Colloids and Surfaces A: Physicochemical and Engineering Aspects* **1998**, *137*, 253–266.

[80] D. Alkekhia, P. T. Hammond, A. Shukla, *Annual Review of Biomedical Engineering* **2020**, *22*, 1–24.

[81] T. Salditt, U. S. Schubert, *Reviews in Molecular Biotechnology* **2002**, *90*, 55–70.

[82] E. I. Goksu, J. M. Vanegas, C. D. Blanchette, W.-c. Lin, M. L. Longo, *Biochimica et Biophysica Acta* **2009**, *1788*, 254–266.

[83] R. K. Iler, *Journal of colloid and interface science* **1966**, *21*, 569–594.

[84] J. J. Kirkland, *Analytical Chemistry* **1965**, *37*, 1458–1461.

[85] G. Decher, J. D. Hong, *Berichte der Bunsengesellschaft für physikalische Chemie* **1991**, *95*, 1430–1434.

[86] G. Decher, *Science* **1997**, *277*, 1232–1237.

[87] K.-S. Kim, S. I. Yoo, M. Kim, B.-H. Sohn, *Macromolecular Chemistry and Physics* **2010**, *211*, 2382–2388.

[88] K.-S. Kim, S. I. Yoo, B.-H. Sohn, *Macromolecular Chemistry and Physics* **2018**, *219*, 1800115.

[89] M. Probst, S. M. Langenegger, R. Häner, *Chemical Communications* **2014**, *50*, 159–161.

[90] S. Rothenbühler, I. Iacovache, S. M. Langenegger, B. Zuber, R. Häner, *Nanoscale* **2020**, *12*, 21118–21123.

[91] C. D. Bösch, J. Jevric, N. Bürki, M. Probst, S. M. Langenegger, R. Häner, *Bioconjugate Chemistry* **2018**, *29*, 1505–1509.

[92] C. D. Bösch, E. Abay, S. M. Langenegger, M. Nazari, A. Cannizzo, T. Feurer, R. Häner, *Helvetica Chimica Acta* **2019**, *102*, 1–6.

[93] Y. Vyborna, M. Vybornyi, R. Häner, *Journal of the American Chemical Society* **2015**, *137*, 14051–14054.

[94] Y. Vyborna, M. Vybornyi, R. Häner, *Chem. Commun.* **2017**, *53*, 5179–5181.

[95] L. Markova, M. Probst, R. Häner, *RSC Advances* **2020**, *10*, 44841–44845.

[96] C. B. Winiger, S. Li, G. R. Kumar, S. M. Langenegger, R. Häner, *Angewandte Chemie International Edition* **2014**, *53*, 13609–13613.

[97] C. D. Bösch, S. M. Langenegger, R. Häner, *Angewandte Chemie* **2016**, *128*, 10115–10118.

[98] M. Kownacki, S. M. Langenegger, S.-X. Liu, R. Häner, *Angewandte Chemie* **2019**, *131*, 761–765.

[99] J. Jevric, S. M. Langenegger, R. Häner, *European Journal of Organic Chemistry* **2020**, *2020*, 4677–4680.

[100] T. Aida, E. W. Meijer, S. I. Stupp, *Science* **2012**, *335*, 813–817.

[101] S. P. Wijnands, E. W. Meijer, M. Merkx, *Bioconjugate Chemistry* **2019**, *30*, 1905–1914.

[102] Y. Yang, M. W. Urban, *Chemical Society Reviews* **2013**, *42*, 7446–7467.

[103] B. Rybtchinski, *ACS Nano* **2011**, *5*, 6791–6818.

[104] E. A. Appel, J. del Barrio, X. J. Loh, O. A. Scherman, *Chemical Society Reviews* **2012**, *41*, 6195–6214.

[105] S. I. Stupp, *Nano Letters* **2010**, *10*, 4783–4786.

[106] C. Gong, S. Sun, Y. Zhang, L. Sun, Z. Su, A. Wu, G. Wei, *Nanoscale* **2019**, *11*, 4147–4182.

[107] K. Petkau-Milroy, L. Brunsveld, *Organic and Biomolecular Chemistry* **2013**, *11*, 219–232.

[108] E. Stulz, *Accounts of Chemical Research* **2017**, *50*, 823–831.

[109] S. K. Albert, M. Golla, N. Krishnan, D. Perumal, R. Varghese, *Accounts of Chemical Research* **2020**, *53*, 2668–2679.

[110] D. Bousmail, P. Chidchob, H. F. Sleiman, *Journal of the American Chemical Society* **2018**, *140*, 9518–9530.

[111] C. A. Hauser, S. Maurer-Stroh, I. C. Martins, *Chemical Society Reviews* **2014**, *43*, 5326–5345.

[112] T. M. Figueira-Duarte, K. Müllen, *Chemical Reviews* **2011**, *111*, 7260–7314.

[113] J. G. Woller, J. K. Hannestad, B. Albinsson, *Journal of the American Chemical Society* **2013**, *135*, 2759–2768.

[114] H. Bui, S. A. Díaz, J. Fontana, M. Chiriboga, R. Veneziano, I. L. Medintz, *Advanced Optical Materials* **2019**, *7*, 1900562.

[115] Y. Zeng, J. Chen, T. Yu, G. Yang, Y. Li, *ACS Energy Letters* **2017**, *2*, 357–363.

[116] M. Vybornyi, A. V. Rudnev, S. M. Langenegger, T. Wandlowski, G. Calzaferri, R. Häner, *Angewandte Chemie International Edition* **2013**, *52*, 11488–11493.

[117] R. Szweda, M. Tschopp, O. Felix, G. Decher, J. F. Lutz, *Angewandte Chemie - International Edition* **2018**, *57*, 15817–15821.

[118] N. Appukutti, C. J. Serpell, *Polymer Chemistry* **2018**, *9*, 2210–2226.

[119] M. Vybornyi, A. Rudnev, R. Häner, *Chemistry of Materials* **2015**, *27*, 1426–1431.

[120] M. Vybornyi, Y. Vyborna, R. Häner, *Chemical Society Reviews* **2019**, *48*, 4347–4360.

[121] R. Häner, F. Garo, D. Wenger, V. L. Malinovskii, *Journal of the American Chemical Society* **2010**, *132*, 7466–7471.

[122] N. F. König, S. Telitel, S. Poyer, L. Charles, J. F. Lutz, *Macromolecular Rapid Communications* **2017**, *38*, 1–5.

[123] Y. Wang, X. Zhan, *Advanced Energy Materials* **2016**, *6*, 1–18.

[124] U. Akiba, D. Minaki, J. I. Anzai, *Polymers* **2017**, *9*, 1–16.

[125] D. Rawtani, Y. K. Agrawal, *Nanobiomedicine* **2014**, *1*, 8.

[126] R. M. Iost, F. N. Crespilho, *Biosensors and Bioelectronics* **2012**, *31*, 1–10.

[127] K. Ariga, M. Nishikawa, T. Mori, J. Takeya, L. K. Shrestha, J. P. Hill, *Science and Technology of Advanced Materials* **2019**, *20*, 51–95.

[128] H. R. Talele, A. R. Chaudhary, P. R. Patel, A. V. Bedekar, *ARKIVOC* **2011**, *9*, 15–37.

[129] J. Jevrić, Light-Harvesting Antenna Based on Polyaromatic Polyamines, Master Thesis, **2016**.

[130] N. Bürki, Towards water-soluble, two-dimensional (2D) fluorescent supramolecular platforms for the controlled DNA arraying, Master Thesis, **2016**.

[131] L. S. Shlyakhtenko, A. A. Gall, Y. L. Lyubchenko, *Methods Mol Biol.* **2013**, *931*, 1–20.

[132] S. D. Meyer, S. L. Schreiber, *The Journal of Organic Chemistry* **1994**, *59*, 7549–7552.

[133] A. F. Abdel-Magid, K. G. Carson, B. D. Harris, C. A. Maryanoff, R. D. Shah, *The Journal of organic chemistry* **1996**, *61*, 3849–3862.

[134] M. Vybornyi, Y. Bur-Cecilio Hechevarria, M. Glauser, A. V. Rudnev, R. Häner, *Chem. Commun.* **2015**, *51*, 16191–16193.

[135] H. Bittermann, D. Siegemund, V. L. Malinovskii, R. Häner, *Journal of the American Chemical Society* **2008**, *130*, 15285–15287.

[136] J. Grimshaw, J. Trocha-Grimshaw, *Journal of the Chemical Society Perkin Transactions 1* **1972**, 1622–1623.

[137] D. M. Connor, R. M. Kriegel, D. M. Collard, C. L. Liotta, D. A. Schiraldi, *Journal of Polymer Science Part A: Polymer Chemistry* **2000**, *38*, 1291–1301.

[138] C. B. Winiger, From DNA-Guided Chromophore Arrays to Light-Harvesting Polymers, PhD Thesis, **2014**.

[139] S. R. Yasa, S. S. Kaki, Y. Poornachandra, C. G. Kumar, V. Penumarthy, *Bioorganic and Medicinal Chemistry Letters* **2016**, *26*, 1978–1982.

[140] D. C. Monkhouse, *Journal of Pharmaceutical Sciences* **1977**, *66*, 1–19.

[141] T. S. Wiedmann, A. Naqwi, *Asian Journal of Pharmaceutical Sciences* **2016**, *11*, 722–734.

[142] G. Picca, Preparation of Mannose-derived 2D Supramolecular Polymers and Synthesis of Mannose/Dolichol mimics for Scramblase identification, PhD Thesis, **2020**.

[143] S. Cerra, L. Fontana, E. Rossi, M. Bassetti, C. Battocchio, I. Venditti, L. Carlini, R. Matassa, G. Familiari, I. Fratoddi, *Inorganica Chimica Acta* **2021**, *516*, 120170.

[144] H. Maeda, R. Horikoshi, M. Yamaji, T. Furuyama, M. Segi, *European Journal of Organic Chemistry* **2020**, *2020*, 3410–3422.

[145] D. G. Whitten, *Accounts of Chemical Research* **1993**, *26*, 502–509.

[146] X. Song, C. Geiger, I. Furman, D. G. Whitten, *Journal of the American Chemical Society* **1994**, *116*, 4103–4104.

[147] R. B. Greenwald, *Journal of Controlled Release* **2001**, *74*, 159–171.

[148] F. Garo, R. Häner, *European Journal of Organic Chemistry* **2012**, 2801–2808.

[149] O. O. Adeyemi, V. L. Malinovskii, S. M. Biner, G. Calzaferri, R. Häner, *Chemical Communications* **2012**, *48*, 9589–9591.

[150] X. Song, J. Perlstein, D. G. Whitten, *Journal of the American Chemical Society* **1997**, *119*, 9144–9159.

[151] X. Song, C. Geiger, S. Vaday, J. Perlstein, D. G. Whitten, *Journal of Photochemistry and Photobiology A: Chemistry* **1996**, *102*, 39–45.

[152] M. Schraub, H. Gray, N. Hampp, *Macromolecules* **2011**, *44*, 8755–8762.

[153] S. Vaday, H. C. Geiger, B. Cleary, J. Perlstein, D. G. Whitten, *Journal of Physical Chemistry B* **1997**, *101*, 321–329.

[154] L. Y. Liao, X. M. Zhang, F. Y. Hu, S. Wang, S. D. Xu, Q. D. Zeng, C. Wang, *Journal of Physical Chemistry C* **2014**, *118*, 7989–7995.

[155] O. Vybornyi, R. Häner, Stimuli-responsive supramolecular polymers from amphiphilic phosphodiester linked azobenzene trimers, Unpublished Data, **2021**.

[156] F. D. Lewis, X. Liu, Y. Wu, S. E. Miller, M. R. Wasielewski, R. L. Letsinger, R. Sanishvili, A. Joachimiak, V. Tereshko, M. Egli, *Journal of the American Chemical Society* **1999**, *121*, 9905–9906.

[157] M. Hariharan, K. Siegmund, F. D. Lewis, *J. Org. Chem* **2010**, *75*, 6236–6243.

[158] F. D. Lewis, H. Zhu, P. Daublain, T. Fiebig, M. Raytchev, Q. Wang, V. Shafirovich, *Journal of the American Chemical Society* **2006**, *128*, 791–800.

[159] F. D. Lewis, Y. Wu, L. Zhang, X. Zuo, R. T. Hayes, M. R. Wasielewski, *Journal of the American Chemical Society* **2004**, *126*, 8206–8215.

[160] F. D. Lewis, Y. Wu, X. Liu, *Journal of the American Chemical Society* **2002**, *124*, 12165–12173.

[161] R. H. Sieber, *Justus Liebigs Annalen der Chemie* **1969**, *730*, 31–46.

[162] H. R. Diéguez, A. López, V. Domingo, J. F. Arteaga, J. A. Dobado, M. M. Herrador, J. F. Quílez Del Moral, A. F. Barrero, *Journal of the American Chemical Society* **2010**, *132*, 254–259.

[163] T. Doi, H. Kashida, H. Asanuma, *Organic and Biomolecular Chemistry* **2015**, *13*, 4430–4437.

[164] D. H. Waldeck, *Chemical Reviews* **1991**, *91*, 415–436.

[165] J. Saltiel, J. T. D'Agostino, *Journal of the American Chemical Society* **1972**, *94*, 6445–6456.

[166] S. Malkin, E. Fischer, *The Journal of Physical Chemistry* **1964**, *68*, 1153–1163.

[167] H. Yu, R. Haner, *Chem. Commun.* **2016**, *52*, 14396–14399.

[168] F. J.-C. Natt, J. Hunziker, R. Häner, S. M. Langenegger, Oligonucleotide synthesis using photocleavable linkers, WO/2007/082713, **2007**.

[169] Y. Shi, X. Cao, D. Hu, H. Gao, *Angewandte Chemie* **2018**, *130*, 525–529.

[170] J. J. Li, Y. Chen, J. Yu, N. Cheng, Y. Liu, *Advanced Materials* **2017**, *29*, 1–5.

[171] C. Li, J. Zhang, S. Zhang, Y. Zhao, *Angewandte Chemie - International Edition* **2019**, *58*, 1643–1647.

[172] S. Guo, Y. Song, Y. He, X.-Y. Hu, L. Wang, *Angewandte Chemie* **2018**, *130*, 3217–3221.

[173] D. Gust, T. A. Moore, A. L. Moore, *Accounts of Chemical Research* **2001**, *34*, 40–48.

[174] R. Ziessel, A. Harriman, *Chemical Communications* **2011**, *47*, 611–631.

[175] M.-S. Choi, T. Yamazaki, I. Yamazaki, T. Aida, *Angewandte Chemie International Edition* **2004**, *43*, 150–158.

[176] H. Imahori, *Journal of Physical Chemistry B* **2004**, *108*, 6130–6143.

[177] Z. G. Fetisova, A. M. Freiberg, K. E. Timpmann, *Nature* **1988**, *334*, 633–634.

[178] A. Ustinov, H. Weissman, E. Shirman, I. Pinkas, X. Zuo, B. Rybtchinski, *Journal of the American Chemical Society* **2011**, *133*, 16201–16211.

[179] M. R. Wasielewski, *Accounts of Chemical Research* **2009**, *42*, 1910–1921.

[180] M. Hao, G. Sun, M. Zuo, Z. Xu, Y. Chen, X.-Y. Hu, L. Wang, *Angewandte Chemie International Edition* **2019**, *58*, 2–8.

[181] W. H. Melhuish, *Journal of Physical Chemistry* **1961**, *65*, 229–235.

[182] B. Albinsson, J. K. Hannestad, K. Börjesson, *Coordination Chemistry Reviews* **2012**, *256*, 2399–2413.

[183] W. Su, V. Bonnard, G. A. Burley, *Chemistry - A European Journal* **2011**, *17*, 7982–7991.

[184] Ö. Persil, N. V. Hud, *Trends in Biotechnology* **2007**, *25*, 433–436.

[185] J. S. Melinger, A. Khachatrian, M. G. Ancona, S. Buckhout-White, E. R. Goldman, C. M. Spillmann, I. L. Medintz, P. D. Cunningham, *ACS Photonics* **2016**, *3*, 659–669.

[186] J. K. Hannestad, P. Sandin, B. Albinsson, *Nucleic acids symposium series (2004)* **2008**, 685.

[187] J. K. Hannestad, S. R. Gerrard, T. Brown, B. Albinsson, *Small* **2011**, *7*, 3178–3185.

[188] X. Zhou, S. Mandal, S. Jiang, S. Lin, J. Yang, Y. Liu, D. G. Whitten, N. W. Woodbury, H. Yan, *Journal of the American Chemical Society* **2019**, *141*, 8473–8481.

[189] F. Nicoli, A. Barth, W. Bae, F. Neukirchinger, A. H. Crevenna, D. C. Lamb, T. Liedl, *ACS Nano* **2017**, *11*, 11264–11272.

[190] P. Ensslen, F. Brandl, S. Sezi, R. Varghese, R. J. Kutta, B. Dick, H. A. Wagenknecht, *Chemistry - A European Journal* **2015**, *21*, 9349–9354.

[191] P. K. Dutta, R. Varghese, J. Nangreave, S. Lin, H. Yan, Y. Liu, *Journal of the American Chemical Society* **2011**, *133*, 11985–11993.

[192] W. P. Klein, B. S. Rolczynski, S. M. Oliver, R. Zadegan, S. Buckhout-white, M. G. Ancona, P. D. Cunningham, J. S. Melinger, P. M. Vora, W. Kuang, I. L. Medintz, S. A. Díaz, *ACS Appl. Nano Mater.* **2020**, *3*, 3323–3336.

[193] E. Boulais, N. P. Sawaya, R. Veneziano, A. Andreoni, J. L. Banal, T. Kondo, S. Mandal, S. Lin, G. S. Schlau-Cohen, N. W. Woodbury, H. Yan, A. Aspuru-Guzik, M. Bathe, *Nature Materials* **2018**, *17*, 159–166.

[194] C. J. Serpell, T. G. W. Edwardson, P. Chidchob, K. M. M. Carneiro, H. F. Sleiman, *J. Am. Chem. Soc* **2014**, *136*, 15767–15774.

[195] Y. Vyborna, M. Vybornyi, A. V. Rudnev, R. Häner, *Angewandte Chemie - International Edition* **2015**, *54*, 7934–7938.

[196] Y. N. Teo, E. T. Kool, *Chemical Reviews* **2012**, *112*, 4221–4245.

[197] B. L. Cannon, D. L. Kellis, L. K. Patten, P. H. Davis, J. Lee, E. Graugnard, B. Yurke, W. B. Knowlton, *Journal of Physical Chemistry A* **2017**, *121*, 6905–6916.

[198] P. K. Dutta, S. Levenberg, A. Loskutov, D. Jun, R. Saer, J. T. Beatty, S. Lin, Y. Liu, N. W. Woodbury, H. Yan, *Journal of the American Chemical Society* **2014**, *136*, 16618–16625.

[199] S. A. Diaz, S. Buckhout-White, M. G. Ancona, C. M. Spillmann, E. R. Goldman, J. S. Melinger, I. L. Medintz, *Advanced Optical Materials* **2016**, *4*, 399–412.

[200] L. Olejko, I. Bald, *RSC Advances* **2017**, *7*, 23924–23934.

[201] S. Wang, B. S. Gaylord, G. C. Bazan, *Journal of the American Chemical Society* **2004**, *126*, 5446–5451.

A. Appendix

A.1. General Methods

NMR Spectroscopy

All the NMR spectra were measured on a Bruker Avance III HD (300 MHz) spectrometer at 298K in the Departement of Chemistry, Biochemistry and Pharmaceutical Sciences of the University of Bern.

Mass Spectrometry

All the MS spectra were obtained on a Thermo Fisher LTQ Orbitrap XL using Nano Electrospray Ionization (NSI) from the Analytical Research and Services of the University of Bern.

UV-vis Measurements

The UV-vis measurements were done on a Varian-Cary-100 spectrophotometer. The samples contained 10 mM acetate buffer (pH 4.69) or 10 mM sodium phosphate buffer (pH 7.01), with varying ethanol, salt and trimer concentration, as stated in the caption of the figures. At every temperature the equilibration temperature was set to 10 min and the probe temperature was controlled and monitored by a reference cuvette.

Fluorescence Measurements

The fluorescence measurements were done on a Varian-Cary-Eclipse spectrofluorimeter. The samples were treated in the same way as already described in the subsection of UV-vis measurements.

AFM Measurements

All the AFM measurements were performed on a Nanoflex AFM instrument (Nanosurf AG, Switzerland) in tapping mode under ambient conditions. Tap190-Al-G cantilevers from Budget-Sensors were used, with a resonant frequency of 190 kHz, a force constant of 48 N/m and a tip radius of 10 nm. Mica sheets (Glimmer "V1", 20mm x 20mm, G250-7, Plano GmbH) were used as substrates. The graphical illustration and evaluation was done with Nanosurf C3000 and SPIP.
30 µl of the solution to be examined were incubated on a non-modified mica-sheet for 10 minutes. Whereas the solution was previously heated up (70-90°C) and cooled to 20°C, using either the UV-vis machine (block or gradient) or the Eppendorf Thermomixer Compact. After the incubation, the mica sheet was washed with 1 ml Milli-Q water and the water was sucked up with a KIMTECH precision wipe from the edges. The mica-sheet was dried under an argon flow. APTES-modified mica was used for the negatively charged molecules. The preparation was the same as previously described, except the washing process. After the 10 minutes of incubation on the mica, the sample was washed off with 2x1 ml of Milli-Q-water and dried under an argon flow.

TEM Measurements

Transmission electron microscopy (TEM) was performed on a Tecnai Spirit instrument with an operating voltage of 80 kV and with either an Olympus-SIS Veleta CCD camera or FEI Eagle CCD camera. Carbon-coated copper grids (300 Mesh, Agar Scientific) were used as a substrate. For a better contrast (e.g. measuring sheets), Holey/Carbon grids were used.
The supramolecular polymers samples were prepared as described in the corresponding chapters. The samples were prepared as followed: 5µl of the supramolecular polymer was dropped onto the grid, waited for 10min, and the solution was blotted. Afterwards the grid was washed by dipping into 20µl of Milli-Q water and blotting two times. The last step was the staining of the sample with a 0.5% aqueous uranyl-acetate solution. This was done according to the washing procedure: the sample was dipped twice into 20µl of the uranyl-acetate solution (0.5%).

DLS Measurements

DLS measurements were carried out on a Zetasizer Nano instrument (Malvern Instruments) by using the standard operation procedure for particle size determination. Pre-washed plastic cuvettes were used for the measurements. The equilibration time at 70°C was 5 minutes, before cooling to 20°C.

A.2. Abbreviations

ACN	acetonitrile
AFM	atomic force microscopy
APTES	3-aminopropyltriethoxy silane
DCM	dichloromethane
DIPEA	N,N-diisopropylethylamine
DMF	N,N-dimethylformamide
DMT-Cl	4,4'-dimethoxytriphenylmethyl chloride
EtOAc	ethyl acetate
Et_3N	triethylamine
FRET	förster resonance energy transfer
Hex	hexane
LHC	light-harvesting complex
PAH	polycyclic aromatic hydrocarbon
PAM-Cl	2-cyanoethyl N,N-diisopropylchlorophosphoramidite
RT	room temperature
TEM	transmission electron microscopy
THF	tetrahydrofuran
TLC	thin layer chromatography

A.3. NMR Spectra

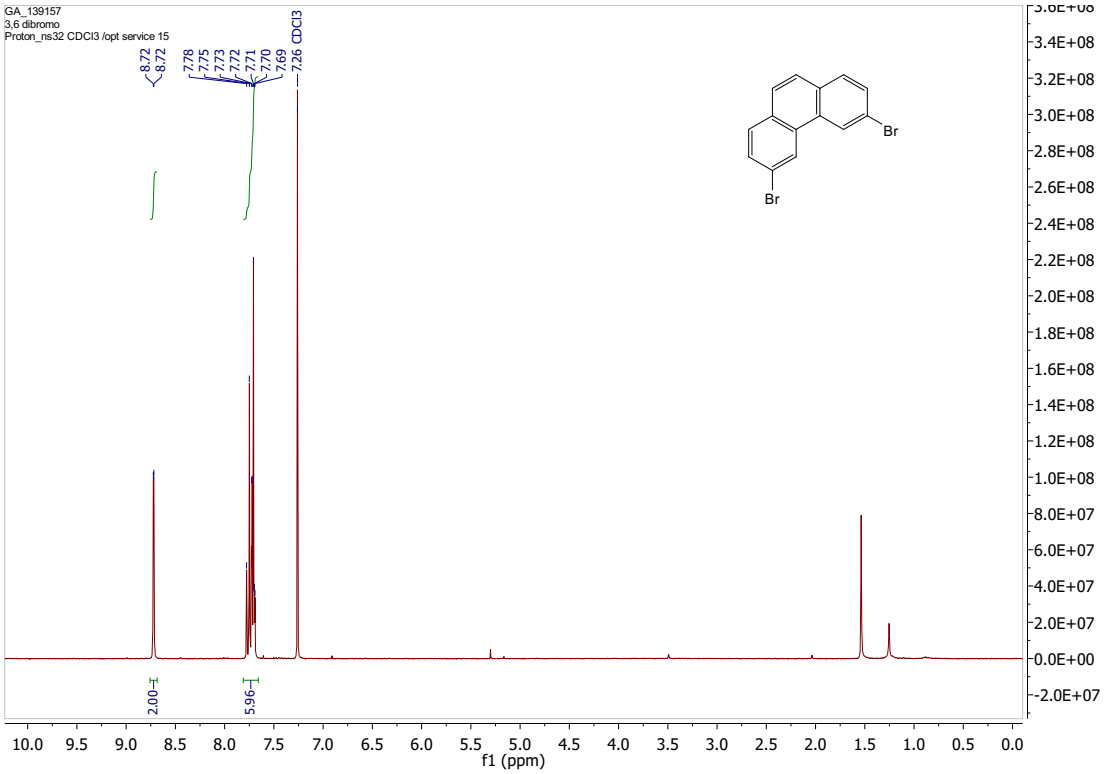

Figure A.1. ^{1}H-NMR of compound **2** in $CDCl_3$.

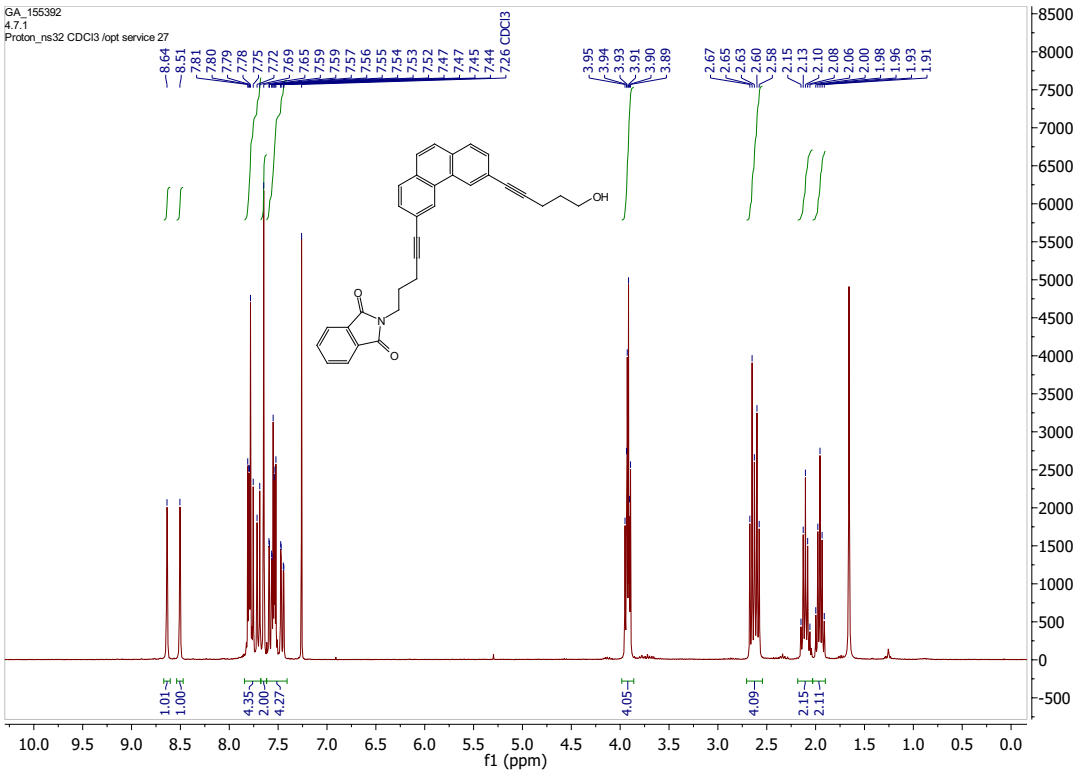

Figure A.2. ^{1}H-NMR of compound **3** in $CDCl_3$.

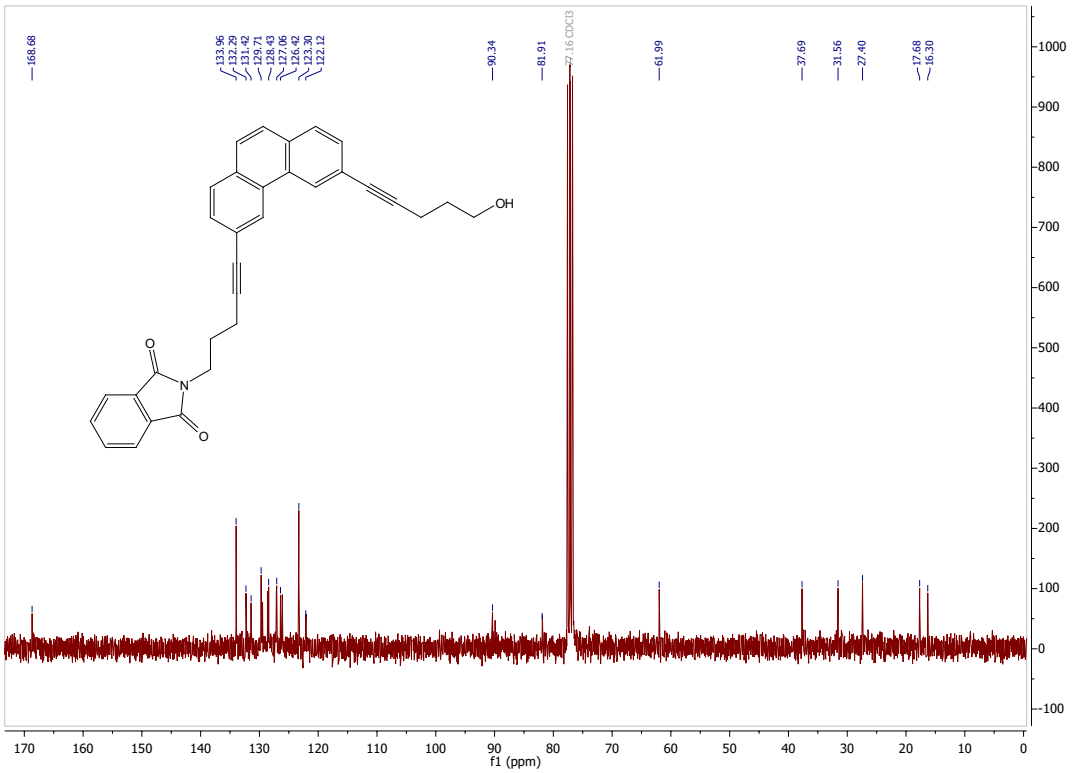

Figure A.3. ^{13}C-NMR of compound **3** in $CDCl_3$.

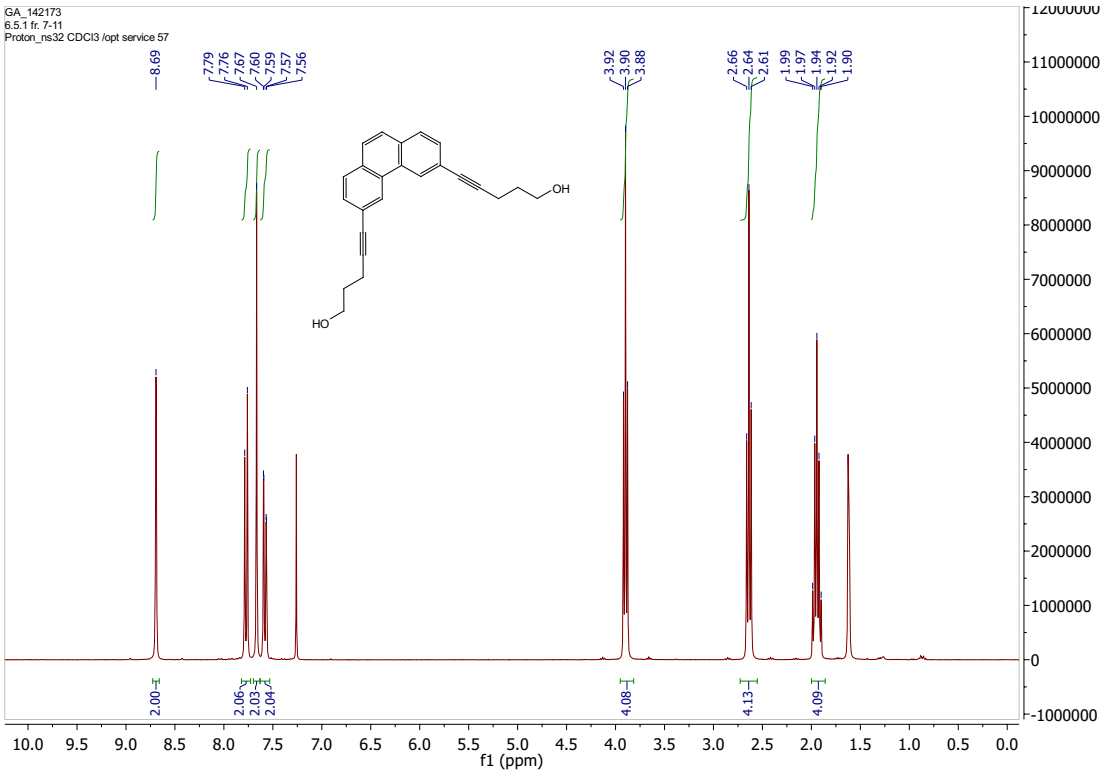

Figure A.4. ^{1}H-NMR of compound **4** in $CDCl_3$.

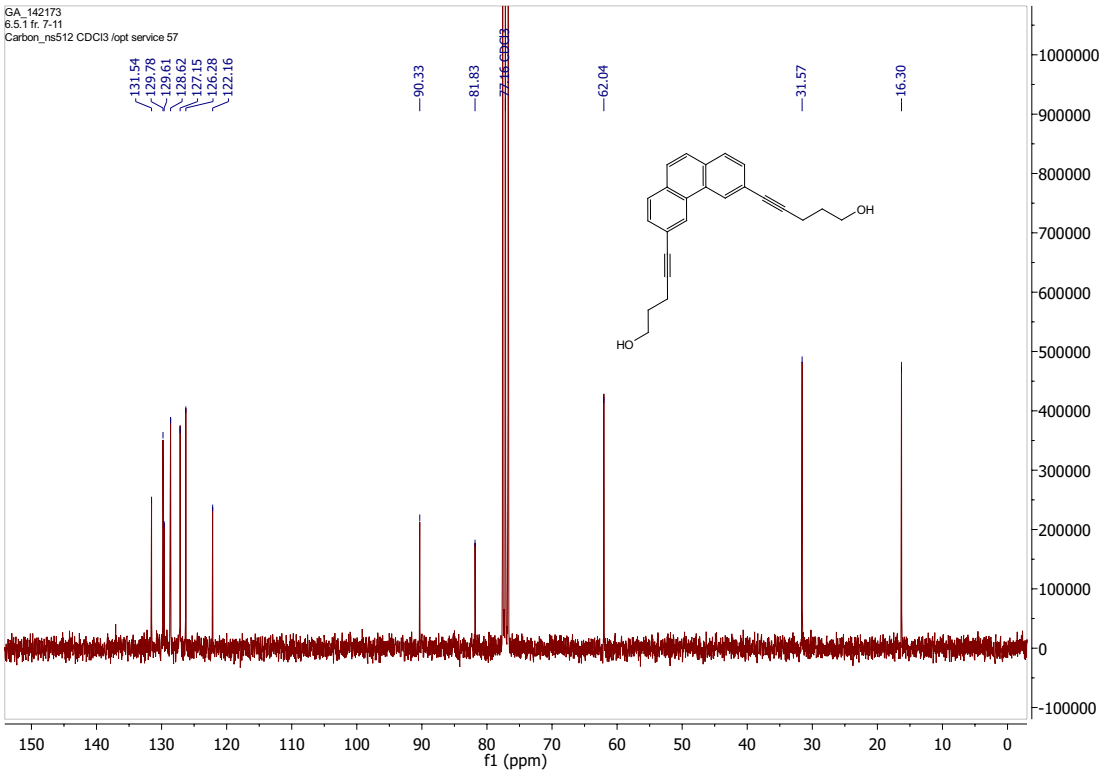

Figure A.5. ^{13}C-NMR of compound **4** in $CDCl_3$.

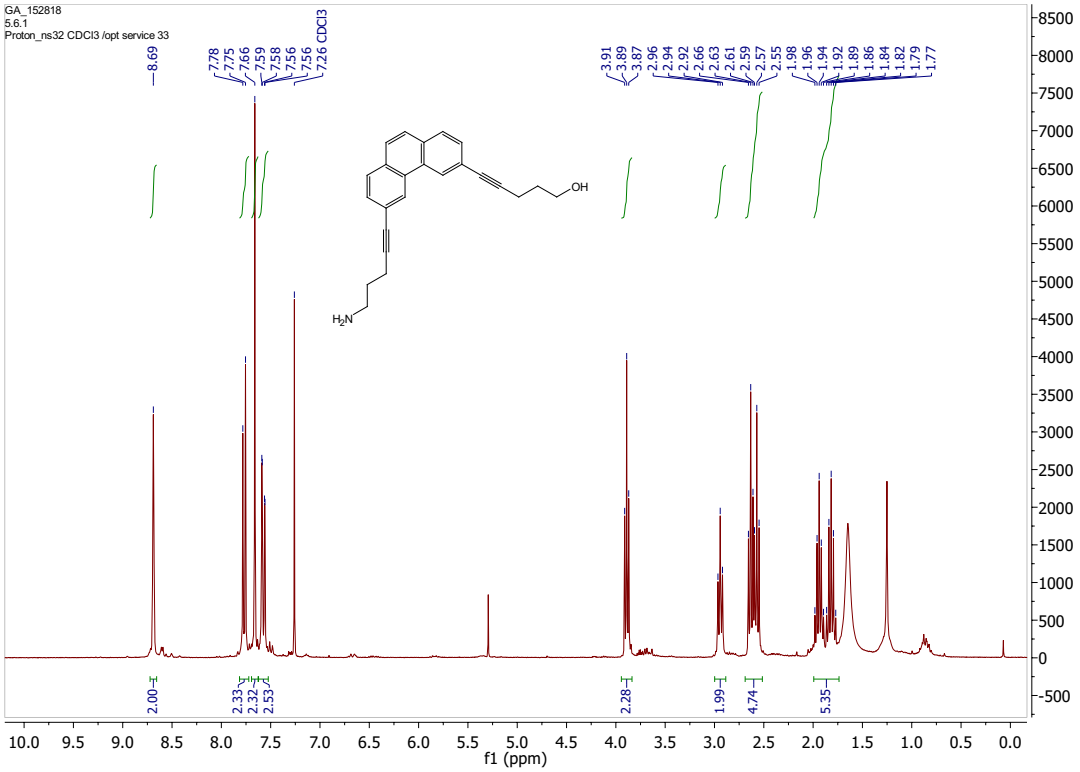

Figure A.6. ^{1}H-NMR of compound **5** in $CDCl_3$.

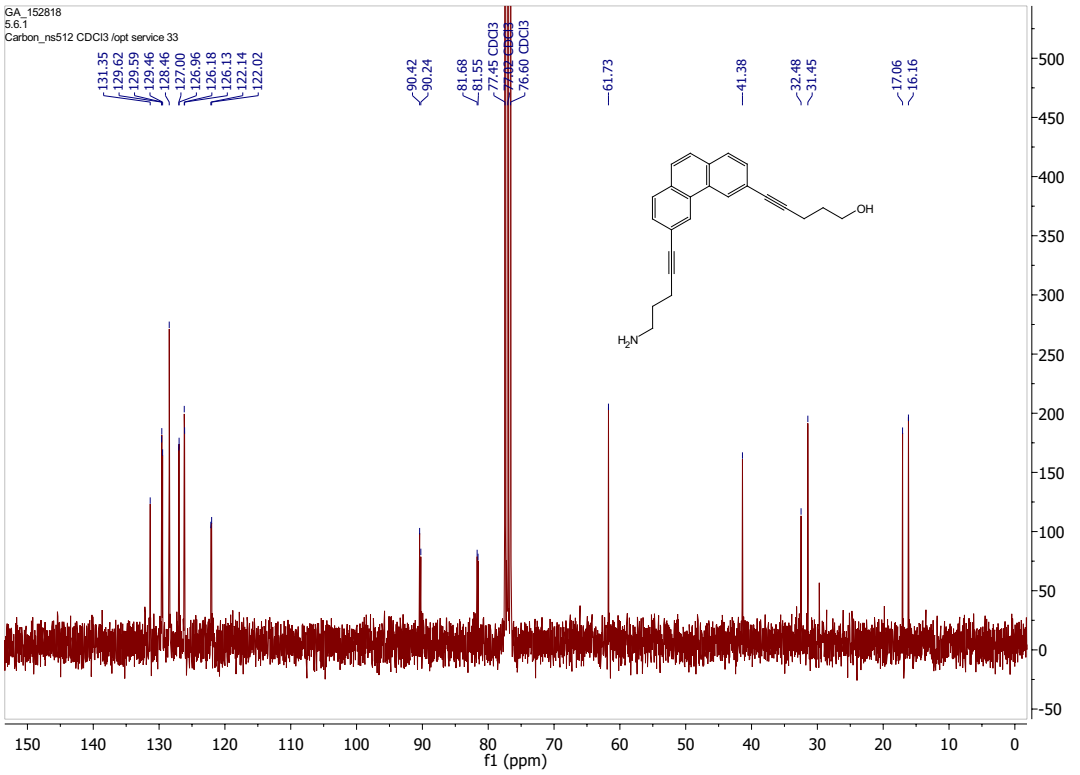

Figure A.7. ^{13}C-NMR of compound **5** in $CDCl_3$.

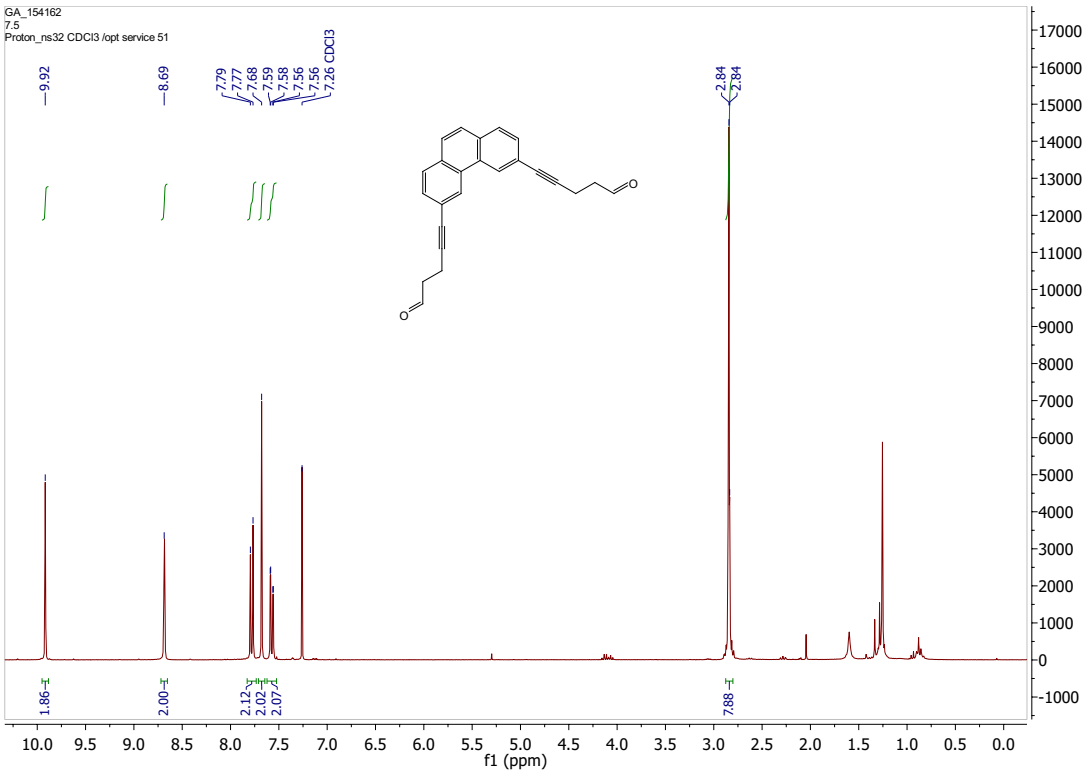

Figure A.8. ^{1}H-NMR of compound **6** in $CDCl_3$.

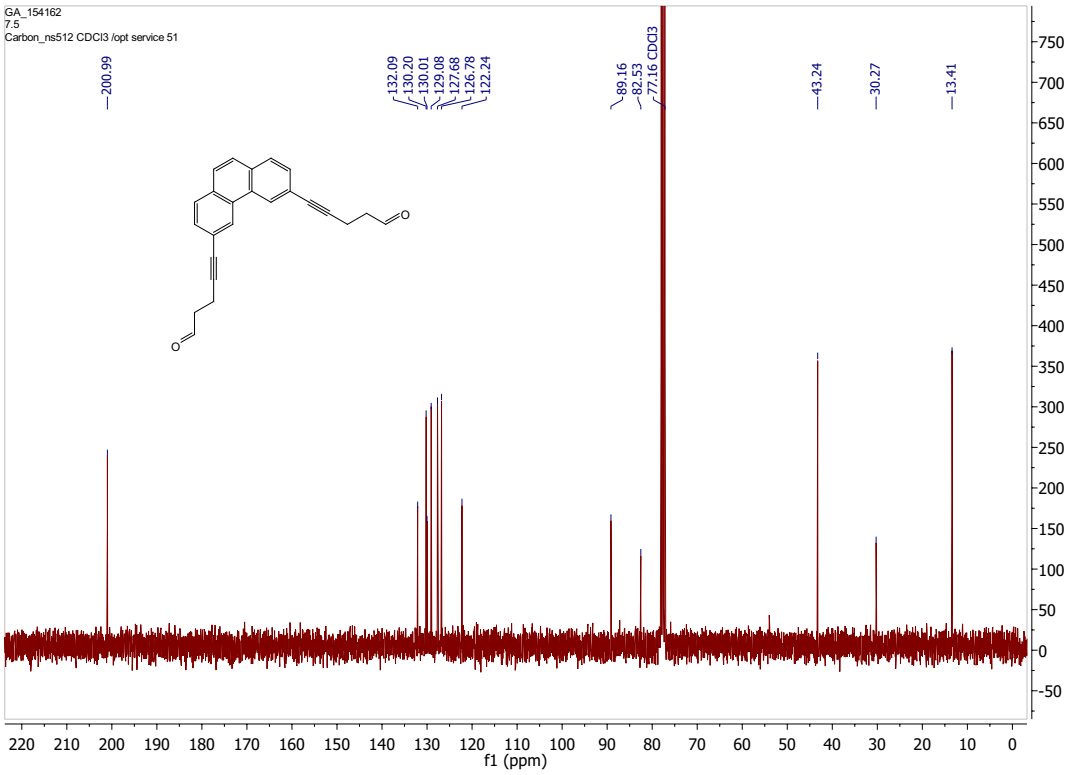

Figure A.9. ^{13}C-NMR of compound **6** in $CDCl_3$.

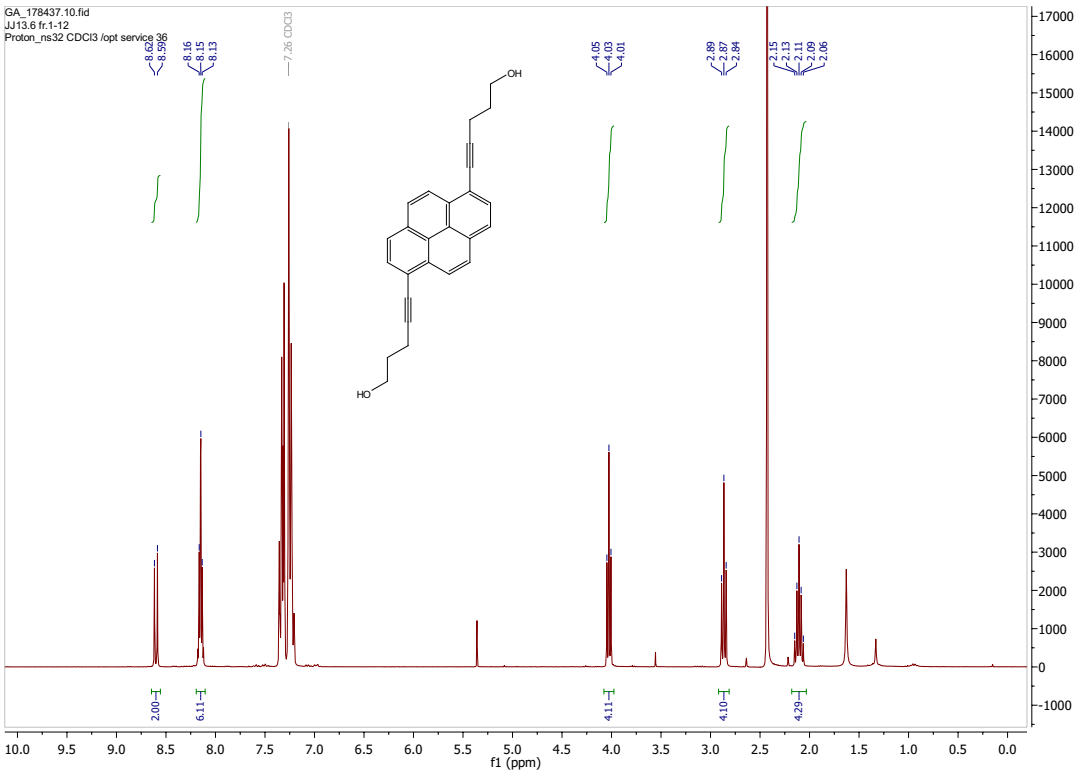

Figure A.10. ^{1}H-NMR of compound **8** in $CDCl_3$.

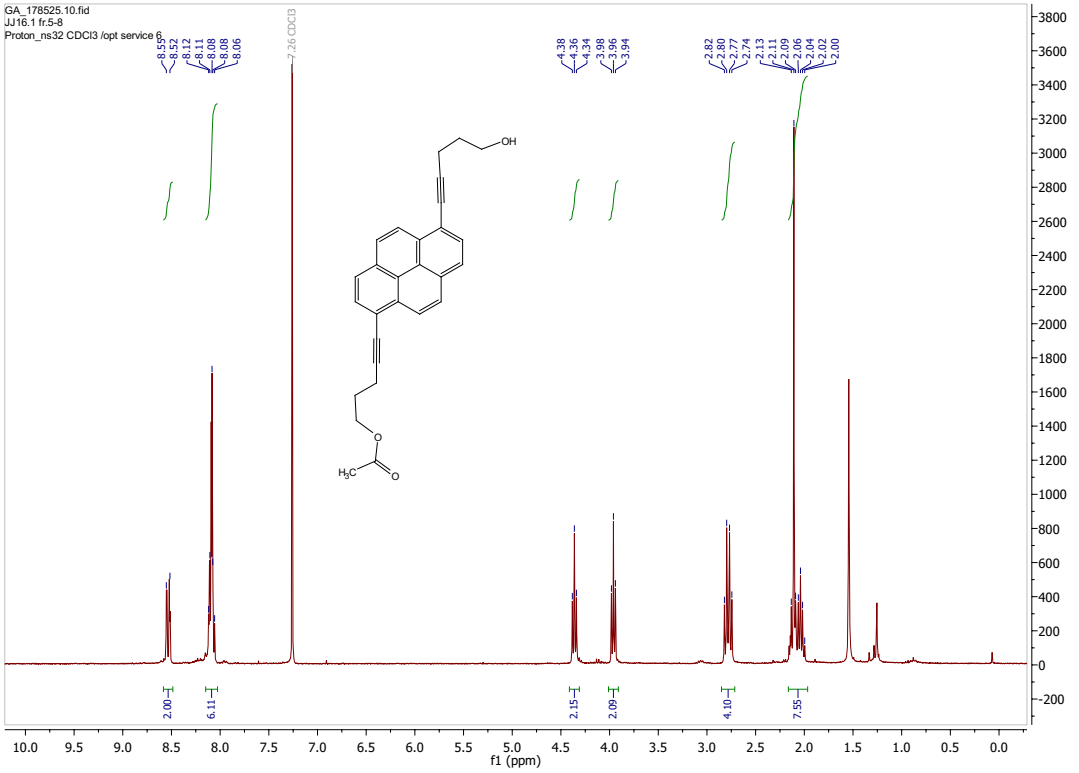

Figure A.11. ^{1}H-NMR of compound **9** in $CDCl_3$.

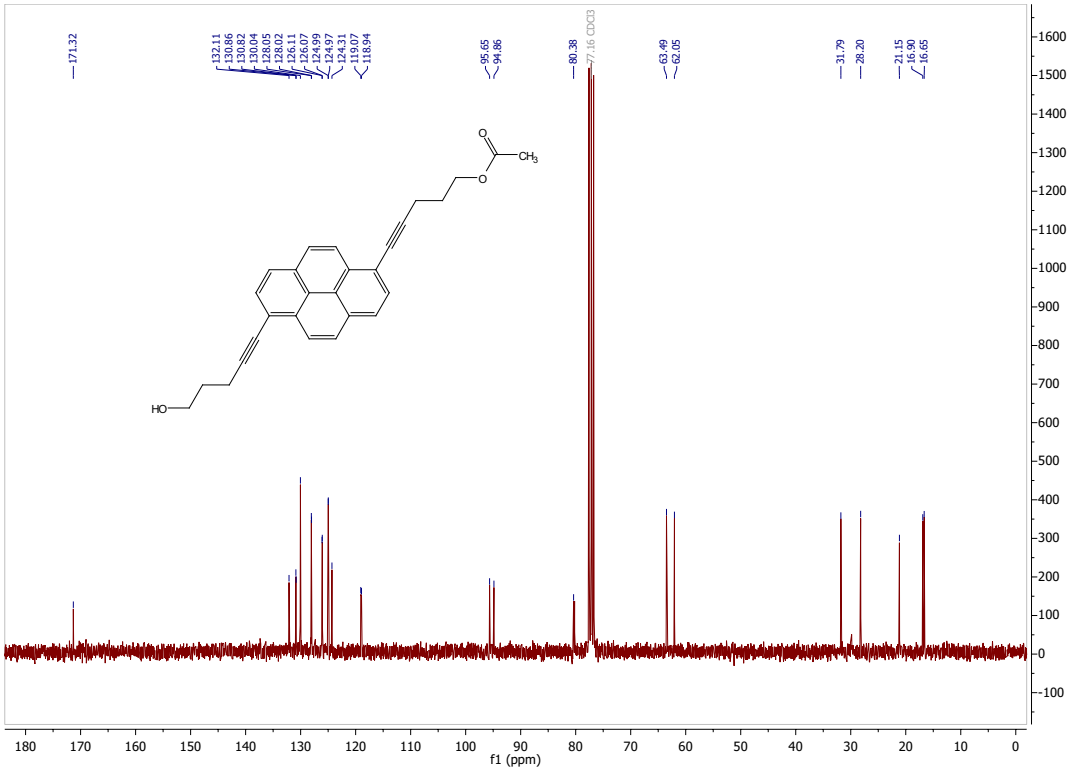

Figure A.12. ^{13}C-NMR of compound **9** in $CDCl_3$.

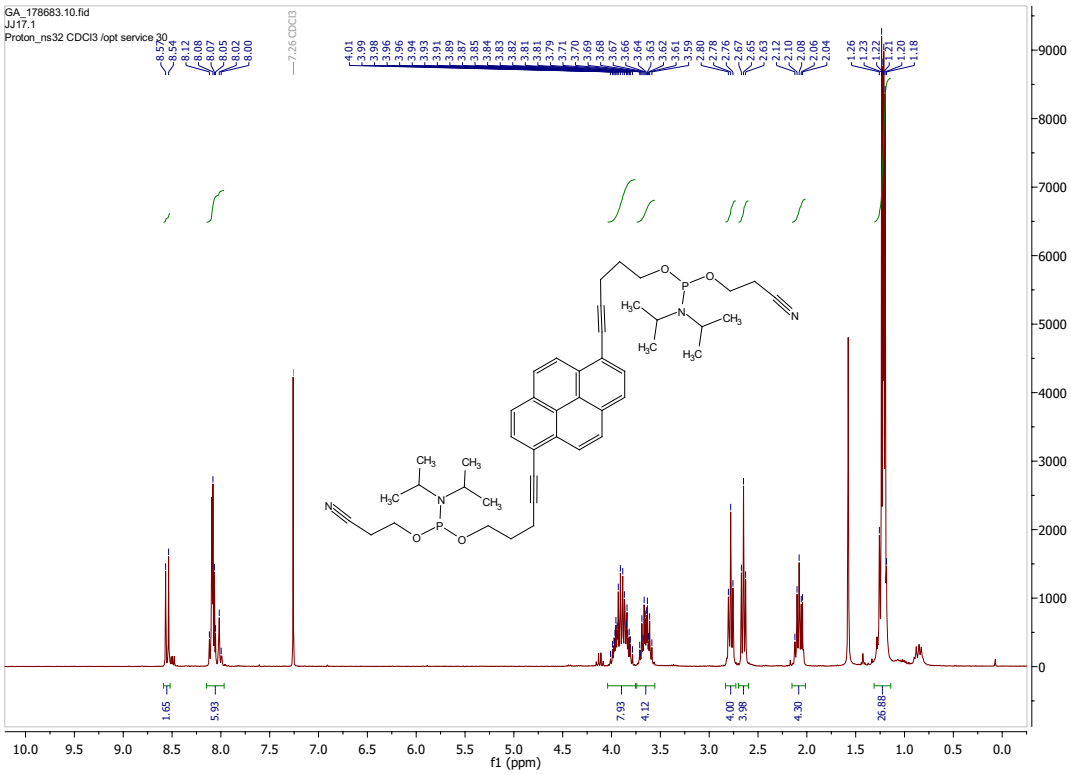

Figure A.13. ^{1}H-NMR of compound **10** in $CDCl_3$.

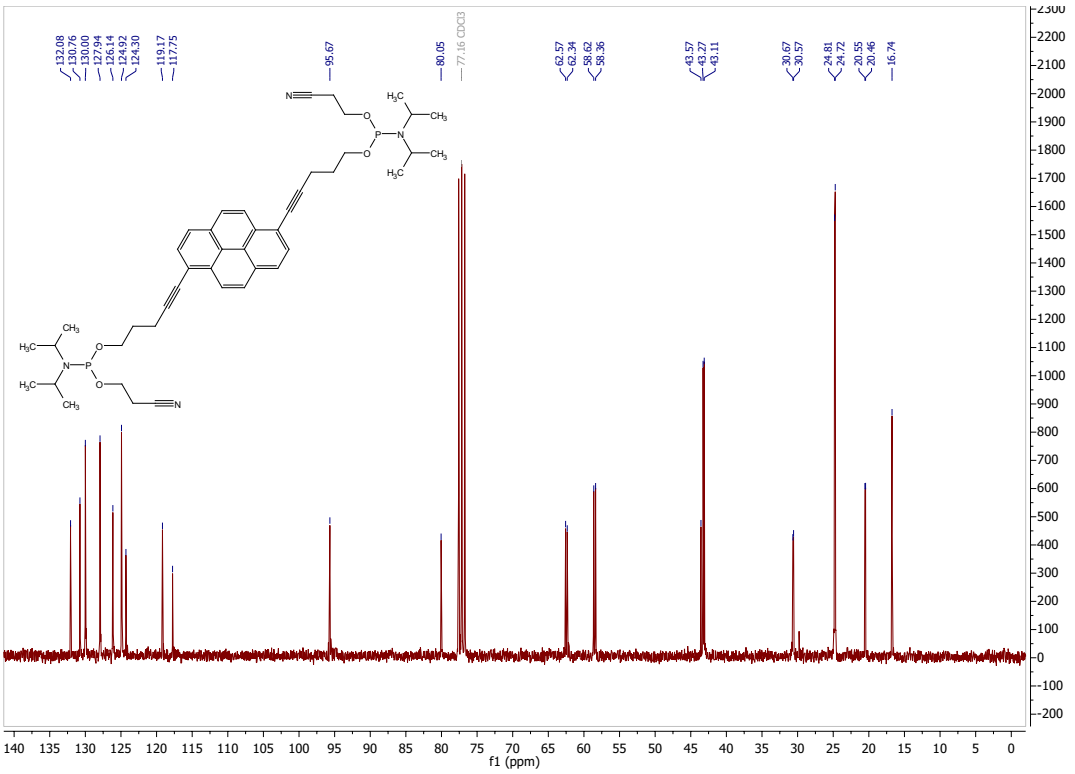

Figure A.14. ^{13}C-NMR of compound **10** in $CDCl_3$.

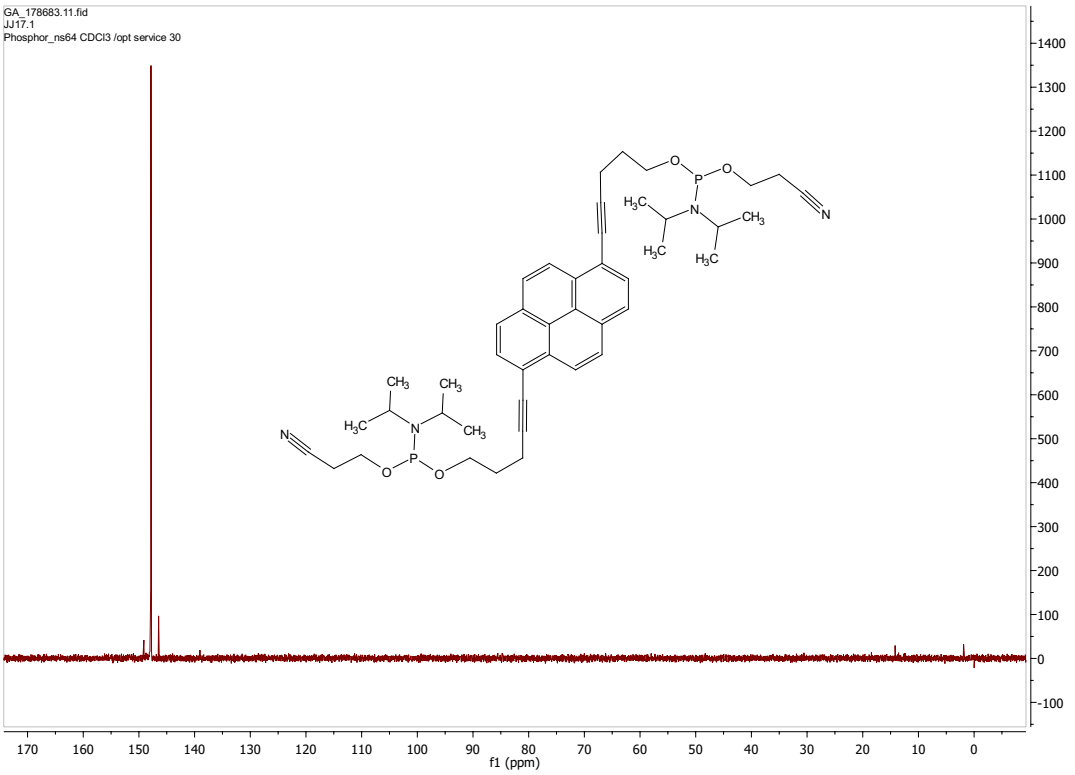

Figure A.15. ^{31}P-NMR of compound **10** in $CDCl_3$.

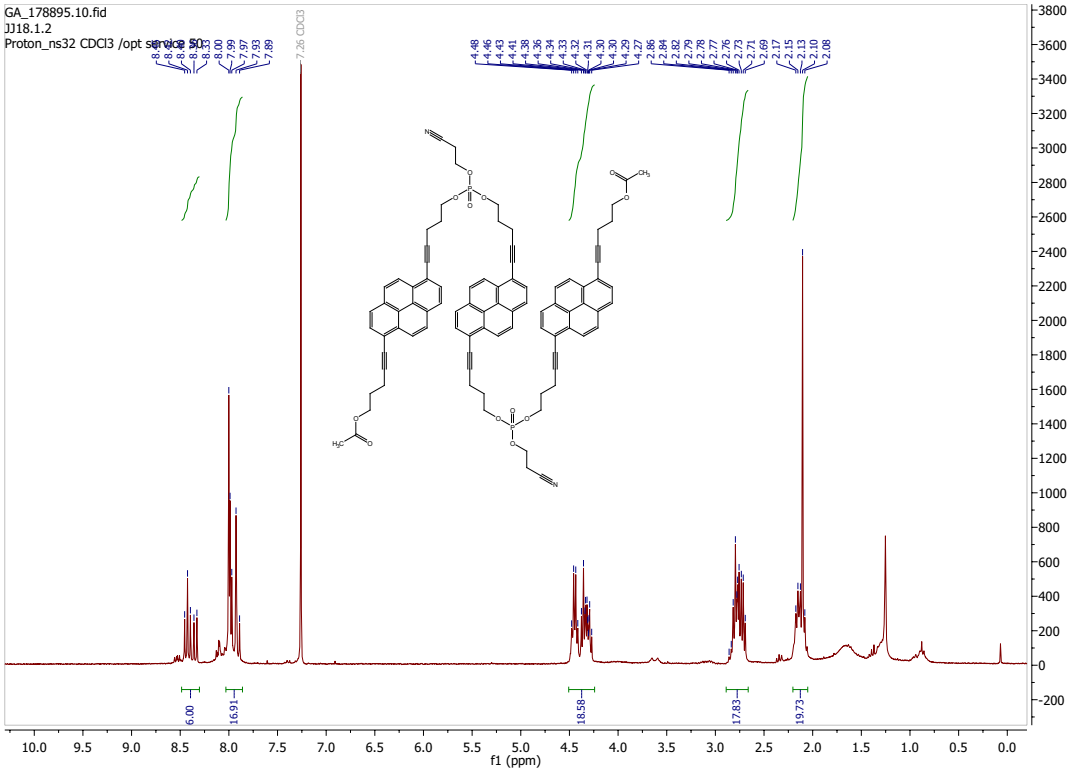

Figure A.16. ^{1}H-NMR of compound **11** in $CDCl_3$.

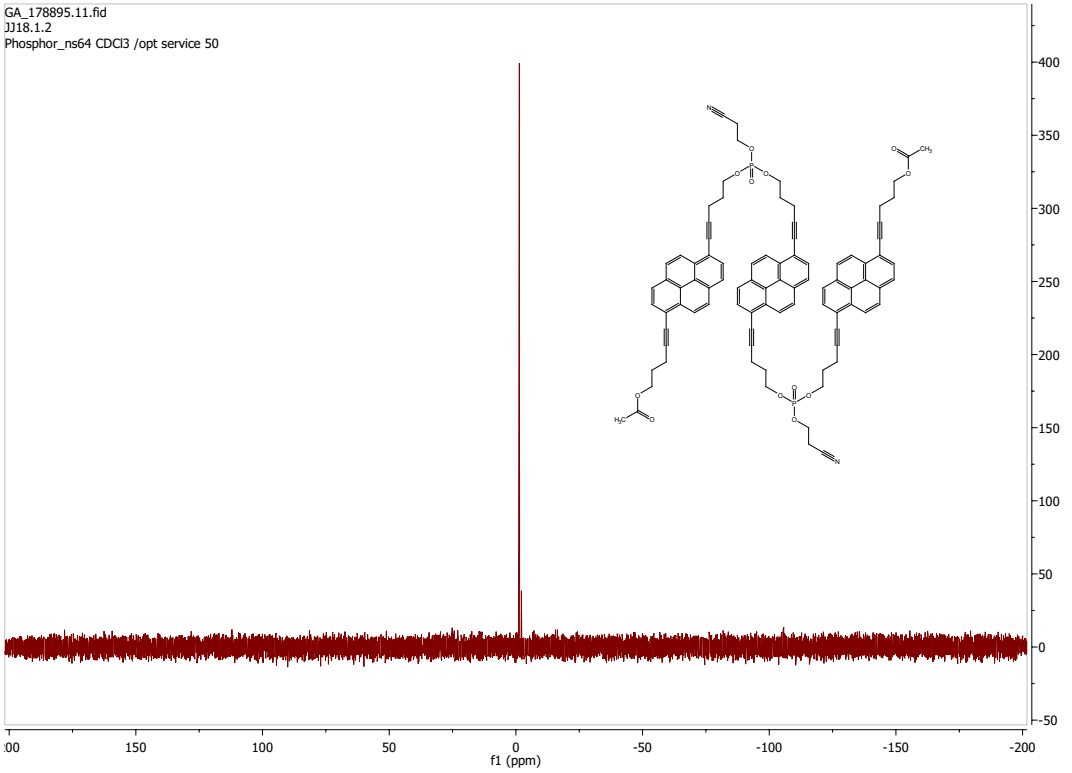

Figure A.17. ^{31}P-NMR of compound **11** in $CDCl_3$.

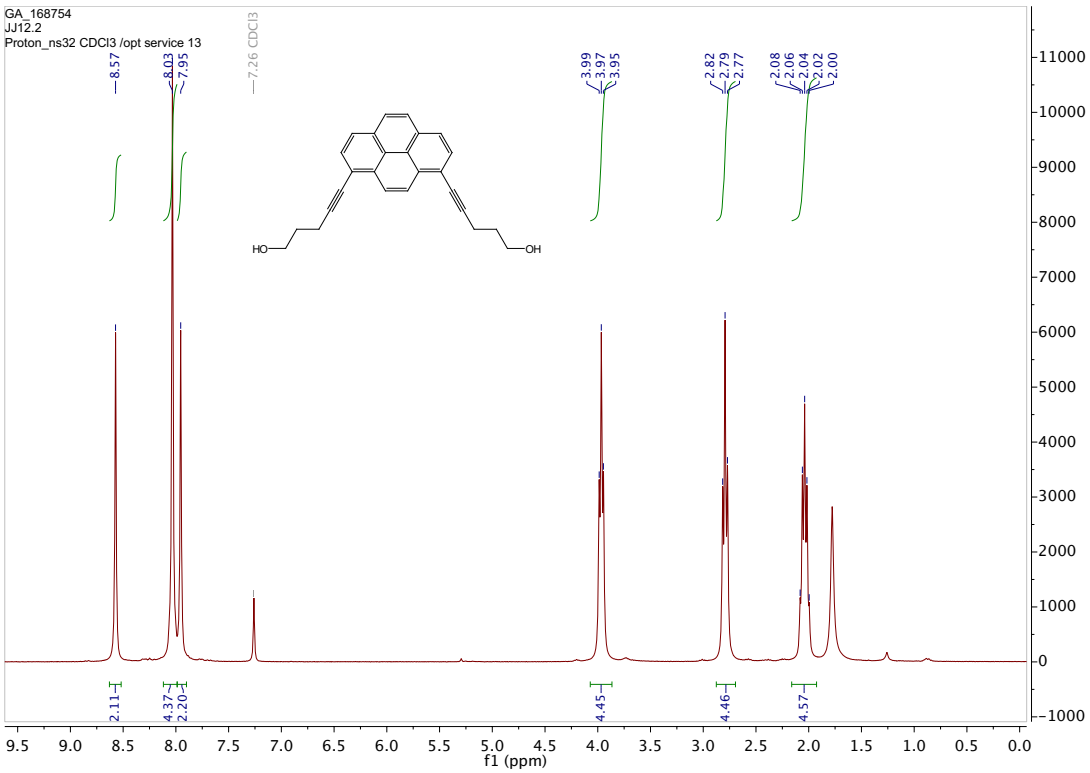

Figure A.18. ^{1}H-NMR of compound **13** in $CDCl_3$.

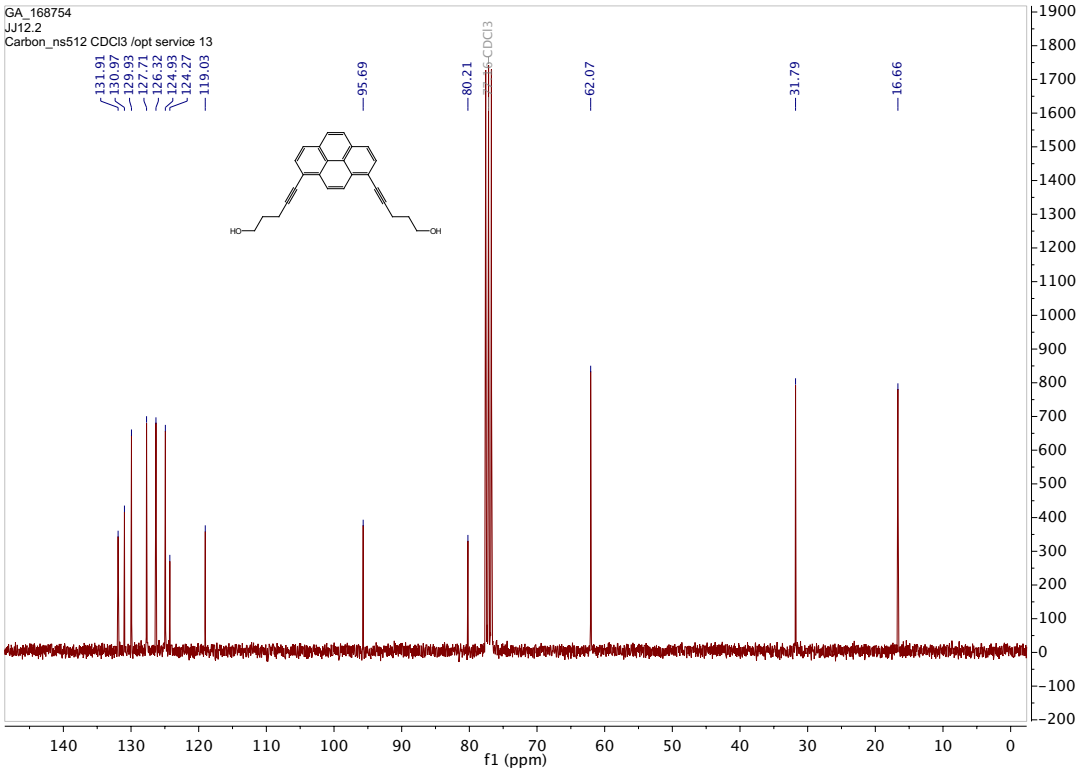

Figure A.19. ^{13}C-NMR of compound **13** in $CDCl_3$.

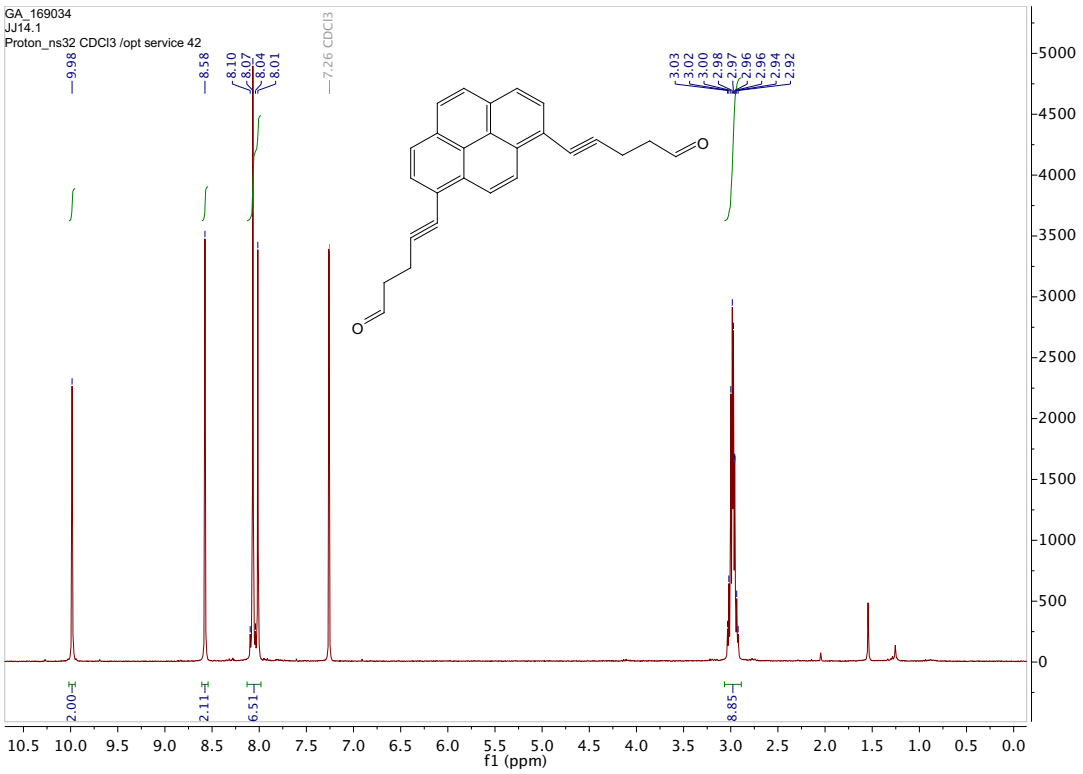

Figure A.20. ^{1}H-NMR of compound **14** in $CDCl_3$.

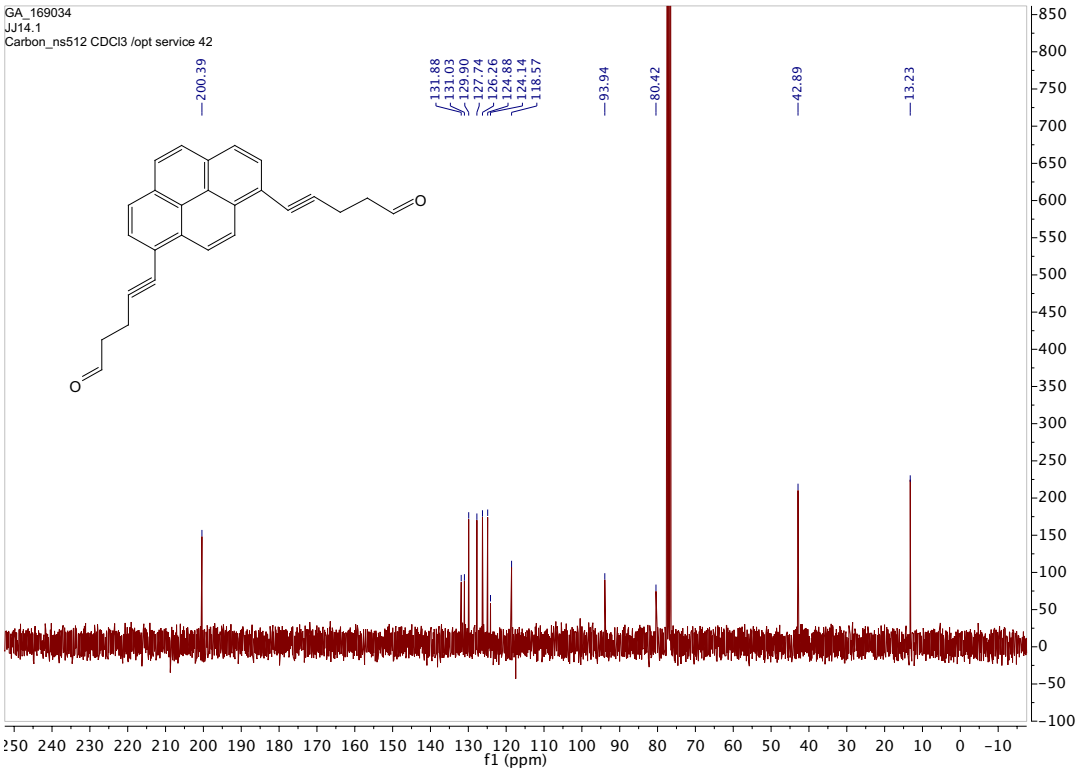

Figure A.21. ^{13}C-NMR of compound **14** in $CDCl_3$.

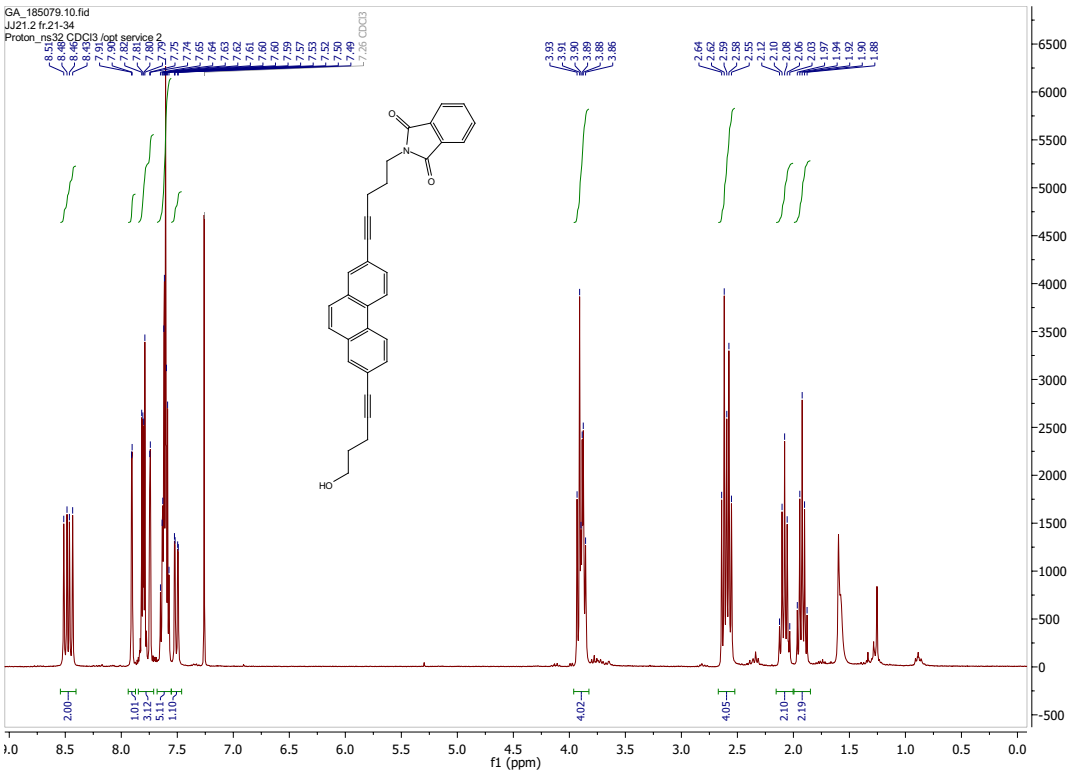

Figure A.22. ^{1}H-NMR of compound **17** in $CDCl_3$.

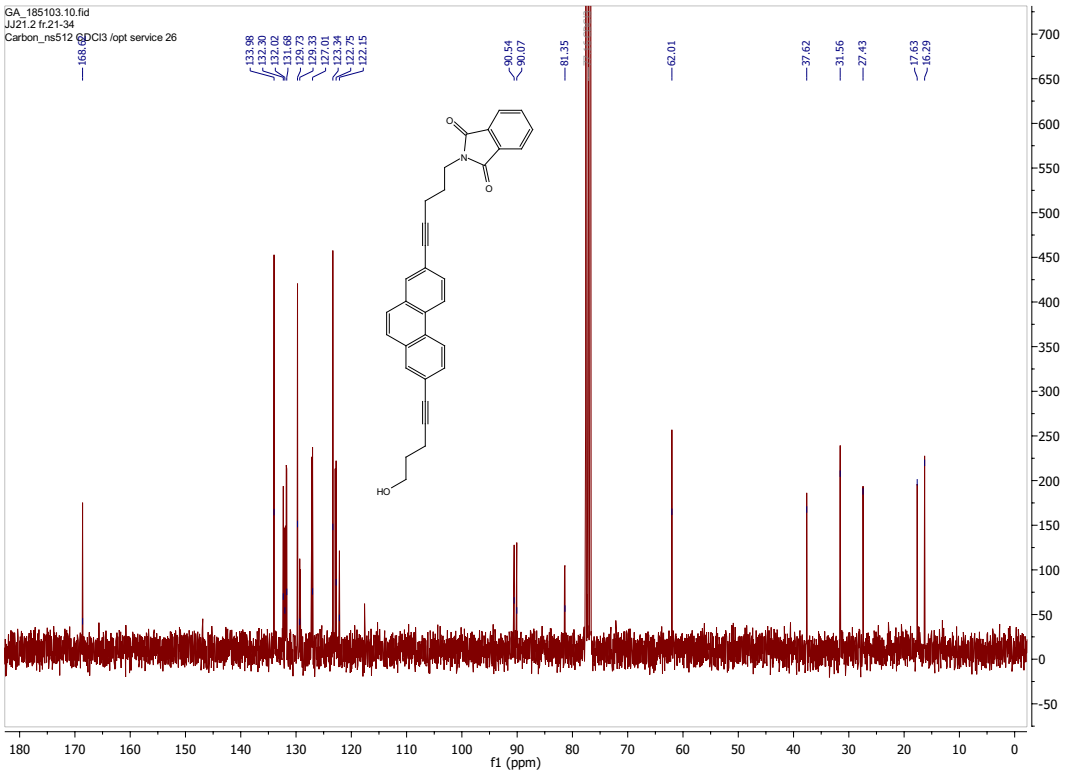

Figure A.23. ^{13}C-NMR of compound **17** in $CDCl_3$.

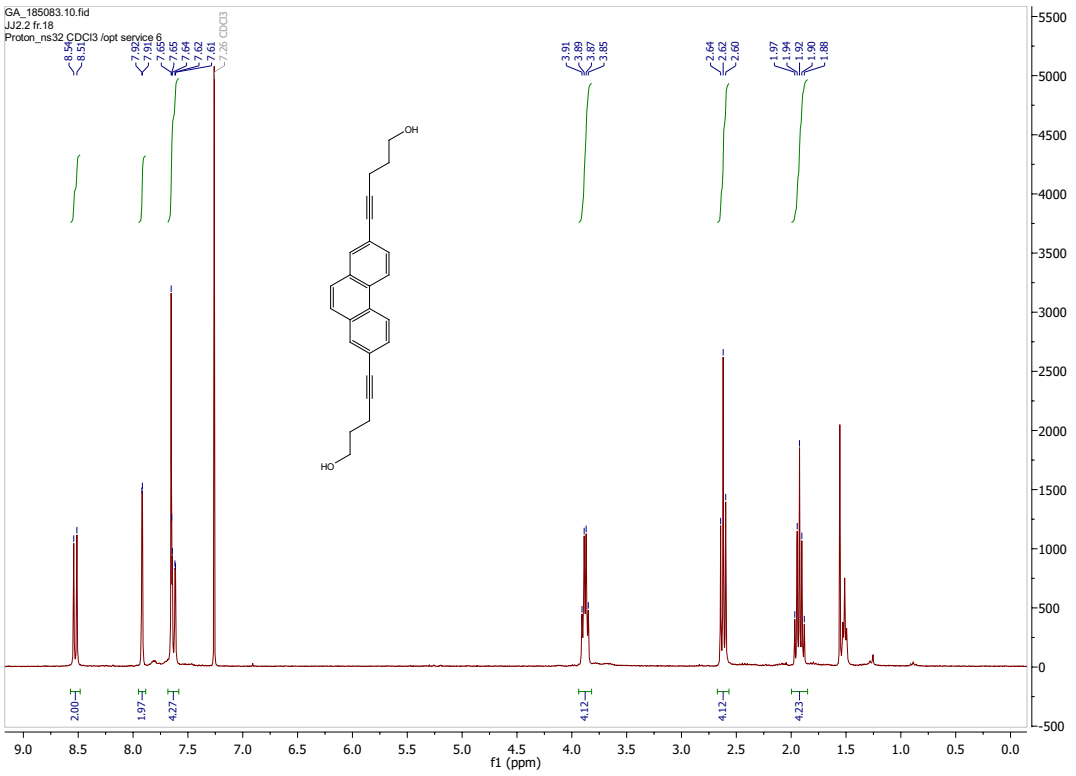

Figure A.24. ^{1}H-NMR of compound **18** in $CDCl_3$.

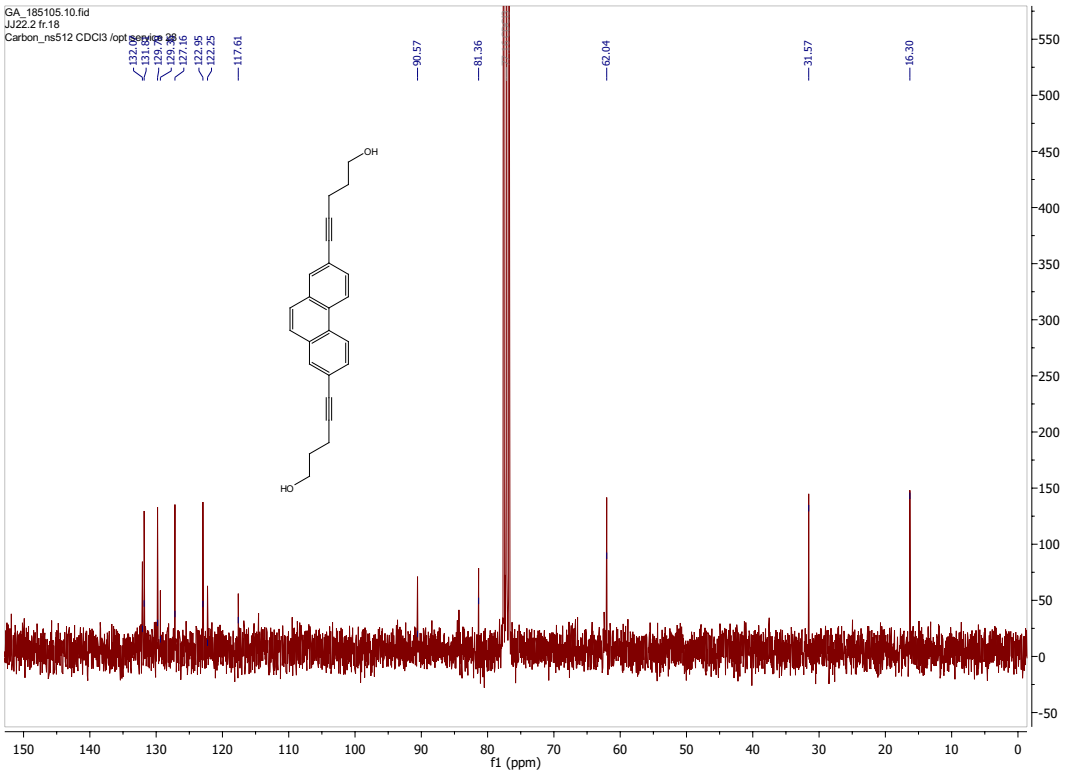

Figure A.25. ^{13}C-NMR of compound **18** in $CDCl_3$.

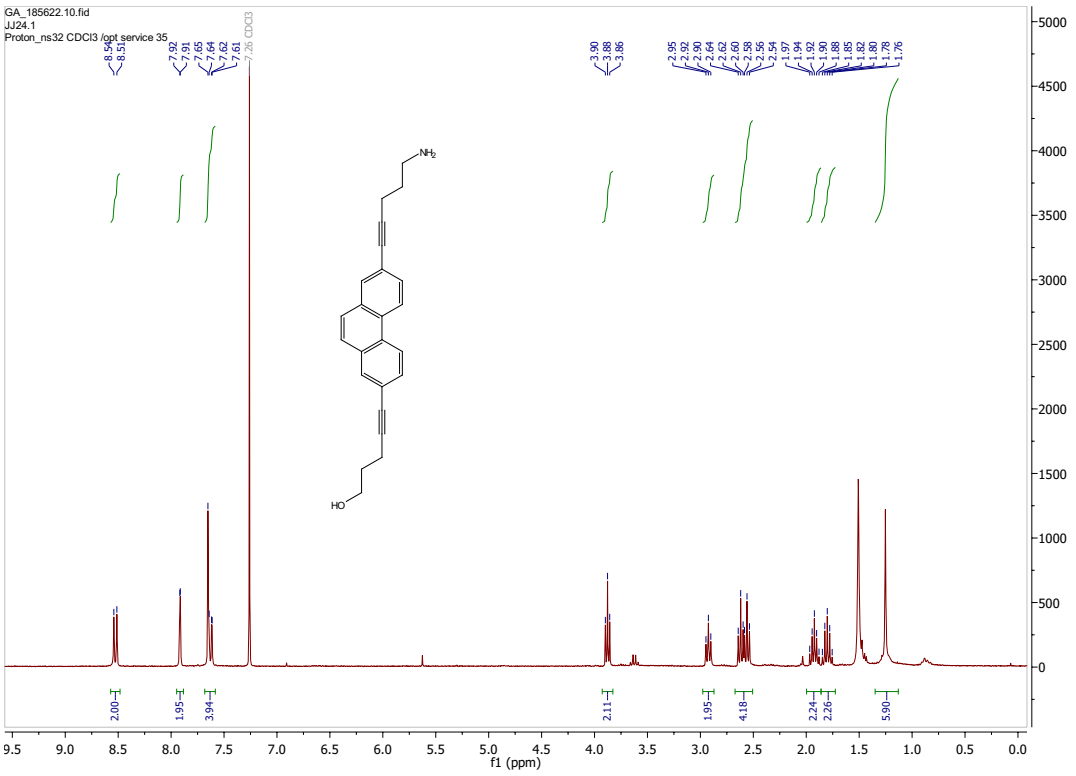

Figure A.26. ^{1}H-NMR of compound **19** in $CDCl_3$.

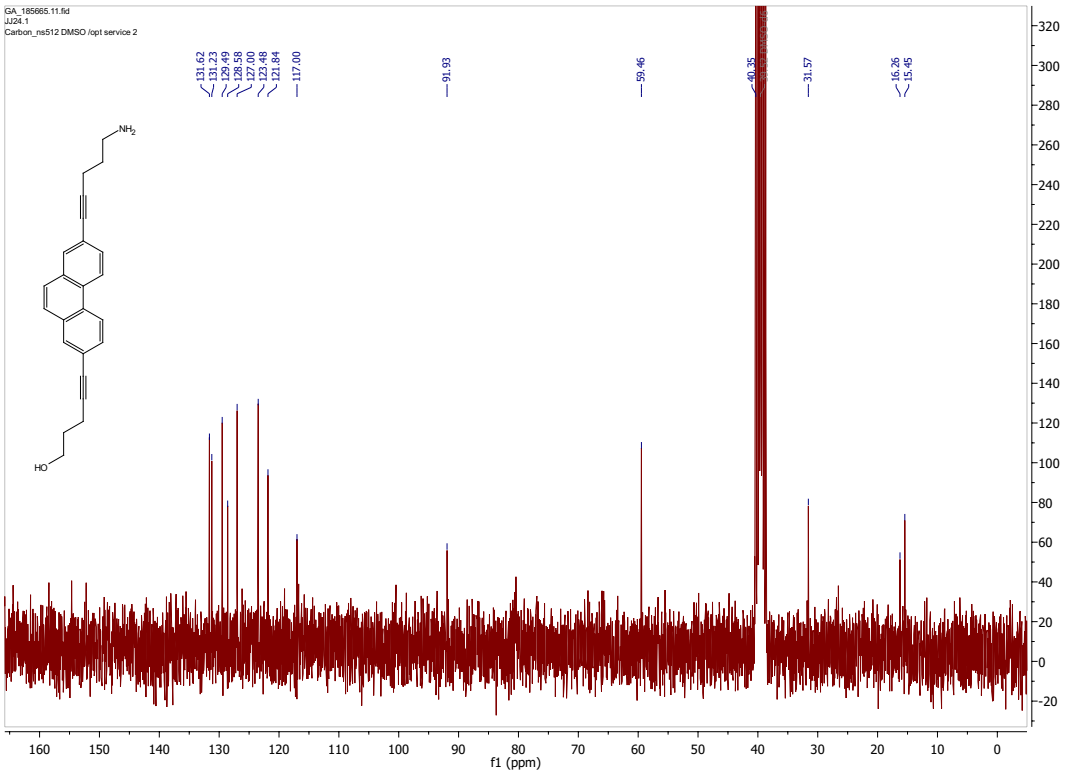

Figure A.27. ^{13}C-NMR of compound **19** in $CDCl_3$.

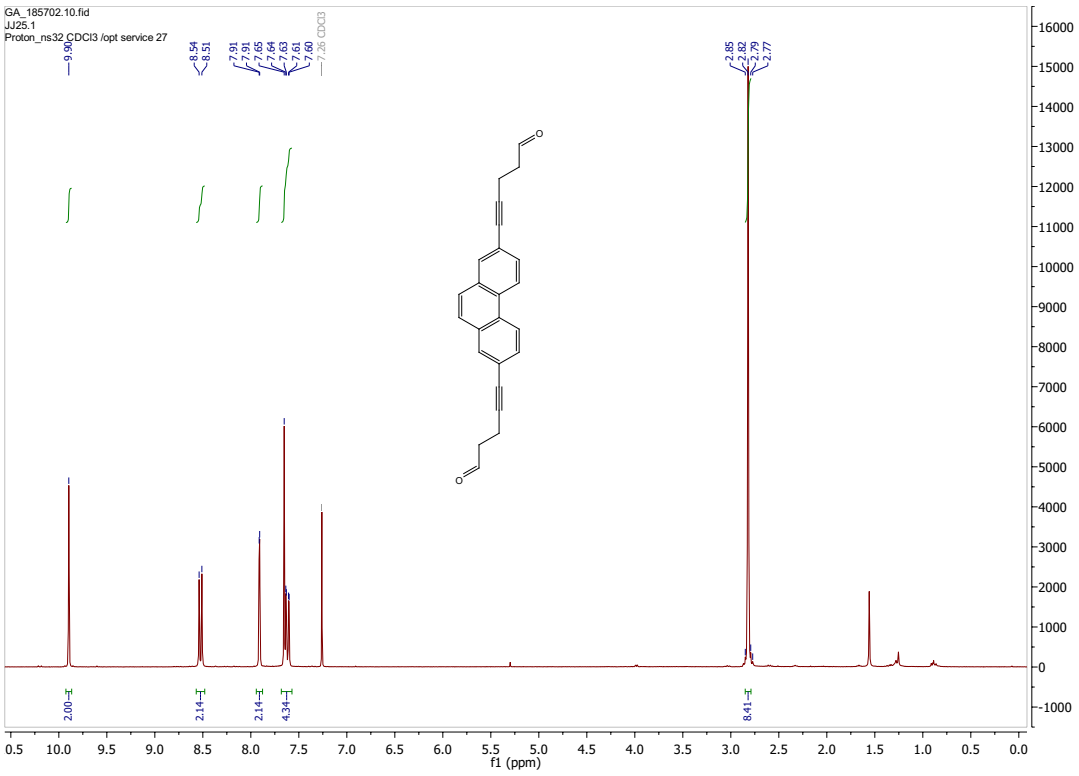

Figure A.28. ^{1}H-NMR of compound **20** in $CDCl_3$.

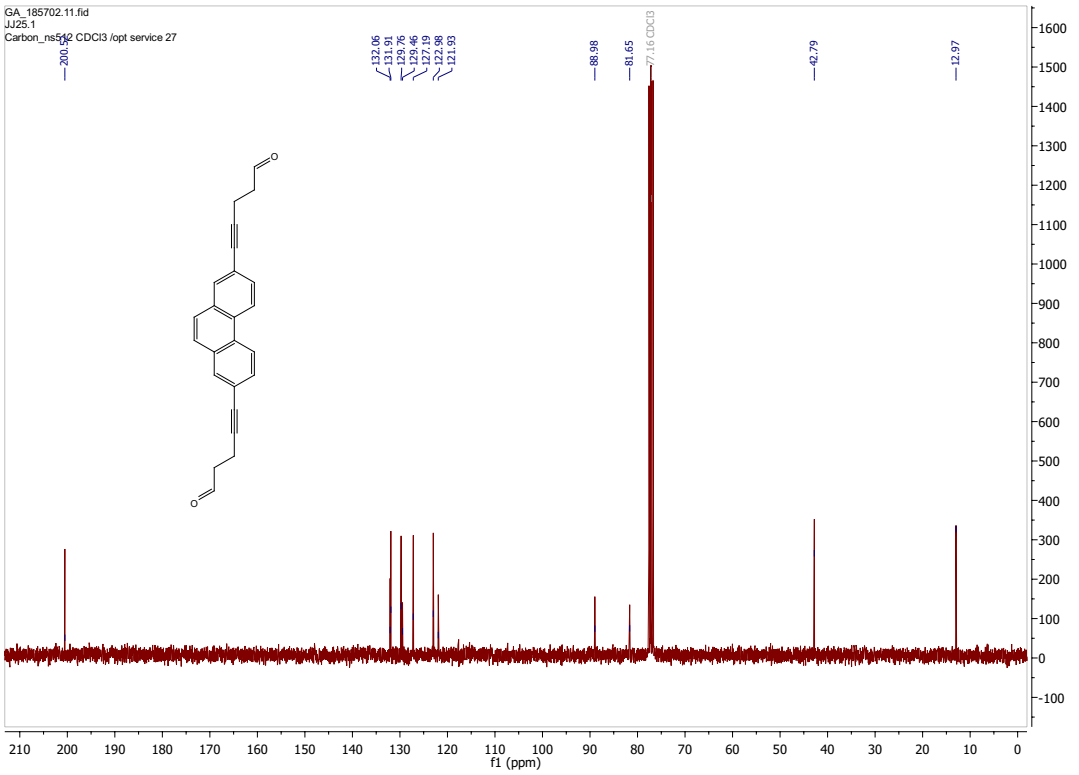

Figure A.29. ^{13}C-NMR of compound **20** in $CDCl_3$.

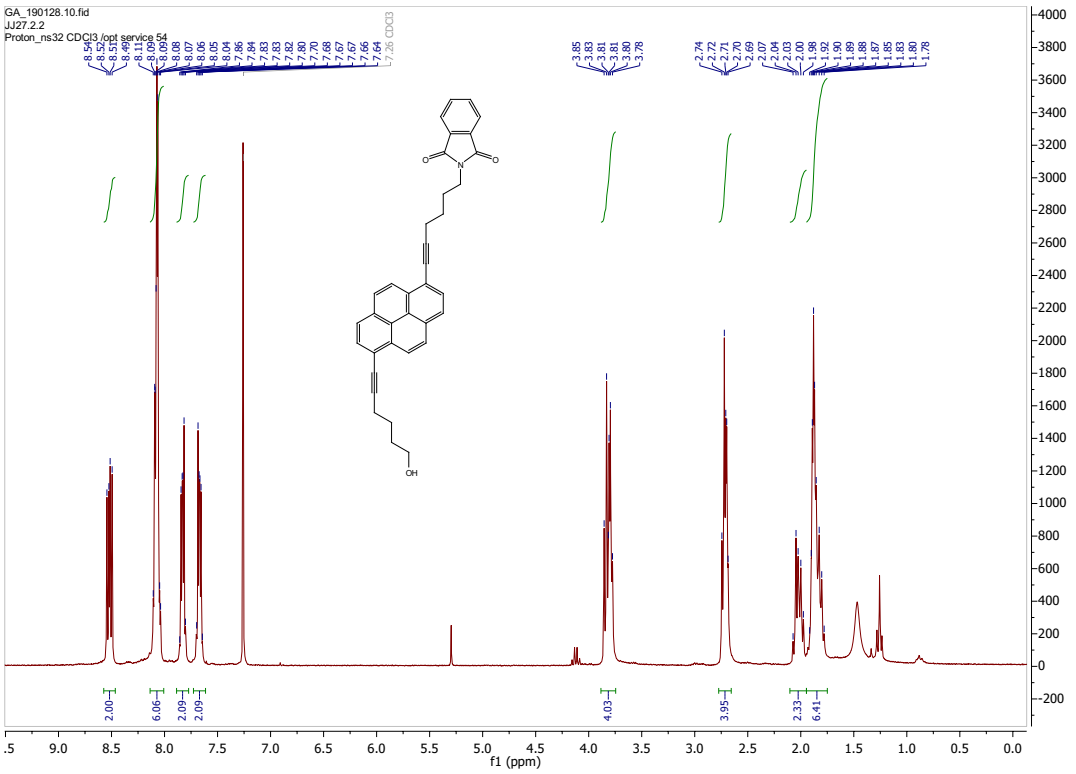

Figure A.30. ^{1}H-NMR of compound **22** in $CDCl_3$.

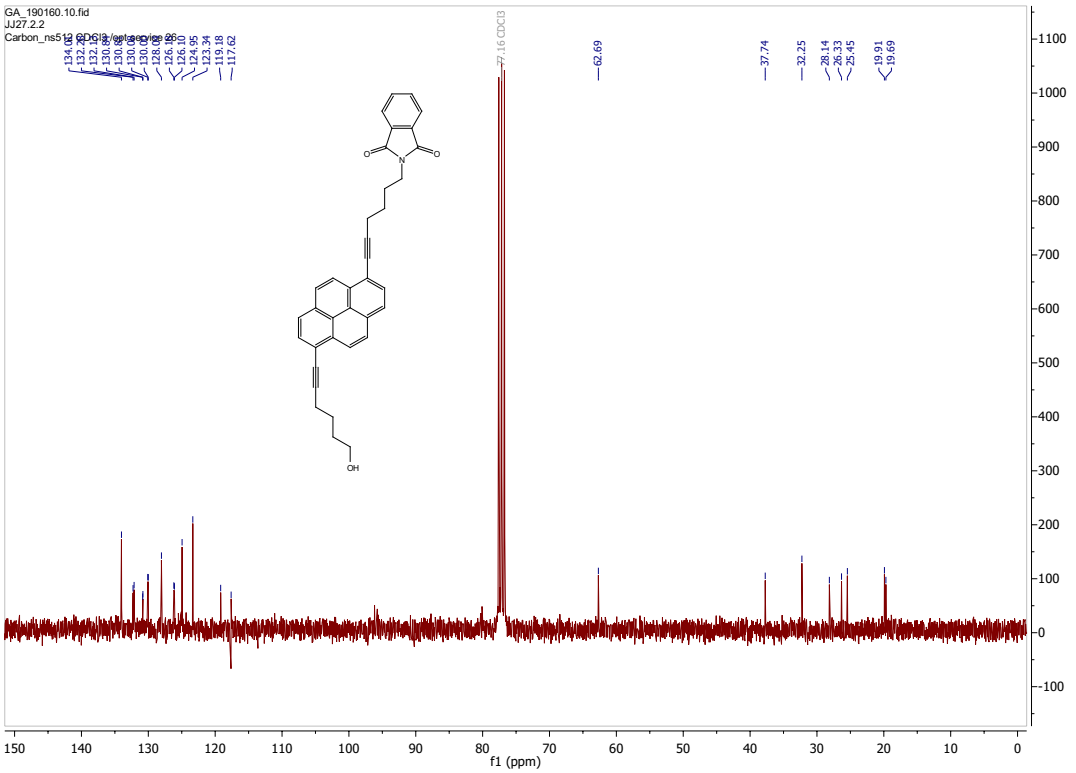

Figure A.31. ^{13}C-NMR of compound **22** in $CDCl_3$.

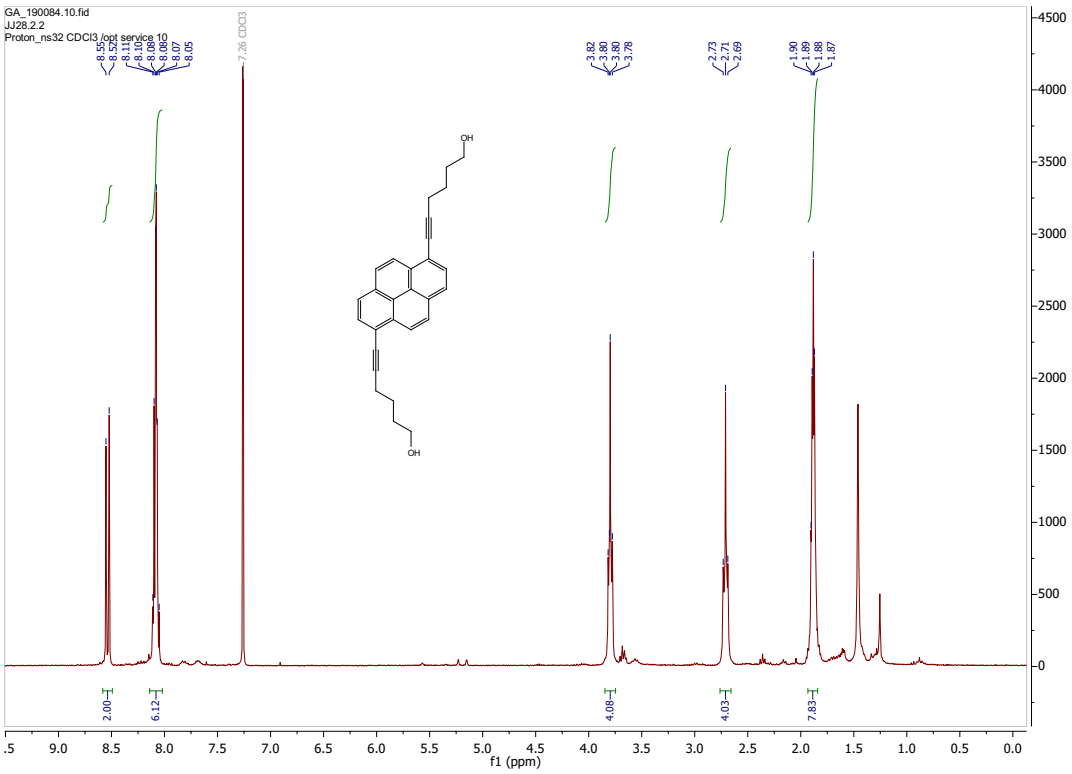

Figure A.32. ^{1}H-NMR of compound **23** in $CDCl_3$.

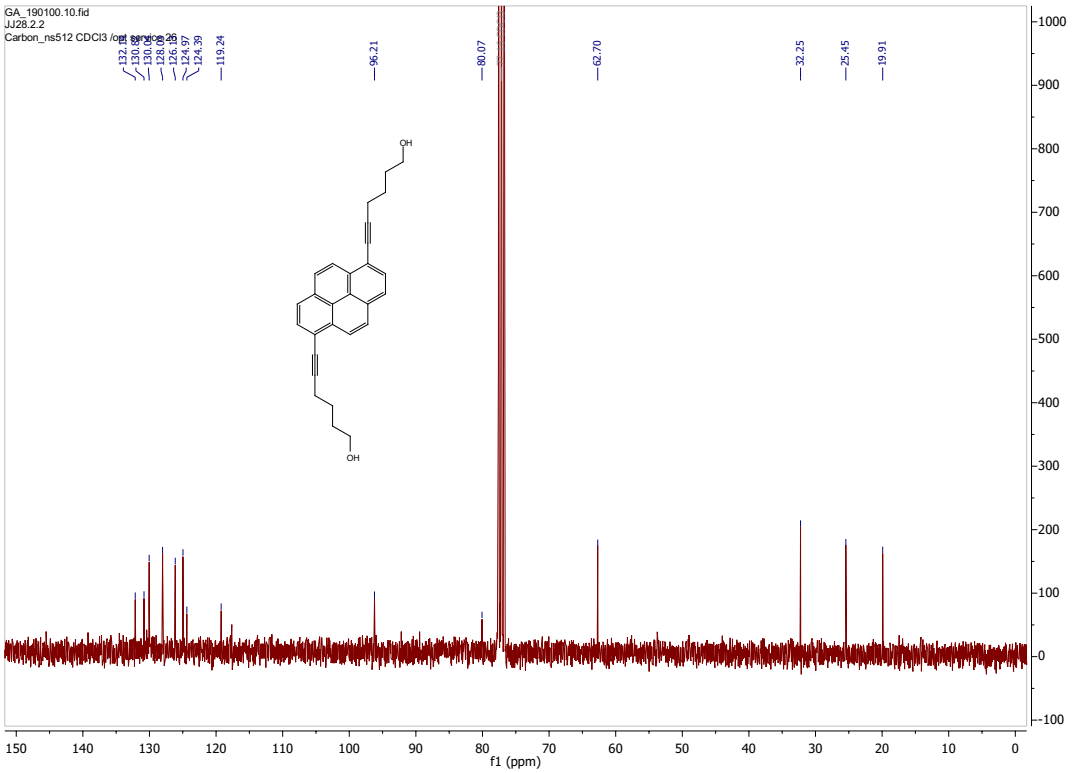

Figure A.33. ^{13}C-NMR of compound **23** in $CDCl_3$.

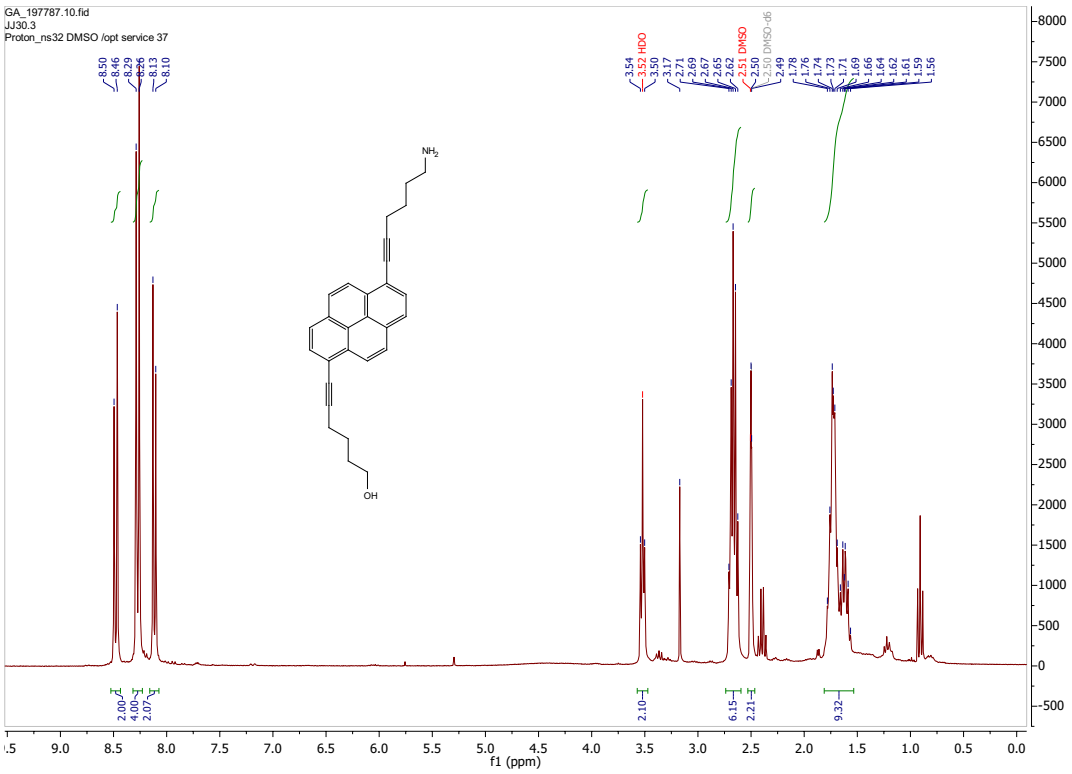

Figure A.34. ^{1}H-NMR of compound **24** in DMSO−d_6.

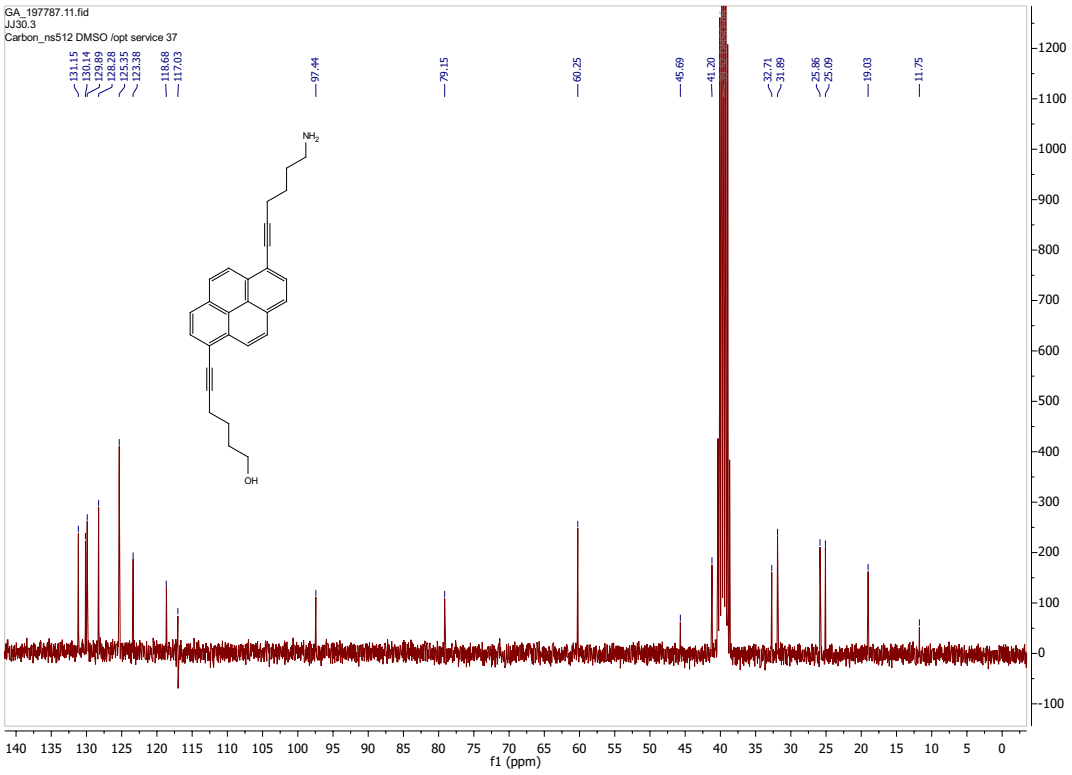

Figure A.35. ^{13}C-NMR of compound **24** in DMSO−d_6.

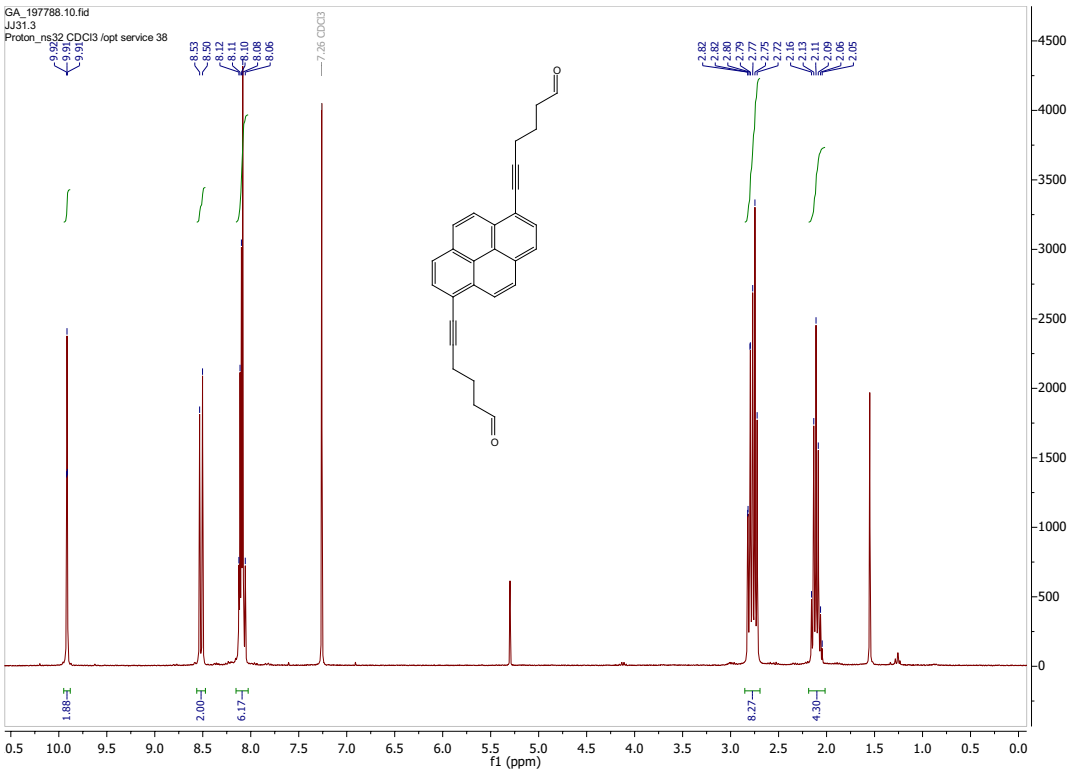

Figure A.36. ^{1}H-NMR of compound **25** in $CDCl_3$.

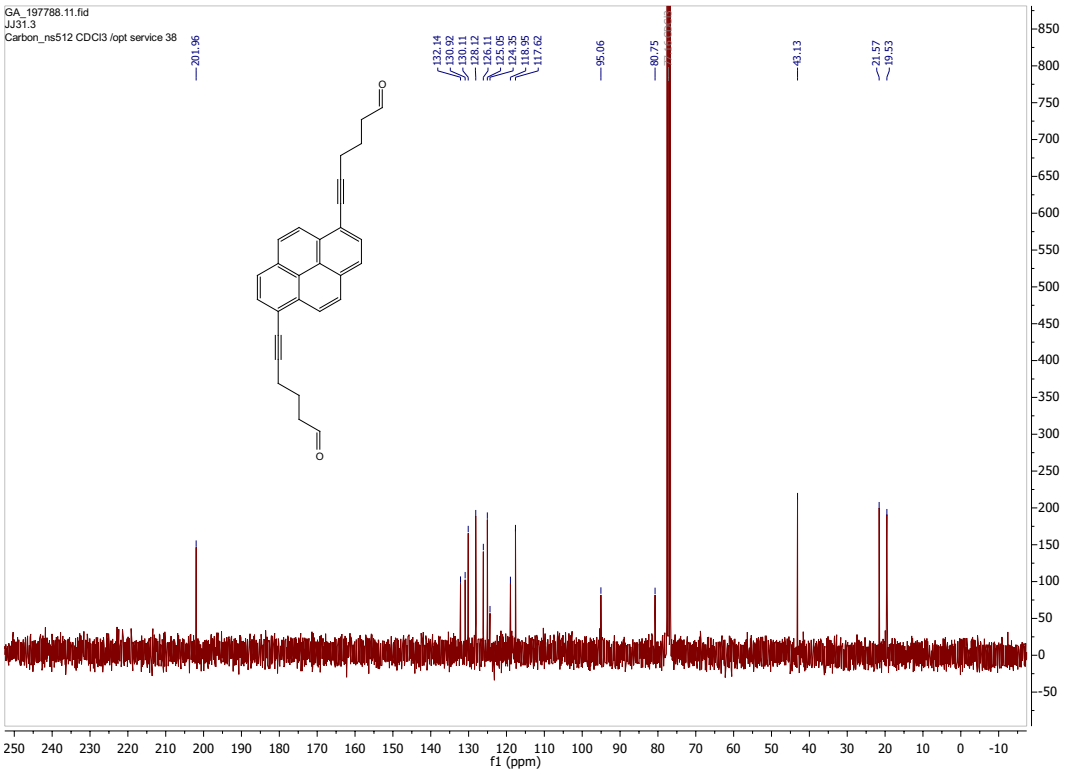

Figure A.37. ^{13}C-NMR of compound **25** in $CDCl_3$.

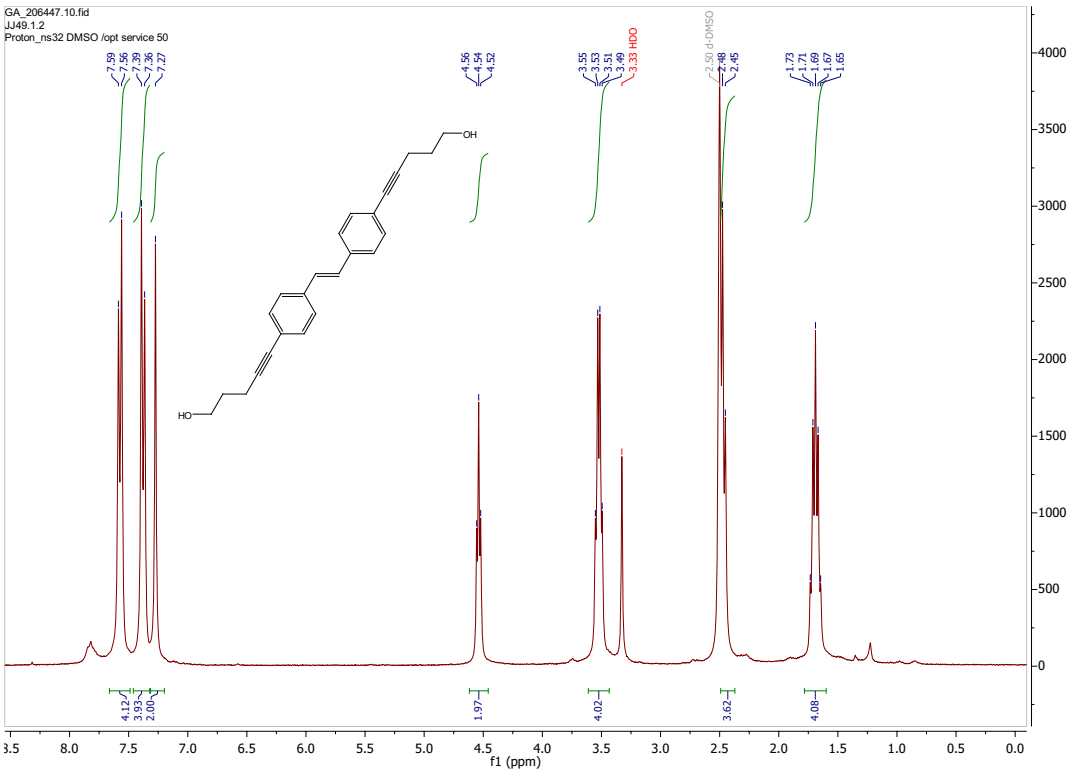

Figure A.38. ^{1}H-NMR of compound **28** in DMSO−d_6.

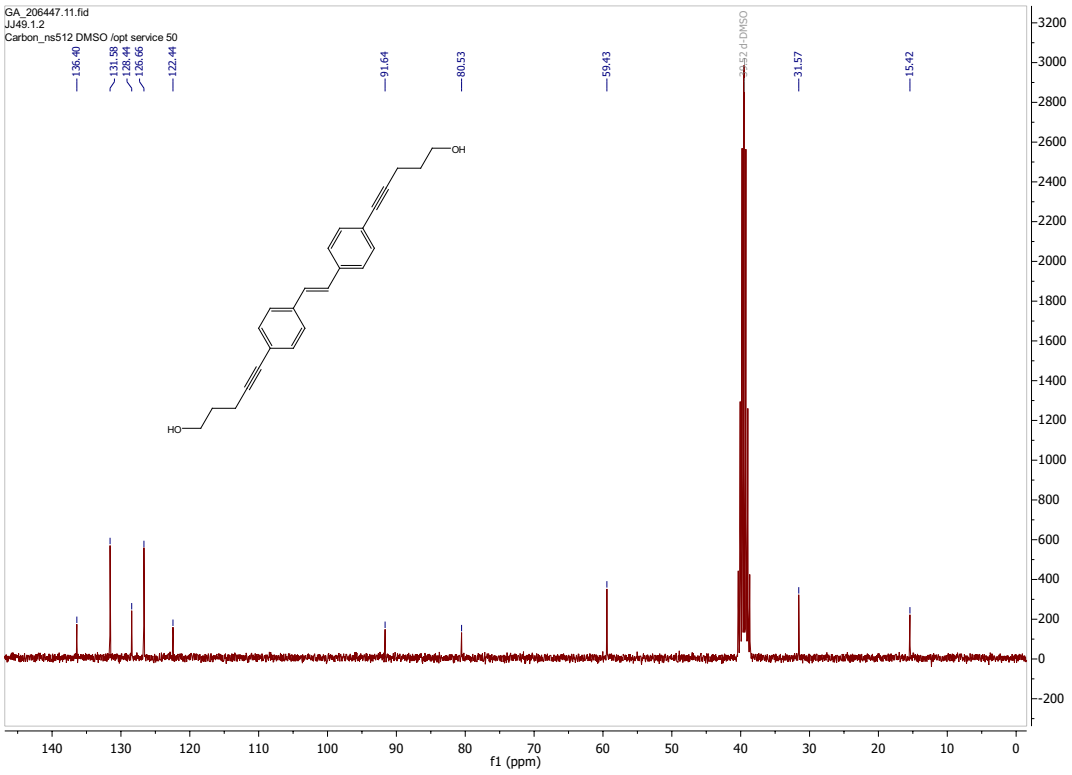

Figure A.39. ^{13}C-NMR of compound **28** in DMSO−d_6.

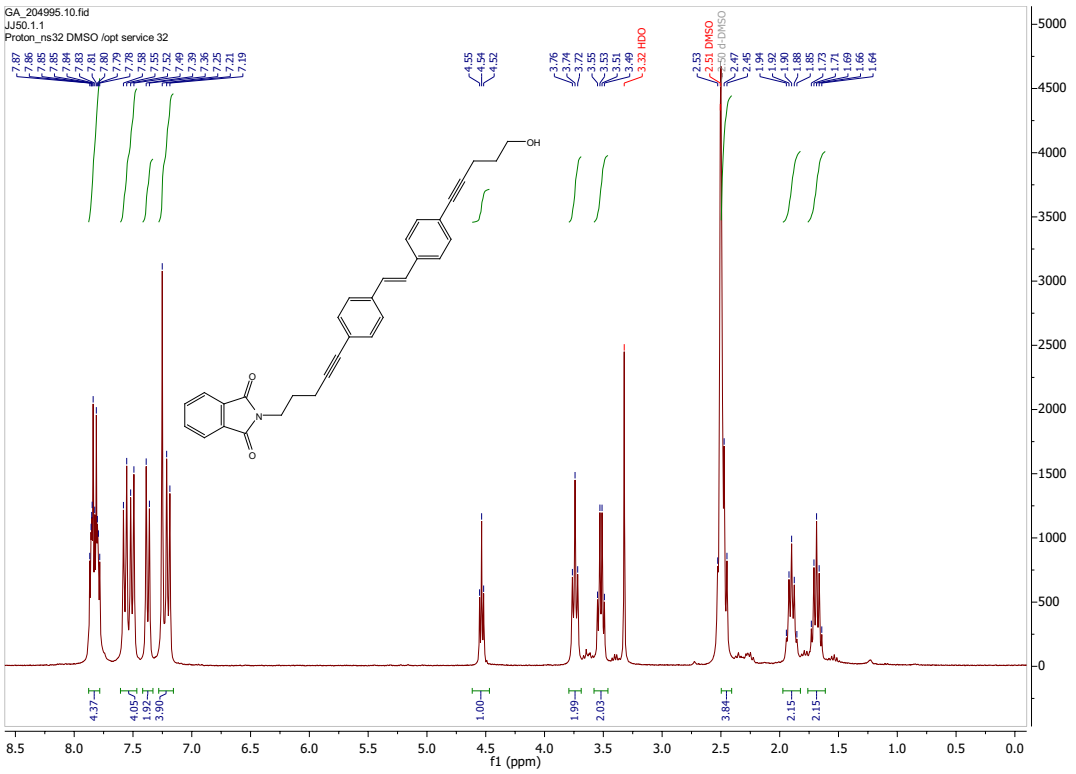

Figure A.40. ^{1}H-NMR of compound **29** in DMSO−d_6.

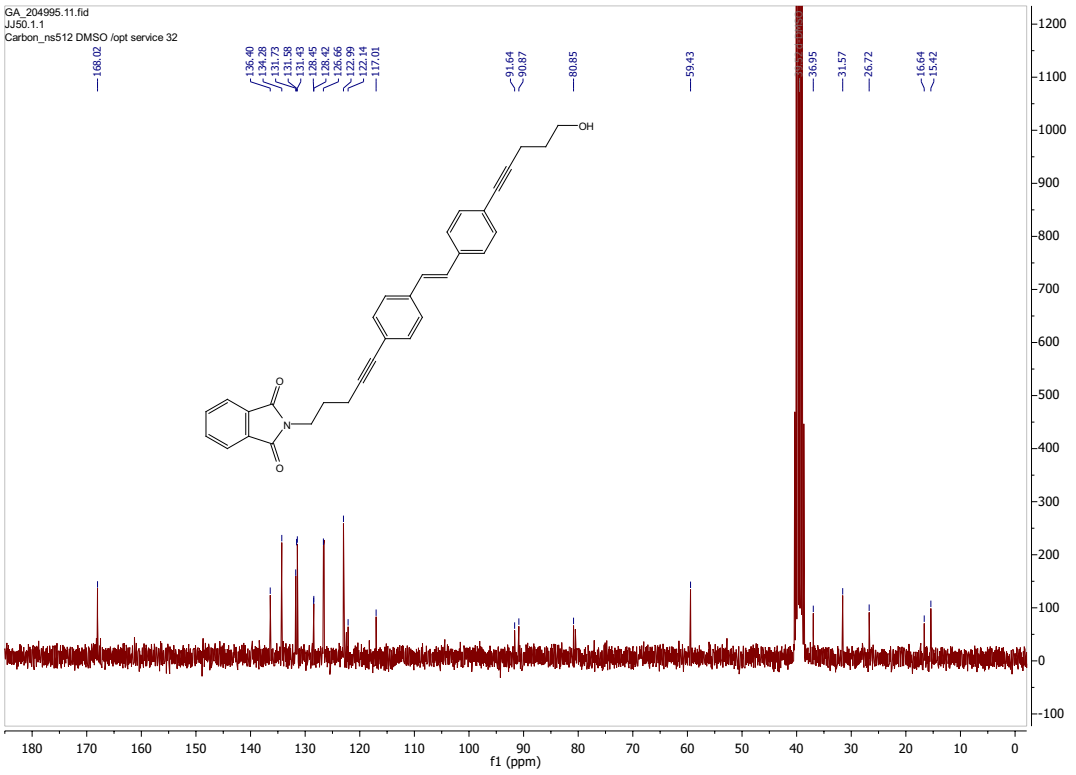

Figure A.41. ^{13}C-NMR of compound **29** in DMSO−d_6.

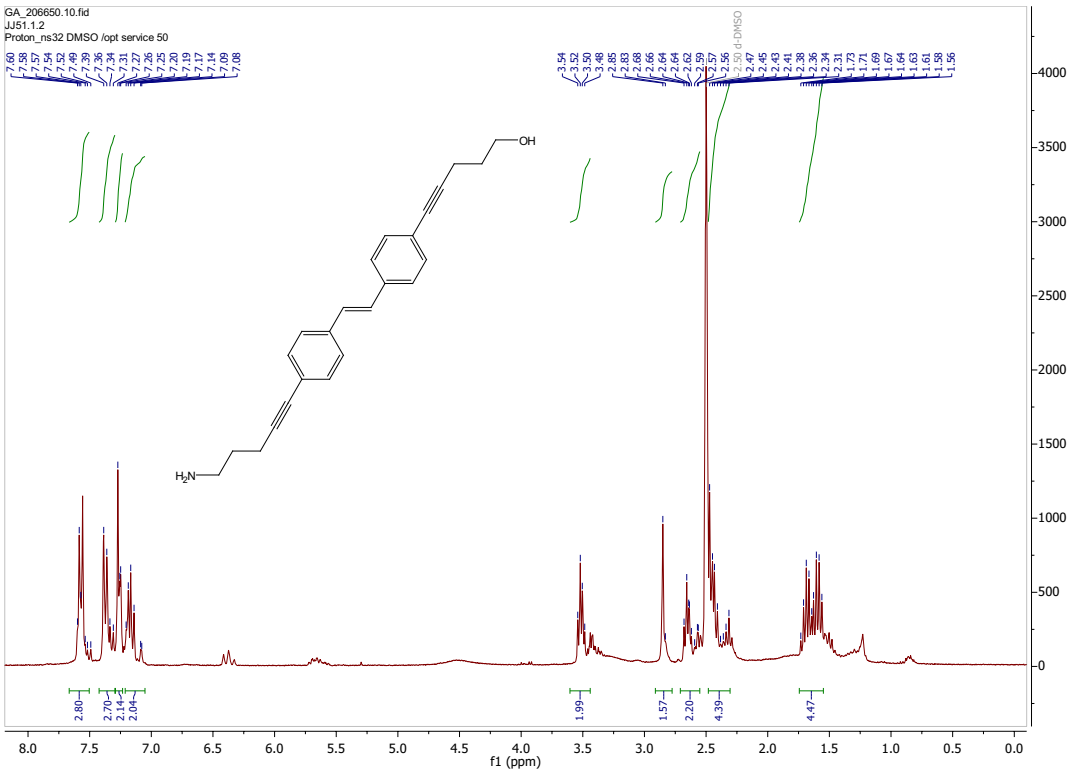

Figure A.42. ^{1}H-NMR of compound **30** in DMSO−d_6.

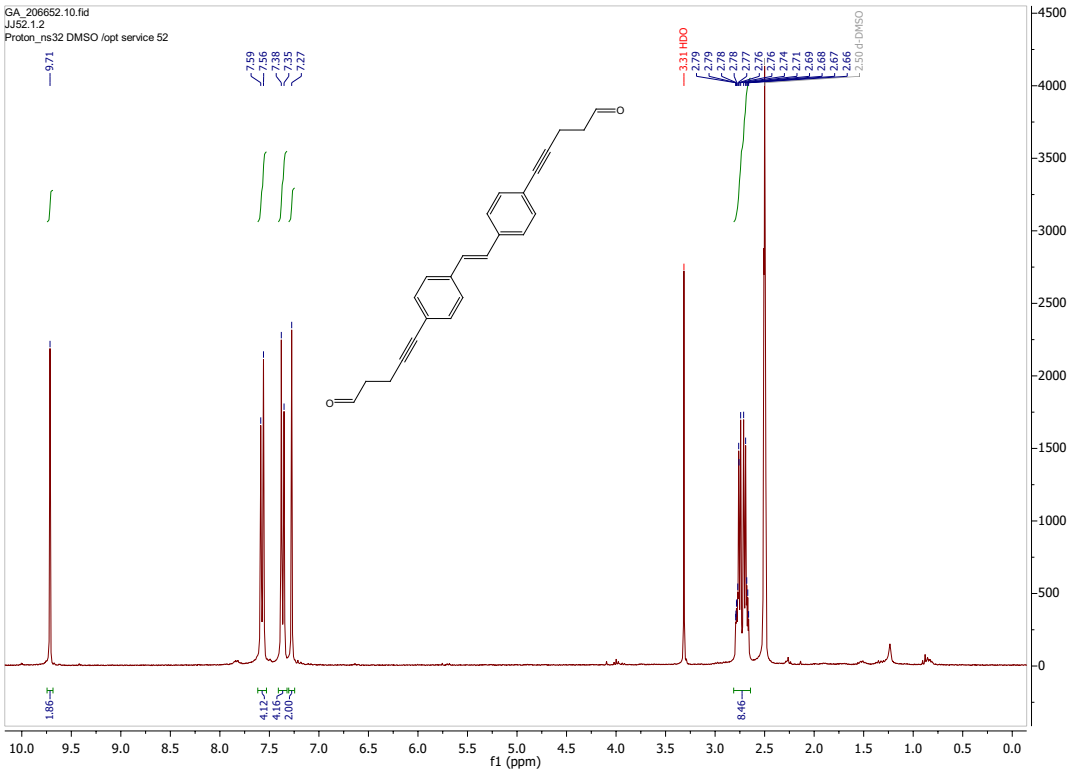

Figure A.43. ^{1}H-NMR of compound **31** in DMSO−d_6.

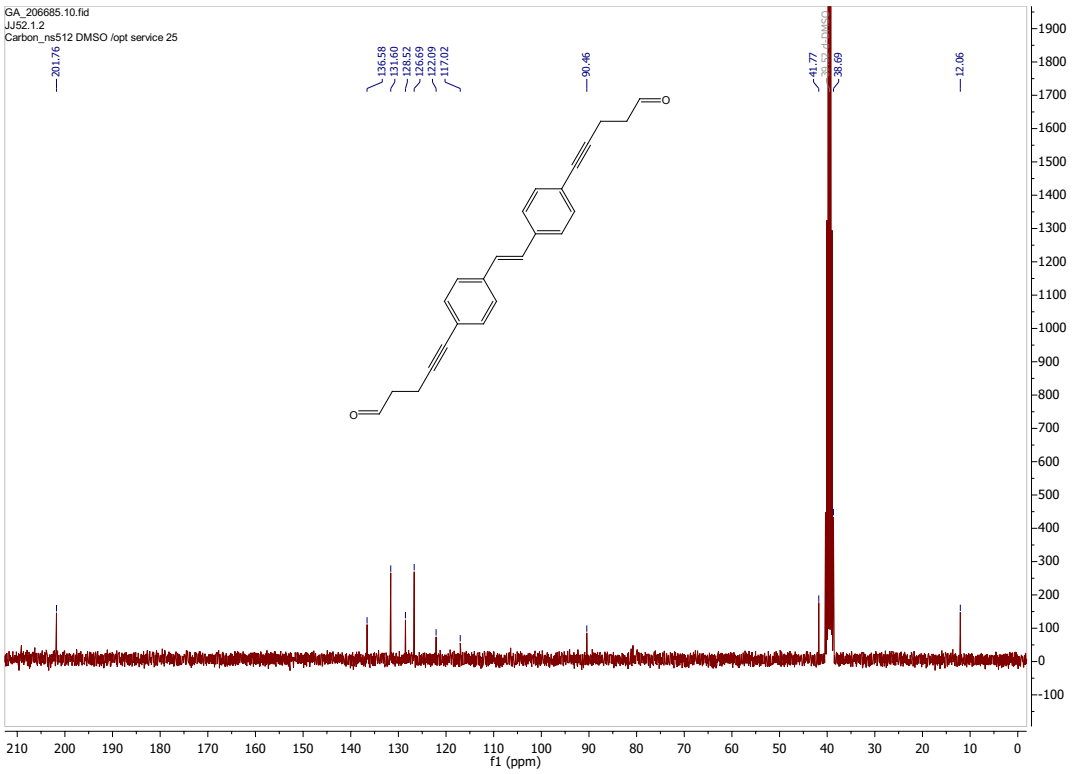

Figure A.44. ^{13}C-NMR of compound **31** in DMSO–d_6.

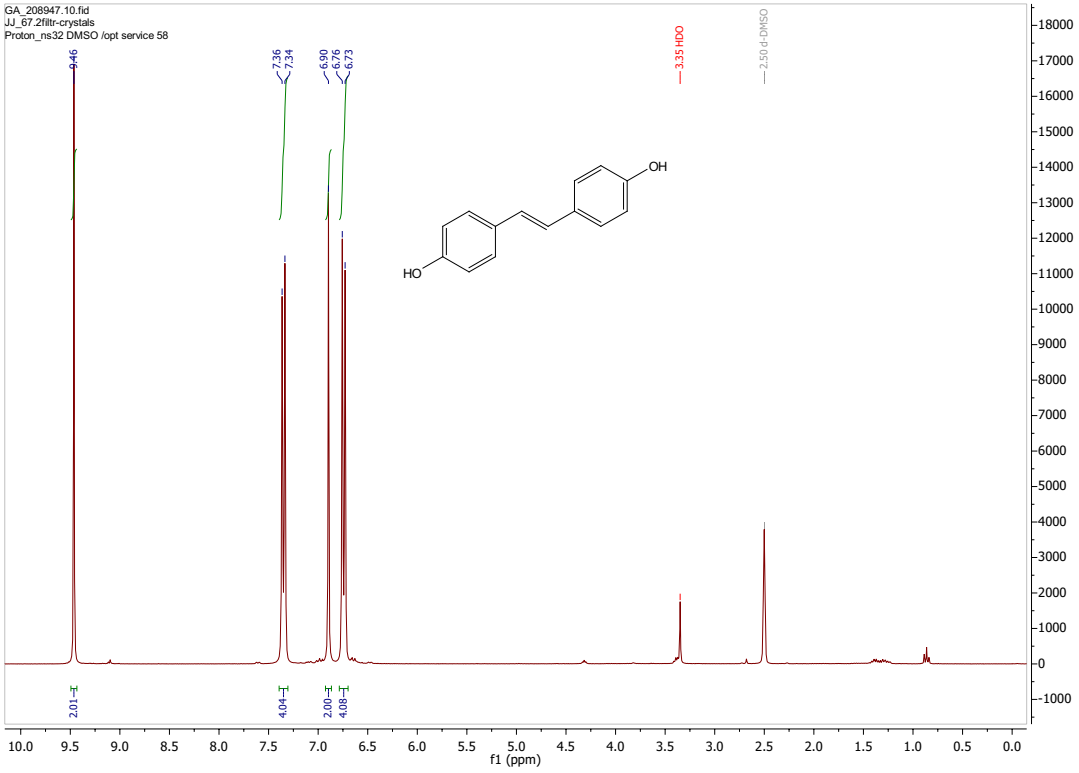

Figure A.45. ^{1}H-NMR of compound **33** in DMSO–d_6.

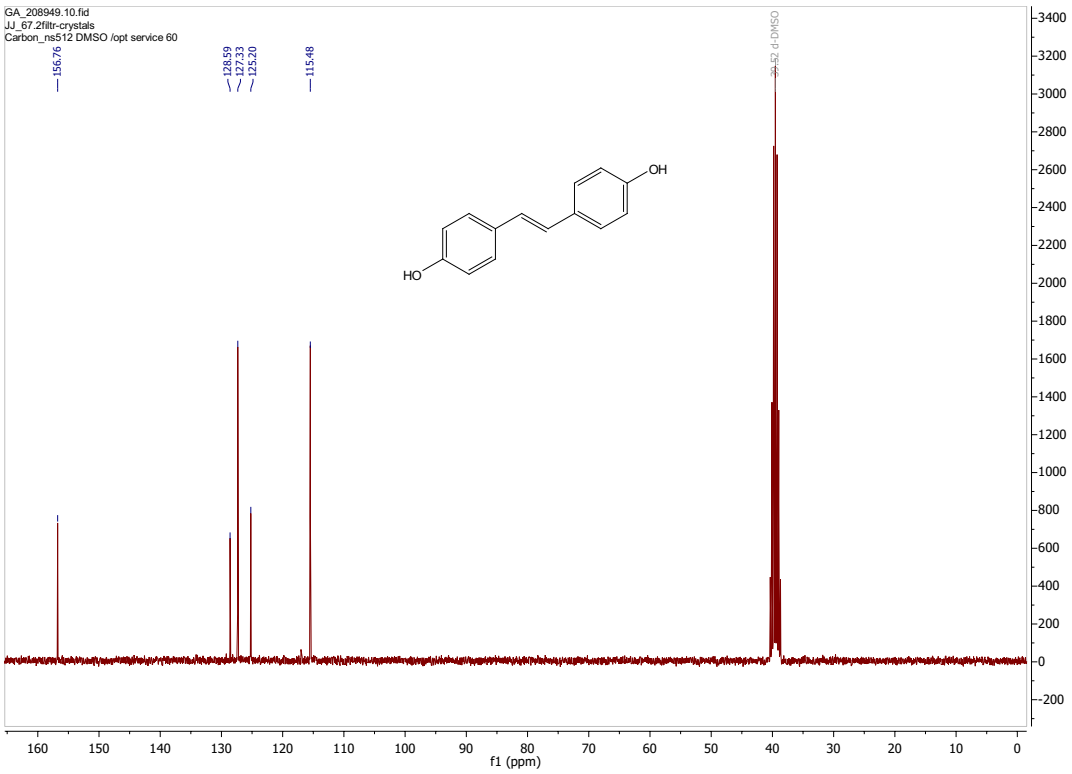

Figure A.46. ^{13}C-NMR of compound **33** in DMSO–d_6.

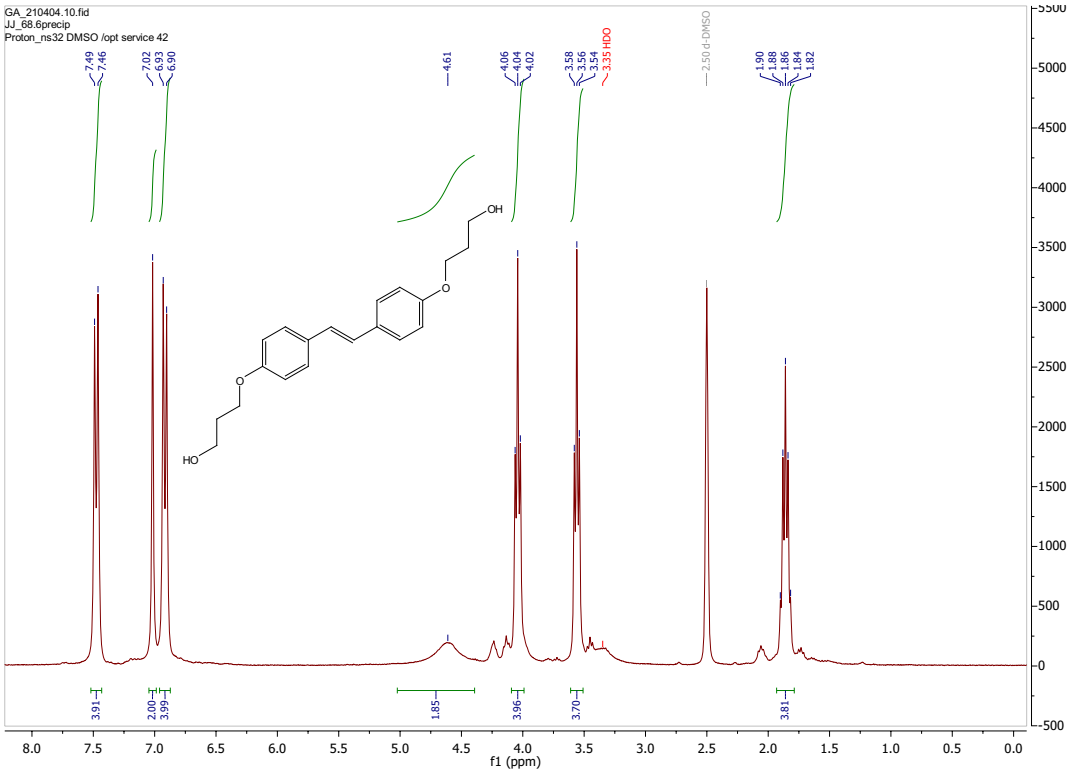

Figure A.47. ^{1}H-NMR of compound **34** in DMSO–d_6.

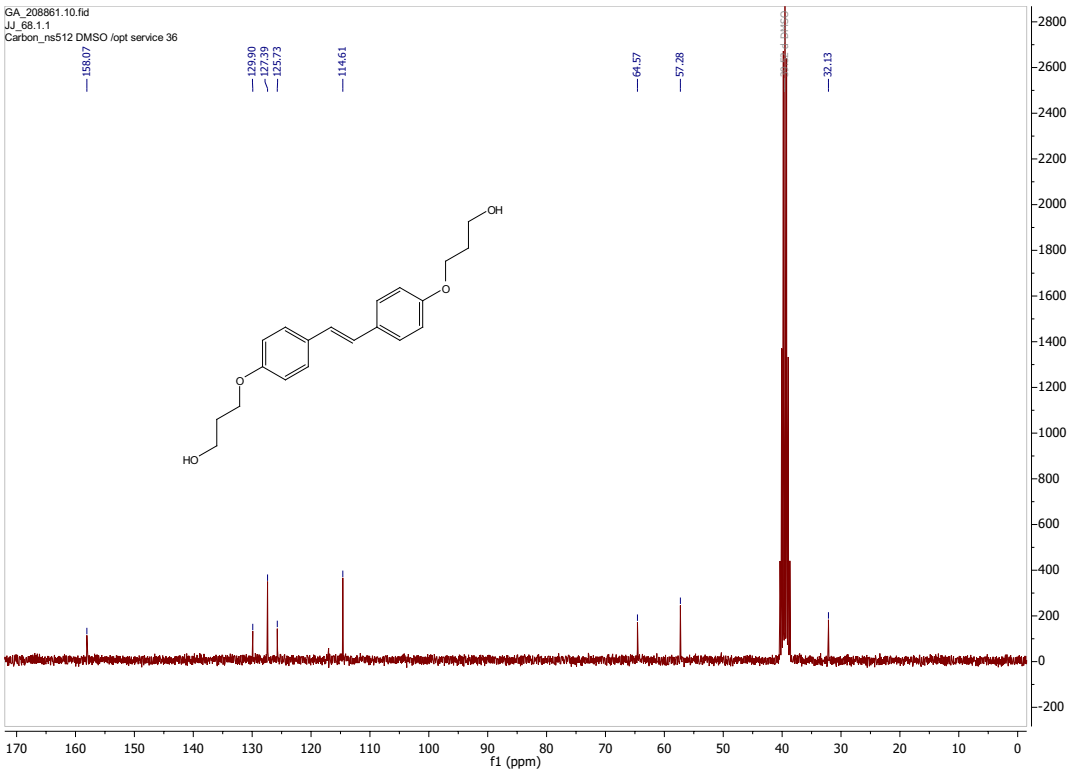

Figure A.48. ^{13}C-NMR of compound **34** in DMSO–d_6.

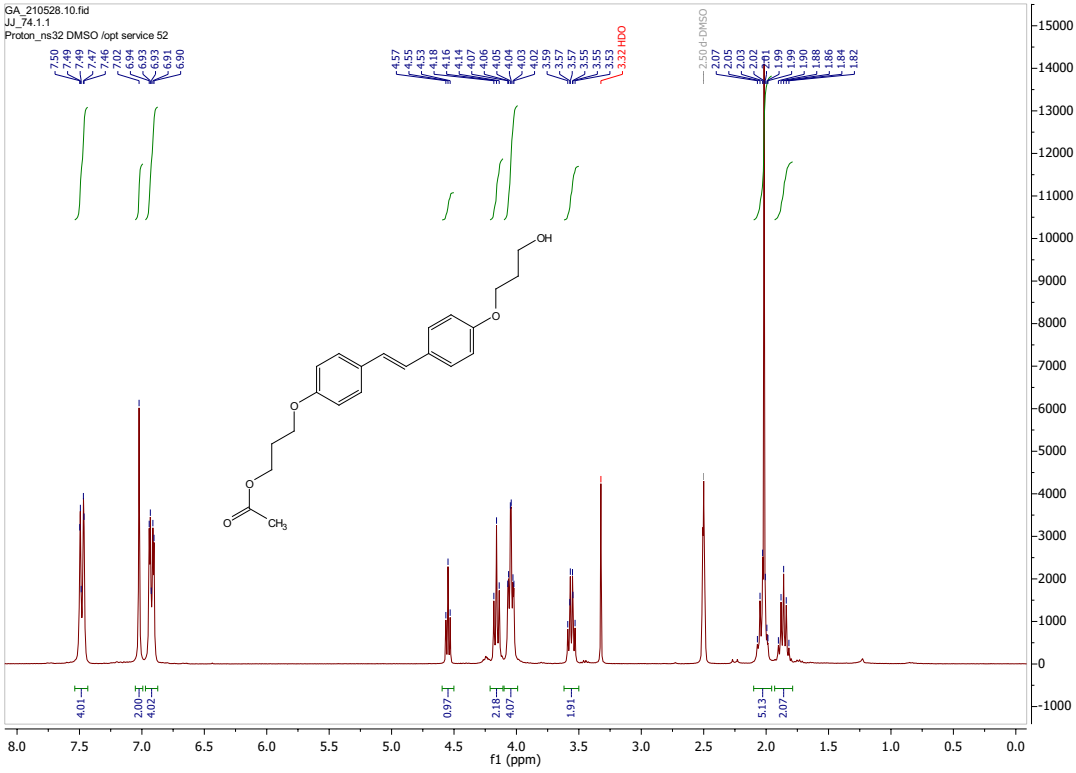

Figure A.49. ^{1}H-NMR of compound **35** in DMSO–d_6.

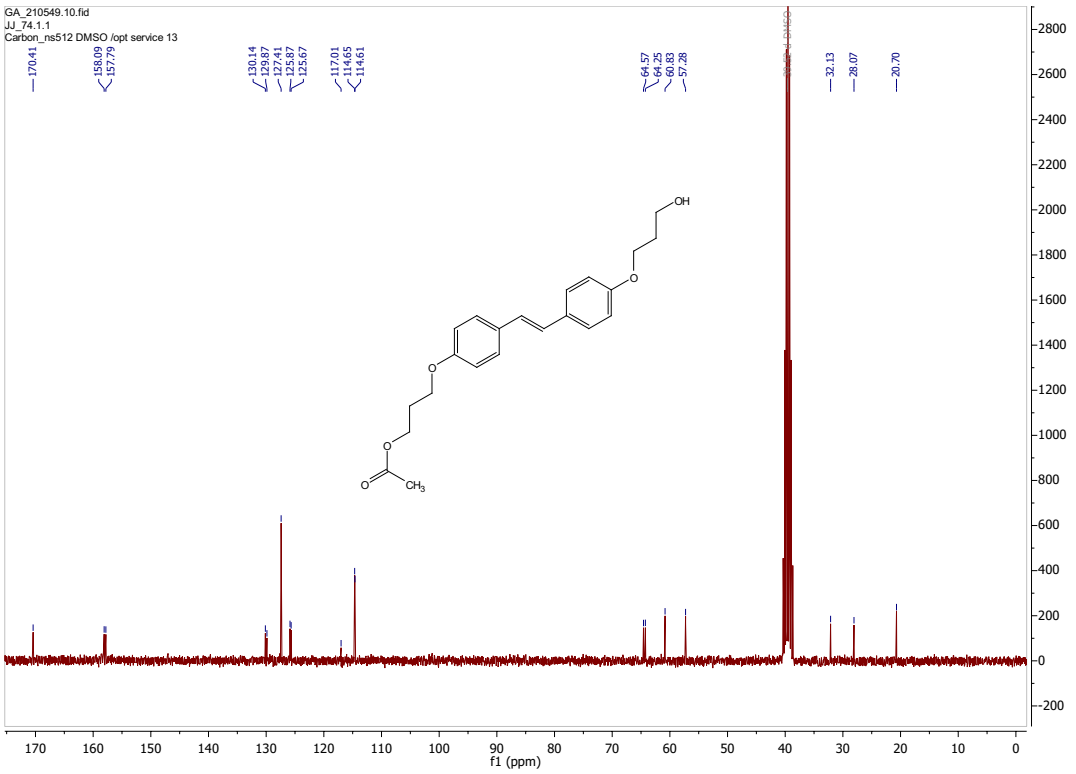

Figure A.50. ^{13}C-NMR of compound **35** in DMSO–d_6.

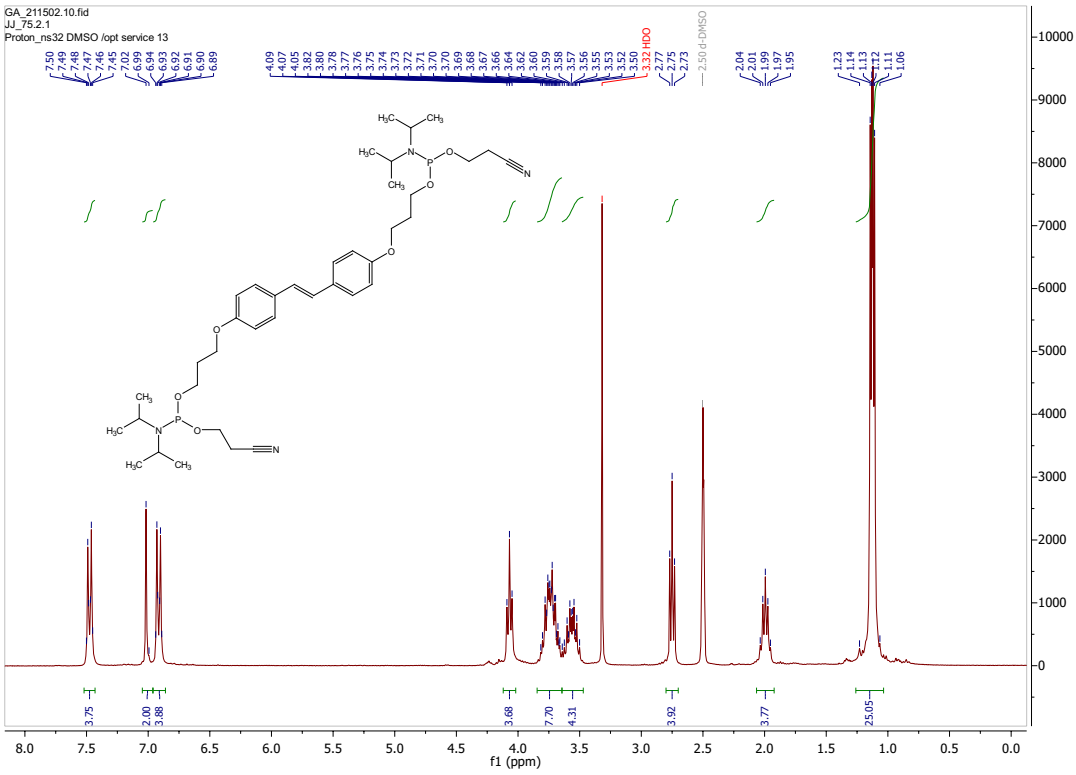

Figure A.51. ^{1}H-NMR of compound **36** in DMSO–d_6.

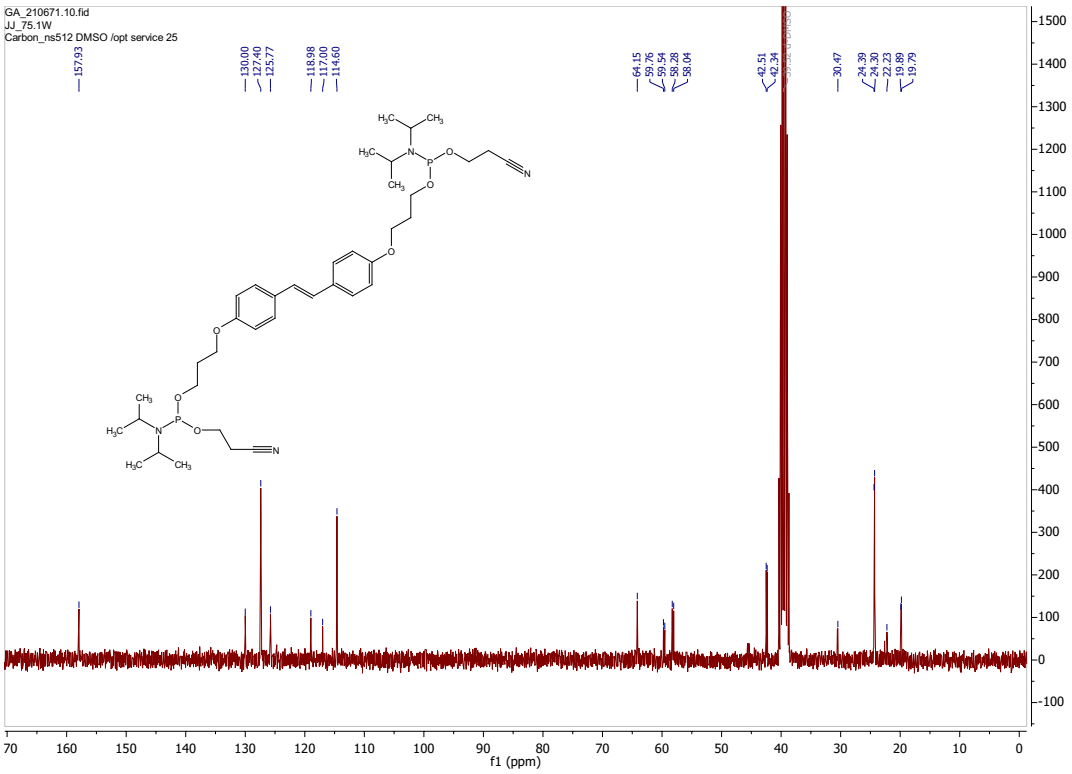

Figure A.52. ^{13}C-NMR of compound **36** in DMSO−d_6.

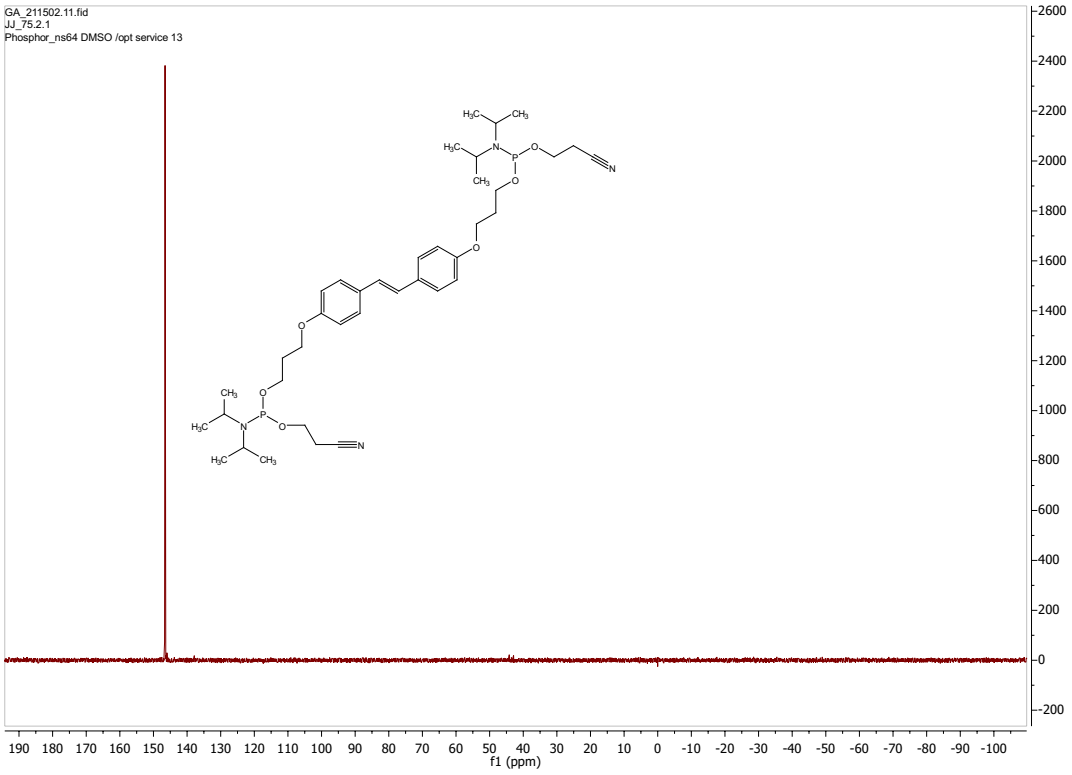

Figure A.53. ^{31}P-NMR of compound **36** in DMSO−d_6.

A.4. Front Cover in *Eur. J. Org. Chem.*, 2020, *30*, 4639

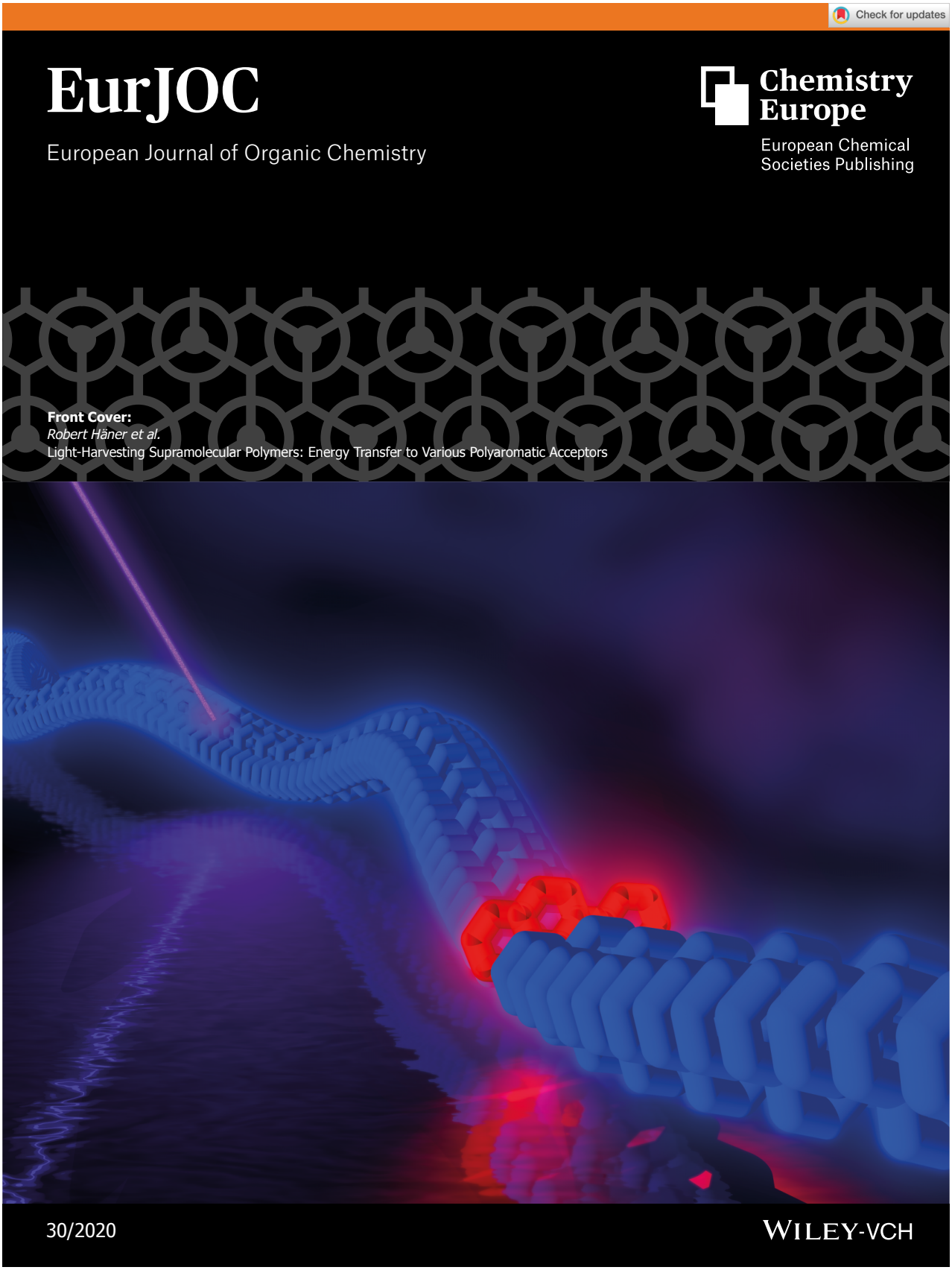

Declaration of consent

Erklärung

gemäss Art. 18 PromR Phil.-nat. 2019

Name/Vorname: Jevric Jovana

Matrikelnummer: 12-113-387

Studiengang: Chemie und Molekulare Wissenschaften

Bachelor ☐ Master ☐ Dissertation ☑

Titel der Arbeit: Amine-Linked Oligomers of Polycyclic Aromatic Hydrocarbons: Synthesis, Properties and Supramolecular Assembly

LeiterIn der Arbeit: Prof. Dr. Robert Häner

Ich erkläre hiermit, dass ich diese Arbeit selbständig verfasst und keine anderen als die angegebenen Quel-len benutzt habe. Alle Stellen, die wörtlich oder sinn-gemäss aus Quellen entnommen wurden, habe ich als solche gekennzeichnet. Mir ist bekannt, dass andern-falls der Senat gemäss Artikel 36 Absatz 1 Buchstabe r des Gesetzes über die Universität vom 5. September 1996 und Artikel 69 des Universitätssta-tuts vom 7. Juni 2011 zum Entzug des Doktortitels be-rechtigt ist.
Für die Zwecke der Begutachtung und der Überprüfung der Einhaltung der Selbständigkeitserklärung bzw. der Reglemente betreffend Plagiate erteile ich der Univer-sität Bern das Recht, die dazu erforderlichen Perso-nendaten zu bearbeiten und Nutzungshandlungen vor-zunehmen, insbesondere die Doktorarbeit zu vervielfäl-tigen und dauerhaft in einer Datenbank zu speichern sowie diese zur Überprüfung von Arbeiten Dritter zu verwenden oder hierzu zur Verfügung zu stellen.

Ort/Datum

Unterschrift